University of Alberta

A Sulphur Concrete Retaining Wall

by

Jose Francisco Garcia Dutari ©

A thesis submitted to the Faculty of Graduate Studies and Research in partial

fulfillment of the requirements for the degree of Master of Science

in

Geotechnical Engineering

Department of Civil and Environmental Engineering

Edmonton, Alberta

Fall 2002

0-612-81397-5

Canada

University of Alberta

Library Release Form

Name of Author: Jose Francisco Garcia Dutari
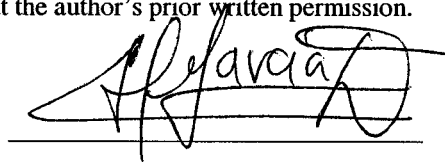
Title of Thesis: A Sulphur Concrete Retaining Wall

Degree: Master of Science

Year this Degree Granted: 2002

Permission is hereby granted to the University of Alberta Library to reproduce single copies of this thesis and to lend or sell such copies for private, scholarly or scientific research purposes only.

The author reserves all other publication and other rights in association with the copyright in the thesis, and except as herein before provided, neither the thesis nor any substantial portion thereof may be printed or otherwise reproduced in any material form whatever without the author's prior written permission.

P.O. Box 6-4818 El Dorado
Panama, Republic of Panama

June 30, 2002

University of Alberta
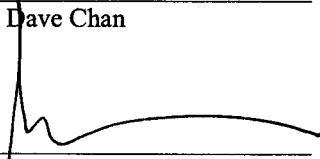
Faculty of Graduate Studies and Research

The undersigned certify that they have read, and recommend to the Faculty of Graduate Studies and Research for acceptance, a thesis entitled A Sulphur Concrete Retaining Wall submitted by Jose Francisco Garcia Dutari in partial fulfillment of the requirements for the degree of Master of Science in Geotechnical Engineering.
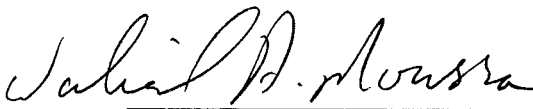
Dr. Dave Sego

Dr. C. Derek Martin

Dr. Dave Chan

Dr. Alaa Elwi

28/June/2002

Dr. Walied Moussa

ABSTRACT

The mining of Oil sands in the Fort McMurray area of northern Alberta constitutes a significant element of Alberta's economy. Over the last 20 years the mining methods have evolved from bucket wheel excavators to truck and shovel operation. A key element of the new truck and shovel mining method is the "Sizer Wall", the dumping areas for the trucks. These sizer walls are currently 15-m high and 204-m long approximately. Presently, these walls are constructed using lean oil sands and reinforced earth technology. The purpose of this thesis was to evaluate the technical feasibility of construction of these sizer-walls using sulphur concrete as sulphur is readily available in the Fort McMurray area. The use of sulphur to build these massive retaining walls may provide an economic and environmental solution to sulphur disposal.

An extensive laboratory program was performed to characterise the strength and deformation behaviour of six mixes of sulphur, tailing sand, and fly ash. Also, a freeze-thaw durability test was developed and carried out. From the results of the laboratory test, a sulphur concrete mix was recommended as a "potential" candidate for constructing the sizer walls.

The external stability of the existing reinforced earth retaining wall was evaluated using traditional Limit Equilibrium Methods. The Factor of Safety of the proposed sulphur concrete wall was evaluated using the same methods. The Finite Element Method, was used to assess the stresses and deformations of the proposed wall, and to evaluate the soil-structure interaction of the sizer wall, backfill, and foundation.

The laboratory data and the analyses show that the construction of massive sulphur-concrete walls is feasible, thus opening the door to the development of novel construction applications of sulphur concrete in the oil sands industry.

ACKNOWLEDGEMENTS

To Melissa, Panchito and Ana

with all my love

TABLE OF CONTENTS

LIST OF FIGURES

LIST OF TABLES

1 INTRODUCTION

Sulphur concrete is relatively new, in comparison to Portland cement concrete, although their physical appearances are similar. The first reference to investigations related to this material originated in 1921; however, it was not until 1975 that sulphur cement, termed as "modified-sulphur cement," was developed. This modified sulphur cement provided the long-term durability that had always been a concern for those working on the applications of this extraordinary construction material (ACI 548, 1988). However, this thesis work does not incorporate modified sulphur cement. Instead, unmodified sulphur cement, i.e., pure sulphur, was used.

At the oil sands mines in the Ft. McMurray area retaining walls of 15 metres high facilitate the unloading of ore from mining trucks and are locally referred to as "Sizer Walls." These walls were originally designed and built implementing reinforced earth technology. The abundance of sulphur, a by-product of oil sands extraction process required an efficient mean of disposal. The construction of these massive retaining walls using sulphur concrete may provide an economical and technical solution to dispose of some of the sulphur in the local region.

This thesis is related to the use of unmodified sulphur cement, combined with material waste from the oil sands industry, to produce a mix of sulphur concrete applicable to the development of civil works. The aggregates of this sulphur concrete are tailing sand and fly ash. No coarse aggregates were included in the mixes, studied throughout this thesis.

1.1 Objective

The objective of this thesis is to evaluate the stability, of a 15 metres high retaining wall, used in the oil sands mining industry; constructed using sulphur concrete.

1.2 Scope

Implementation of the sulphur-concrete retaining wall requires an understanding of material behaviour. A laboratory testing program aimed at characterising the material properties of different mixes was undertaken. In order to define these properties, a uniaxial compression test, split tensile test, and a test of resistance of concrete to rapid freezing and thawing cycles, were performed. At the end, strength and deformation properties (after having subjected the sulphur concrete mixes to freeze-thaw cycles) are suggested.

The evaluation of the retaining wall stability involves the use of the Limit Equilibrium Method and the Finite Element Method. Commercial software packages are used to perform such evaluations. A comparison between the existing and proposed structures based on Limit Equilibrium, results from these analyses. Furthermore, sensitivity analyses, using the Finite Element Method are presented, to predict the stresses and deformations throughout the sulphur concrete wall.

1.3 Outline of Thesis Content

Chapter 1 provides a general introduction to the sulphur disposal problem which exist in Alberta, particularly in the oil sands industry. A brief description of the retaining wall is presented in this thesis, as well as the intended objective, and the scope of the thesis required to achieve the objective.

Chapter 2 presents an extensive literature review of sulphur and sulphur concrete. The basic chemistry of sulphur is presented. The characteristic of sulphur concrete and its development are also included. Information about the environmental and safety concerns in the use of sulphur is compiled. Furthermore, the current practice implemented in the Limit Equilibrium Method is detailed, and the basic theory of the Finite Element Method is included.

Chapter 3 describes the laboratory test performed in order to characterise the material properties of six, sulphur concrete mixes. A test of resistance of the concrete to the rapid freezing and thawing cycles is performed, in order to evaluate the impact on the strength and deformation parameters of the sulphur concrete mixes.

Chapter 4 provides an evaluation, using the Limit Equilibrium Method on the existing reinforced earth retaining walls. Also, the proposed wall is evaluated, in the same manner, in order to compare the results. The sliding, overturning, and bearing capacity of the proposed structure is also evaluated.

Chapter 5 presents results from the Finite Element analyses. The material properties evaluated in Chapter 3 are used in the strain-softening constitutive model proposed for the sulphur concrete, to simulate its brittle behaviour. In addition, the hyperbolic and "Cam Clay" models are used to represent the backfill and foundation material. Also, the soil-structure interfaces are incorporated into the analysis.

Chapter 6 provides the conclusions related to the use of sulphur concrete for the sizer walls and the impact of its use on the environment. Conclusions gathered from

evaluations derived from using the Limit Equilibrium Method and Finite Element Method of the existing and proposed retaining walls are stated. Topics of further research are identified and discussed.

2 LITERATURE REVIEW

2.1 Elemental Sulphur and Sulphur Concrete

Sulphur concrete consists of elemental sulphur, stone and fine aggregates and contains no water or Portland cement (Malhotra, 1979); however, its final appearance is similar to the Portland cement concrete (ACI 548, 1988). The best proportions of sulphur, fine aggregate and coarse aggregate will vary greatly depending on the surface texture, size and gradation of the aggregates (Loov, 1974).

The early sulphur concretes ("unmodified") lacked durability to resist repeated freeze-thaw cycles and their failures were caused by stress relief resulting from thermal cycling (Duecker, 1934). Therefore, early research programs were focused on improving the durability of sulphur concrete.

These investigations resulted in a "modified sulphur cement" by introducing some additives, mainly hydrocarbons, to overcome the stability and durability problems by reducing the expansion-contraction of sulphur concrete during thermal cycling. The resulting modified sulphur concrete was first produced for commercial use in Calgary, Alberta, in 1975 (ACI 548, 1988).

A brief description of the development of sulphur cements is included in this section. However, this thesis focuses on unmodified sulphur cements (pure elemental sulphur) because of its abundance in the oil sands mines, and only the characteristics of the unmodified sulphur cement are addressed here.

2.1.1 Development of Sulphur Concrete

Pure solid sulphur is yellow in appearance and weighs between 2000 and 2100 kg/m^3. Its melting point is about 119°C, and the liquid ranges in colour from transparent straw yellow to dark reddish brown. Depending on its temperature, its viscosity changes markedly, particularly above 159°C. Some properties are summarised by Malhotra (1979) and presented in Table 2.1.

Viscosity	
At 120°C	11.8 x 10^{-3} Pa.s
At 159°C	6.6 x 10^{-3} Pa.s
At 188°C	100 Pa.s
Specific Gravity	
Of solid	1.96 – 2.07
Of liquid at 120°C	1.80
Compressive Strength	
On 75 x 150 mm cylinders	28 MPa
Thermal Coefficient of Expansion	
At 25°C	74 x 10^{-6} / °C

Table 2.1 Some Properties of the Element Sulphur (Malhotra, 1979)

Sulphur concrete is relatively new and very similar to the final appearance of Portland cement concrete (ACI 548, 1988). However, its manufacture, handling, use, and testing are different from Portland cement based concretes. Sulphur concrete is a Thermoplastic material prepared by hot-mixing sulphur cement, coarse aggregates, and fine aggregates. It does not contain water or Portland cement. This material solidifies and gains strength rapidly after cooling. "Sulphur concrete" is a generic term involving a family of materials composed of different proportions of sulphur cement and aggregates.

6

Bacon and Davis (1921) tested many (suggested) additives to modify sulphur's properties. They found that a mixture of 60% sand and 40% sulphur showed excellent resistance to acids and provided high strength.

In the middle of the 1960's , Dale and Ludwig (1966 and 1968) pointed out the need for well-graded aggregates to obtain optimum strength. This work was followed by the investigations of Crow and Bates (1970) into the development of high-strength sulphur-basalt concretes. The United States Department of the Interior's Bureau of Mines and The Sulphur Institute (Washington, D.C.) launched a co-operative program in 1971 to investigate and develop new uses for sulphur. At about the same time, the Canada Centre for Mineral and Energy Technology (CANMET) and the National Research Council (NRC) of Canada initiated a research program into the development of sulphur concrete. At the University of Calgary, Loov (1974) followed up on this work.

In 1973, the Sulphur Development Institute of Canada (SUDIC), jointly founded by the Canadian Federal Government, the Alberta Provincial Government, and Canadian sulphur producers was established to develop new markets for the increasing Canadian sulphur stock-pile. In 1978, CANMET and SUDIC sponsored an international conference focusing on sulphur in construction (Malhotra et al., 1978). Also during this period, a number of investigators published papers and reports dealing with various aspects of sulphur and sulphur concrete: Malhotra (1974), Loou (1974), Sullivan et al. (1975), Sullivan and McBee (1976), Vroom (1977), McBee and Sullivan (1976, 1979, and 1982), McBee et al (1981, 1983 and 1986), Funke and McBee(1982), and Sullivan (1986). All of these activities led to an increased awareness of the potential use of sulphur as a construction material.

7

Sulphur concrete prepared through the hot-mixing of unmodified sulphur and aggregate lacked durability. Unmodified sulphur concretes failed when exposed to repeated cycles of freezing and thawing, humid conditions, or immersion in water (ACI 548, 1988). When unmodified sulphur and aggregate are hot-mixed, cast, and cooled to prepare sulphur concrete products, the sulphur binder, after cooling from the liquid state, first crystallises as monoclinic sulphur (S_β) at 114°C with a volume decrease of 7 percent. On further cooling to below 96°C, the S_β starts to transform into orthorhombic sulphur (S_α), which is the stable form of sulphur at ambient temperatures. This transformation is rapid, generally occurring in less than 24 hrs. As the S_α form is denser than S_β, the sulphur binder can become highly stressed internally and can fail prematurely. Duecker (1934) observed this phenomenon in mortar prisms made with sulphur and sand.

The increasing demand since 1976 for corrosion-resistant sulphur concrete has led to the installation of pre-cast and / or cast-in-place sulphur concrete instead of Portland cement concrete in industrial plants. The typical installations, as described by Pickard (1984), included floors, slabs on grades, overlays, curbs, walls, trench drains, sump pits, tanks, electrolytic cells, pumb bases, column piers, foundations, and pipes.

2.1.2 Modified Sulphur Cement

The previous section notes the inconvenience of using unmodified sulphur cement (elemental sulphur with no additives). Therefore, sulphur cements are modified by introducing additives to improve stability and durability and reduce the expansion-contraction of sulphur concrete during thermal cycling.

In 1973, A. H. Vroom developed a process, with assistance from the National Research Council of Canada and A. Ortega of McGill University, involving modifying sulphur by reacting it with olefinic hydrocarbon polymers (Vroom, 1977 and 1981). The resulting sulphur concrete was first produced for commercial use in Calgary, Alberta, in 1975. McBee and Sullivan (1982) produced a modified sulphur cement that was stable in the S_β form and was not temperature sensitive in the mixing temperature range for producing sulphur concrete. This process utilised a controlled reaction of cyclopentadiene (CPD).

Other researchers have reported various methods to produce modified sulphur concretes: Leutner and Dieh (1977) introduced the use of dicyclopentadiene (DCPD); Gillott et al. (1980), crude oil and polyol additives; Schneider and Simic (1981), DCPD or glycol; Woo (1983), phosphoric acid to improve freeze-thaw resistance; and Nimer and Campbell (1983), organosilane to improve water stability.

Two modified sulphur concretes currently used in North America are given in Table 2.2.

Materials	Method 1 (in % by weight)	Method 2 (in % by weight)
Sulphur	95.0 ± 1.0	80
Carbon	5.0 ± 0.5	18
Hydrogen	0.5 ± 0.05	2

Table 2.2 – Material of Modified Sulphur Concrete used in North America, taken from ACI 548.2R-88.

Method 1 shown in Table 2.2 is based on the polymeric reaction, in which 100% of the sulphur reacts with a modifier containing equal parts of cyclopentadiene oligomer and

9

dicyclopentadiene (DCPD) (McBee and Sullivan, 1982). DCPD is a hydrocarbon in the form of a colourless liquid with double bonds suitable for reacting with sulphur, and it also retards and prevents the crystallisation of sulphur (Sullivan and McBee, 1976). This process is known as the Chempruf® Process and uses a proprietary composition called "Chement 2000"(Crick and Whitmore, 1998).

Method 2, also shown in Table 2.2, uses a modified sulphur concrete prepared by combining sulphur with olefinic hydrocarbon polymers such as Escopol (Vroom, 1981). This concentrate is then mixed with locally available pure sulphur in the ratio of 10 parts of sulphur to 1 part of concentrate, by weight. Actually, this process is used commercially to produce the concrete product named STARcrete™. Its predecessor Sulfurcrete® was first marketed in Canada in 1976.

While various additives are available to enhance the properties of sulphur concrete, this thesis has focused on unmodified sulphur concrete. Hence only the characteristics of unmodified sulphur concrete are discussed in the following sections.

2.2   Characteristics of Sulphur Concrete

2.2.1   Compressive Strength Development

Loov et al. (1974) compared the rate of compressive strength development of sulphur concrete and Portland cement concrete (Figure 2.1). Sulphur concrete develops about 70% of its ultimate strength within a few hours after cooling, and usually 75% to 85% after 24 hours at 20°C; however, it reaches its ultimate strength after 180 days at 20°C (McBee et al., 1983). The rate of strength development depends on the temperature at which the material is aged. Strength gain is slower at elevated temperatures and faster at

lower temperatures. Therefore, larger masses gain strength slowly because they cool more slowly; however in the end, sulphur concrete reaches the same ultimate strength (McBee and Sullivan, 1979). Johnston (1979) emphasised that there is no evidence of strength retrogression during a six-month period following placement of sulphur concrete.

Lee et al. (1978) showed that the addition of fly ash in a proportion of 7.3% by weight of the total mix to the unmodified sulphur concrete improved the compressive strength by 73%.

Czarnecki and Gillot (1989) studied the effect of different admixtures on the strength of sulphur concrete. Their conclusions included the following:

- The strength of sulphur concrete did not depend entirely on the amount of sulphur binder.

- The strongest rock aggregate did not produce the strongest concrete. Moreover, the aggregate particle shape and texture played a major role in the overall strength and density of concrete.

- The addition of crude oil resulted in lower strengths.

- Sulphur concrete continuously immersed in water developed lower strengths than that exposed to normal laboratory air.

- Silane admixtures affected positively the moisture durability and strength in air and water.

Abel-Jawad and Al-Qudah (1994) determined the compressive strengths of sulphur concrete using limestone, basalt, and sandstone aggregates after curing times of 2, 4, 7,

14, and 28 days at room temperature (20°C). They found that the peak strength did not change with time.
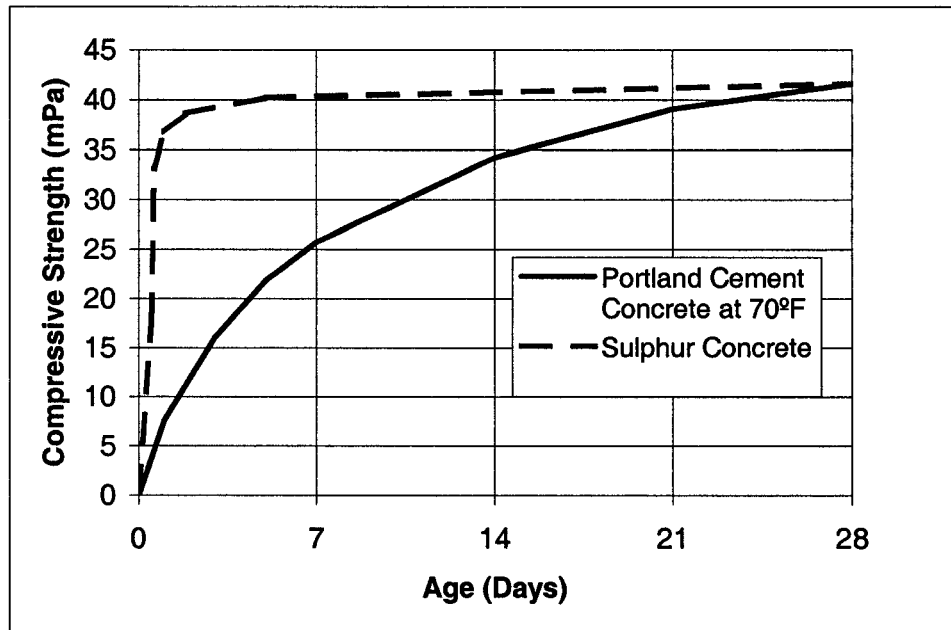
Figure 2.1 Comparison of the strength gain of sulphur concrete and Portland cement concrete, modified from Loov et al. (1974)

2.2.2 Stress-Strain Relationships

Unmodified sulphur concrete has a near linear stress-strain curve up to failure. Czarnecki and Gillot (1989) considered sulphur concrete to be "brittle" when during an unconfined compressive test, a sudden noise followed by a rapid reduction in load are observed within seconds of the ultimate load being reached. Concrete that produced a descending post peak response or fails in a less violent manner is considered "ductile".

Shrive et al. (1977) and Loov (1975) reported that sulphur, sulphur mortars, and sulphur concrete are extremely brittle materials, far more so than Portland cement mortars and concretes. Loov also published stress-strain curves showing that there was no gradual reduction in stiffness when the ultimate load was approached. Moreover,

12

failure occurred at a strain of approximately 0.0014. The Young Modulus of sulphur concrete and Portland cement concrete are comparable, and its value is about 30 GPa for a sulphur concrete with a strength of 40 MPa (Loov, 1974; Malhotra, 1979). Moreover, after one day of cooling, the ACI 548 (1988) reported that for sulphur concrete with a compression strength of 27.6 MPa of the Young Modulus ranged from 20.7 to 27.6 GPa.

Lee et al. (1981) found that admixtures, such the olefins and thiocols, stabilised the bonding structure and converted the sulphur concrete into a more ductile material. However, the effect of these admixtures was time-dependent, and the ductility disappeared with time. An explanation of this effect can be found in Currel et al. (1975).

Gillot et al. (1980) studied another type of admixture that they believed could alter the bond characteristic between the sulphur matrix and the aggregate and between the sulphur crystals within the matrix. Petroleum additives and some polyols improved the strain capacity, and the effect remained during large periods of time (Gillot et al., 1982 and 1983).

2.2.3 Fatigue Behaviour

A material is said to fail in "fatigue" if failure takes place after a number of repeated loads, each smaller than the static strength. This characteristic is important in structures such as pavement subject to repetitive loads. Lee et al. (1978) investigated the fatigue behaviour of sulphur concrete. They found that sulphur concrete exhibited different fatigue properties than those of conventional Portland cement concrete. Unmodified sulphur concrete withstood repeated loading at a much higher percent of the modulus of rupture than conventional concrete. This finding means that for pavements of the same

13

thickness and of equivalent compressive strength, sulphur concrete is able to carry many

more applications of traffic loads than Portland cement concretes.

Furthermore, Lee et al. (1978) indicated that sulphur concrete with fly ash as an

additive had higher fatigue life and improved considerably the compressive strength.

Finally, all the sulphur concrete mixes studied by Lee et al. (1978) presented a better

fatigue behaviour than Portland cement concrete (Figure 2.2). The difference in the

modulus of rupture between the regular Portland cement concrete and the unmodified

sulphur concrete is particularly noteworthy. The behaviour of the fly-ash-modified

sulphur concrete is far better than that of the DCPD-modified sulphur concrete.
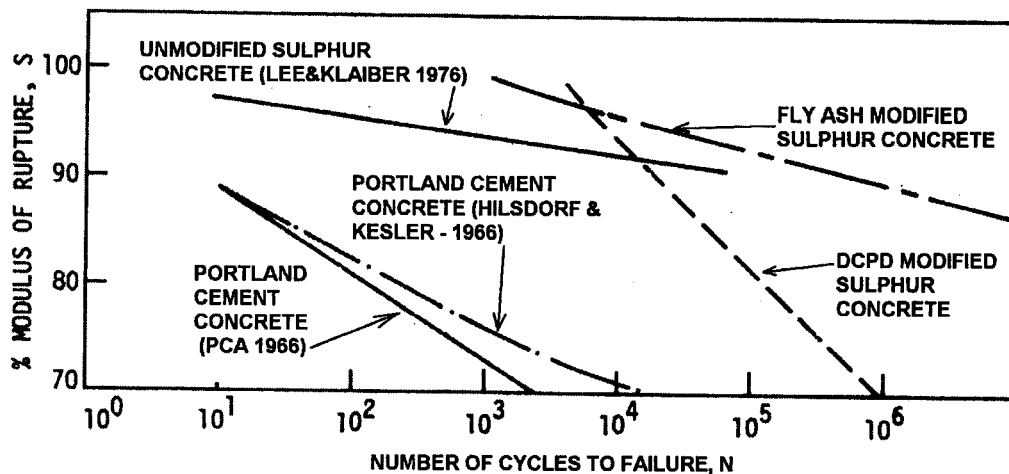
Figure 2.2– Fatigue curve for different series of sulphur concrete and Portland
cement concrete, modified from Lee et al.(1978).

2.2.4 Creep

Loov (1975) and Malhotra (1979) indicated that sulphur concrete exhibited

considerably more creep than Portland cement concrete. Gamble and Shrive (1978)

suggested several mechanisms of creep in sulphur and also mentioned that the creep in

elemental sulphur was greatly affected by the methods of preparation and curing. Figure

14

2.3 presents the creep behaviour of sulphur concrete compared to the Portland cement concrete.
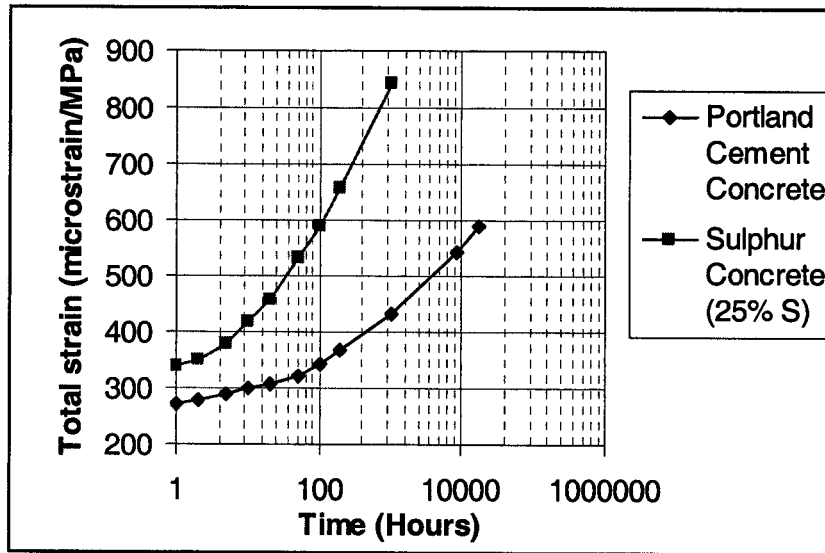
Figure 2.3 Creep behaviour of sulphur concrete at 21°C, modified from Loov

(1974)

2.2.5   Freeze – Thaw Durability

The durability of sulphur concrete subjected to freeze-thaw cycles has been studied extensively (Malhotra, 1973; Beaudoin and Sereda, 1974; Loov, 1975; Sullivan and McBee, 1976). Their laboratory results showed sulphur concrete to have poor freeze-thaw durability.

Duecker (1934) proposed a theory explaining the deterioration of the sulphur concrete under freeze-thaw cycles, and it has been supported by many workers such as Currel (1976), Sullivan and McBee (1978), Malhotra (1979), and Vroom (1977). Duecker suggested that since sulphur has a low thermal conductivity, large internal temperature gradients develop when the ambient temperature changes externally by a few degrees. These temperature gradients, when coupled with the unusually high coefficient of thermal expansion of sulphur ($\approx 55 \times 10^{-6}$ / °C), generate high thermal stresses. These stresses were thought to be responsible for the development of fissures or fractures within the

15

material (Shrive et al., 1981). However, Shrive et al. (1981) concluded that the lack of freeze-thaw durability of sulphur concrete resulted from some mechanism involving the thawing and freezing of water in the specimen. This failure mechanism was the same as that proposed for Portland cement concretes under freeze-thaw cycles and involved the effect of moisture in the material. It was thought that moisture migration associated with the growth of ice crystals was the principal factor in the creation of cracks and fractures. Powers (1975) remarked that pressure great enough to exceed the tensile strength of the material has been attributed to an osmotic-type mechanism. In addition, Litvan (1976) suggested that differences in vapour pressure between the more stable ice and unfrozen water absorbed on internal surfaces also increased the pressure. Therefore, the ice is understood to form in large voids or cracks. This failure mechanism is controlled by entraining an air and void system, which is created such that the distance between voids within the matrix is sufficiently small (on average) to avoid development of large internal pressures.

Therefore, Shrive et al. (1981) showed that moisture reaches the interior of the samples despite the low permeability of the sulphur concrete. They inferred that both the mechanism of failure and the potential solution could be the same as for Portland cement concretes. Shrive et al. (1977) remarked that many sulphur concretes can support many freeze-thaw cycles, although these concretes fail in the presence of water at constant temperatures. This phenomenon was attributed to the presence of expansive clays in the aggregate

The air content and the void spacing factor are important parameters considered in Portland cement concretes for freeze-thaw durability and are measured by the ASTM C-457. An air content of at least 7% and a void spacing factor of at most 0.2 mm are

considered necessary to provide an adequate durability for severe exposure conditions in Portland cement concretes. However, no consistent trend was found in sulphur concrete specimens. Shrive et al. (1981) argued that the durability of sulphur concrete must also be a function of the permeability, tensile strength, stress-strain behaviour, and water absorption properties of the concrete.

Cohen (1987) performed an investigation to evaluate the freeze-thaw durability based on the mechanism proposed by Shrive et al. (1981). They received 12 bars of 2x2x12-inches of regular grade and cut 6 bars in cubes of 2x2x2-inches. The samples were immersed in water, petroleum base oil and in air (in sealed plastic containers) and stored in a freeze-thaw apparatus with a temperature range from $-12°C$ to $32°C$ at 27 cycles per week. Figure 2.4 shows the weight change versus the number cycles, and Figure 2.5 shows the relative compressive strength versus the number of cycles. It can be observed that after 300 cycles, the weight and the relative compressive strength of the air- and water-stored samples hardly changes. However, Figure 2.6 shows the dynamic Young's modulus decreasing to values below 60%. The ASTM C-666 indicates that when this kind of decrease occurs, the specimen fails to pass the durability test. Cohen (1987) remarked that the interesting point was that the water- and air-stored samples behave similarly during freeze-thaw testing.

Even though the samples failed according to the ASTM C-666, analyses of the relative compressive strengths, surface conditions, and weight loss data of the water- and air-stored samples seemed to indicate good freeze-thaw resistance. Moreover, no appreciable differences were found in the strength behaviour of the water- and air-stored samples. Consequently, Cohen (1987) suggested that the mechanism by Duecker (1934) should not be dismissed from consideration. In other words, cyclic freezing and thawing in sulphur

concrete may be equivalent to thermal cycling, in which water does not have any significant role. Furthermore, the fact that mortars bars failed the ASTM C-666, when at the same time the cube strength showed satisfactory resistance, showed that the ASTM C-666 test cannot be used effectively for sulphur concrete (Cohen, 1987).
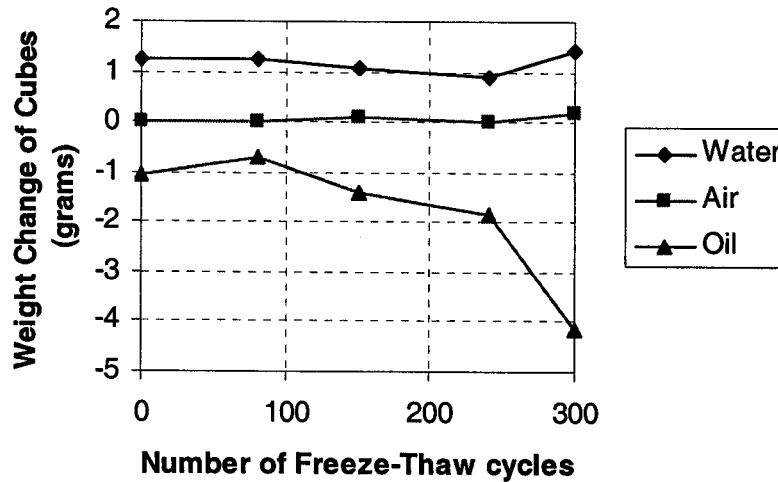
Figure 2.4 Weight change of cubes versus number of freeze-thaw cycles, modified
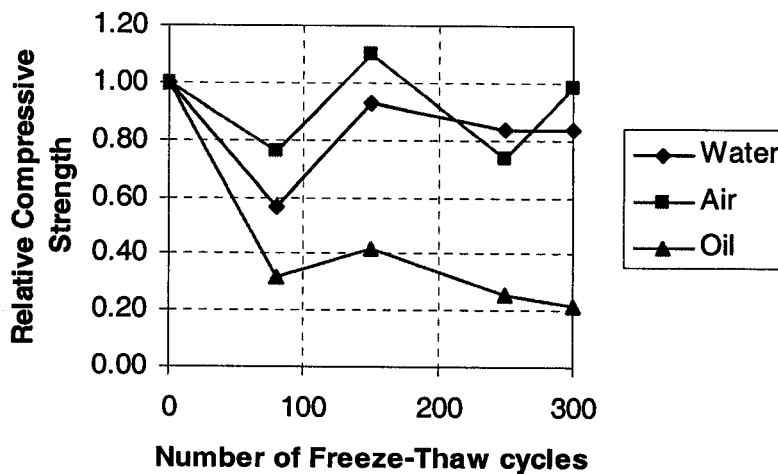
from Cohen (1987).

Figure 2.5 Relative compressive strength of cubes versus number of freeze-thaw cycles, modified from Cohen (1987)
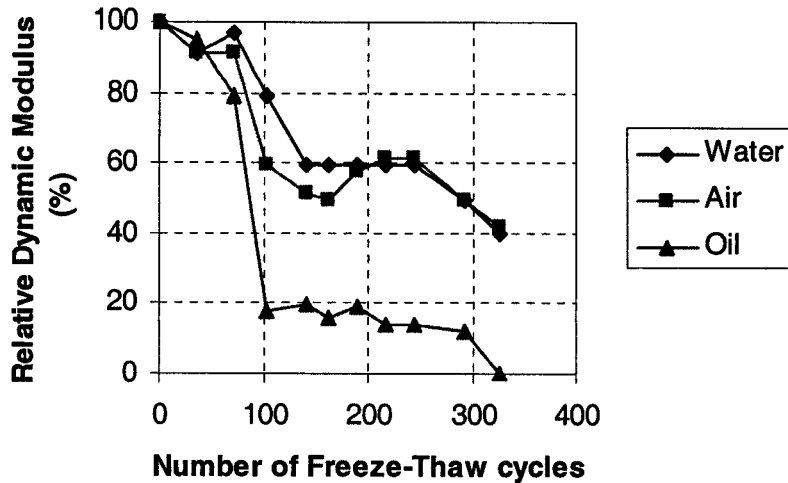
Figure 2.6 Relative modulus of bars versus number of freeze-fhaw cycles, modified from Cohen (1987).

2.2.6 The Effect of Water Under Constant Temperature

The immersion in water under constant temperature also affects the durability of the sulphur concrete. Gillot et al. (1983) and Czarnecki and Gillot (1989 and 1990) showed that sulphur concrete is subject to excessive expansion, cracking, and strength loss as a result of continuous immersion in water at room temperature. Their results indicated that sulphur concrete made with good quality aggregates may show poor durability in the presence of water. However, glycerine and silanes were found to reduce the moisture expansion. Their effectiveness depends of the type of admixture and the type of aggregate.

Czarnecki and Gillott (1989) also found no correlation between the expansion of the rocks and the expansion of the concretes made with these rocks. They observed much greater expansion in the concretes than in the rocks, leading to the conclusion that the expansion resulted from a physical phenomenon within the sulphur.

Abdel-Jawad and Al-Qudah (1994) studied the combined effect of water and temperature on compressive strength by using different kind of aggregates. Figures 2.7 (a, b, and c) summarise the results of the study of the compressive strength of sulphur concrete samples using crushed limestone, sandstone and basalt aggregates. These figures show clearly that the sulphur concrete gained its strength after few hours of casting and that no further strength was gained, as is shown by the curves of the samples cured in air at 20°C. Therefore, the sulphur concrete strength may be considered independent of time (Abdel-Jawad and Al-Qudah, 1994). The specimens cured by being immersed in water showed that most of the strength reduction took place after the first three days, and that afterward the strength remained practically unchanged. As well, cracks and cavities appeared in the samples prepared with aggregates of crushed limestone and basalt, possibly because of the presence of clay minerals.

2.2.7 Corrosion Resistance

Sulphur concrete is a desirable material for use in construction in the fertiliser and metal-refining industries because of its resistant to attacks by a wide range of acids and corrosive materials. Sullivan and McBee (1978) showed that concretes prepared with silica aggregates and modified sulphur binder were superior to those made with unmodified sulphur. Dielhl (1976) presented some data showing the sulphur and dicyclopentadiene modified sulphur's resistance to aggressive chemical attacks. More recently, Crick and Whitmore (1998) presented a list of the sulphur concrete's chemical resistance to various solutions at room temperature (Table 2.3).
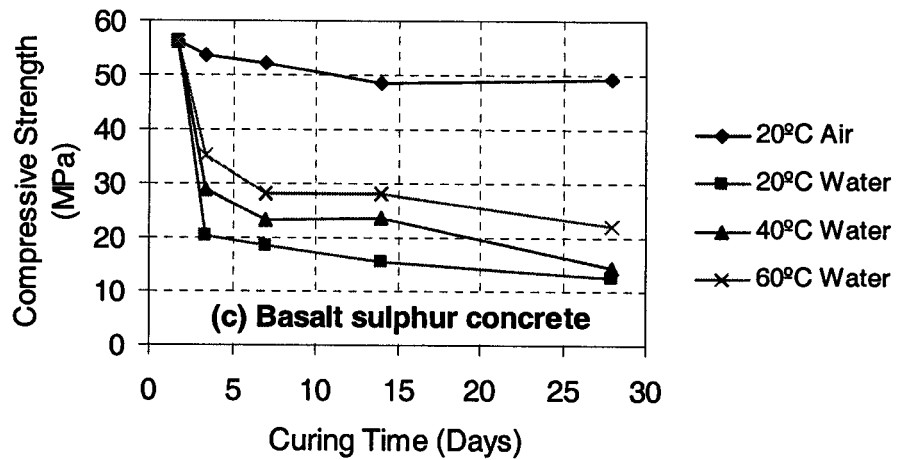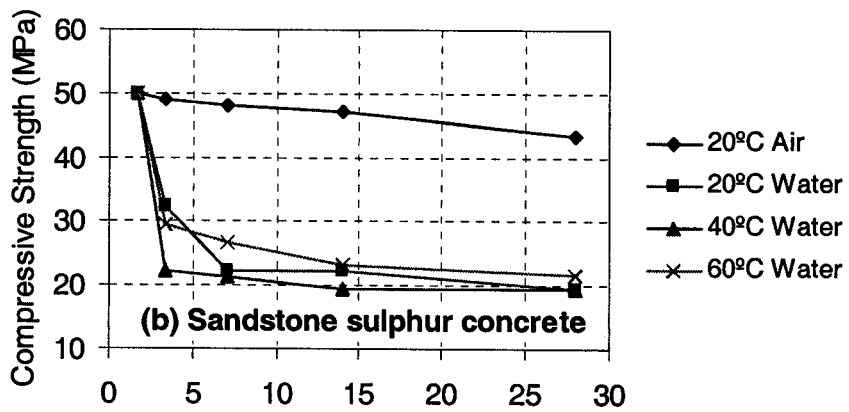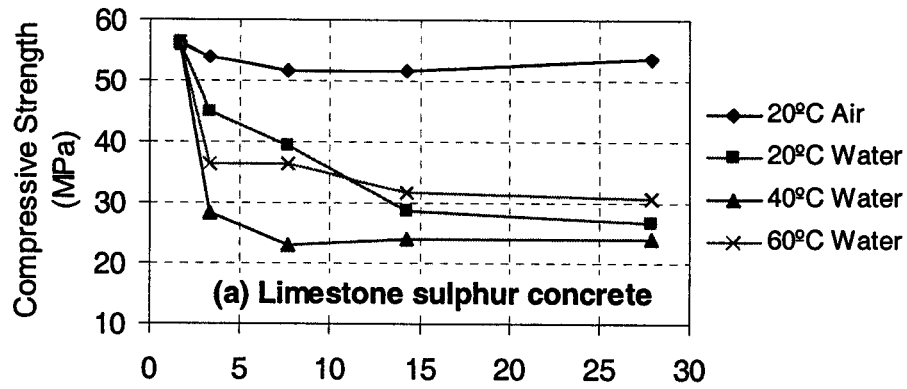
Figure 2.7 Compressive strength versus the curing time for sulphur concretes at different curing conditions:(a)Limestones, (b) Sandstones, and (c) Basalt; modified from Abdel-Jawad and Al-Qudah (1994)

However, Malhotra (1979) mentioned that sulphur concrete can be attacked or dissolved by strong oxidising agents such as concentrated sulphur, nitric, and chromic acids; sodium hypochloride; strong alkalis at pH 10; polysulphide solutions; and certain organic chemicals (carbon disulphide, phenols and others). Sulphur also reacts with a number of metals in solutions like copper and beryllium to form insoluble sulphides, Sheppard (1975).

Recently studies by Okamura (1998) showed that sulphur concrete performed well over time, and that quality control in design, production, and placing were paramount for success against chemical attacks.

Acids	Concentration* (%)	Chemicals	Concentration* (%)
Boric acid	100	Ammonium sulphate	100
Hydrochloric acid	32	Calcium chloride	100
Nitric acid	50	Copper sulphate	100
Phosphoric acid	85	Ferric chloride	100
Sulphuric acid	93	Magnesium chloride	100
		Magnesium sulphate	100
		Potassium chloride	100
		Nickel chloride	100
		Nickel sulphate	100
		Sodium chloride	100
		Sodium Sulphate	100
		Zinc chloride	100
		Zinc sulfate	100

*Maximum concentration resisted by sulphur concrete.

Table 2.3 Chemical resistance at room temperature after Crick and Whitmore (1998).

2.2.8 Resistance to Biological Attack

Loov (1974) and Malhotra (1979) pointed out that sulphur concretes were susceptible to attack by bacteria, primarily thiobacillus thiooxidans, resulting in the production of sulphuric acids (H_2SO_4); therefore, a drop in medium pH indicates growth of this organism. Frederick and Starkey (1948) reported that the oxidation of elemental sulphur by Thiobacillus thiooxydans was dependent upon particle size – the smaller the sulphur particle, the faster its rate of oxidation in pure culture experiments. Fjerdingstad (1960) pointed out that the optimum growth temperature for Thiobacillus thiooxydans is between 28 and 30°C; therefore, the attack would be more severe in soil in countries with hot climate.

Investigations have reported the use of bactericides to counter this attack (Duecker et al., 1948; Laishly and Tyler, 1978). Laishly and Tyler (1978) indicated in Table 2.4 the effect of Thiobacillus thiooxidans on sulphur concrete.

Sulphur Limestone Concrete Bars	Cell Count of Thiobacillus thiooxidans/ ml		pH		SO$_4$ mg/ml		Length of Bars in inches		Flexure Test (psi)
	Initial	Final	Initial	Final	Initial	Final	Initial	Final	
Inoculated[*]	3.1×10^6	7×10^7	3.3	1.8	0.5	9.5	10.06	10.06	384(±37)
Uninoculated[*]			4.5	4.8	0.5	1.6	10.08	10.08	381(±35)
Dry Control[**]							10.07	10.06	481(±36)

[*] Average of 4 different experiments.
[**] Average of 3 different experiments.
[***] Measured with Demec Extensometer.
( ) Standard deviation of the mean.

Table 2.4 Effect of thiobacillus thiooxidans on sulphur concrete, modified from Laishley and Tyler (1978)

2.2.9 Resistance to Fire

Sulphur melts at about 119°C, and sulphur concrete subjected to about this temperature will lose all its strength; consequently, its use is limited to conditions in which temperatures are no more than 80°C (Malhotra, 1979). Regardless of the development of new fire retardant, sulphur concrete cannot be considered stable in a fire. In addition, Malhotra (1979) mentioned that sulphur combustion is self-sustained and that once ignited, sulphur will continue to burn until extinguished.

2.2.10 Recycling

One attractive feature of sulphur concrete has been that, if necessary, it can be melted to recover the sulphur and aggregates, so that the recycled materials can be used again for concrete (Malhotra, 1979). Limited data by Lee et al. (1978) showed that the strength properties of concrete made with recycled sulphur were comparable to the original strength values.

2.3   Environmental and Safety Aspects in the Use of Sulphur

The material presented in this section was condensed from the works of Saylak et al. (1981) and Deuel and Saylak (1981). Their studies were sponsored by the Federal Highway Association (FHWA) and performed in the Texas Transportation Institute (TTI). The first part of these studies dealt with the pollution from the mix preparation and construction (Saylak et al., 1981). The second part investigated those aspects related to post-construction exposures to the elements, and to the problems that can occur while the pavement is in use (Deuel and Saylak, 1981).

2.3.1   Use of Sulphur in Construction

One of the major concerns with the use of sulphur in construction applications has been the generation of toxic gases (such as the Hydrogen Sulphide (H_2S) and Sulphur

24

Dioxide (SO₂)) and the sulphur itself. Saylak et al. (1980) concluded that as long as the temperature of the mix is maintained below 300°F (149°C), the concentrations of the H_2S, SO_2, and sulphur remained below the maximum allowable concentrations (MAC) suggested by the American Conference of Governmental Industrial Hygienists (ACGIH). Many other organisations have sponsored research on this topic, such as the Sulphur Institute (Izatt, 1977), Gulf (Kennepohl et al., 1975), Shell (Deme, 1974), and SUDIC (Rennie, 1978). These researchers supported the previous conclusions by Saylak et al. (1980). The above conclusion did not apply when the mixtures containing sulphur were processed or stored for prolonged periods of time in closed environments such as silos and hoppers.

2.3.2 Toxicity of Sulphur Initiated Pollutants

2.3.2.1 Hydrogen Sulphide (H₂S)

Hydrogen Sulphide is known for its characteristic odour of "rotten eggs" and is noticeable at low concentrations of about 0.02 ppm. However, the odour is not a good indicator because H_2S paralyses the sense of smell; therefore, higher concentrations cannot be noticed. During the TTI research project, the toxicity of H_2S was based on the relationships between its concentration and the effects on humans, as specified by the ACGIH. Those concentrations and their effects are given in Table 2.5.

H₂S Concentration (ppm)	Effect
0.02	Odour Threshold
0.10	Eye Irritation
5-10	Suggested MAC for prolonged exposure
70-150	Slight symptoms after exposure of several hours
170-300	Maximum concentration which can be inhaled for one hour without serious consequences
400-700	Dangerous after exposures for 30 to 60 minutes.
600	Fatal with 30 minutes exposure.

Table 2.5 – Effects of H₂S on Humans, taken from Saylat et al. (1981)

On the basis of these, effects a MAC value of 5 ppm is normally specified as the upper

threshold limit for continuous exposure to H_2S emissions in areas expected to be

normally occupied by construction or plant personnel.

2.3.2.2 Sulphur Dioxide (SO_2)

Sulphur Dioxide is a colourless gas with an odour, and which, unlike the H_2S, gives

ample warning of its presence. The National Institute for Occupational Safety and Health

and the Manufacturing Chemists Association provided the relationships between its

concentrations and its effects on humans (Table 2.6).

SO_2 Concentrations (ppm)	Effect
0.3-1	Detected by taste
3	Noticeable odour
5	MAC (ACGIH)
6-12	Immediate irritation of nose and throat
20	Irritation of eyes
50-100	MAC for 30 to 60 minutes exposures
400-500	Immediately dangerous to life

Table 2.6 Effect of SO_2 on Humans (Saylat et al., 1981)

A concentration of 5 ppm is the MAC specified as the upper threshold limit for SO_2

emissions in areas expected to be normally occupied by construction or plant personnel.

26

2.3.2.3 Sulphur

Vapours emitted during the mixing and dumping operations contain undissolved and unreacted sulphur. As the vapours come in contact with air and cool, the sulphur crystallises into small particles that are carried by the wind. Since no practical way exists to eliminate this pollutant; its effect on both the environment and personnel must be considered.

Saylat et al. (1981) pointed out that the principal problem related to sulphur dust is the irritation of the eyes after contact. Sulphur is capable of irritating the inner surfaces of the eyelids. Sulphur is virtually non-toxic, and no evidence has been found that systematic poisoning results from the inhalation of sulphur dust. Also, sulphur dust rarely irritates the skin. The primary hazard in handling solid sulphur results from the fact that sulphur dust suspended in the air may be ignited. This problem is almost always limited to enclosures and unventilated areas such as storage silos and hoppers (Saylat et al., 1981).

2.3.3 Post-Construction Exposure

During the second part of the study performed by the TTI (Deuel and Saylak, 1981), selective sulphur asphalt and sulphur concrete paving mixtures were subjected to a variety of simulated in-service weathering traffic conditions including hot temperatures, actinic light (Ultra-Violet radiation), rainfall, freeze-thaw, biological activity, chemical spills, and fires. Pollutants in the form of dust, fumes, and run-off products were collected and analysed for their safety-and-environmental-impact assessment.

2.3.3.1 Weathering Studies

The combined effects of temperature, actinic light, and rainfall on emissions and run-off products were achieved by exposing slabs of six selected mix designs of asphalt, sulphur-asphalt, and sulphur concrete to natural daily and seasonal weathering.

Their results showed that the discharge of H_2S and SO_2 from the sulphur concrete and sulphur concrete modified with dicyclopentadiene were approximately equal in magnitude to that of the lower sulphur-asphalt pavement material, although they contained more than 10 times the total sulphur than the sulphur-asphalt mixes. To put the magnitude of the flux values of H_2S and SO_2 in perspective, the maximum value of H_2S measured during the test was 955 $\mu g/m^2/hour$ (reported from the high sulphur-asphalt blend). This value corresponded to a concentration in the air of 2.6 ppm, which was half of the maximum allowable concentration recommended in section 2.3.2.1. Moreover, the maximum values measured for the sulphur concrete mix were 159 $\mu g/m^2/hour$ of H_2S and 201 $\mu g/m^2/hour$ of SO_2, and for the sulphur concrete modified with dicyclopentadiene were 164 $\mu g/m^2/hour$ of H_2S and 232 $\mu g/m^2/hour$ of SO_2. These values were well below the recommended maximum allowable concentrations.

2.3.3.2 Simulated in Service Conditions

- **Temperature, Actinic Light and Run-off Effects**

Compacted specimens of sulphur-asphalt, asphalt, and sulphur concrete were exposed to actinic light and temperature. After 6 months of exposure, the outer edges were chipped away, then ground in a ore crusher for subsequent total sulphur analysis. The most relevant results were that UV radiations from full sunlight did not affect the total sulphur measured and that the conservation of sulphur suggested no losses from a rainfall run-off mechanism.

- **Freeze-Thaw**

Compacted specimens of sulphur-asphalt, asphalt, and sulphur concrete were subjected to the weathering impact of freeze-thaw cycling as indicated in the ASTM C-666. Following the final thaw, the water used as the surrounding matrix was filtered and extracted. Analyses of this water showed contents of organic leachate ; however, further analysis demonstrated that these leachates were not constituents of the samples and also did not contain sulphur.

Chips were taken from the beam samples for total sulphur analyses suggesting no loss of sulphur from the sample following the multiple freeze-thaw weathering sequence.

- **Chemical Weathering**

Deuel and Saylak (1981) analysed for hydrolysates by using gas chromatographic techniques. This analysis revealed that organic material was not solubilised by hydrolysis reaction in either pH2 or pH10 water at a reaction temperature equivalent to the maximum surface temperature. Many more acidic or basic reactions at the pavement surface were required to induce chemical hydrolysis of sulphur asphalt pavements. The total sulphur lost as H_2S was small in magnitude, suggesting that hydrolysis reactions would at best be significant in the weathering of sulphur-asphalt pavements over a long term. Deuel and Saylak (1981) also concluded that the chemical oxidation of sulphur was an exceedingly slow reaction at ambient temperatures in the natural environment.

- **Biological Weathering**

The mentioned mixes were ground to pass through a 1 mm mesh sieve, and 10 grams of samples were incorporated into 100 grams of fresh soil matrix to determine the

potential biological degradation. The data suggested that the sulphur tended to increase the biological activity of the soil. A mechanism of weathering was not reported for the sulphur concrete mixes. The study also revealed that no significant levels of sulphur were lost from the specimens exposed to a natural weathering environment over a relatively short period of time. However, the results suggested that soil-borne microbes might be important in the long term.

- **Simulated Traffic Effects**

Deuel and Saylak (1981) studied the following degrading factors affecting the surface road: skiding, snow low friction, tire-pavement interaction, and exhaust fumes. With the exception of the exhaust fumes, the other three factors produced dust from erosion or friction. This dust could be transported by wind or rain to adjacent stream and ground surfaces. Sulphur was detected in the dust generated during the test; however, it was believed that the test exaggerated the mechanism of degradation.

- **Simulated Fire Test**

Deuel and Saylak (1981) showed that putting compacted specimens of asphalt-sulphur and sulphur concrete mixes in direct contact with a natural gas flame resulted in significant sulphur losses as H_2S and SO_2. Compared with the sulphur losses (in the form of SO_2) of the asphalt sulphur mixes, those of the concrete mixes were extremely high. The SO_2 emissions of sulphur concrete and sulphur concrete modified with DCPD were 2800 and 3400 ppm, respectively compared with the highest asphalt-sulphur emissions of 750 ppm. However, the H_2S emissions of the sulphur concrete mix was nil, and the emissions of mix modified with DCPD was 25 ppm, comparable with the lowers emissions from the asphalt-sulphur mix. Another important issue was that only the DCPD-modified sulphur concrete remained on fire once the burner flame was removed.

30

2.4   Batching, Transporting, Placing and Finishing of Sulphur Concrete

The ACI 548 (1988) guideline provides recommendations for batching, transporting, placing and finishing sulphur concrete. The minimum and maximum temperatures of a sulphur concrete mixture are controlled because: 1) the sulphur cement melts at 119°C and 2) above 149°C, the viscosity of sulphur cement rapidly increases to an unworkable consistency. For these reasons, 132°C to 141°C has been found to be an optimum temperature range to allow time for transportation, placement, and finishing of the sulphur concrete before solidification. The ACI 548 (1988) indicated that the keys to successful placing and finishing of sulphur concrete are: 1) having the sulphur concrete mass heated from 132° to 141°C at the moment of the placement; and 2) speed in placing and finishing. Furthermore, the ACI 548 (1988) guidelines also added that sulphur concrete should be worked in as large a mass as possible to maintain heat. The maximum dimensions for slabs are normally limited by the ability of the finishing crew to finish the concrete while it is sufficiently hot.

The ACI 548 (1988) pointed out that if the sulphur concrete has a stiff, dry appearance when is heated above 149°C, additional sulphur cement should not be added. When this happens, the temperature should be checked to determine whether the mixture is too hot. If it is, the mixture temperature should be quickly reduced below 149°C. If the right amount of sulphur cement was originally added, the sulphur concrete will return to more fluid and workable consistency.

In wall construction, the ACI 548 (1988) indicated that preheating the reinforced steel and forms using infrared of other suitable heaters is usually necessary to preclude poor consolidation due to flash-setting of sulphur concrete. Insulation will provide additional

31

time at working temperatures to assure adequate consolidation of successive lifts, resulting in a monolithic wall. The ACI 548 (1988) pointed out that internal vibration (light) maybe used to ensure consolidation; however, excessive vibration can result in segregation. External vibration has been used effectively for consolidation.

2.5   Cement-Stabilized Soil Retaining Walls

Morris and Crockford (1990) provided a review of cement stabilized soil retaining walls. They remarked that the stabilized backfill itself essentially forms the retaining wall. If the strength of the stabilized soil is sufficiently improved by the addition of cement, then the stability analysis is straightforward, and the stabilized cross section can be considered a monolithic structure. Consequently, the structure becomes a conventional mass gravity structure, and the overall stability is provided by the self-weight of the stabilized soil.

The finite element analysis performed by Morris and Crockford (1990) showed that the system will perform satisfactorily under typical field conditions to a height well in excess of those normally required for highway construction (typically 10 m to 20 m). However, because of the stress concentrations and the brittle nature of the materials, a factor of safety of at least 3 (preferably 5) against the crushing of the stabilized fill is recommended, as defined as

$$F_s = \frac{f_c}{\gamma H} \ ,$$
(2.1)

where f_c is the unconfined compression strength of the fill, H is the wall height, and γ the unit weight of the stabilized soil.

2.6 Summary

Sulphur concrete is a thermoplastic material prepared by hot-mixing sulphur cement, coarse aggregate and fine aggregates. This material solidifies and gains strength rapidly after cooling. The characteristics of this construction material are:

1. *Strength Development:-* Sulphur concrete develops about 70% of its ultimate compressive strength within a few hours after cooling, and usually 75% to 85% after 24 hours at 20°C (MacBee et al., 1983). It reaches its ultimate strength after 180 days and Johnston (1979) emphasised that there is no evidence of strength retrogression once achieved.

2. *Stress-Strain relationship:-* Unmodified sulphur concrete has a linear stress-strain curve up to failure (Czarnecki and Gillot, 1989). Moreover, Shrive et al. (1977) and Loov (1974) reported that sulphur, sulphur mortars and sulphur concrete are extremely brittle materials, far more so than Portland cement mortars and concretes.

3. *Fatigue Behaviour:-* Lee et al. (1978) concluded that all the sulphur concrete mixes, in their research, presented a better fatigue behaviour than Portland cement concrete.

4. *Creep:-* Loov (1974) and Malhotra (1979) indicated that sulphur concrete exhibited considerably more creep than Portland cement concrete (Figure 2.3).

5. *Freeze-Thaw Durability:-* Sulphur concretes subjected to freeze-thaw cycles have poor durability (Beaudoin and Sereda, 1974; Malhotra, 1975; Loov, 1975; Sullivan and McBee, 1976). Duecker (1934) suggested that since sulphur has a low thermal conductivity, large internal temperature gradients develop when the ambient temperature changes a few degrees, and couple with the unusually high coefficient of thermal expansion of sulphur induced high thermal stresses responsible for the development of fissures and fractures within the sulphur concrete materials. Cohen (1987) pointed out that water does not have any significant role in the mechanism suggested by Duecker (1934). Cohen (1978) also pointed out the fact that sulphur

33

concrete mortars bars failed the ASTM C 666, when at the same time cube samples of the same material showed satisfactory compressive strength. Therefore, Cohen (1978) concluded that the ASTM C 666 test cannot be used effectively to evaluate durability of sulphur concrete.

6. *The Effect of Water under Constant Temperature:-* Results of investigations indicated that sulphur concrete made with good quality aggregates may show poor durability in the presence of water (Gillot et al., 1993; Czarnecki and Gillot, 1989 and 1990). Abdel-Jawad and Al-Qudah (1994) indicated that the sulphur concrete specimens cured by being immersed in water showed that most of the strength reduction took place after the first three days, and that afterward the strength remained practically unchanged.

7. *Corrosion Resistance:-* Sullivan and McBee (1978) showed that concretes prepared with silica aggregates and modified sulphur cement were superior to those made with unmodified sulphur.

8. *Resistance to Biological Attack:-* Sulphur concretes are susceptible to attack by bacteria, primarily thiobacillus thiooxidans (Loov, 1974; Malhotra, 1979). The attack of this bacteria would be more severe in soils in countries with hot climate (Einer, 1960).

9. *Resistance to Fire:-* Malhotra (1979) indicated that the use of sulphur concrete is limited to conditions in which temperatures are no more than 80°C.

10. *Recycling:-* Limited data by Lee et al. (1978) showed that the strength properties of concrete made with recycle sulphur were comparable to the original strength values.

The effect of sulphur in the human health and environment was addressed in Section 2.1.4. Saylak et al. (1980) concluded that as long as the temperature of the mix is maintained below 300°F (149°C), the concentrations of the H_2S, SO_2, and sulphur

remained below the maximum allowable concentrations (MAC) suggested by the American Conference of Governmental Industrial Hygienists (ACGIH).

Deuel and Saylak (1981) carried out a post-construction study to evaluate the impact of the sulphur pollutants in the environment, and was concluded that exposure to weathering and in-service conditions had a negligible effect on the sulphur concrete materials. Run-off, either by wind or rain, produced little or no effect in the immediate environment.

ACI 548 (1988) indicated that between 132°C and 141°C has been found to be an optimum temperature range to allow time for transportation, placement and finishing of the sulphur concrete before solidification. Specifically in wall construction, the ACI 548 (1988) indicated that preheating of reinforced steel and forms is usually necessary to preclude poor consolidation due to flash setting of sulphur concrete. Moreover, insulation will provide additional time at working temperatures to assure adequate consolidation of successive lifts, resulting in a monolithic wall.

A sulphur concrete wall such as the proposed in this thesis has not been constructed yet. However, Morris and Crockford (1990) reported a similar retaining structure but using Portland cement to stabilise in-situ soils. They indicated that the wall can be considered a monolithic structure and recommended a factor of safety of at least 3 (preferably 5) against the crushing of the stabilised fill (see equation 2.1).

3   LABORATORY TESTS

The construction of a 15-metre-high retaining wall using sulphur concrete requires knowledge of the strength properties and deformation characteristics of this material. To fully characterise the sulphur concrete-behaviour, forty-two compression tests were performed in order to measure the peak compressive strength, yield compressive strength, Young's modulus, and Poisson's ratio of the six different mixes under study; moreover, the stress-strain curve of these mixes were also obtained. The tensile strength was also measured using twelve splitting tensile tests. The materials selected to prepare the mixes presented in this thesis were sulphur, tailing sand, and fly ash. Three mixes contained all three materials, but the other three did not include the fly ash. Its effect on the stress-strain curve and strength will also be discussed.

The resistance of sulphur concrete to freeze-thaw cycles is most important to its application in northern locations. The parameters measured to evaluate the freeze-thaw durability differed from those recommended in the standards for Portland cement concrete; however, they were consistent with the observations found in the literature review (Chapter 2). A sulphur concrete mix was selected based on the results from the resistance to the rapid freezing and thawing tests used in this study. The strength properties and elastic parameters of this mix are established.

3.1   Materials and Proportions

Environment Canada (1984) give three main sources of sulphur. The primary source of elemental sulphur is from sour natural gas (containing hydrogen sulphide), with smaller amounts from sour petroleum. Other sources include sulphuric acid and sulphur dioxide recovered from smelter gases, and sulphuric acid from pyrites concentrates, and

minor amounts from direct mining operations. Moreover, Meyer (1977) pointed out that one way to produce sulphur is from the extraction of ores mined primary for lead, zinc, and copper. Particularly in Alberta, sulphur is recovered from hydrocarbons as a by-product of the oil and gas industry. Near Fort McMurray waste sulphur is a by-product of the oil sands bitumen extraction and upgrading process. Environment Canada (1984) remarked that Alberta accounts for 90 percent of the total production of sulphur in Canada, with the various oil-industry facilities distributed throughout the province.

The oil sands extraction process also produces other waste materials such as tailing sand and fly ash. After the oil is extracted from the oil sands ore, the sand is disposed of in the tailing dams, giving it the name of "tailing sands". The fly ash is a waste product from power plants as a result of burning coke a byproduct of the bitumen upgrading process. These two materials were selected as potential aggregates to produce the sulphur concrete materials under study because of their availability at a typical oil sands extraction facility.

3.1.1 Sulphur

The sulphur used in the laboratory to produce the specimens for testing was 99.5% pure elemental sulphur manufactured by Bulldog Bag from Richmond, British Columbia, and distributed by Tigger Industries Inc. from Calgary, Alberta.

3.1.2 Tailing Sand

The tailing sand was transported from the tailing dams located at the Suncor Energy Mine in sealed barrels to the University of Alberta. A wash-sieve analysis was performed at the University of Alberta, and the results are presented in Figure 3.1. The author classified this material as "SP" under the Unified Soil Classification System.

37

Suncor Tailing Sand
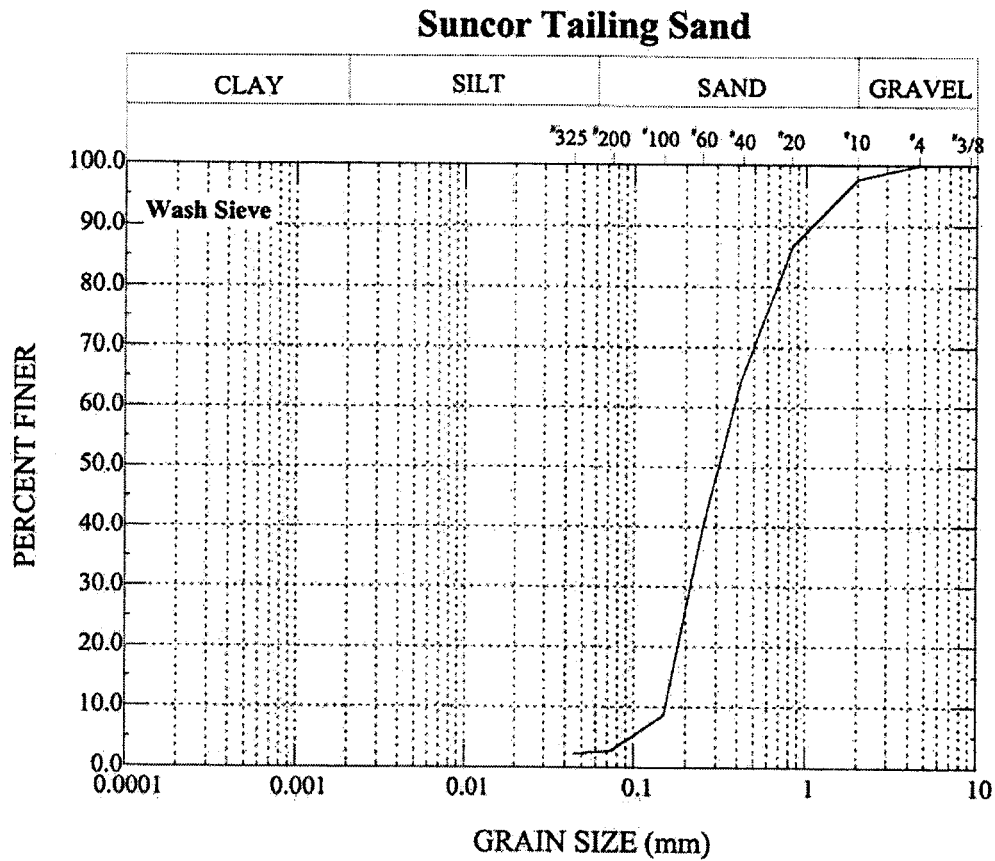
Figure 3.1 Suncor tailing sand grain size curve

3.1.3   Fly Ash

The fly ash is a waste material from the Power Plant at the Suncor site in Fort McMurray, Alberta.   The fly ash can be described as a fine dark-grey powder with similar appearance to Portland cement.

3.1.4   Sulphur and Aggregates Proportions

The mixes were prepared in six different proportions by weight by using sulphur, fly ash and tailing sand and the proportions are presented in Table 3.1. Also, in this table, are

abbreviations to designate each mix. These abbreviations are used throughout this thesis when discussing the results.

Percentage by weight			Consistency	Key
Sulphur	Fly Ash	Tailing Sand		
10%	-	90%	mortar	10Su90Sa
15%	-	85%	mortar	15Su85Sa
30%	-	70%	fluid	30Su70Sa
10%	2%	88%	mortar	10Su2FA
15%	3%	82%	mortar	15Su3FA
25%	5%	70%	fluid	25Su5FA

Table 3.1 Sulphur and aggregates proportions

3.2 Sample Preparation

The preparation of sulphur concrete specimens of any mix requires the sulphur to be molten in order for it to mix with the aggregates; furthermore, the aggregates also need to be heated to prevent the sulphur from quickly solidifying when it is in contact with the aggregates during the mixing process. Two mixing process have been used; 1) the open hot mix and 2) the dry post-heating mix.

The open hot mix process requires the sulphur to be molten and the aggregates to be heated before mixing. This process produces toxic gases like Hydrogen Sulphide (H_2S) and Sulphur Dioxide (SO_2). However, as was mentioned in Section 2.3.1, as long as the temperature of the mix is maintained below 149°C, the concentrations of these gases remain below the Maximum Allowable Concentrations (Saylak et al., 1981).

39

In the dry mix post-heating process, the granular sulphur and the aggregates are mixed before heating, and then enough heat is applied for the sulphur to melt. The mixing process could be performed at room temperature, and the temperature raised in a sealed container controlling the emission of gases, but even then, avoiding some exposure to the fumes is difficult.

Because of the simplicity of the equipment required, the open hot mix process was selected to produce the specimens in the laboratory. A sealed rubber mask and goggles were worn at all time during the preparation process, and the specimens were prepared using a fume hood to vent all gases emissions.

3.2.1 Procedure for Sample Preparation

The ACI 548 (1988) requires that sulphur concrete samples be cast in steel molds from materials raised to between 132°C and 141°C. The molds should be pre-heated to approximately 138°C before adding the mixture. This specification requires compacting the sulphur concrete, as it is added to the mold by tamping with a heated 16-mm hemispherical tipped rod . The samples are cast in an upright position and allowed to cool to room temperature before being removed from the molds. This procedure was followed during the preparation and casting of all samples reported in this thesis. This procedure also complies with the requirements of the standard procedure described by ASTM C 1312.

The steel molds were approximately 76-mm in diameter by 152-mm high. These dimensions were selected to facilitate the investigation of the stress-strain curve of the materials and determine the Young's modulus (ACI 548, 1988). Also, Malhotra (1978)

40

and the ACI 548 (1988) pointed out that small cylinders gained strength faster; thus, to investigate the compressive strength, this size was convenient.

Laboratory ovens were used to melt the sulphur and heat the aggregates to a temperature ranging from 135°C to 139°C. A heavy-duty commercial mixer with a metal bowl of 4-litre capacity was used to mix the heated aggregates and the molten sulphur. The sulphur was melted in the mixing bowl which was preheated to the same temperature. The mixing paddle, tamper, spoon, and trimming tool were also pre-heated at the same temperatures mentioned above. The aggregates and steel molds were heated in a different oven to temperatures between 145°C and 150°C. Figure 3.2 shows the mixer, bowl, paddle, tamper and trimming tool used to prepare the samples.
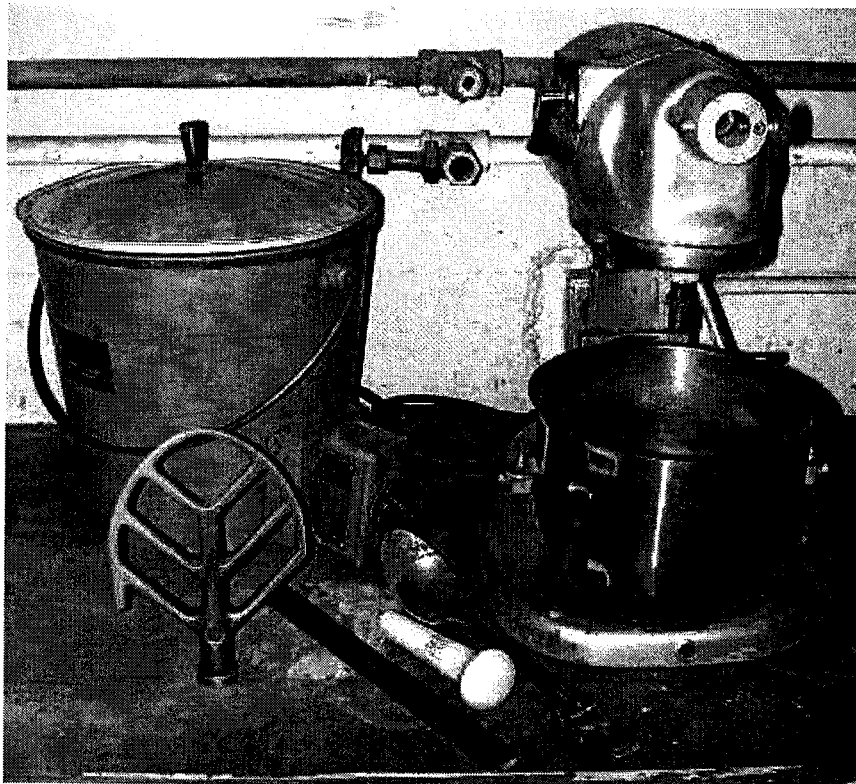
Figure 3.2 Tools used to prepare sulphur-concrete

Sulphur cement and aggregates were mixed until they formed a uniform mixture, usually obtained after 30 to 60 seconds of mixing at a medium velocity. Mixes with higher content of sulphur (25% or 30 %) become uniform faster. The mixtures with 25% and 30 % sulphur content turned into a viscous-fluid material like a cement mortar. The mixes with 10% and 15% sulphur content were similar to asphalt, requiring tamping for placement into the molds.

The 10% and 15% sulphur mixtures, after mixing and before casting into the steel molds, were poured into a heating pot while the temperature was maintained at approximately 135°C. A porcelain tamper, typically used to pulverise soil, was used to tamp the sulphur concrete into the steel molds. The sulphur concrete was compacted in 2 or 3 layers. After each tamping, this tool was returned to the oven to be heated for compaction of the next layer. The sample was tamped to a height above the top of the mold and trimmed with a preheated steel trimmer. Care was taken during trimming to maintain the compaction and provide a finished surface.

The 25% and 30% sulphur mixes did not require the use of the heating pot and were poured directly into the preheated steel molds. A gentle pressure was applied to one or two layers to prevent the formation of voids within the sample. Vibration was avoided to diminish the segregation ; however, some segregation of aggregate to the bottom of the mold was observed.

After being poured into the molds, the specimens were cured in air at room temperature (20°C) in the air. The molds were removed after the specimens cooled to room temperature.

3.2.2 Measurements of Specimens and Unit Weight

The diameter and height of each sample were measured at least 24 hours after casting by using a digital calliper. The diameter was measured on the top and bottom ends and in the middle. At each location, two measurements were taken at right angles to each other.

The weight of the samples was taken by using laboratory scales with a precision between 0.0001 and 0.00001 kg. A total of 148 samples were measured and weighed. The unit weights are calculated and presented in Table 3.2.

Type of Mix	10Su90Sa	10Su2FA	15Su85Sa	15Su3FA	25Su5FA	30Su70Sa
Statistical Value	(Unit Weight in kN/m^3)					
Mean	18.73	18.42	19.63	19.96	20.70	20.86
Standard Error	0.22	0.30	0.20	0.18	0.08	0.08
Median	18.76	18.25	19.82	20.26	20.66	20.90
Std.Deviation	1.10	1.42	0.98	0.97	0.40	0.38
Sample Variance	1.22	2.01	0.96	0.94	0.16	0.14
Range	4.21	4.94	3.09	3.36	1.45	1.44
Minimum	16.74	16.38	17.77	17.91	19.85	20.00
Maximum	20.95	21.32	20.86	21.27	21.31	21.45
Num. of samples	26	23	23	28	27	21

Table 3.2 - Unit weight statistics of the mixes used in this study

3.3 Compressive Strength, Young Modulus and Poisson's Ratio

Two types of compression tests were conducted. The first series of tests were uniaxial compression loading of the specimens to failure, measuring the load and axial displacement throughout the test. The unconfined compressive strength (peak strength), the Young modulus and the stress-strain curve were determined from these tests. The second series of tests were uniaxial compression loading up to 50% of the peak strength,

43

measuring the load, axial displacement, and the circumferential displacement. From the last series of tests, the Young's modulus and the Poisson's ratio were determined. All tests were performed in accordance with the recommended procedure given in ACI 548 (1988), ASTM C 39 and ASTM C 469. Details of the testing procedure are given in Appendix D. Figures 3.3 and 3.4 show the test set up for recording the axial deformation and the circumferential deformation, respectively. The sulphur-concrete samples were capped with sulphur mortar (ASTM C 617).
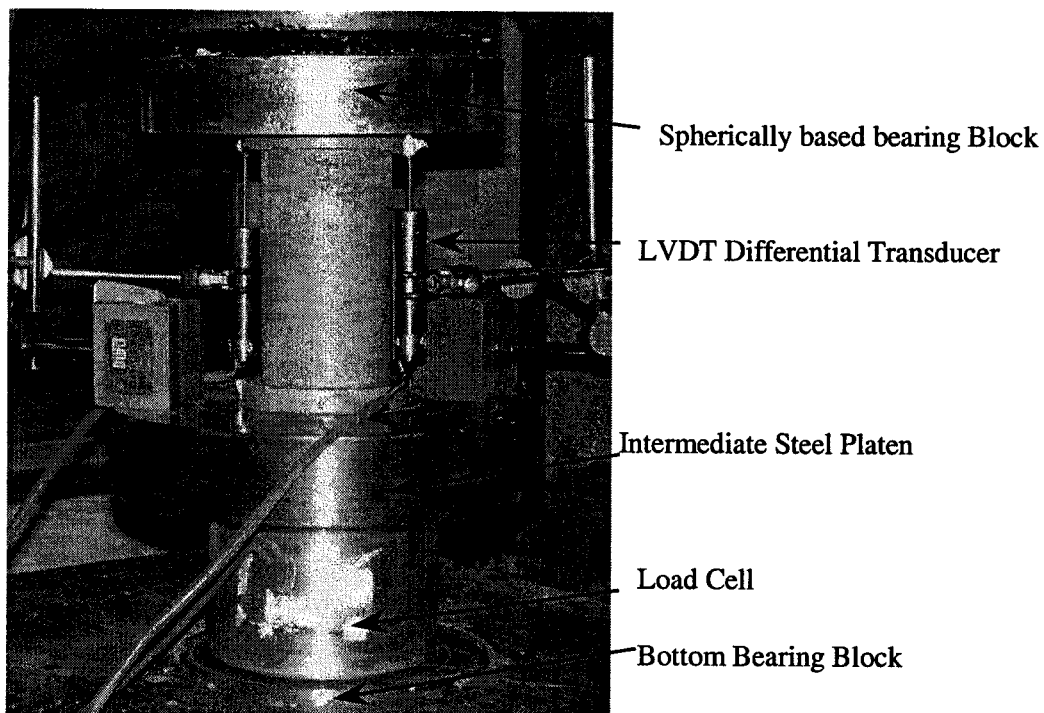
Figure 3.3 - Compression test set-up for 3-by-6-inch samples

3.3.1 Test Series I

Specimens representative of the mixes shown in Table 3.1 were tested to failure, and measurements of the axial deformations and loads recorded. Two compression-testing machines were used during this investigation. One compression machine was a load controlled hydraulic type, and the other a displacement-controlled screw type.

The hydraulic compression machine was a Baldwin manufactured by Southwark Tate-Emery Testing Machines, with a maximum capacity of 1,350 kN. The Baldwin testing machine had been calibrated recently prior to carrying out this series of tests. This compression machine provides two dial gauges, one for readings up to 220 kN and the other for up to 1,350 kN of applied load. Two-control valves are used in its operation, one for loading and another for unloading. It also has two steel-bearing blocks. The upper block was spherically seated and fixed. The bearing block at the bottom moved vertically, applying the compression load to the specimens.

The vertical displacement measurements in the Baldwin machine were the average of two displacement transducers located diametrically opposite approximately at the same distance from the specimen centre. These transducers were linear variable differential transformers (LVDT) with a built-in 24-volt DC excited carrier oscillator and phase-sensitive demodulator systems. The transducer's model was the 24DCDT-250 manufactured by Hewlett- Packard, with ±0.25-inch displacement range and proportioned with a scale factor of 28 Volt/inch. (1.1 Volt/mm) The full-scale output of these displacement transducers was 7 volts, with a maximum non-linearity of ±0.5% of the full scale. This type of transducer provides unlimited resolution, high accuracy and sensitivity. Figure 3.3 shows a picture of the LVDT's transducer set-up. An acrylic pipe was located between the sample and the LVDT's transducers as a protection measure but is not shown in Figure 3.3. Also in Figure 3.3, beneath the intermediate steel platten is a load cell used to measure the applied load at the same interval of time as the LVDT transducers are measured. The readings of the transducers and the load cell were recorded through a data logger with an interval of time between 3 and 5 seconds. The model of this data logger was the Data Dolphin DD-124 manufactured by Optimum Instruments, Inc. The reading precision of this device was about 1×10^{-7} Volts. The

maximum load applied to the samples was read from the machine dial gauge. The loading range was very low (between 75 and 150 kPa/sec approximately) about the half of the specified range to obtain accurate readings as failure was approached. The failures were always sudden and noisy, characteristic of failure of brittle materials, and sometimes were explosive. It was not possible to record a post-peak response for any of the test specimens.

The displacement controlled compression machine used was an Instron Universal Testing Instrument Model 4206. This testing machine was equipped with a built-in load cell with a maximum load capacity of 150kN. The axial deformation also was measured through a built-in mechanism in the testing machine itself. The loading rate was always set to 1 mm/min. These features enabled the tracking of the load and displacement up to the sample's failure and were very convenient for investigating the stress-strain behaviour. Unfortunately, the device measuring the axial deformation was found to be in error resulting in too large axial deformations as recorded. However, the stress-strain curve measured showed that this error occurred in a constant manner in each test; therefore a correction factor was determined and applied to establish the correct displacement for the individual test. After an examination by qualified technicians, it was concluded that the loads had been measured correctly throughout all tests.

3.3.2 Test Series II

For this test only, the hydraulic Baldwin compression apparatus was used. Two samples representative of each mix shown in Table 3.1 were prepared for this compression test. The samples were measured and weighed as explained in Section 3.2.2.

A similar arrangement to that presented in Figure 3.3 was utilised. The load cell and the LVDT differential transducers (measuring axial strains) were the same as those used during the tests presented in Section 3.3.1. To estimate the Poisson's ratio, the circumferential change was measured with a chain device placed around the specimens at midheight (Figure 3.4). This device was able to expand during loading of the specimens, and the circumferential change was measured by a LVDT differential transducer mounted horizontally in the chain device. Just one transducer was used to measure this deformation. The model of the LVDT differential transducer was the 24DCDT-100 with a full scale output of 9 volts; the displacement range was ±2.54 mm, the scale factor was 90Volt/in., and the full scale had a maximum non-linearity of ±0.5% . As the scale factor indicates, this transducer was 3 time more sensitive than the transducers used to measure the axial deformation.

The samples were capped, with sulphur mortar (ASTM C 617), before the chain device was assembled on them. To set the chain device and the transducer on the samples, they were unassembled completely. The chain was placed first by unscrewing it, wrapping it around the sample, and screwing it together. The transducer was then placed in the ring of the chain device and tightened. The final set-up of the instruments on the specimen is shown in Figure 3.4.

Each sample was loaded twice, and a data logger recorded the readings continually every 5 seconds. The data logger was the same as the one used in the previous test. The loading rates were approximately from 35 to 120 kPa/sec. These rates allowed several readings to be taken along each loading increment.
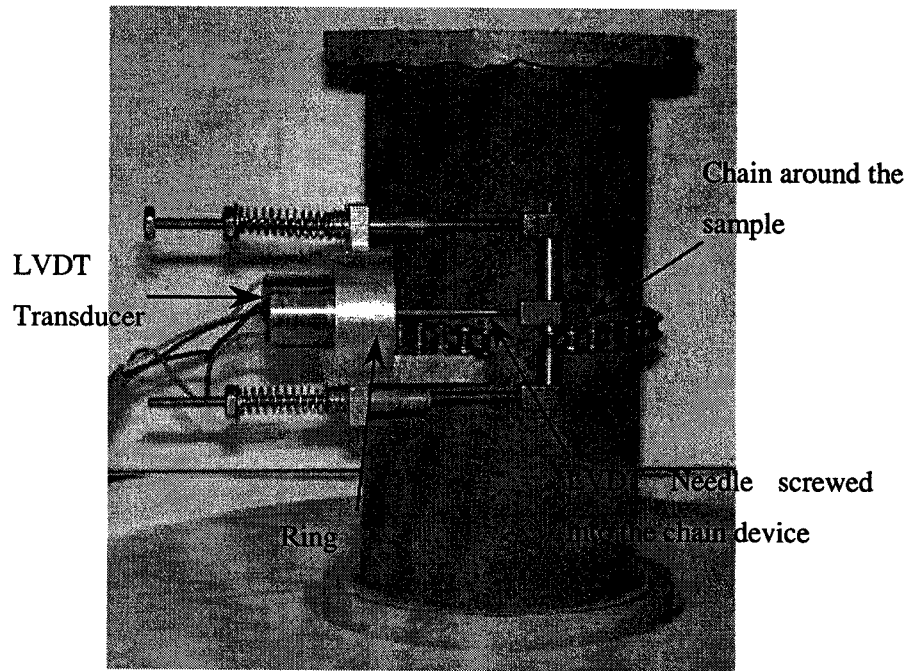
Figure 3.4 Chain device to measure circumferential strains

Furthermore, two samples of the 15Su3FA mix were tested using strain gauges instead of the chain device for comparison with and to verify the previous results. The strain gauges type was Micro Measurements CEA-06-250UT-350. These devices enable reading on both the axial and circumferential strains. Three strain gauges were placed around the mid height of the sample and were located approximately at 120° to each other. This time a data logger was not used; however, the loading rate was low permitting readings at approximately equal time intervals.

3.3.3   Results of Compression Tests

The results from the compression test are summarised in Figures 3.5 through 3.9. Figure 3.5 presents the typical stress-strain curves of the mixes prepared with sulphur and tailing sand only, and Figure 3.6 shows the stress-strain curves of the sulphur concrete

48

mixes prepared with sulphur, fly ash, and tailing sand. Appendix A presents the remaining stress-strain curves from this study.
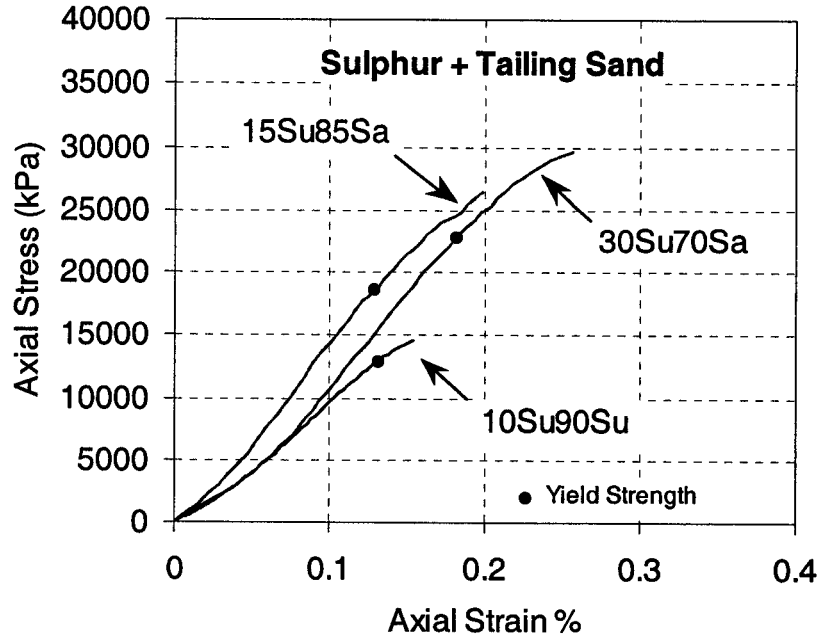
Figure 3.5 Stress-strain curve of the sulphur and tailing sand mixes
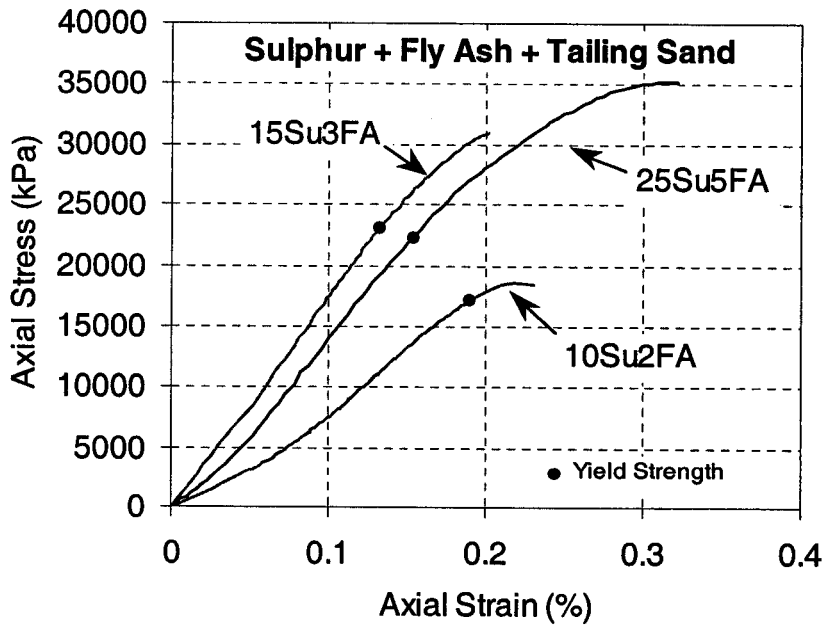
Figure 3.6 Stress-strain curve of the sulphur, fly ash, and tailing sand mixes

49

Figure 3.7 summarises the peak compressive strengths. The values in Figure 3.7 are the mean, maximum, minimum, standard error, standard deviation, and the number of samples tested. Figure 3.8 presents the same statistical data but for the Yield compressive strengths. Appendix A presents the peak and yield strengths of each test, and additional statistical information.

The Young's moduli were calculated from the compression tests and are summarised in Figure 3.9. Appendix A presents the Young's moduli calculated from all the tests.
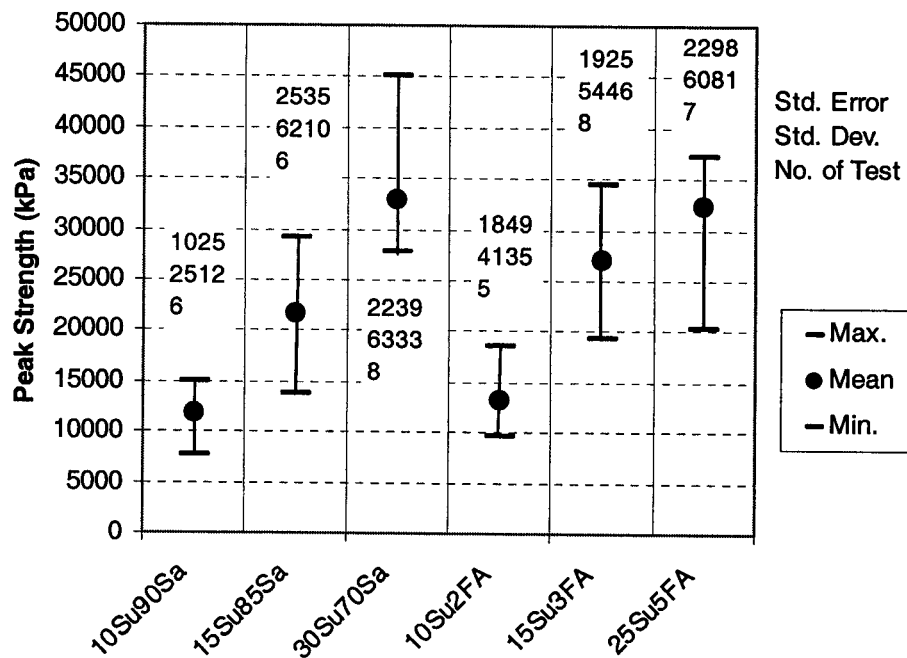
Figure 3.7 Peak strength summary
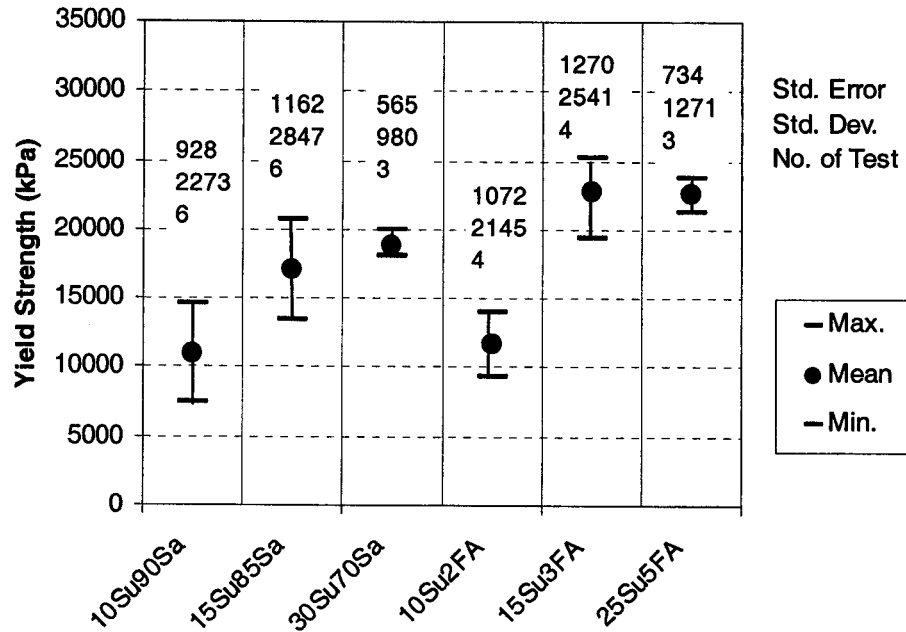
Figure 3.8 – Yield strength summary
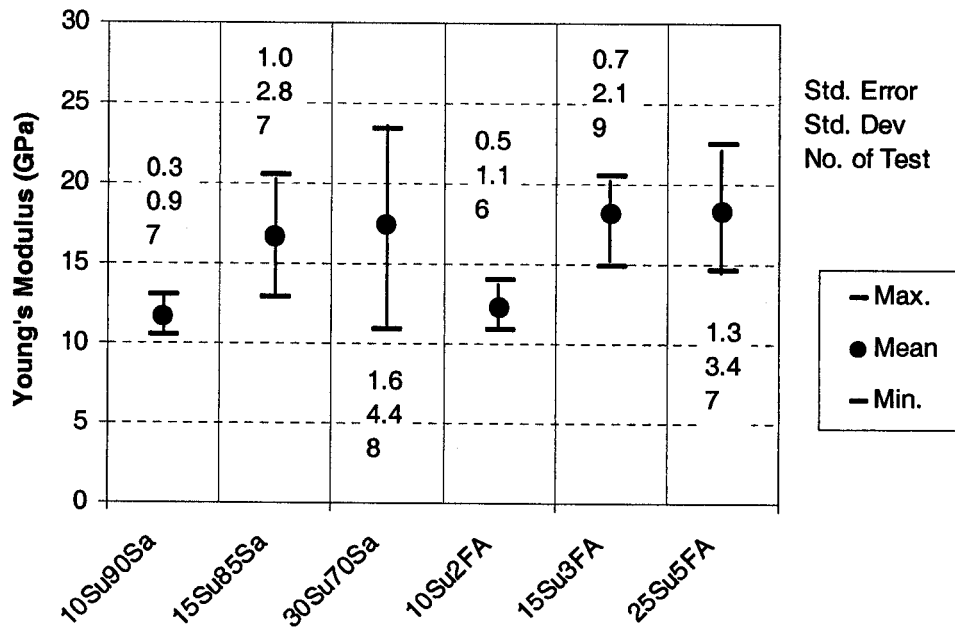
Figure 3.9 Young's modulus summary

51

The measurements of the Poisson's ratio were not successful using the chain device. Therefore, strain gauges were used on two 15Su3FA samples. The measured Poisson's ratios were 0.20 and 0.15 which are consisted with the value reported by R.M. Hardy & Associated in 1975, on similar sulphur-concrete.

3.4   Tensile Strength

The tensile strength of the sulphur concrete specimens was investigated by using the split cylinder tensile test, as recommended by the ACI 548 (1988), following the procedure outlined in ASTM C 496.

After the 76-mm by 152-mm specimens were prepared and cured in air at room temperature (two for each mix), they were marked so that the marked lines were on the same plane. In this case, two diametric lines at right angles were marked on both ends, and lines were drawn along the sides of the cylinder, as shown in Figure 3.10. The longitudinal lines were marked to locate two LVDT differential transducers in a perpendicular line to the loading plane, between cylinder ends.

The LVDT differential transducers were used to measure the maximum strain at the moment of failure by adding the measurement from each transducer. These transducers were the same as those used to measure the axial displacement during the compression test. The black bands located at the cylinder ends were electric plastic tapes to protect the transducer. After failure, the samples split apart pushing the transducer, so the electric tapes only kept the broken pieces together. This tape was wrapped loosely around the cylinders to prevent it having any effect during the test. The load was measured by using the same load cell for the compression tests (not shown in Figure 3.10); however, the

maximum load was taken from the readings of the Baldwin compression machine at the moment of failure.
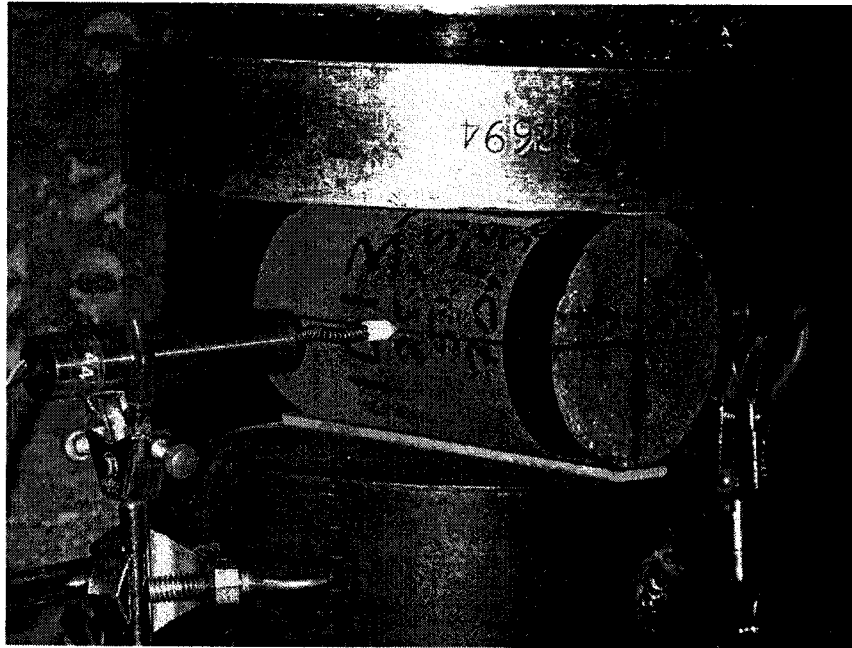
Figure 3.10 Splitting tensile test set-up

Two specimens of each sulphur concrete mix specified in Table 3.1 were tested. The results of all the split tensile tests are included in Appendix A, and the average splitting tensile strengths and the maximum measured strains are summarised in Table 3.3:

Mix Name	Avg. Splitting Tensile Strength (σ_t) (kPa)	Avg. Maximum Strain (%)	Avg. UCS (σ_c) (kPa)	Ratio of σ_t / σ_c
10Su90Sa	883	0.11	11718	0.07
15Su85Sa	1205	0.07	21671	0.05
30Su70Sa	1927	0.66	32860	0.06
10Su2FA	832	0.11	13159	0.06
15Su3FA	1189	0.06	27030	0.04
25Su5FA	2805	0.27	32251	0.08

Table 3.3 Splitting tensile strengths and maximum strains

3.5 Freeze-Thaw Durability Test

The durability of the sulphur concrete as a construction material is an important consideration. When unmodified sulphur cement is used to prepare the sulphur concrete, the freeze-thaw durability is paramount. The ACI 548 (1988) recommended evaluating the resistance to freeze-thaw cycles, as specified by the ASTM C 666, by using Procedure A, implying that the rapid freezing and thawing of the specimens must be in water. Furthermore, the dynamic modulus of elasticity must be determined in accordance with ASTM C 215.

Although the ASTM C 666 is recommended by the ACI 548, it was not followed rigorously. Using the literature review presented previously, one can argue that the dynamic modulus of elasticity did not accurately represent the degree of deterioration of the sulphur concrete during the rapid freezing and thawing test. Therefore, it was decided to perform a uniaxial compressive test thus measuring the static modulus of elasticity, the compressive peak strength, and the compressive yield strength in order to evaluate any freeze-thaw induced damage.

3.5.1 Rapid Freeze and Thaw Test Procedure

This test's objective was to evaluate the durability of the specimens subjected to rapid freeze-thaw cycles using the compression test instead of measuring the dynamic Young's modulus. From the compression test, the static Young's modulus, the peak compressive strength, and the yield compressive stress were determined. They were then compared to the behaviour before application of any freeze-thaw cycle. The samples used were cylinders 76-mm in diameter and 152-mm high, complying with the requirement to have aspect ratios of 2 for the compression test.

Because the compression test is a destructive test, the samples cannot continue to be used in the freeze-thaw cycles. Four groups of samples, two per each mix type, were prepared for this test, making a total of 48 samples. Originally, it was planned to test samples after 50, 100, 200 and 300 cycles. Each group started the freeze-thaw cycles after three days of curing in air at 20°C. Each group was made on a different day, one after the other; therefore, the different groups were in different cycles.

To measure the temperature, four samples were prepared by putting a thermo-electrical transducer into the specimens, at about the midheight. These devices were Omega's Precision Interchangeable Thermistors model 44007, with a resistance of 5,000 Ohms at 25°C. The Thermistors were manufactured from oxides of nickel, manganese, iron, cobalt, magnesium, titanium, and other metals. They provided precise temperature information, and their accuracy was ±0.2°C in a working range from −80 to 120°C. The temperature data of the four transducers were recorded using a data logger. The model of this data logger was the Data Dolphin DD-124 manufactured by Optimum Instruments, with the same specifications as those mentioned previously in the compression test. The temperatures of the rooms and the heat transfer media (water, glycol or air) were verified by using regular mercury thermometers. The freeze-thaw cycles were performed using a freezer and a cooler room. (The cylinders were moved from one room to the other.) At night, the specimens were frozen to −19°C, the normal temperature in the freezer room. The minimum temperature permitted was −19.4°C. The temperature of the cooler room was not easy to set up. After a week of trial and error, it was found that a temperature of 14°C was appropriate to warm the temperature as specified by the ASTM.

Procedure A of the ASTM C 666 required that the samples must be in water during the freezing and thawing periods. Stainless steel containers with an internal diameter of 83.2 mm were used, leaving a gap of approximately 3.5-mm around the cylinders. An O-

ring 2.5 mm thick and approximately 50 mm in diameter was used at the bottom to support the sample. The O-ring maintained a space between the container and the bottom of the sample. Furthermore, a twisted rubber band approximately 2-mm thick was placed around the top third of the specimens, ensuring that a gap was maintained between them and the container's wall.

For thawing, the steel containers were introduced randomly into plastic tubs of water, as is shown in Figure 3.11, and the samples took between 30 and 60 minutes to thaw, depending on the initial temperature of the water. Keeping the initial water temperature constant for each thawing period was difficult because the time the water required to recover its initial temperature after thawing was longer than the period of time that the samples were in the freezer; therefore, each thawing period was longer than its previous period. Heating and changing the water were required to correct the temperature to the optimum of 14°C. During the thawing period, the temperatures were monitored constantly to prevent the samples from reaching temperatures higher than the maximum permitted of 6.1°C.

Figure 3.11 Specimens in steel containers during the thawing period

Freezing the samples was less complicated. Initially, the samples were frozen as shown in Figure 3.11; however, instead of water, glycol was used to surround the metal containers. Its use involved many problems such as spilling and making the surface of the containers slippery. After two weeks, it was found that placing the containers with the specimens in just air at −19°C worked well. The time required to reach the specified temperature of −16.1°C was about the same as the time required when using glycol as a freezing medium. Therefore, the freezing medium was changed to air, and the cylinders were randomly placed in the freezer room in front of the cooling fans during every freezing period.

As mentioned previously, after the cycling, the samples were tested in compression to failure. Two events have to be mentioned prior to presenting the results. After 41 cycles an incident resulted in 8 broken samples, which were replaced with a new group to re-start the freeze-thaw cycling. However, for the first time, a construction joint was observed in the samples. Unfortunately, almost all the broken samples were part of the group scheduled to be tested after 50 cycles. The remaining samples apparently were in good conditions up to this point of the test.

The freeze-thaw cycling continued normally until cycle 88 when pop-out along a construction joint were discovered in many of the test samples. Figure 3.12 shows a construction joint formed during the compaction process when the hot mix was placed into the steel mold. The round shape of the tamper on both sides can be observed. This shape was found in the samples consisting of 10% and 15% sulphur. Although this shape did not appear in the specimens prepared using 30% and 25% sulphur, they also split apart.

57
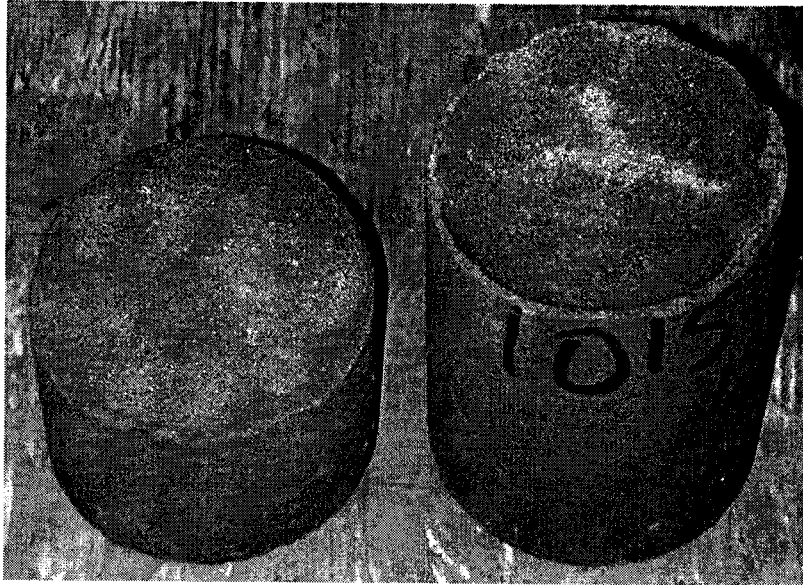
Figure 3.12 Construction joint in samples

Furthermore, after 88 cycles, the specimens of mixes with 10% sulphur content were found not only with pop-outs at the joint surface; they also presented a high degree of deterioration. They had split apart along more than 2 joints, and the material crumbled between ones fingers. Consequently, it was determined that these samples had failed to pass the freeze-thaw test.

After 100 cycles, the samples with 15%, 25%, and 30% sulphur content were taken for compression testing. At this point, two groups still remained with samples of 15%, 25%, and 30% sulphur content. The test continued until the groups reached 150 and 162 cycles, respectively. All the samples failed to pass the freeze-thaw durability test.

Figure 3.13 shows a specimen of 25Su5FA after 162 cycles, and Figure 3.14 shows a specimen of 15Su85Sa, which also failed after 162 cycles. These two figures show the condition of the samples consisting of 15%, 25% and 30% sulphur after failure.
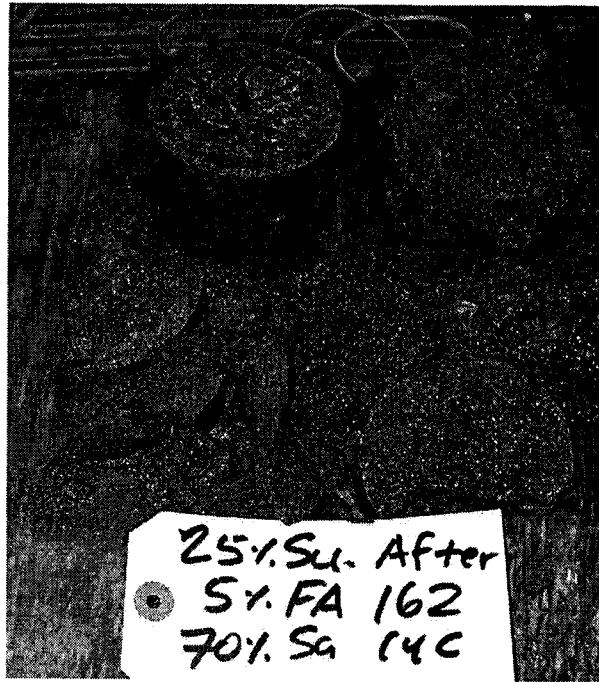
Figure 3.13 25Su5FA sample after failed the freeze-thaw durability test
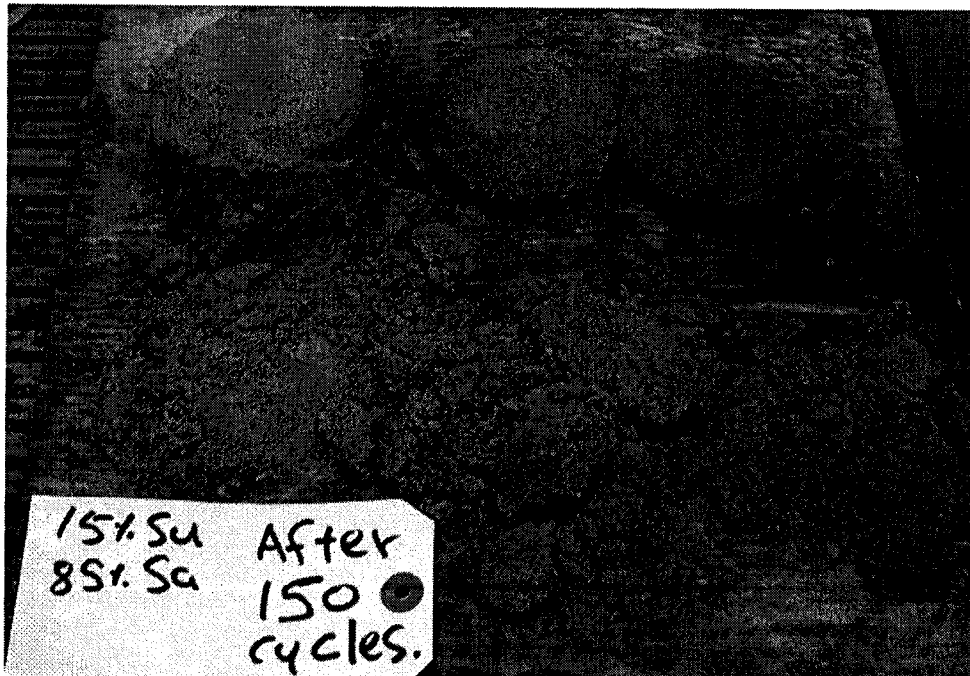
Figure 3.14 15Su85Sa sample failed to pass the freeze-thaw durability test

59

3.5.2 Results of the Rapid Freezing and Thawing Test

All the samples eventually failed to pass the rapid freezing and thawing test. This section presents the results of the Young's Modulus, peak compressive strength, and yield strength tests, which were performed before these failures occurred. In the 10Su90Sa and 10Su2FA mixes, the samples tested were made from pieces with aspect ratio of approximately one, defined as the ratio between the height and the diameter of the sample (h/d). These were sound pieces of samples that had already failed along the construction joints, like the bigger piece shows in Figure 3.14. The rest of the samples (15Su85Sa, 15Su3FA, 25Su5FA, and 30Su70Sa) were tested after 50 and 100 cycles. The mixes of 15Su3FA and 30Su70Sa were subjected to compression testing after 162 and 150 cycles, respectively; however, they had companion specimens of the same age that failed to pass the freeze-thaw durability test. The 15Su3FA specimen tested after 162 cycles had already deteriorated at the bottom, so the sample was trimmed to a shorten length to perform the test. .

Figures 3.15 and 3.16 present only the test results after 50 and 100 cycles, respectively, which are the results that can be used to evaluate the materials that could be used to build a sulphur concrete sizer wall. All the results are summarized and presented in Appendix A. Figure 3.15 presents the average peak compression strength, yield compression strength, and the Young's modulus results after 50 cycles. Figure 3.16 shows the same information after 100 cycles. Figures 3.17, 3.18 and 3.19 present the variation of the peak compressive strength, yield compressive strength, and Young's modulus with the number of freeze-thaw cycles. Results after 150 and 162 cycles were also included; however, this are not considered for design because specimens of the same age failed to reach the same number of cycles.

After 50 Freeze-Thaw Cycles
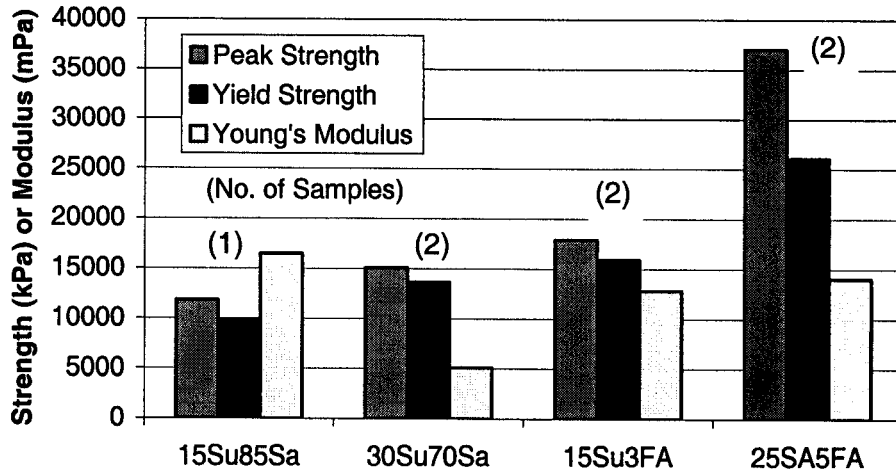
Figure 3.15 Average peak strength, yield strength, and Young's modulus after 50 cycles

After 100 Freeze-Thaw Cycles
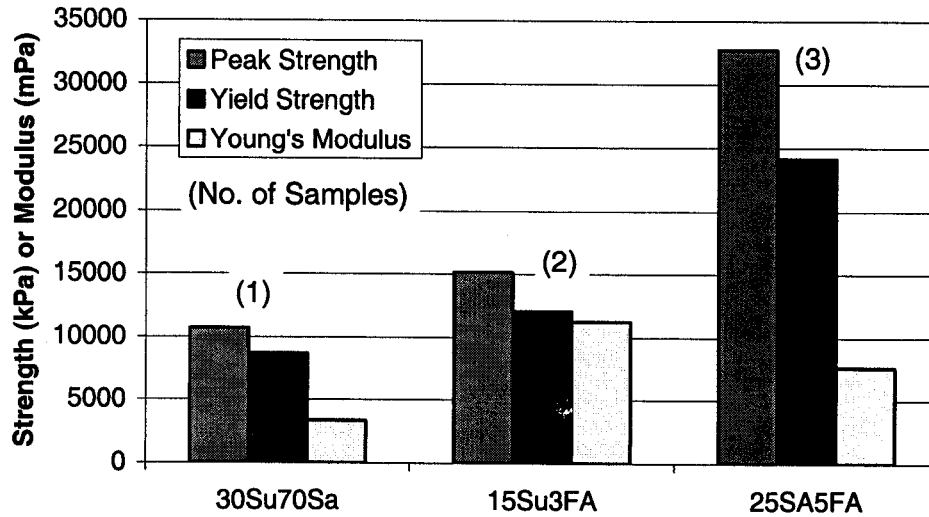
Figure 3.16 Average peak strength, yield strength, and Young's modulus after 100 cycles

σ_{cd} = Damaged Peak Strength

σ_{ci} = Initial Peak Strength
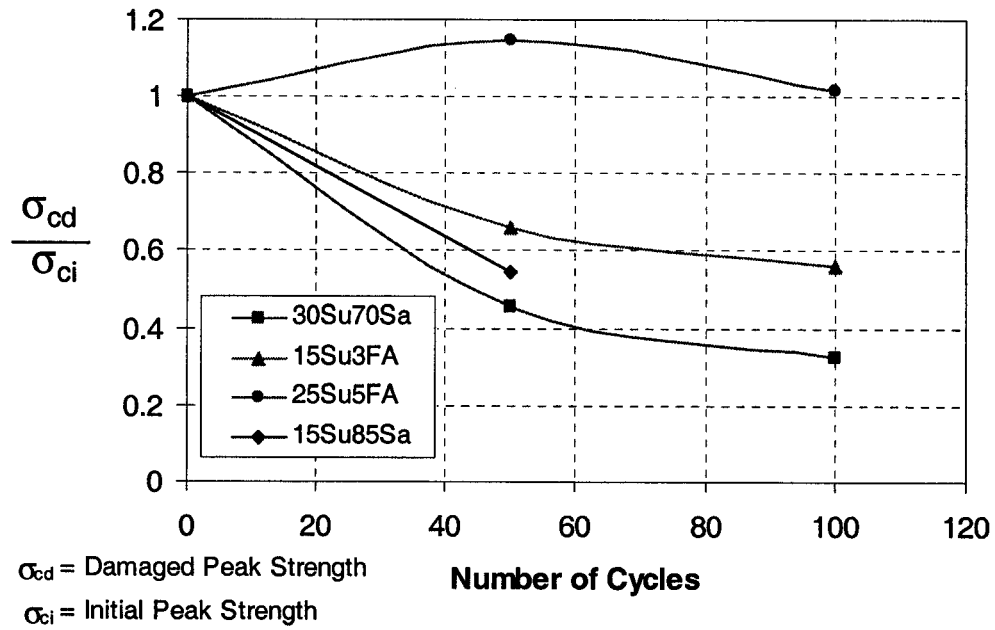
Figure 3.17 Variation of σ_{cd} / σ_{ci} with the number of freeze-thaw cycles

σ_{yd} = Damaged Yield Strength

σ_{yi} = Initial Yield Strength
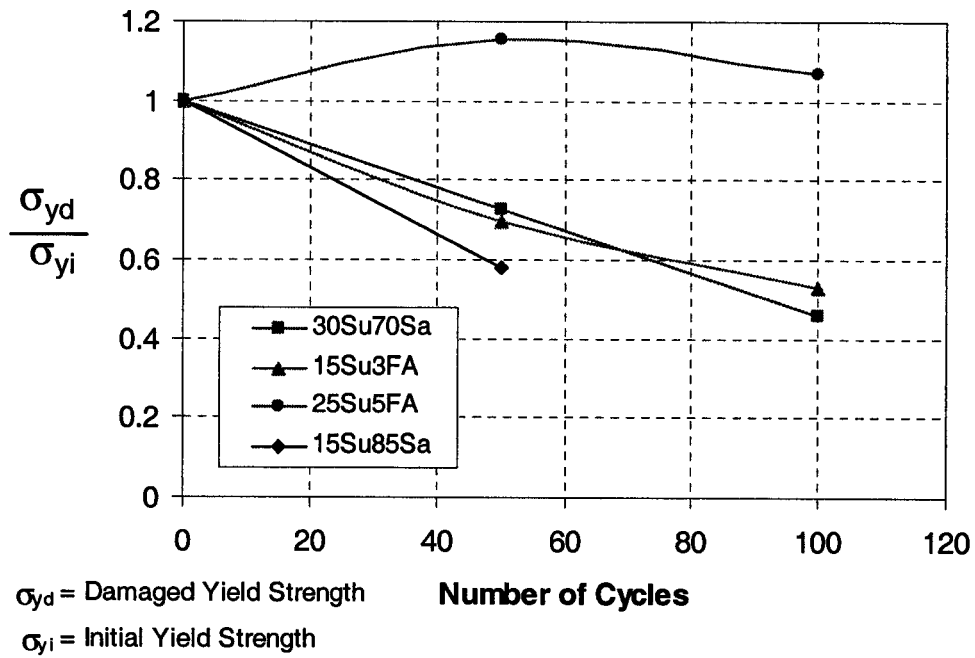
Figure 3.18 Variation of σ_{yd} / σ_{yi} with the number of freeze-thaw cycles

62

E_d = Damaged Young's Modulus
E_i = Initial Young's Modulus
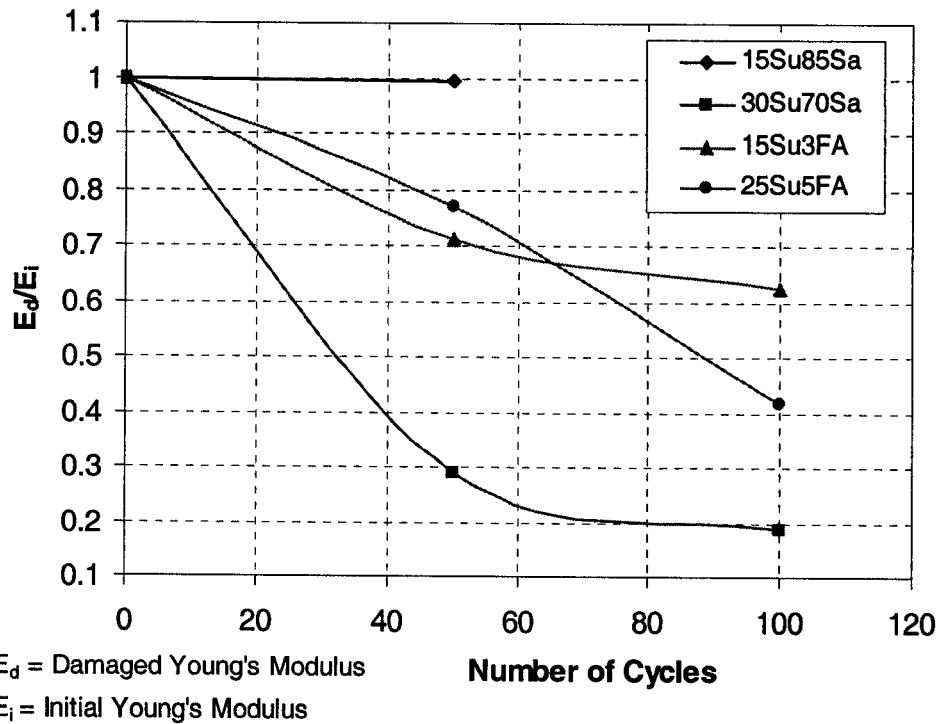
Figure 3.19 Variation of E_d / E_i with the number of freeze-thaw cycles

3.5.3 Correction of the Young's Modulus Measured in the Instron Compression Machine

Section 3.4.1.2 mentioned that the Instron compression machine produced errors in measuring the axial deformation. Unfortunately, some samples after the freeze-thaw cycles were tested using this machine before the technical problem was discovered. Therefore, a correction factor was required to correct the Young's modulus. Initially, the stress-strain curves of the 10% and 15% sulphur concrete mixes, before the freeze-thaw cycles, were determined by using the Instron machine; however, the measurements had to be carried out again using the Baldwin compression apparatus. The stress-strain curves measured by the Instron compression machine showed that the error was constant because these curves were reproduced more than two times for each mix. Therefore, a correction factor comparing the two initial Young's modulus results, in both machines, was obtained and applied to the Young's modulus measured from the Instron machine

63

after the freeze-thaw cycles. The loads measurements did not require correction; therefore, the peak and yield strengths were taken directly from the test data produced using in the Instron machine.

Table 3.4 shows the corrections applied to the samples of the 15Su3FA mix. In comparing the initial modulus (E_o) from the Instron compression machine, and the modulus measured after the freeze thaw cycles, a percentage referred to "the initial modulus" is presented. To estimate the corrected Young's modulus, this same percentage is applied to the initial modulus measured by the Baldwin compression machine. This table also reveals that the Young's modulus decreased as the number of cycles increased; thus, in the 15Su3FA mix after 100 freeze-thaw cycles, the modulus decreased to a value of 11,247 MPa representing 62% of the original measured modulus.

Appendix A presents the corrections of the modulus of elasticity, when required, and their ratio to the original Young's modulus values for all 6 mixes under study. The results shown in Figures 3.15 and 3.16 are corrected as required, and all the values presented are related to the modulus measured by the Baldwin compression machine.

Material: 15Su 3FA							
Description	No. of Cycles	E_{AVG} MPa	E_{MIN}	E_{MAX}	No. of Samples	% of E_o	E related to the Baldwin
Eo Baldwin		18065	12885	20496	7		16578
Eo Instron		1732	1406	2028	4		
E Instron	50	1340	967	1714	2	77	12826
E Instron	100	1078	923	1427	2	62	11247
E Baldwin	162	6231	N/A	N/A	1	38	6231

Table 3.4 Correction of the Young's modulus measured with the Instron compression machine

3.5.4 Correction Factor Applied to the Cylinders with a Length to Diameter Ratio of Approximately 1

Section 3.5.1 indicated that some cylinders split apart along a plane called "a construction joint," which was created during the casting of the samples into the steel heated molds. Figure 3.12 shows that these weakness planes were formed when the sulphur concrete was compacted into the molds. These weakness planes were not a problem during the compression test of the samples not subjected to freeze-thaw cycles, because the failure planes and these weakness planes were not coincident; therefore, the joint did not negatively impact the measured compressive strength and yield strength.

Pieces close to or greater than a length-to-diameter ratio (l/d) of 1 were selected to measure the strengths and the modulus, and a correction factor was applied to the measured peak compression strength to relate the measured data to samples with l/d of 2. Although the factors used were developed for the peak strength, they also were applied to the yield strength. Hudson et al. (1971) presented a series of stress-strain curves to show how the change in aspect ratio (l/d) affects the shape of the stress-strain curve itself; however, no effect was found along the elastic portion of the stress-strain curve. Thus, the Young's modulus did not have to be corrected because of the change in the length-to-diameter ratio of the sample being tested.

Bartlett and MacGregor (1994) presented a revision of the effect of the core length to diameter ratio (l/d) on the concrete strength. These authors mentioned that short specimens fail at greater loads because the steel platens of the testing machine restrain lateral expansion throughout the specimens more effectively; furthermore, they added that the end restraint is conventionally assumed to be negligible for specimens with a

length-to-diameter ratio of 2. The ASTM C 42 recommended correction factors for specimens with a l/d ratio of less than 1.8, and the same correction factors are included in the ASTM C 39. However, the strengths from this test program were corrected using the expressions developed by Bartlett and MacGregor (1994):

$$f'_{c,S} = \left[1 + \left(-0.144 + 0.027 Z_{mc} + 0.00044 f'_{c,NS}\right)\left(2 - \frac{l}{d}\right)^2\right] f'_{c,NS} \,, \qquad (3.6)$$

where $f'_{c,S}$ is the average strength of standard cores with l/d=2, $f'_{c,NS}$ is the average strength of companion cores with l/d ratios not equal to 2, and Z_{mc} indicates the moisture condition of the cores at the time of testing and equals 0 for air dried cores, 1 for soaked cores, or 0.5 for sealed cores. For the case under study, a value of Z_{mc} equal to 0.5 was selected.

Figure 3.20 presents the correction factors ($F_{l/d}$) found for the specimens tested and shows a linear trend with the increment in l/d ratio. $F_{l/d}$ is the term between the brackets in equation 3.6. There is 3 values enclosed by a circle out of this trend line; however, Bartlett and MacGregor (1994) concluded that the required strength correction is significantly reduced for high-strength concretes; consequently, as the concrete strength increases, correction factors closer to 1 are appropriate. For the sulphur concrete strengths of 33, 36, and 43 MPa the calculated correction factor were 0.96, 0.97, and 0.99 respectively. Also, Appendix A shows the correction factor for all the samples.
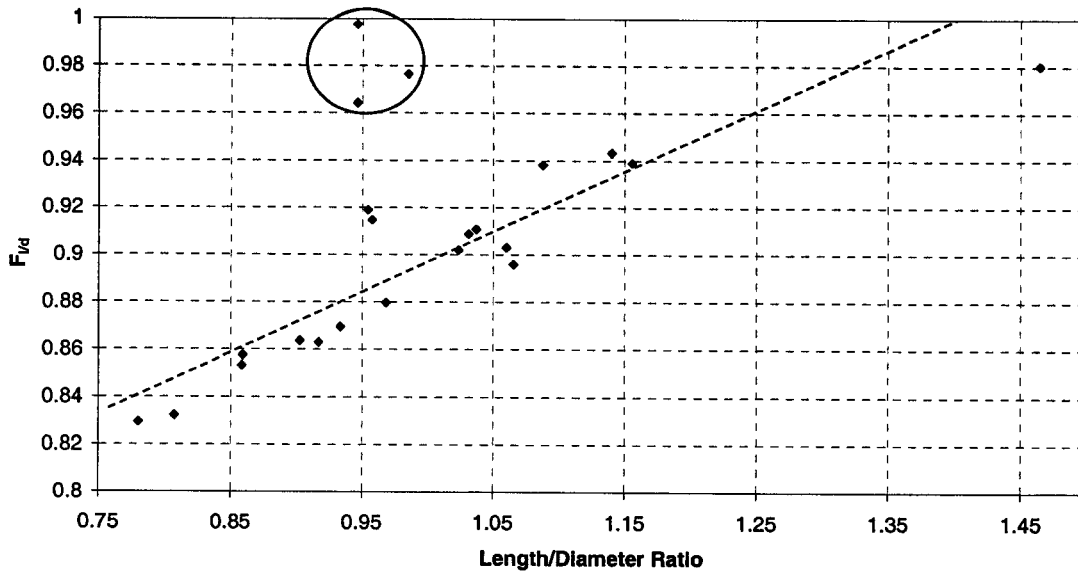
Figure 3.20 Correction factor ($F_{l/d}$) for specimens with l/d ratio less than 2

3.6 Summary

Sulphur concrete is often described as a brittle material (Loov, 1974; and Malhotra, 1979). The sulphur mixtures tested in this research program had relatively linear stress-strain curves until the peak strength was approached. Near the peak strength the samples containing the fly ash display greater axial straining from the on-set of yielding to reach peak strength compared to the samples containing only the sulphur and tailing sand (Figures 3.5 and 3.6). In all samples, the post-peak response ended with a sudden loss of load, supporting the observation that sulphur concrete samples tested behaved in a brittle manner.

From the test program carried out the following is concluded:

1. Figure 3.7 shows that the fly ash increased the mean peak strength of the mixes. Figure 3.7 shows for the mixes 10Su90Sa and 15Su85Sa that the mean peak strengths were 11,720 kPa and 21,670 kPa, respectively. The mean peak strengths for mixtures 10Su2FA and 15Su3FA were 13,160 kPa and 27,030 kPa,

respectively, showing an increment in the mean peak strength due to the addition of fly ash in the mixes.

2. Fly ash also increased the yield strength of samples (Figure 3.8).

3. Figure 3.9 shows that the fly ash did not significantly affect the Young's modulus.

4. Table 3.3 shows a comparison of the results of the splitting tensile strength with the compressive strength shows that the measured tensile strengths were less than 10% of the compressive strengths for all the sulphur concrete mixes. Nevertheless, the tensile strength data are limited to two samples for each mix. This finding is important because the rule of thumb that 10% of the compressive strength is approximately equal to the tensile strength is not applicable for the mixes under study.

5. The Poisson's ratio measured on two samples was 0.15 and 0.2. These values are comparable to those reported in the literature.

A standard procedure for assessing the rapid freezing and thawing durability was adapted. Cohen (1987) concluded that the dynamic modulus of elasticity does not correlate well with the behaviour of the sulphur concrete during the rapid freezing and thawing cycles; therefore, it was decided to measure the peak compressive strength, yield strength, and the static Young's modulus. The results of this test were definitive, and all the samples failed to reach 300 cycles, thus failing to pass the test. However, the structure under consideration has a lifespan of only ten years, so the material that survived 100 cycles may still be used to build the required structure, depending on how

many freeze-thaw cycles can be expected in a environment such as Fort McMurray, Alberta. The following was noted from the freeze-thaw studies:

1. The "pop out" of the samples along the weakness planes created by the action of tamping the material during casting was noticed only during the freeze-thaw cycles. Moreover, this pop out may occur during construction because of the sulphur concrete requires compaction during placement; therefore, a construction procedure accounting for this behaviour must be developed.

2. An analysis of the results reveals that unmodified sulphur concrete mixes of 10 % sulphur content by weight cannot be used in an environment subjected to freeze-and-thaw cycles. The mixes failed before they had undergone 50 cycles; consequently, even a temporary structure cannot be built from this material subject to freeze-thaw environment. Figure 3.15 shows that after 50 cycles, the strength properties and the modulus of the mix of 30Su70Sa were reduced to below 60% of the initial modulus. Although the mix of 15Su85Sa did not show deterioration after 50 cycles, it failed to reach the test of 100 cycles.

3. The only two mixes to survive to 100 cycles were the 15SU3FA and 25SU5FA. Although the peak strength after 100 cycles of the 25Su5FA was above 30 MPa, its modulus was reduced to 40% of the initial modulus (Figure 3.19). The 15Su3FA mix presented lower compressive strength (peak and yield), but Young's modulus was reduced to 60% of the initial value after 100 cycles (Figure 3.19). The reduction of the modulus in some way is a measure of the broken bonds within the sulphur matrix; thus the 25Su5FA shows more deterioration than the 15Su3FA mix.

Given the above findings, the material selected for use in a structure that will undergo fewer than 100 freeze-thaw cycles should be the 15Su3FA. Table 3.5 presents the recommended strength and modulus to be used for design purposes under the initial

condition after construction and after 100 freeze-thaw cycles. Also, included are the recommended properties for the 25Su5FA mix for comparison.

Material Properties	15Su3FA		25Su5FA	
	Initial Condition	After 100 cycles	Initial Condition	After 100 cycles
Peak Compressive Strength (kPa)	27,030	13,200	32,250	32,251
Yield Compressive Strength (kPa)	22,800	11,700	22,560	22,560
Tensile Strength (kPa)	1,189	660	2,800	1,120
Young's Modulus (MPa)	18,000	11,200	18,260	7,600
Poisson's Ratio	0.1	0.1	0.1	0.1

Table 3.5 Recommended values for the 15Su3FA and 25Su5FA mixes to be used in the initial condition and after 100 freeze-thaw cycles

4 LIMIT EQUILIBRIUM ANALYSIS

A retaining wall is a man-made steep slope designed for a particular function. The traditional manner for determining the design dimensions and geometry of a retaining wall is via use of Limit Equilibrium Analysis while applying an appropriate Factor of Safety.

The condition that establishes limiting equilibrium is a stress condition along a predefined slip plane and the strength required to satisfy equilibrium. The Factor of Safety is a key feature of limiting equilibrium condition and the geotechnical community widely accepts Morgenstern's (1992) definition: "The Factor of Safety is that factor by which the shear strength parameters may be reduced in order to bring the slope into a state of limiting equilibrium along a given slip surface" (p. 3).

The Factor of Safety has two well-recognized features in practice: 1) a factor of ignorance regarding of the strength of the materials, and 2) a means for controlling deformations. The first depends on the knowledge of the problem under study. A good understanding of the problem provides a good understanding of the processes and material behaviour. In contrast, ignorance or poor knowledge of the problem results in a poor understanding of the expected performance. Our confidence in the outcome is reflected in the value of the Factor of Safety.

The Factor of Safety's second feature is the indirect control of deformation. A Limit Equilibrium Analysis does not provide any information about the internal or external deformation. However, a judicious choice of a Factor of Safety, greatly influenced by experience, limits the deformation to acceptable values.

According to Terzaghi et al. (1996) the possible failure mechanism of a retaining structure based on Limit Equilibrium Analysis for which a factor of safety must be determined are:

a) Internal Stability: relates to a failure mechanism developed within the retaining structure itself.

b) Sliding: refers to a slip plane underneath the structure, probably between the foundation material and the structure.

c) Overturning: a rotation of the entire structure around its toe or a nearby point of rotation.

d) Global Stability: refers to the general condition of stability of the soil around the structure.

e) Bearing Capacity: the maximum soil pressure is computed from static equilibrium and compared with the allowable soil pressure estimated from bearing capacity theory and settlement considerations.

This chapter evaluates the existing reinforced earth structure used to construct a "sizer wall" and the proposed sulphur concrete structure using the limit equilibrium method of slices that involve checking for internal and global stability. The remaining failure mechanisms in the checklist provided above are verified for the sulphur concrete wall. However, since both types of retaining wall are considered monolithic structures for the sliding, overturning and bearing capacity failures, and giving that their unit weight are similar; therefore, the calculations of these failure mechanisms are valid for both retaining walls. In order to compare both solutions the same geometry, pore water pressures, material properties of the foundation, backfill, pavements, sub-grades, and drainage are used throughout this thesis.

72

4.1 Stability Analysis (Soil Slope)

In limit equilibrium techniques, slope stability is analysed by first computing the factor of safety and this value must be determined for the surface that is most likely to fail by sliding, the so-called critical slip surface (Duncan, 1996). He also indicated that to evaluate the stability of a slope by limit equilibrium methods, it is necessary to perform a considerable number of possible slip surface in order to determine the location of the critical slip surface and the value of the minimum factor of safety.

The most useful method of analysis for slope stability is the method of slices, so called because they subdivide the potential sliding mass into slices for purposes of analysis. Duncan (1996) pointed out that the equilibrium conditions are considered slice by slice, and if a condition of equilibrium is satisfied for each and every slice, it is also satisfied for the entire mass. However, define this condition of equilibrium is a statically indeterminate problem, and assumption are required to make up the imbalance between the equations and unknowns. Therefore, the slope stability methods based on limit equilibrium differ from each other in the assumptions proposed to solve the unknowns.

In this thesis, the slope stability analyses were performed using Slope/W, and this software offers to the user the option to select the Morgenstern-Price method for the stability analysis. This method of slices satisfies all conditions of equilibrium and is applicable to any shape of slip surface (Morgenstern and Price, 1965).

The Canadian Foundation Engineering Manual (1992) recommended that the stability of the soil mass containing a retaining structure must have a minimum factor of safety of at least 1.5 for the most critical slip plane.

4.2   Earth Pressures

The "at rest condition" is a state of stress that depends on the process that formed the deposit and its subsequent stress history (Morgenstern and Eisentein, 1970). At-rest pressures only apply rigorously in the case of walls that were placed into the ground with a minimum of disturbance and that remain unmoved during the process of loading, or when unmoving frictionless walls with a backfill placed with a minimum of compactive effort, a condition rarely achieved in practice (Clough and Duncan, 1992). These authors also add that at-rest pressures are still useful in design, either as a baseline or as an assumed conservative choice for the design loading.

From the theory of elasticity the lateral and vertical stresses in a confined mass are related by the Poisson's ratio, v, as follow:

$$K_o = \frac{\sigma_h}{\sigma_v} = \frac{v}{1-v} \tag{4.1}$$

For normally consolidated soils, Jaky (1944) proposed a relationship based on the drained friction angle ϕ':

$$K_o = 1 - \sin\phi' \tag{4.2}$$

Bishop (1958) presented the results of a comprehensive investigation into the determination of K_o in the laboratory and found that for all practical purposes, equation (4.2) was substantiated for initial loading. Additional studies by Brooker and Ireland (1965) and Maine and Kulhawy (1982) also justified Jaky's equation.

Terzaghi et al. (1996) indicated that the change of stress from the K_o condition depends on whether the soil after being deposited was stretched or compressed. If a semi-infinite mass of soil is stretched, the horizontal stress decreases to a minimum value known as "the active state of stress." On the other hand, if the semi-infinite mass of soil

74

is compressed, the horizontal stress is increased to a maximum value known as "the passive state of stress." These conditions are known as the general states of plastic equilibrium. Terzaghi et al. (1996) defined that the soil as being in a state of limiting equilibrium when every part of it is on the verge of failure. Rankine (1857) studied both conditions and proposed the following well-known expressions to estimate the active (K_a) and passive (K_p) coefficients of earth pressures:

$$K_a = \tan^2\left(45^\circ - \frac{\phi}{2}\right) \tag{4.3}$$

$$K_p = \tan^2\left(45^\circ + \frac{\phi}{2}\right) \tag{4.4}$$

The ideal condition for a wall is for the pressure to be exerted at the active state. If the wall is considered smooth (no friction between the wall and the soil mass) and the backfill is horizontal, the Rankine coefficient of earth pressure, defined in equations (4.3) and (4.4), can be used. A wall in this condition supports an active earth pressure p_a calculated from the Morh-Coulomb failure criterion suggested by Clough and Duncan (1992):

$$p_a = K_a z \gamma - 2c\sqrt{K_a} \ , \tag{4.5}$$

where γ is the unit weight; c is the cohesion; z is the depth below the ground surface; and K_a is the Rankine active earth pressure defined in (4.3). For the passive state against a frictionless wall , Clough and Duncan (1992) recommended that the lateral earth pressure p_p is calculated similarly as follows:

$$p_p = K_p z \gamma + 2c\sqrt{K_p} \ , \tag{4.6}$$

75

where K_p is the Rankine coefficient of passive earth pressure. Equations (4.5) and (4.6) are for soil that has mobilised shear strength from friction and cohesion, and in the case of cohesionless soils, the second term is eliminated.

The Coulomb theory is one of the theories most used in practice; however, it is well known to overestimate the passive resistance and, hence, acts on the unsafe side (Morgenstern and Eisentein, 1970; Driscoll, 1979). Moreover, Terzaghi et al. (1996) argued when the wall friction is equal to the effective friction angle, the magnitude of the error of the Coulomb theory is about 30%.

Clough and Duncan (1992) pointed out that in the active state, the log-spiral shape is reasonably approximated by a straight-line, and that the resultant load predicted by using the simple straight-line failure mechanism is within 10 percent of that obtained with the more exact log-spiral mechanism. The Coulomb theory allows for the consideration of wall friction, sloped backfill and sloped walls; the Coulomb coefficient of active earth pressure presented here has been taken from Das (1994):

$$K_a = \frac{\cos^2(\phi - \theta)}{\cos(\delta + \theta)\cos^2\theta \left[1 + \sqrt{\dfrac{\sin(\phi + \delta)\sin(\phi - \alpha)}{\cos(\delta + \theta)\cos(\theta - \alpha)}}\right]^2} , \qquad (4.7)$$

where ϕ is the angle of soil friction, δ is the angle of wall friction, α is the inclination of the backfill slope ($\alpha = 0$ for horizontal slope), and θ is the angle of the back-face ($\theta = 90°$ for vertical face).

Duncan et al. (1990) pointed out the following consideration for retaining walls with granular backfill and foundations of sand or gravel: Sand and gravels foundations are sufficiently compliant to allow the movement required to reduce the earth pressures to values significantly smaller than the at rest values. Therefore, if the design provides adequate safety against sliding and overturning, active earth pressures calculated by using the Coulomb theory can be used in the design. The shear load generated between the wall and the backfill when it settles more than the wall (in the usual condition) must be included in the analysis because it plays an important role in enhancing the wall's stability. Also, the normal reaction at the base must be located in the middle third, and the horizontal force against the wall must be located approximately at 0.4 of the restrained height rather than at the theoretically predicted 1/3 height.

4.2.1 Earth Pressures due to Surface Loads

A uniform surcharge pressure applied under a large area (theoretically, an infinitely large area) generates a constant increment in the vertical pressure and in the horizontal pressure at all depths. Clough and Duncan (1992) showed that the increment in the vertical pressure and the horizontal pressure are in the following form:

$$\Delta p_v = q_s \qquad (4.8)$$

$$\Delta p_h = K q_s \ , \qquad (4.9)$$

where Δp_v and Δp_h are the increment in the vertical and horizontal stress, respectively; q_s is the surface surcharge; and K is an earth pressure coefficient. For the active earth pressure condition, $K = K_a$; for at-rest condition $K = K_o$; and for the passive condition $K = K_p$.

77

Bousinesq (1885) developed expressions for the stresses induced within an elastic

mass by a point load acting in the surface. Clough and Duncan (1992) indicated that this

solution can be used to develop an expression to estimate the horizontal stress on the wall

if the wall does not move and if no shear is present between the soil and the wall. Peck

and Mesri (1987) derived the following expression for a finite load perpendicular to the

wall as shown in Figure 4.1:

$$\Delta p_h = \frac{Q}{z\pi}\left(\frac{1}{\left[1+\left(\frac{z}{x_2}\right)^2\right]^{3/2}} - \frac{1-2\upsilon}{\left[1+\left(\frac{z}{x_2}\right)^2\right]^{1/2} + \frac{z}{x_2}} - \frac{1}{\left[1+\left(\frac{z}{x_1}\right)^2\right]^{3/2}} + \frac{1-2\upsilon}{\left[1+\left(\frac{z}{x_1}\right)^2\right]^2 + \frac{z}{x_1}}\right) \quad (4.10)$$
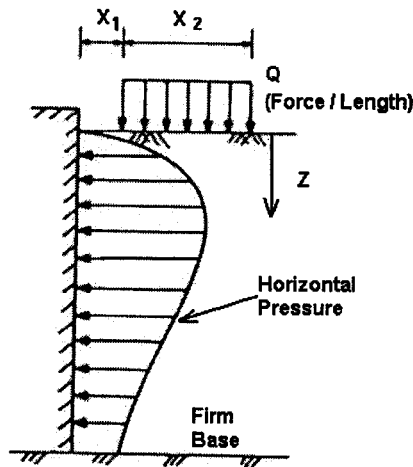
Figure 4.1 Finite Line Load Perpendicular to Wall (Modified from Clough and
Duncan, 1992).

where Q is the magnitude of the line load , x_1 and x_2 are defined in Figure 4.1, and z is

the depth below the surface.

4.3 Reinforced Soil

Mitchell and Christopher (1990) explained that "Reinforced soil" is a generic name applied to combinations of soil and distributed linear or planar inclusions (e.g., steel strips, steel or polymeric grids, geotextile sheets, and steel nails) that are capable of withstanding tensile loading and, in some cases, bending and shear stresses as well. These authors also mentioned that "mechanically stabilized earth" refers principally to reinforced soil placed as fill and also includes anchored systems.

The Reinforced Earth system was invented by the French architect and engineer Henri Vidal in 1963, and the first wall was built in France in 1965. Vidal's method use parallel steel strips as reinforcement. Vidal (1966) originally proposed the "concertina" construction method, which accommodates the differential settlements by using a flexible face closing in a manner similar to a set of bellows or a concertina (Rourke and Jones, 1990). Some of the largest reinforced soil structures have been built using this method.

Metallic and polymeric grids have also been used as reinforcement, although Europe was not a pioneer in this area. The first grid reinforced soil retaining structure (welded wire bar mat) was constructed in the USA in 1974, along interstate Highway 5, near Dunsmuir, California (Forsyth, 1978). The bar mat/soil interaction is complex and involves both friction along the longitudinal bars and passive resistance against the transversal elements (Schlosser, 1990).

4.3.1 Mechanism of Reinforcement

Mitchell and Christopher (1990) related the soil-reinforcement interaction to design by using the following three criteria:

1. Pullout capacity. The pullout resistance of each reinforcement should exceed the design tensile force by a specified factor of safety.

2. Allowable displacement. The relative soil-to-reinforcement displacement needed to mobilize the design tensile force should be less than the allowable displacement.

3. Long-term displacement. The pullout load should be less than the critical creep load for the reinforcement or the soil (in the case of cohesive soils).

Mitchell and Christopher (1990) also mentioned that the reinforcement pull-out resistance is mobilized by two interactions: interface friction and passive soil resistance against transverse elements such as bar mats and wire meshes. The same authors stated that the major load transfer mechanism (in granular soils) for bar mats is passive resistance with a high dilatancy effect, although for the welded wire mesh, this mechanism is frictional. The displacement required to develop the pullout resistance for the bar mats is between 2 and 4 inches and for the welded wire mesh is only from 0.5 to 0.8 inches. Schlosser (1990) mentioned that because of the mobilized passive resistance, bar mats are more resistant in pull-out than strips, but only for large displacement (from 5 to 10 centimetres). If the required lateral displacement to generate the passive resistance is acceptable for the structure, bar mat reinforcement permits the use of poor quality backfill material with a relatively large fine grain portion.

4.3.2   Behaviour and Design of Reinforced Soil Walls.

Terzaghi et al. (1996) summarised the requirements for the design of the internal stability of a reinforced earth wall:

- The tension in any tie must not exceed the strength of the tie, and the frictional resistance between the tie and the soil of the resisting zone must be great enough to prevent the tie from pulling out of the backfill.

Schlosser (1971) showed that the earth mass of a reinforced retaining wall is divided into active zone and a resistant zone (Figure 4.2). Schlosser (1990) explained the behaviour as follows:

- In the active zone, the soil tries to move away from the structure, but is restrained by friction developed along the inclusions.

- The mobilized shear forces are directed toward the front of the wall, resulting in an increase of the tensile force with distance from the facing.

- The maximum tensile force in the reinforcement does not occur at the wall facing, but rather at some distance away from the facing.

- In the resistant zone, the shear stresses are oriented away from the facing and prevent slippage of the reinforcement at the soil/inclusion interface.
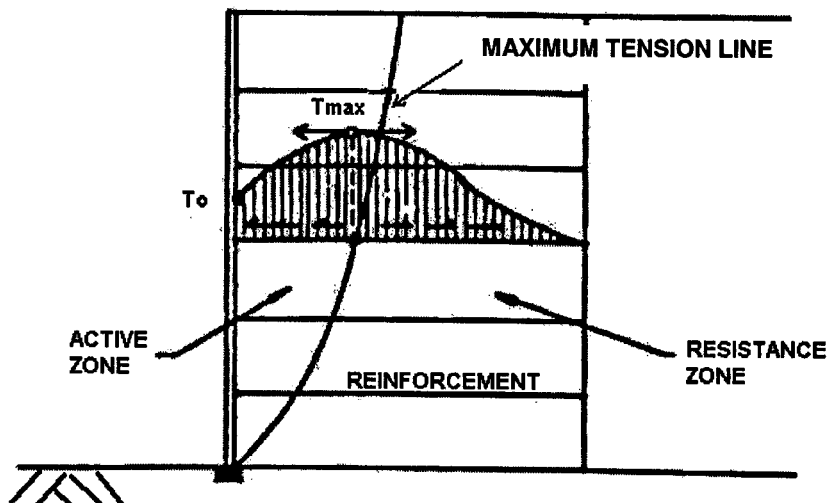
Figure 4.2 Maximum Tension Line (Modified from Mitchell and Christopher (1990)).

In addition, Schlosser (1990) mentioned that reinforced retaining walls (using inextensible reinforcement) with larger L/H, where L is the reinforcement length and H the height of the structure, failed by breakage of the reinforcement, and that the failure zone corresponded to the line of maximum tensile force. Furthermore, Schlosser (1990) remarked that the wall height that generates failure is greater than the one predicted by the Mohr-Coulomb failure wedge, and that the failure surface intercepted the top of the backfill at a closer distance from the facing than that predicted by the Rankine Theory.

Mitchell and Christopher (1990) stated that the extensibility of the reinforcement compared to the deformability of the fill controls the magnitude of the horizontal stresses in the backfill. They commented that closely spaced, inextensible reinforcements produce an unyielding mass that can retain essentially a K_o state of stress; moreover, the reinforcement with passive interaction can develop lateral stresses higher than K_o in the upper few feet because of the compaction effect. Mitchell and Christopher (1990) remarked about extensible reinforcement that the fill yields laterally so that an active condition can develop before failure of the reinforcement. Therefore, the current practice is to design the retaining structures with extensible reinforcement to resist the limiting condition of active earth pressure. On the other hand, the current practice for inextensible reinforcement is to assume a K_o stress condition at the ground surface, with K decreasing to the active value (K_a) at a depth of six metres.

Figure 4.2 shows the maximum tensile force line as presented by Mitchell and Christopher (1990) and a scheme representing the distribution of the tensile forces along the reinforcement. It can be observed how the tension changes from an initial value T_o to the maximum value T_{max} at some distance from the facing.

82

Figure 4.3 presents an approximation of the maximum tension line for inextensible and extensible reinforcement. Schlosser (1990) explained that for steel reinforcement (inextensible), the high stiffness of the inclusion results in only small deformations in the soil mass. As a result, the maximum tensile force line is vertical (Figure 4.3 (a)). Schlosser (1990) mentioned also that geosynthetics (extensible) have relatively low stiffness and therefore undergo sufficient deformation to attain an active state; consequently, the maximum tension is similar to that of the Mohr-Coulomb failure plane (Figure 4.3 (c)).
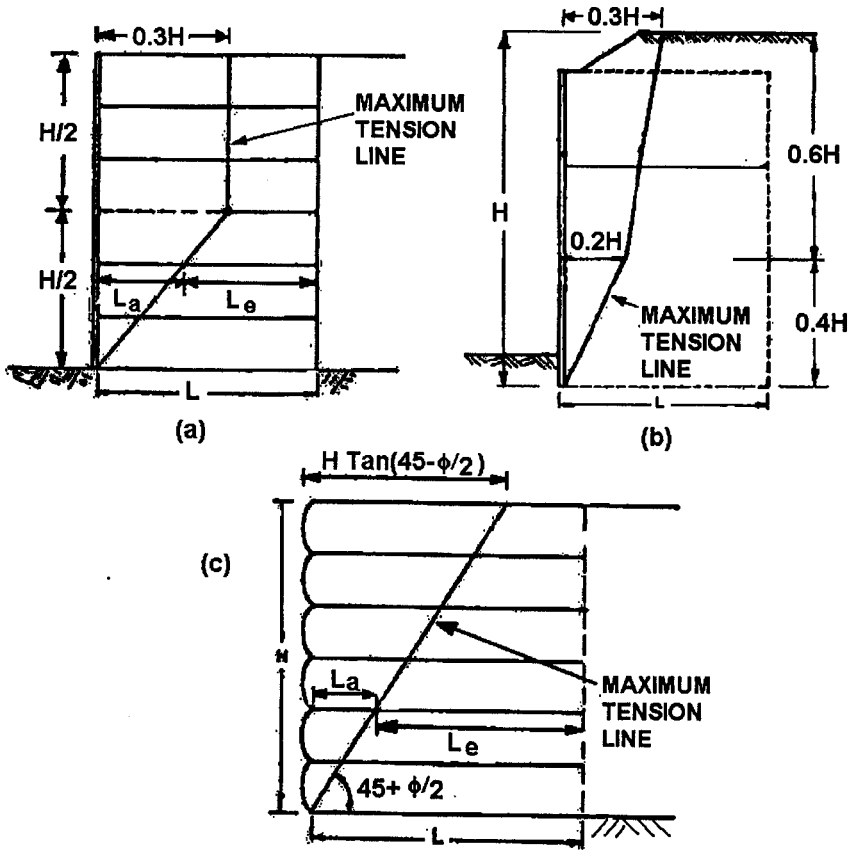
Figure 4.3 Maximum Tensile Force Line (a) and (b) Inextensible Reinforcement and (c) Extensible Reinforcement (Modified from Mitchell and Christopher, 1990; and Schlosser,1990).

In addition, Schlosser (1990) presented another bi-linear distribution for the maximum tension force for reinforced earth walls with inextensible reinforcement based on reduced and full-scale tests and finite element calculations (Figure 4.3(b)).

4.4   Use of Compacted Oil Sand as Backfill

Compacted oil sand was used for the construction of a Reinforced Earth dump wall in 1990 by Syncrude Canada Ltd in Fort McMurray, Alberta. Brockbank et al. (1992) described this application. Granular backfill material in the area of Fort McMurray is in very short supply and costly; consequently, the use of lean oil sand becomes necessary. Lean oil sand is excavated oil sand from the mining operation, with a bitumen content of 6% or less.

A Reinforced Earth test wall was built by using the traditional metal strips, although a wire mesh facing called Terratrel® was used because it was able to accommodate the expected displacements. A surcharge load representing the 240-ton Mining Trucks was used. Bockbank et al. (1992) were concerned that the presence of oil would act as a lubricant and reduce the strips' pull-out capacity. An apparent friction angle of about 35° was determined from laboratory tests carried out at the University of Alberta under the supervision of Dr. Don Scott. However, Brockbank et al. (1992) reported that an angle of 30° was used in the design.

The compaction characteristics of oil sand were investigated by Lord and Cameron (1985). Oil sand has a composition of four elements: gases, water, bitumen and solids. As mentioned by Lord and Cameron (1985), the key for the success of the computation of the dry density is to recognise the bitumen as part of the fluid phase and relate the fluids to solids. The maximum dry density was found to be 1800 kg/m³, and the desirable

average was 1750 kg/m^3. The typical compacted unit weight of the oil sand was found to be about 19.5 kN/m^3. In their conclusions, Lord and Cameron (1985) recommended not using a bitumen content greater than 9%, where the bitumen content is defined as the mass of bitumen divided by the total mass (including water, bitumen, and solids). Furthermore, direct shear testing was also performed. Lord and Cameron (1985) found an effective peak friction angle of 35° and an effective residual friction angle of 32°. Oil sand compacted at 1750 kg/m^3 is expected to have the residual friction angle mentioned above; however, whether the peak friction angle can be reached is uncertain because the shear tests were performed on samples with a dry density of 1850 kg/m^3.

In 2000, the Mine Engineering Division of Suncor Energy started a research to improve the design methodology of their Haul Roads (Suncor 2000). For this work, material samples were sent to the University of Alberta for testing; the tests consisted of monotonic loading to failure and cyclic loading with maximum stresses limited to 50% of the peak strength. The specimens were compacted to 98% Standard Proctor. Table 4.1 presents an extract of the results.

Sample	Description	Wet Density (kg/m^3)	Young Mod[1] (MPa)	Young Mod[2] (MPa)	Young Mod[3] (MPa)
1a	Gravel-20mm	2314	18	-	>200
1b	Gravel-20mm	2277	14	103	
1c	Gravel-20mm	2309	7.1	77	
4a	Lean oil sand	2071	3	-	30
4b	Lean oil sand	2035	14	63	
4c	Lean oil sand	2957	4	32	

1 Young Modulus for first loading cycle.
2 Young Modulus after 2 to 3 loading cycles.
3 Recommended Young Modulus for numerical modelling.

Table 4.1 Measured Moduli and Wet Density (From Haul Road Design, Suncor Energy)

4.5 Evaluation of the Existing Reinforced Earth (RE) Retaining Wall

Figure 4.4 shows the layout for the RE retaining wall used by Suncor for the sizer-wall construction. The structure's height is approximately 15 metres and has a foundation base of granular material connected to a sloped drainage layer (4). The backfill material is compacted lean oil sand (3). The structure also has a 1-metre thick concrete pavement (1) and 2-metre thick granular material sub-base (2). The reinforcement is composed of steel-welded wire mesh (7) with pre-cast concrete facing panels for approximately the first 3 metres and a facing of wire mat on the rest. Typical in-situ materials of the McMurray formation are oil sands (5) and limestone bedrock(6).
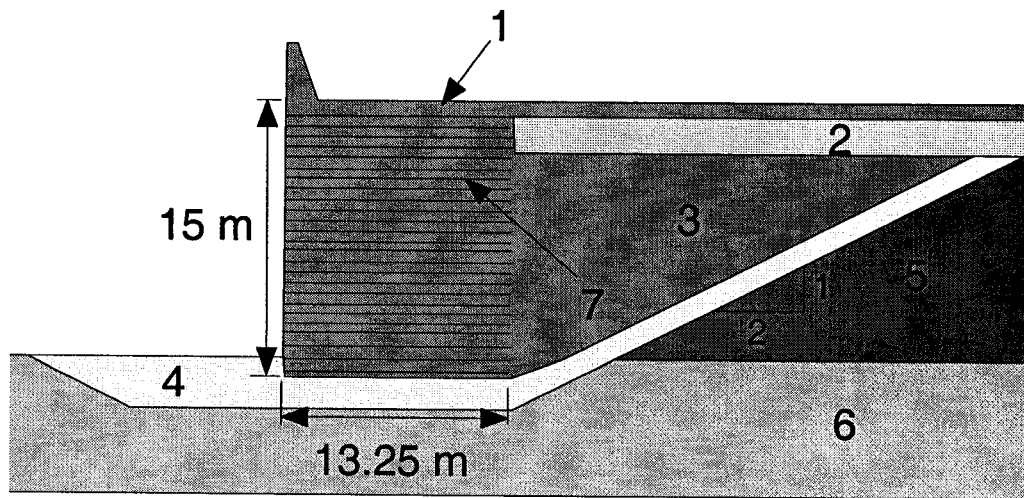
1. Concrete Pavement
2. Gravel Sub-base
3. Compacted Lean Oil Sand
4. Gravel Base and Drain
5. Oil Sand
6. Limestone Bedrock
7. Steel Welded Wire Reinforcement

Figure 4.4 Reinforced Earth retaining structure used by Suncor for their Sizer-wall construction

The stability of this RE wall geometry is evaluated in the following sections by:

a) Estimating the external surcharge design loads by the mining trucks parked on top of the wall.

b) Comparing the tensile forces generated on the earth reinforcement to the allowable tensile forces base on the material properties.

c) Carrying out slope stability limit equilibrium analysis using the software Slope/W.

d) Evaluating the RE wall for base sliding, overturning and bearing capacity.

4.5.1 Mining Trucks Surcharge

The RE retaining wall is designed to support the latest generation of Mining Truck from Caterpillar, the CAT® 797 with a payload of approximately 360 tons. Therefore, the proposed sulphur concrete wall will have to support the same loads. Table 4.2 presents the truck loads used for design purposes. These are incremented by 15% to accommodate possible overloading with oil sand.. Also, Figure 4.5 shows the truck dimensions in millimetres.

	Load in kg	Load in kN
Front Axle	198,892	2,243.8
Rear Axle	398,381	4,494.3
Gross Weight	686,864	6,738.1

Table 4.2 Cat 797 truck loads

Figure 4.5 shows the distance between the front and rear axle of 7.2 m and the maximum width of the rear axle of 9.154 m. These dimensions are used to define the area where the loads are applied.
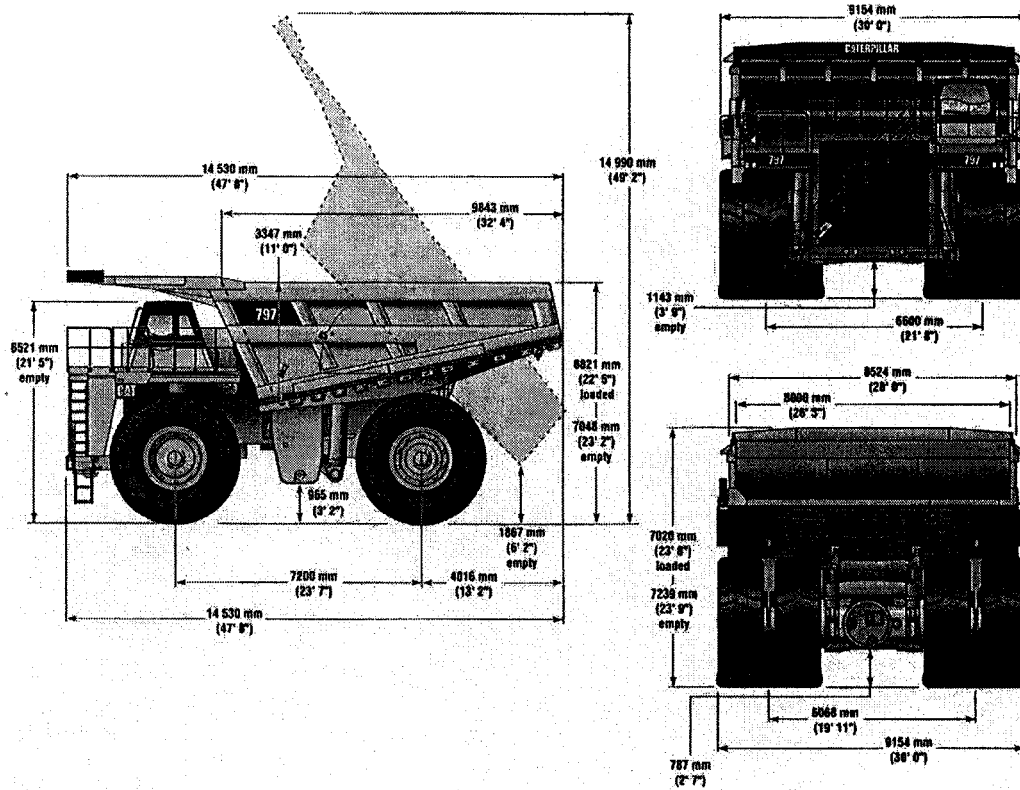
Figure 4.5 Dimensions of Cat®797 mining truck (in millimetres)

Two simple distributed loads are assumed to represent the loading conditions resulting from the mining trucks:

a. The first distributed load results when the Mining Truck is dumping on top of the retaining structure, and the steel box is in its vertical position shown in Figure 4.5 by the dotted line. This operation assumes that the rear axle supports the entire load, so the load is distributed over the rear half-size area below the truck. The

total load of 6738.1 kN is distributed over the rear area of 3.6 m by 9.154 m, resulting in a pressure of approximately 205 kPa (Brockbank et. al., 1992).

b. The second distributed load results when the box of the Mining Truck is in the horizontal position and both axles support the load. In this situation, the total load of 6738.1 kN is distributed over the entire area below the truck, 7.2 m by 9.154 m, resulting in a pressure of 102.5 kPa.

These pressures allow us to represent two loading conditions of interest, the partial and full loading condition, respectively. The partial loading condition occurs when only one Mining Truck is dumping on top of the structure, with no waiting line of trucks. A pressure of 205 kPa, as shown on Figure 4.6, results. The full loading condition occurs when there is a waiting line of mining trucks and results in a distributed pressure of 102.5 kPa, as shown in Figure 4.7.

4.5.2   Evaluation of Tensile Forces

A RE wall is not a trivial structure. The design process focuses on the external stability of the entire reinforced mass (sliding, overturning, and bearing capacity) and on the internal stability within the reinforced mass (reinforcement spacing, anchorage length and connection strength).

This section does not intend to verify the design of the existing wall, but to evaluate its behaviour by using Limit Equilibrium Analysis in order to compare the results with those obtained using the new proposed wall. To make this comparison, the forces provided by the reinforcement in the system must be estimated. The design details (geometry and materials characteristics) were obtained from Suncor's construction drawings. By using a

back-calculation process, the tensile forces resisted by the reinforcement can be estimated.
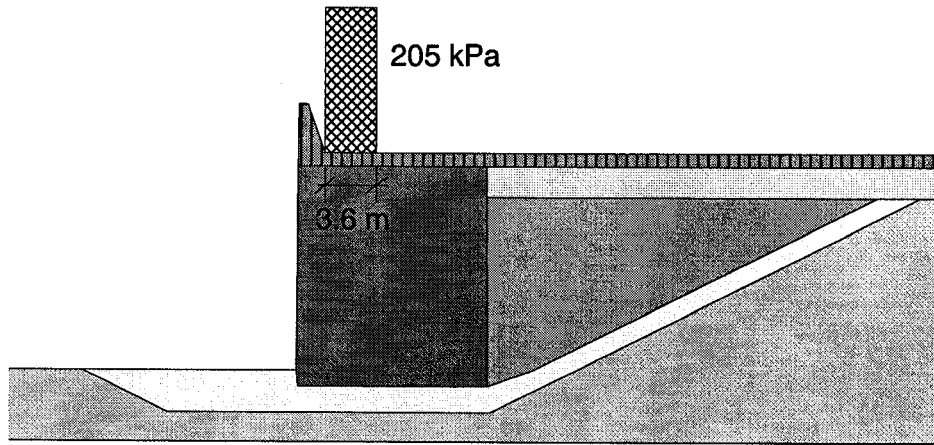
Figure 4.6 Partial loading condition
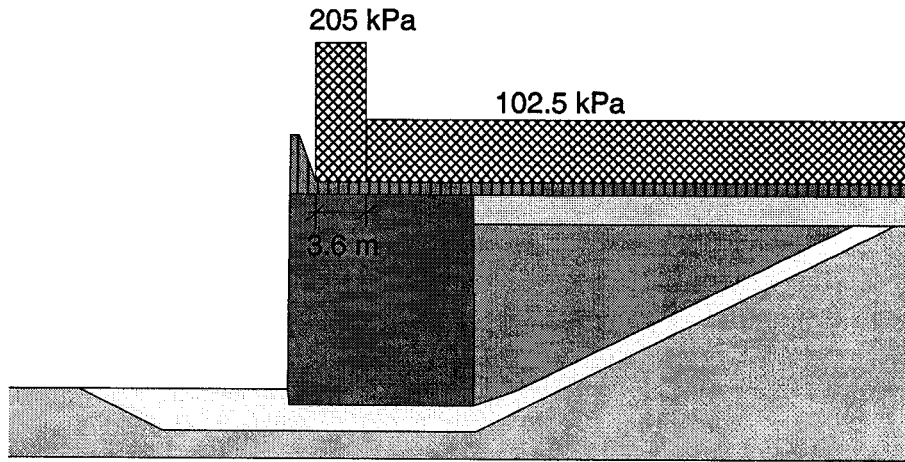
Figure 4.7 Full loading condition

4.5.2.1 Calculation of Demand Forces

The demand forces are defined as the tensile forces generated by the applied loads into the inclusion layers. The following information is used to establish internal stability:

- The backfill material is compacted lean oil sand with a unit weight of 20 kN/m³ and a friction angle of 32°, Lord and Cameron (1985).

90

- The sources of surcharge are the concrete pavement, the concrete guard-rail wall and the Mining trucks. The contributions of the concrete pavement and the guard-rail wall are 19 kPa and 7 kPa, respectively. The full loading condition (Figure 4.7) is assumed to estimate the tensile forces. To estimate the truck surcharge, a uniform line pressure of 102.5 kPa is applied, and, in addition, a finite pressure area of 102.5 kPa under the first half of the truck is superimposed on the line surcharge. The result is a finite pressure of 205 kPa below the first half of the truck and an infinite uniform surcharge of 128.5 kPa on the rest of the area.

The earth horizontal stress changes with depth and can be calculated from the following expression:

$$\sigma_h = \gamma(z)K + qK + \Delta P_h \ , \tag{4.11}$$

where γ is the unit weight of the backfill material, z is the depth, q is uniform surcharge pressure (128.5 kPa), and K is the ratio between the vertical stress and the horizontal stress. ΔP_h is defined, as shown in equation 4.10, from the applied pressure of 102.5 kPa (as indicated in the previous paragraph). For comparison purposes, K varies between the coefficient of the active earth pressure (K_a) and the coefficient of the earth pressure at rest (K_o). These coefficients are estimated from equations 4.3 and 4.2, respectively

Figure 4.8 shows a schematic layout of one reinforcement layer where σ_h is applied against the facing and is resisted by the allowable strength of the reinforcement. The friction and passive forces generated at the soil-reinforcement interface drag the reinforcement on both sides, transmitting the force to the facing and generating tensile forces similar to those presented in Figure 4.2. T_{allow} is the maximum allowable tensile

91

strength to be used for final design purposes and is defined from the ultimate tensile

strength of the reinforcement (T_{ult}) divided by an appropriate Factor of Safety.
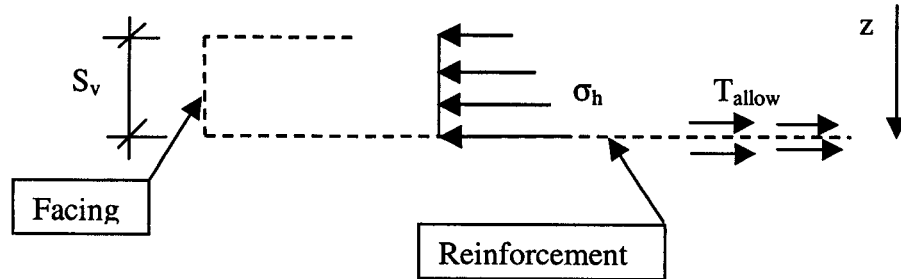
Figure 4.8 Schematic section view of the reinforcement in the RE wall

From static equilibrium of the forces shown in Figure 4.8, the demand force (T_{demand})

is estimated as follow:

$$T_{demand} = \sigma_h S_v FS \qquad (4.12)$$

$$T_{demand} \leq T_{allow} \; , \qquad (4.13)$$

where σ_h is the horizontal stress calculated from equation 4.11, S_v is the vertical spacing

of the reinforcement, and FS is the Factor of Safety currently used in design practice that

amplifies the demanded forces. In Table 4.3, T_{demand} is calculated throughout the entire

height of the retaining structure for $K_a = 0.3073$ and $K_o = 0.4701$, based on a friction

angle of 32° (see Section 4.5.2.1). The spacing and the depth (z) of each reinforcement

layer was determined from the contract drawings.

4.5.2.2   Calculation of Allowable Forces

As indicated in the previous section, T_{allow} is the allowable tensile force of the

reinforcement. The contract drawings S01A and S03A, both dated 02/16/00 by

McCavour Engineering Limited, provided the information for estimating the maximum

allowable forces for each reinforcement layer. Table 4.4 shows the reinforcement mat under consideration.

The contract drawings also specify a minimum allowable tensile strength of 450 MPa for the welded wire mesh. Table 4.4 presents the distribution of the welded wire mesh reinforcement using the standard convention presented on the contract drawings. This convention specifies that the wire size number represents the area of the wire in mm^2. The first number is the longitudinal wire size, and the second one is the transverse wire size.

The maximum allowable tensile force for each combination of longitudinal and transverse wire spacing specified in Table 4.4 is calculated in Table 4.5. The spacing and the cross-section area of the longitudinal wires define the amount of steel reinforcement area per metre. The calculations of the allowable forces are performed for each reinforcement layer through the entire wall height and are presented in Table 4.6.

Figure 4.2 shows the profile of the RE wall. The mat width and spacing cannot be seen in this figure. The mat reinforcement has a width of 1.219 metres (in the direction perpendicular to the paper) and is spaced 0.305 metres. Because the reinforcement is not continuous, a factor of 0.8 is applied to reduce the allowable force per metre (Koerner, 1994). This factor is shown in Table 4.6 as well.

			K=Ka=0.3073			K=Ko=0.4701	
Layer No	Sv (m)	Z(m)	σ_h (Ka) kPa	FS	T demanded KN/m	σ_h (Ko) kPa	T demanded KN/m
1	0.61	0	39.48	1.3	58.48	60.41	89.47
2	0.61	0.61	69.77	1.3	61.45	92.68	94.01
3	0.61	1.22	87.63	1.3	64.42	112.52	98.56
4	0.61	1.83	93.98	1.3	67.40	120.87	103.11
5	0.61	2.44	94.50	1.3	70.37	123.37	107.66
6	0.61	3.05	93.01	1.3	73.34	123.86	112.20
7	0.61	3.66	91.32	1.3	76.31	124.16	116.75
8	0.61	4.27	90.14	1.3	79.29	124.97	121.30
9	0.61	4.88	89.69	1.3	82.26	126.50	125.85
10	0.61	5.49	89.95	1.3	85.23	128.75	130.40
11	0.61	6.1	90.85	1.3	88.20	131.64	134.94
12	0.61	6.71	92.29	1.3	91.18	135.06	139.49
13	0.61	7.32	94.16	1.3	94.15	138.92	144.04
14	0.61	7.93	96.39	1.3	97.12	143.13	148.59
15	0.61	8.54	98.89	1.3	100.09	147.63	153.14
16	0.61	9.15	101.62	1.3	103.07	152.34	157.68
17	0.61	9.76	104.53	1.3	106.04	157.24	162.23
18	0.61	10.37	107.59	1.3	109.01	162.28	166.78
19	0.61	10.98	110.75	1.3	111.98	167.43	171.33
20	0.61	11.59	114.02	1.3	114.96	172.68	175.87
21	0.61	12.2	117.36	1.3	117.93	178.01	180.42
22	0.442	12.64	119.82	1.3	87.01	181.91	133.12
23	0.762	13.4	124.12	1.3	154.64	188.69	236.59
24	0.762	14.17	128.49	1.3	159.28	195.55	243.69
25	0.762	14.93	132.92	1.3	163.92	202.45	250.79

Table 4.3 Calculation of T_{demand}

Figure 4.9 shows a comparison between the estimated demand forces and the allowable forces. The shape of the demanded forces up to a 4-metre depth is due to the influence of ΔP_h on equation 4.11. The allowable tensile forces (T_{allow}) are very similar to the demand forces (T_{demand}) using K_o until a 12-metre depth. Beneath the 12-metre depth,

94

T_{allow} increases considerably, more so than K_o values. This practice ensures that the critical slip surface will pass underneath the structure. Consequently, the agreement shown in Figure 4.9 provides a basis for selecting T_{allow} as the appropriate force to evaluate the stability in the next section.

Mats are arranged from the top to the bottom of the wall					
Size	Number	Longitudinal Wire spacing (mm)	Transverse wire spacing (mm)	Mat vertical spacing (mm)	Mat Length (metres)
W61.4xW32.3	2	305	203	610	13.25
W61.4xW32.3	7	305	508	610	13.25
W77.4xW32.3	8	305	914	610	13.25
W90.3xW45.2	4	305	914	610	13.25
W90.3xW45.2	2	152	914	762	13.25
W103xW45.2	2	152	914	762	13.25

Table 4.4 – Reinforcement mat schedule (as shown on the contract drawings S01A
and S03A, dated 02/16/00)

Minimum Allowable Strength = 450 mPa					
Welded Wire Mesh Size	Number of wires per mesh	Area per wire (mm^2)	Area per mesh (m^2)	T_{allow} per mesh (kN/m)	T_{allow} per metre (kN/m)
W61.4xW32.3	3	614	0.000307	138.15	113.33
W61.4xW32.3	3	61.4	0.000307	138.15	113.33
W77.4xW32.3	3	77.4	0.000387	174.15	142.86
W90.3xW45.2	3	90.3	0.0004515	203.17	166.67
W90.3xW45.2	6	90.3	0.0008127	365.71	300.01
W103xW45.2	6	103	0.000927	417.15	342.20

Table 4.5 – Calculation of T_{allow} for each combination of longitudinal and transverse
wire spacing

95

Layer No.	Sv (m)	Z(m)	T_{allow} KN/m	T_{allow} by 0.80 (a) KN/m	Layer No.	Sv (m)	Z(m)	T_{allow} KN/m	T_{allow} by 0.80 (a) KN/m
1	0.61	0	113.33	90.66	14	0.61	7.93	142.86	114.29
2	0.61	0.61	113.33	90.66	15	0.61	8.54	142.86	114.29
3	0.61	1.22	113.33	90.66	16	0.61	9.15	142.86	114.29
4	0.61	1.83	113.33	90.66	17	0.61	9.76	142.86	114.29
5	0.61	2.44	113.33	90.66	18	0.61	10.37	166.67	133.39
6	0.61	3.05	113.33	90.66	19	0.61	10.98	166.67	133.39
7	0.61	3.66	113.33	90.66	20	0.61	11.59	166.67	133.39
8	0.61	4.27	113.33	90.66	21	0.61	12.2	166.67	133.39
9	0.61	4.88	113.33	90.66	22	0.442	12.642	300.01	240.01
10	0.61	5.49	142.86	114.29	23	0.762	13.404	300.01	240.01
11	0.61	6.1	142.86	114.29	24	0.762	14.166	342.206	273.76
12	0.61	6.71	142.86	114.29	25	0.762	14.928	342.206	273.76
13	0.61	7.32	142.86	114.29					

(a) T_{allow} is multiplied by 0.8 because the reinforcement mats are spaced 0.305 m. Mats with =1.219 m (1.219/{0.305/2+1.219+0.305/2}=0.80)

Table 4.6 Calculation of tensile forces for stability analysis

4.5.3 Stability Analysis of Reinforced Earth-Retaining Structure.

An appropriate stability analysis must represent the site conditions where the earth structure will be build. In this case, the in-situ conditions were based on the information given in the contract drawings, and on the project site geology. The typical in-situ conditions were assumed to be a foundation material of moderately weathered limestone underlying a layer of oil sand. Figure 4.3 shows the simplified profile and Table 4.7 gives the associated material strengths used for the analysis in this thesis.

96
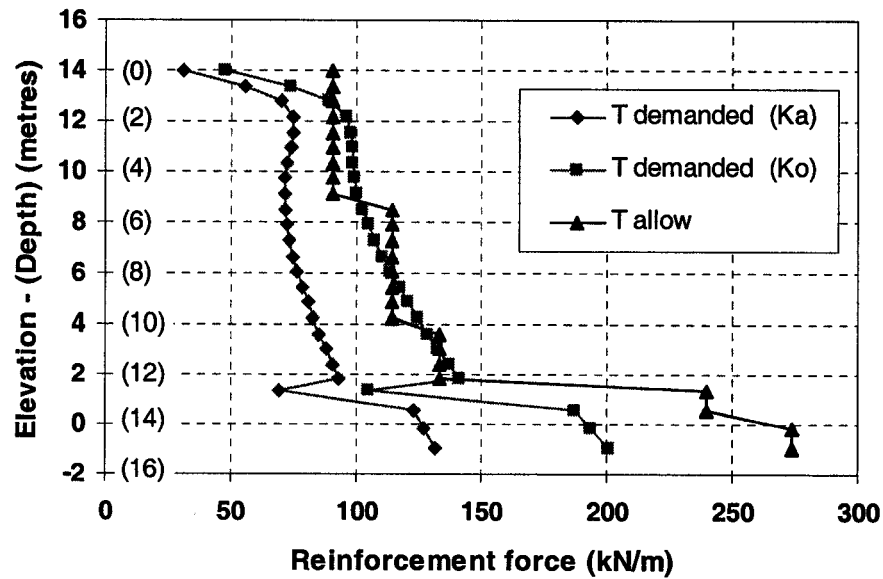
Figure 4.9 T_{allow} and T_{demand} versus depth

The two main parameters controlling the stability of a retaining wall are the shear strength and the pore water pressure. The shear strength of soil and rock given in Table 4.7 were taken from published values. Hoek and Bray (1981) recommended for limestone a friction angle between 35° and 40° and a cohesion from 10,000 to 30,000 kPa. Because some weathering of the limestone is anticipated, the lower bound values were selected with a friction angle of 35° and the cohesion of 10,000 kPa.

Dusseault and Morgenstern (1978) described oil sand as a material with a locked structure providing high friction angles. The lowest value these authors reported was 40°. The properties of the compacted oil sand were taken from Lord and Cameron (1985), who suggested a residual friction angle of 32° if a density of 1750 kg/m³ is reached after compaction. The properties selected for the gravel sub-base and the gravel footing and drain are typical for compacted GW materials and were taken from NAVFAC (1982). For the concrete pavement, a tension crack is introduced into the model through its entire depth. In this way, the strength of concrete is ignored in the analysis.

No.	Description	Unit Weight (kN/m³)	Cohesion (KPa)	Friction angle φ
1	Concrete Pavement	23	10,000	0
2	Gravel Sub-base	22.5	0	38°
3	Compacted Oil Sand	21	0	32°
4	Gravel Base and Drain	22.5	0	38°
5	Oil Sand	20	0	40°
6	Limestone Bedrock	23	10,000	35°

Table 4.7 Material properties for stability analysis

The water table is considered to be below the structure because of the drainage layer. Therefore, two pore water pressure conditions are considered: 1) there is no water table and 2) the water table is located between the gravel sub-base and the compacted oil sand. This is a horizontal water table 3 metres below the concrete pavement surface. The second condition represents the worst-case scenario and assumes the drainage layer is not functioning due to blockage of the under drain.

Slope/w provides two options, constant and variable, to represents the reinforcement in the RE Wall. Figure 4.10 shows a typical case of an earth-reinforced wall; if the constant option is selected, the anchors 1 through 4 are ignored, and the full force of anchor 5 is applied. If the variable option is selected, as in the case under study, anchors 1 and 2 are ignored, and anchors 3, 4, and 5 are considered for equilibrium in the stability analysis. For anchors 3 and 4, the forces are calculated as a fraction of the total force specified for each anchor. This fraction is calculated as follow:

$$anchor \ load = \frac{b}{a} x(allowable \ tensile \ force) \qquad (4.14)$$

$$\frac{b}{a} \le 1.0 \ ,$$

where *a* and *b* are defined in Figure 4.10. The force of anchor 5 is fully applied.
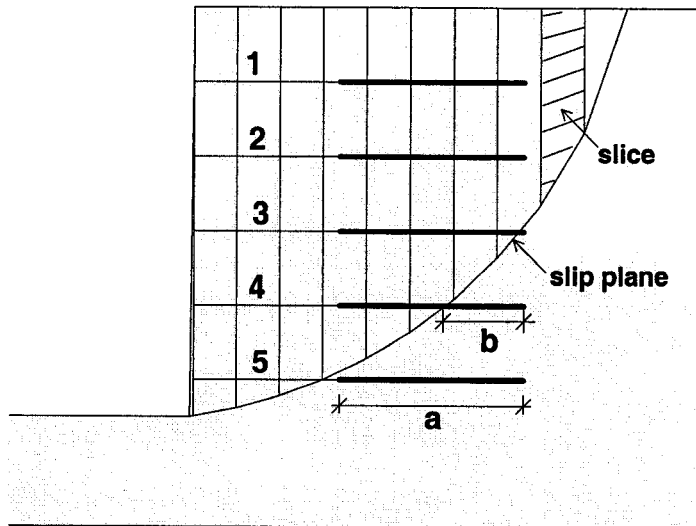
Figure 4.10 Typical representation of a earth reinforced wall

Mitchell and Christopher (1990) suggested that the distribution of the tensile force along the reinforcement could be represented as that given in Figure 4.2. Figure 4.3 (a) and (b) present a schematic maximum tensile force line for inextensible reinforcement and (c) for extensible reinforcement, where L_e is the embedment length and L_a is the distance from the facing to the point of maximum tensile force.

The retaining wall under study uses steel welded wire mesh reinforcement and is therefore classed as "inextensible." Consequently, the maximum tension line must be as shown in Figure 4.3(a) or (b). Therefore, the maximum tension line shown in Figure 4.3(b) was used to estimate the reinforcement embedment length. The distances L_e and L_a are computed in Table 4.8, and the calculated values of L_e are the embedment lengths used in the stability analysis. Figure 4.11 presents a graphical representation showing the reinforcement in the Slope/W model. The anchor load was set to the variable condition

99

(in Slope/w) and defined according to equation (4.14) during the stability calculations. The forces introduced in each reinforcement layer are calculated and presented in Table 4.6.

Layer	Depth (m)	L_a (m)	L_e (m)	Layer	Depth (m)	L_a (m)	L_e (m)
1	0	4.478	8.772	14	7.93	3.156	10.094
2	0.61	4.376	8.874	15	8.54	3.054	10.196
3	1.22	4.274	8.976	16	9.15	2.986	10.264
4	1.83	4.173	9.077	17	9.76	2.584	10.666
5	2.44	4.071	9.179	18	10.37	2.279	10.971
6	3.05	3.969	9.281	19	10.98	1.974	11.276
7	3.66	3.868	9.382	20	11.59	1.669	11.581
8	4.27	3.766	9.484	21	12.2	1.364	11.886
9	4.88	3.664	9.586	22	12.642	1.146	12.107
10	5.49	3.563	9.687	23	13.404	0.762	12.488
11	6.1	3.461	9.789	24	14.166	0.381	12.869
12	6.71	3.359	9.891	25	14.928	0.000	13.250
13	7.32	3.258	9.992				

<p align="center">Table 4.8 Calculation of L_a and L_e</p>

The reasons for modeling the reinforcement using Slope/w in this way are the following:

- The first layer of reinforcement is the critical layer because its L_e is the shortest.

- L_e is used to determine the length required to develop T_{allow} that produces a reasonable and economical design. For this reason, it is assumed that L_e of the first layer is not longer than is required to develop T_{allow} .

- The subsequent layers of the same welded wire mesh type must have the same L_e that is specified for the first one because if it is longer, it will exceed T_{allow}.

- In the same manner, the following groups of layers are defined as shown in Figure 4.9.

A series (no less than 8) of Slope/W analyses were carried out to determine the global Factor of Safety and the location of the critical slip surface. Table 4.9 summarises these stability analyses results. From these results, the following conclusions are made:

- The results numbered 2, 4, 6, and 8 (Table 4.9) include the pore water pressure given in section 4.5.3 and give the lowest Factor of Safety (1.14 to 1.8). This condition is considered as the worst-case scenario, with the drainage layer not functioning while the wall is subjected to the maximum surcharge

- The results 1 and 5 (Table 4.9) concern the mining trucks during the dumping operation. Under this loading condition, the Factor of Safety for RE wall ranges from 1.9 to 2.7 RE wall performs well, in a conservative manner. Figure 4.13 (a) and (b) shows a graphical view of results 1 and 5, respectively.

- The results 3 and 7 (Table 4.9) are considered representative for the RE wall functioning under normal working condition. For these conditions the Factor of Safety range from 1.5 to 2.3. In Figure 4.14 (a) shows that the slip plane passes through the lower portion of the reinforcement, giving a FS=1.52. In Figure 4.14 (b), a FS=2.35 is obtained from a slip surface passing beneath the wall.

- A Factor of Safety of 1.52 (Result 3, Table 4.9) is the minimum safety factor found under the condition of a functioning drainage layer (No PWP) and maximum surcharge. This result represents the global factor of safety under the most probable and reasonable working conditions.

No.	Loading Condition	Forces	PWP	Location of Failure	F. of S.
1	205 kPa	T_{allow}	No	Through the wall	1.933
2	205 kPa	T_{allow}	Yes	Through the wall	1.343
3	205 & 102.5 kPa	T_{allow}	No	Through the wall	1.527
4	205 & 102.5 kPa	T_{allow}	Yes	Through the wall	1.144
5	205 kPa	(1)	No	Below the wall	2.780
6	205 kPa	(1)	Yes	Below the wall	1.800
7	205 & 102.5 kPa	(1)	No	Below the wall	2.355
8	205 & 102.5 kPa	(1)	Yes	Below the wall	1.677

(1) The reinforcement forces are not included in the analysis because they are completely inside the sliding mass.

Table 4.9 – Results of stability analyses of the reinforced earth wall
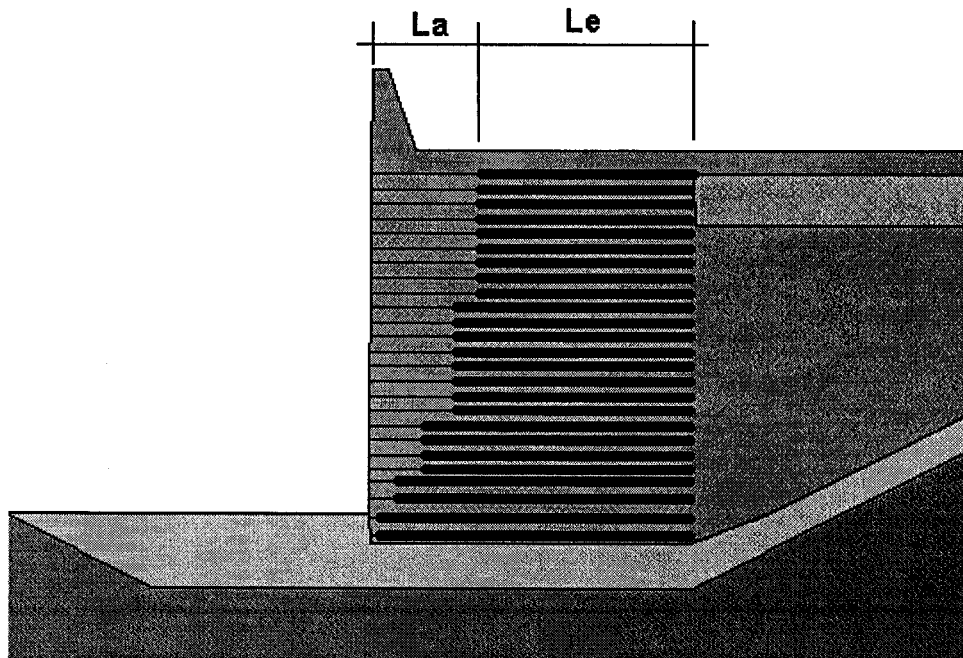
Figure 4.11 Graphical representation of the reinforcement in Slope/w (Ver. 4)

A FS=3.64 was found for the slip plane passing through the maximum tension line (Figure 4.12). The safety factor shown was calculated using the Ordinary method of slices as convergence problems were encountered using the rigorous methods such as Spencer's and Morgernstern-Price. This result is consistent with design practice in which a high factor of safety is used to control internal stability.

3.639

205 KPa

102.5 KPa
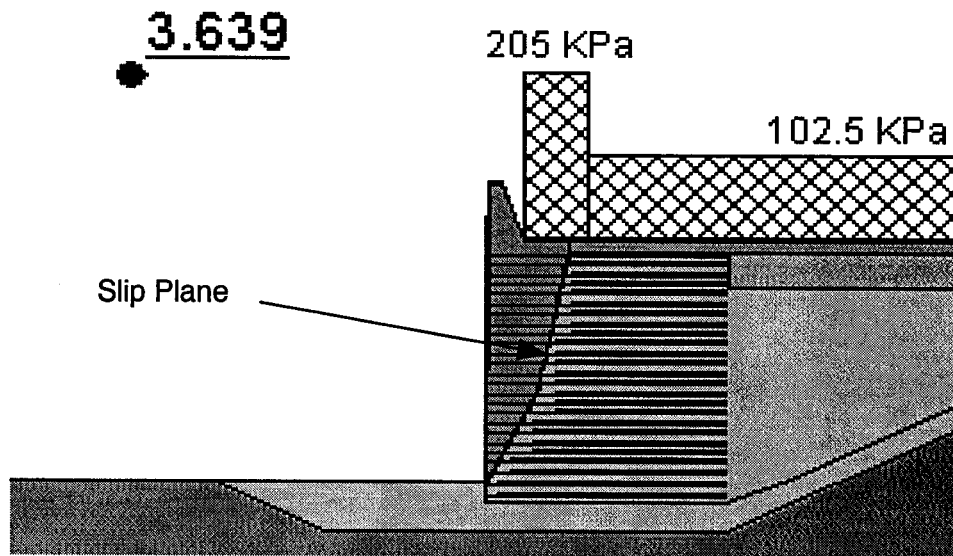
Slip Plane

Figure 4.12 Slip plane at the maximum tension line using ordinary method of slices
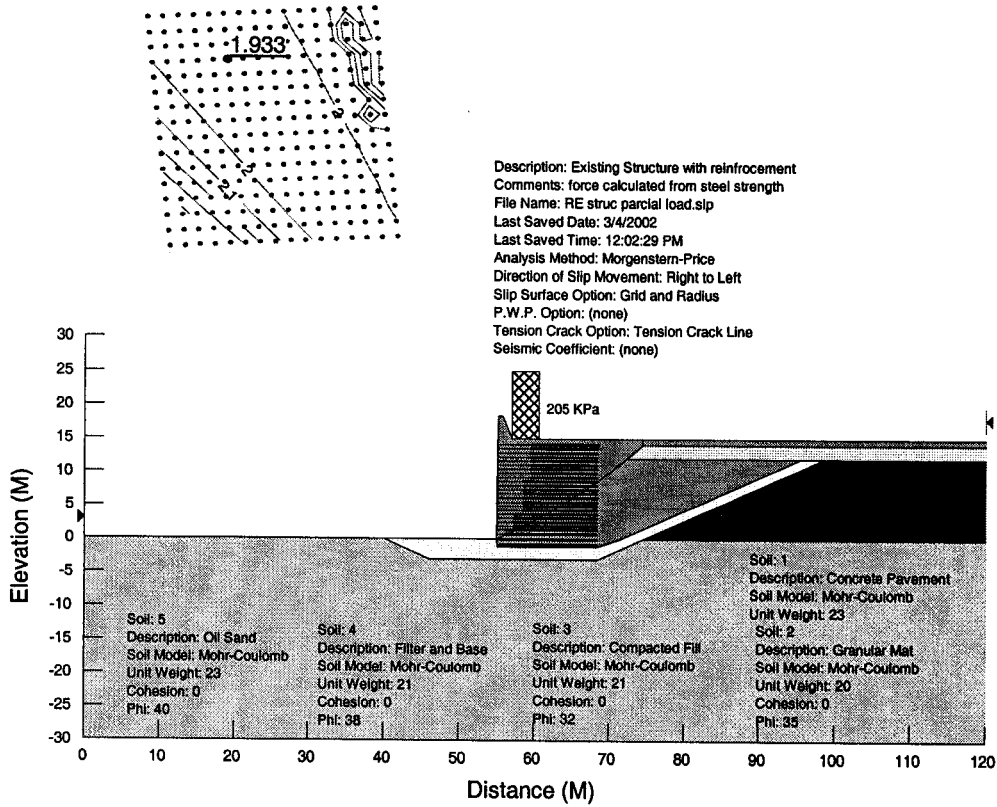
(a)
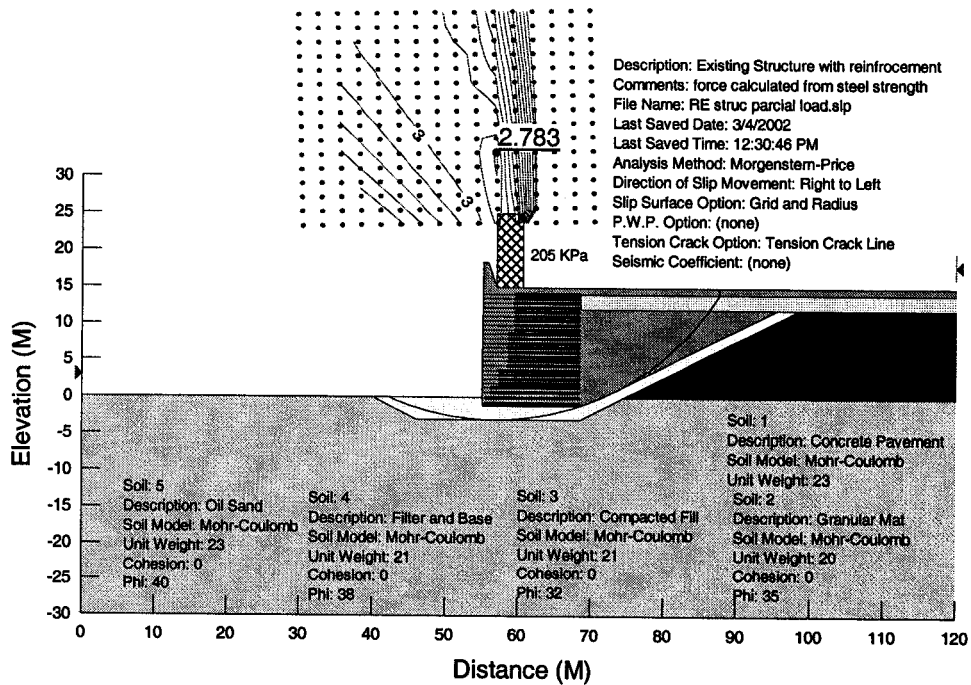
(b)

Figure 4.13 Graphical views of results 1 and 5

104

Description: Existing Structure with reinfrocement
Comments: force calculated from steel strength
File Name: RE struc full load.slp
Last Saved Date: 3/4/2002
Last Saved Time: 12:57:10 PM
Analysis Method: Morgenstern-Price
Direction of Slip Movement: Right to Left
Slip Surface Option: Grid and Radius
P.W.P. Option: (none)
Tension Crack Option: Tension Crack Line
Seismic Coefficient: (none)

1.527

205 KPa

102.5 KPa

Soil: 1
Description: Concrete Pavement
Soil Model: Mohr-Coulomb
Unit Weight: 23

Soil: 5
Description: Oil Sand
Soil Model: Mohr-Coulomb
Unit Weight: 20
Cohesion: 0
Phi: 40

Soil: 4
Description: Filter and Base
Soil Model: Mohr-Coulomb
Unit Weight: 21
Cohesion: 0
Phi: 38

Soil: 3
Description: Compacted Fill
Soil Model: Mohr-Coulomb
Unit Weight: 21
Cohesion: 0
Phi: 32

Soil: 2
Description: Granular Mat
Soil Model: Mohr-Coulomb
Unit Weight: 20
Cohesion: 0
Phi: 35

Elevation (M)
Distance (M)

(a)

Description: Existing Structure with reinfrocement
Comments: force calculated from steel strength
File Name: RE struc full load2.slp
Last Saved Date: 3/4/2002
Last Saved Time: 1:01:25 PM
Analysis Method: Morgenstern-Price
Direction of Slip Movement: Right to Left
Slip Surface Option: Grid and Radius
P.W.P. Option: (none)
Tension Crack Option: Tension Crack Line
Seismic Coefficient: (none)

2.355

205 KPa

102.5 KPa

ement

Unit Weight: 23

Soil: 2
Description: Granular Mat
Soil Model: Mohr-Coulomb
Unit Weight: 20
Cohesion: 0
Phi: 35

Soil: 5
Description: Oil Sand
Soil Model: Mohr-Coulomb
Unit Weight: 20
Cohesion: 0
Phi: 40

Soil: 4
Description: Filter and Base
Soil Model: Mohr-Coulomb
Unit Weight: 21
Cohesion: 0
Phi: 38

Soil: 3
Description: Compacted Fill
Soil Model: Mohr-Coulomb
Unit Weight: 21
Cohesion: 0
Phi: 32

Elevation (M)
Distance (M)

(b)

Figure 4.14 Graphical views of results 3 and 7

4.6 Evaluation of the Proposed Sulphur Concrete Retaining Wall.

In this section, an evaluation of the proposed sulphur-concrete wall is carried out using Slope/w (Version 4). The sulphur-concrete retaining wall has exactly the same geometry, the mining trucks surcharges, and the pore water pressures used to analyse the reinforced earth retaining wall in the previous section. The only change is that a mix of sulphur concrete composed of sulphur, fly ash and tailing sand replaces the compacted lean oil sand reinforced with welded wire mesh. The strength of sulphur concrete, the wall itself, is modelled by using cohesion only.

4.6.1 Shear Strength of Sulphur Concrete.

The shear strength of soils and rock is frequently characterized by the well known Mohr-Coulomb failure envelope give as:

$$\tau = c + \sigma \tan \phi \quad ,\qquad (4.15)$$

where τ is the shear strength, c is the cohesion, σ is the normal stress, and ϕ is the angle of internal friction. This equation suggests that the cohesion and fiction are mobilized instantly and simultaneously. However, as noted by Hajiaabdomajid et al. (2000) the strength of brittle materials, such as sulphur-concrete, is best represented by portioning cohesion and friction as a function of plastic strain. In their model, they propose that the cohesive strength component in equation 4.15 controls the strength of brittle materials at small plastic straining. Therefore, the cohesion is mobilized first and by the time that friction is mobilized, most of the cohesion is lost because the bonding around the grains of sand, created by the sulphur, are broken. A structure built with this type of material collapse after losing its cohesion.

106

The peak strength of the sulphur-concrete is based on cohesion only, and the friction is ignored. This simplifies equation (4.15) to:

$$\tau = c \tag{4.16}$$

To define the cohesion, unconfined or uniaxial compression tests with different proportions of sulphur, fly ash and tailing sand were carried out. In these compression tests, the cohesion was evaluated from the Mohr circle as follows:

$$c = \frac{\sigma_1 - \sigma_3}{2} \tag{4.17 a}$$

Because in the uniaxial test the minor principal stress (σ_3) is equal to zero and the major principal stress (σ_1) is equal to the peak stress, equation (4.17 a), reduces to:

$$c = \frac{\sigma_1}{2} \quad , \tag{4.17 b}$$

where σ_1 at failure is equivalent to the Peak Unconfined Compressive Strength (UCS).

4.6.2 Preliminary Stability Analysis of the Sulphur Concrete Retaining Wall

Figure 4.15 presents a schematic layout of the sulphur-concrete retaining wall. The material properties are the same as those presented in Table 4.7. The only new material is the sulphur concrete, and its shear strength is varied. The surcharges from the Mining Trucks are applied in the same way as was explained in Section 4.5.1 and by applying the Partial and Full loading conditions as shown in Figures 4.6 and 4.7, respectively. Again, the pore water pressure is specified for two conditions, as was explained in Section 4.5.3.

Table 4.10 presents the results of the preliminary stability analysis, and they are plotted in Figure 4.16, showing that as the cohesion of the sulphur concrete increases the Factor of Safety nonlinearly.
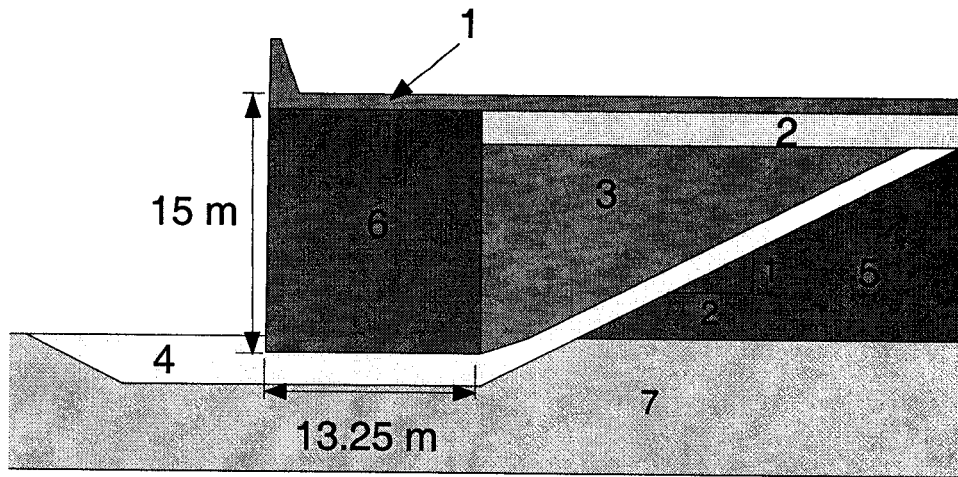
107

1. Concrete Pavement
2. Gravel Sub-base
3. Compacted Lean Oil Sand
4. Gravel Base and Drain
5. Oil Sand
6. Sulphur Concrete
7. Limestone Bedrock

Figure 4.15- Sulphur-concrete retaining wall scheme

Load Condition	Pore Water Pressure	F of S C=200 φ=0	F of S C=300 φ=0	F of S C=350 φ=0	F of S C=400 φ=0	F of S C=500 φ=0
205 & 102.5 kPa	Yes	1.148	1.535	1.585	1.618	1.618
205 & 102.5 kPa	No	1.176	1.668	1.914	2.096	2.216
205 kPa	Yes	1.482	1.772	1.772	1.772	1.772
205 kPa	No	1.516	2.159	2.487	2.654	2.764

205 & 102.5 kPa: means that the full loading condition is applied.

205 kPa: means that the partial loading condition is applied.

Table 4.10 Preliminary stability analysis results of the sulphur-concrete wall
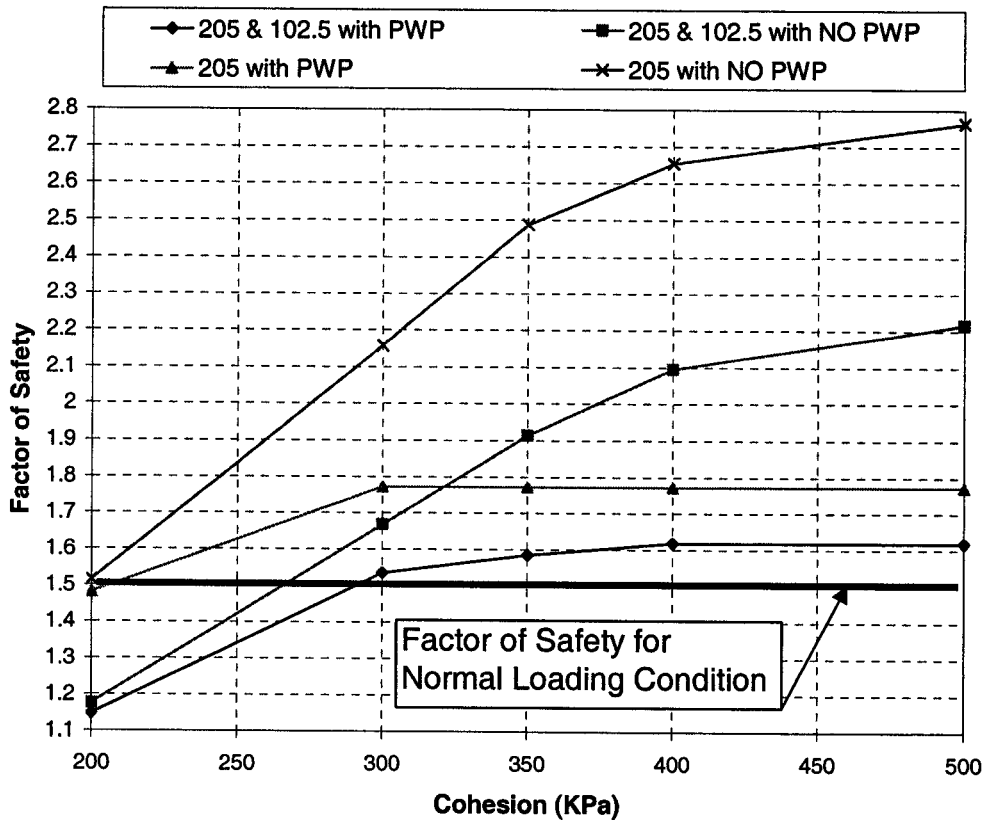
Figure 4.16 Sulphur-concrete retaining wall Factor of Safety versus cohesion

Figure 4.16 shows that to achieve a Factor of Safety of 1.5 for all loading conditions the minimum uniaxial strength of the sulphur-concrete must be 600 kPa (c = 300 kPa). Figure 4.16 also shows that if cohesion reduced to 200 kPa the Factor of Safety is reduced to 1.1 for some loading situation. Figure 4.17 shows the critical slip circle for a factor of safety of 1.53, with cohesion equal to 300 kPa, and under the condition of no functioning the drainage layer (including PWP) and maximum surcharge.

These finding suggest that to meet the Factor of Safety of 1.5 obtained for the RE wall the cohesion of the sulphur concrete must be equal to 300 kPa. However, because the sulphur concrete is a brittle material and the cohesion is lost after a small amount of

plastic strain, a minimum factor of safety for design of 2.0 is recommended. Figure 4.16

indicates that increasing the cohesion to 400kPa provide a range in the Factor of Safety

from 1.6 to 2.6 with 1.6 being the condition for no drainage. Figure 4.18(b) shows a

Factor of Safety of 2.09 for the sulphur-concrete wall, with a cohesion of 400 kPa, under

the most probable and reasonable working condition that include a functioning drainage

layer (No PWP) and maximum surcharge. From equation (4.17) a cohesion of

approximately 400 kPa could be reached with a unconfined compressive strength of 800

kPa for sulphur concrete.
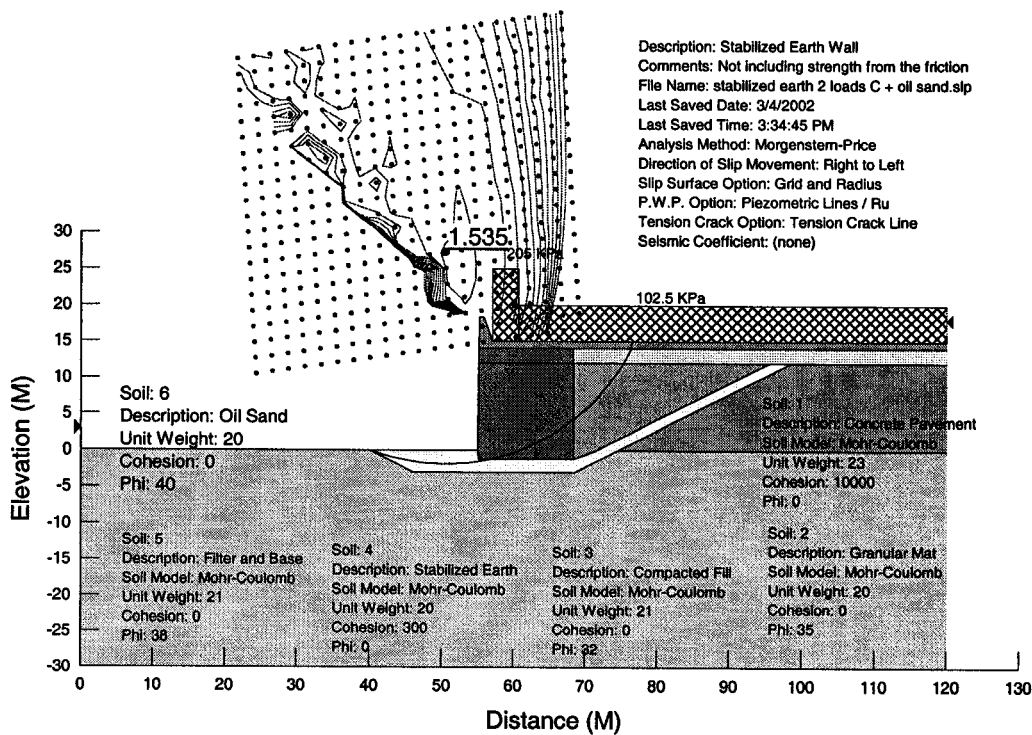
Figure 4.17 Results of sulphur-concrete wall under PWP and full load condition
with a C=300 kPa
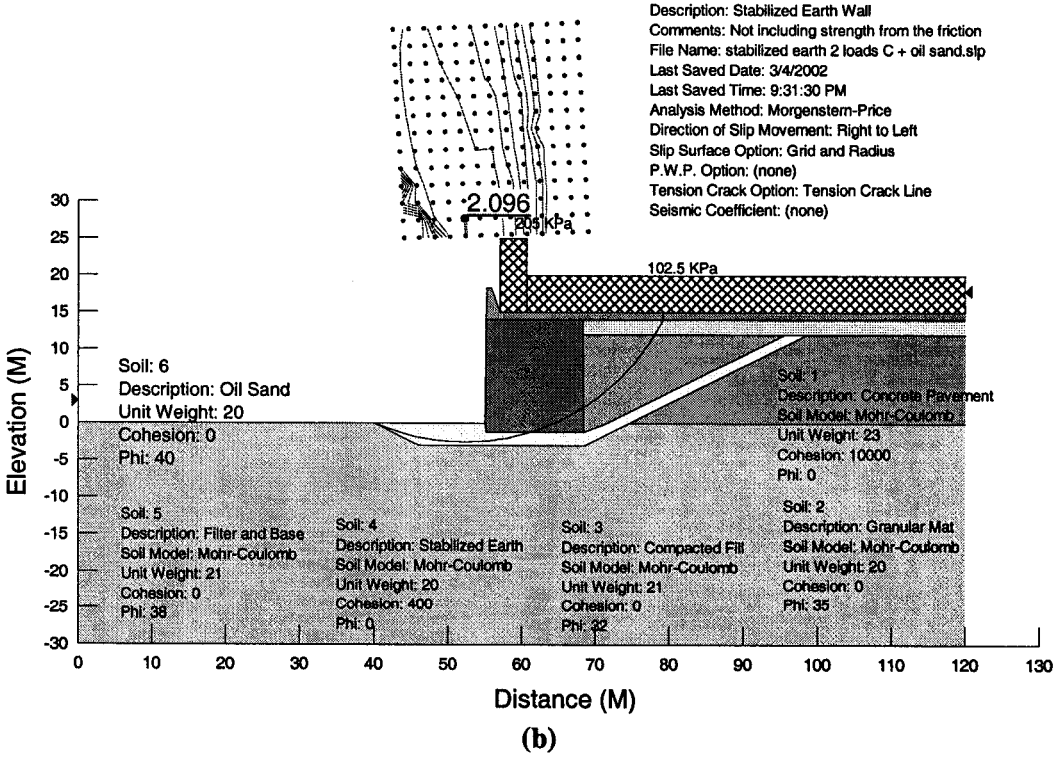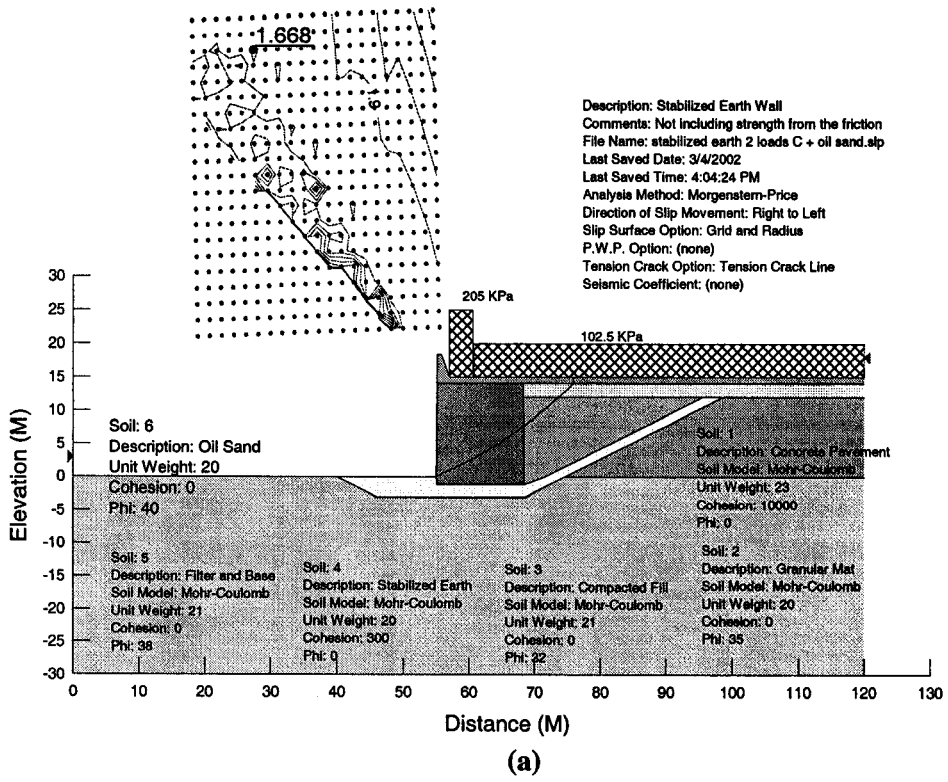
Figure 4.18 Results of the sulphur concrete retaining wall under full load and no PWP: a) C=300 kPa and b) C=400 kPa

4.6.3 Final Stability Analysis of the Sulphur Concrete Retaining Wall

The freeze-thaw durability of the sulphur concrete is the major concern regarding the use of this material for building the retaining wall. It was observed in the freeze-thaw durability test during this investigation that the mixes proposed in Section 3.2.4 deteriorated and failed to pass the test. However, the sulphur concrete mix 15Su3FA showed no significant deterioration in strength and deformation properties for up to 100 freeze-thaw cycles. The yield compressive strength after 100 freeze-thaw cycles was 11,700 kPa which would provide a cohesive strength of 5,850 kPa. Table 4.11 presents the factor of safety calculated with this cohesion.

Load Conditioin	Pore Water Pressure	Factor of Safety C=5850 kPa
205 & 102.5 kPa	Yes	1.618
205 & 102.5 kPa	No	2.296
205 kPa	Yes	1.772
205 kPa	No	2.764

Table 4.11 Final stability analysis with a C=5,850 kPa

Figure 4.19 (a) shows the results under full loading condition and including pore water pressures. Figure 4.19 (b) involves the same loading condition but with no pore water pressures. The figures show that when the cohesion reaches a certain magnitude the slip surfaces touches the heel of the wall, rather than going through the wall as is shown in Figures 4.17 and 4.18, this is the reason for the non-linear relationship of Factor of Safety versus cohesion in Figure 4.16. For all loading conditions Figure 4.16 indicates that with a value of cohesion equal to 500 kPa the critical slip surface does not pass through the retaining wall. Hence the sulphur concrete could withstand more than 100 freeze-thaw cycles before the strength is reduced to c = 500 kPa. Because the sulphur concrete wall has enough strength not to fail in shearing.

(a)

(b)
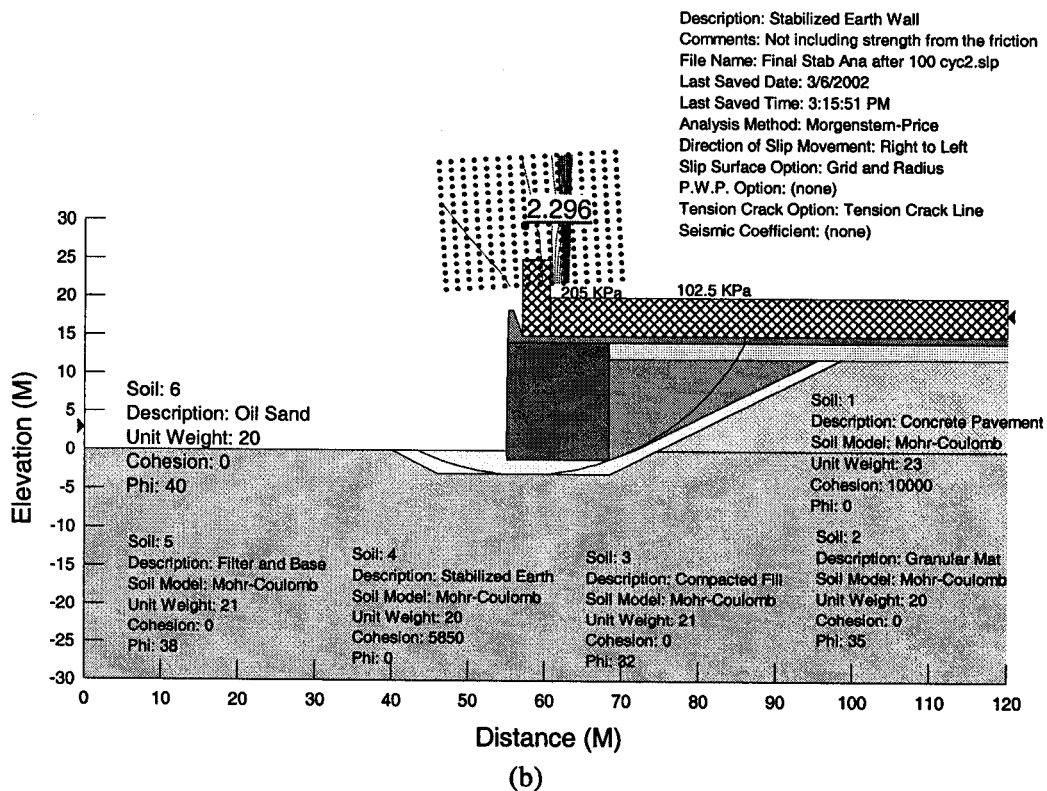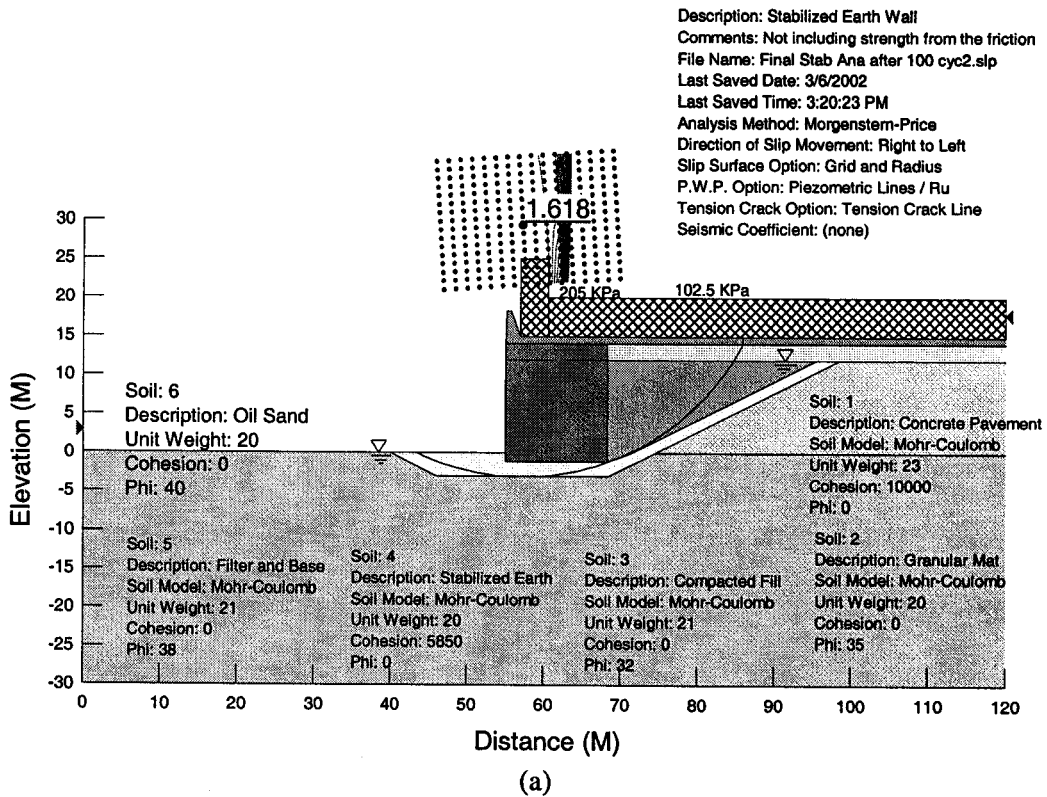
Figure 4.19 Final stability analysis of the sulphur concrete wall

113

4.7   External Stability

The sliding, overturning and bearing capacity failures are referred to as the external stability because these mechanisms involve the earth around the wall while the wall itself is considered as a monolithic structure. The common practice for the evaluation of these mechanisms is addressed in the next section.

4.7.1   General Practice

4.7.1.1   Sliding

The factor of safety against sliding is computed by dividing the horizontal resisting force (P_R/b) by the horizontal driving force (P_D/b), as described by Coduto (1994):

$$SF_s = \frac{\sum (P_R / b)}{\sum (P_D / b)} \quad ,$$

(4.18)

where b is the unit length of the wall. The Canadian Foundation Engineering Manual (1992) recommended an SF_s greater or equal to 1.5, and stated that if the passive pressure in front of the wall is considered, then the SF_s must be greater than 2.0. For cohesionless soils, Wu (1975) emphasised that usually the critical slip surface is through the active zone (in the back of the wall), and that it continues through to the bottom of the wall and reach the surface, in front of the wall, through the passive zone. However, the Canadian Foundation Engineering Manual (1992) noted that if weak layers are present in the soil or rock, the mechanism of sliding along the weak layer must be considered in the analysis. Furthermore, the authors of this manual also pointed out the need to consider the effect of the pore water pressures and seepage.

4.7.1.2   Overturning

Coduto (1994) presented the factor of safety against overturning as follows:

$$FS_M = \frac{\sum (M_R / b)}{\sum (M_D / b)} \tag{4.19}$$

where M_R/b is the sum of resisting moments per unit length of the wall; M_D/b is the sum of the overturning moments per unit length of the wall; and b is the unit length. Traditionally, the point of rotation was taken about the toe, but doing so implies that the soil is infinitely strong. Observations of walls that have failed in overturning have shown that the point of rotation is somewhere between the toe and the midpoint of the footing. Coduto (1994) mentioned that as the wall overturns, a bearing capacity failure occurs in the soil below the toe of the footing. If the soil is strong, the ultimate bearing capacity is large, so the centre of overturning is closer to the toe; if the soil is weak, it is closer to the midpoint. Coduto (1994) also recommended the use of trial and error to find the centre of rotation that will produce the lowest factor of safety and mentioned that it is usually found between 0.1B and 0.3B measured from the toe, where B is the width of the footing.

Moreover, Coduto (1994) pointed out the following:

- The footing may move rearward if an overturning failure occurs; consequently, the resistance offered by the passive force in front of the footing is not reliable and should be neglected in the overturning analysis.

- In a limit equilibrium condition (i.e., if the wall is in the process of overturning), only the part of the footing forward of the point of rotation would be in contact with the soil, and the soil beneath this zone would be experiencing a bearing capacity failure. Therefore, for overturning analysis, the normal force acting below the footing acts over a width equal to the distance from the toe to the centre of rotation and is calculated by using the ultimate bearing capacity.

- The shear force between the footing and the ground does not affect the overturning stability because it has no moment arm.

- The required factor of safety is at least 1.5 for cohesionless soils, and 2.0 for cohesive soils.

4.7.1.3 Allowable Bearing Pressure and Settlement

The maximum soil pressure should not exceed the allowable soil pressure derived from considerations of bearing capacity and settlement. The lateral earth pressure against the back of the wall produces a moment, and the distribution of the soil pressure on the footing is not uniform, being higher at one end of the footing than the other. A retaining wall can be designed by using the same considerations about footing with eccentric or moment loads.

An eccentric load or a moment can be represented in terms of the eccentricity, e, of the resultant force that acts on the base of the footing. If an eccentric load is applied, then the resultant at the base acts immediately below the applied load, and both have the same eccentricity. If a moment is applied, then the eccentricity is calculated as:

$$e = \frac{M}{P} \quad , \tag{4.2}$$

where M is the applied moment, and P is the applied load (P times e will produce the effect of M). The maximum and minimum net-bearing pressure can be estimated from the following expressions:

$$q_{min} = \frac{P}{A}\left(1 - \frac{6e}{B}\right) \tag{4.21}$$

116

$$q_{mas} = \frac{P}{A}\left(1 + \frac{6e}{B}\right) \ ,$$ (4.22)

where q_{min} and q_{max} are the minimum and the maximum net-bearing pressures, respectively; A is the base area of footing; and B is the width of footing. If e<B/6, the bearing pressure has a trapezoidal distribution, or if e=B/6, then the bearing pressure is a triangular distribution (q_{min}=0). However, if e>B/6, the resultant force is outside the middle third, and the footing is on tension to some extent, generating high bearing pressures at the toe that may cause large settlement with excessive tilting, which is not desirable

Coduto (1994) remarked that walls that meet the previous criteria of e ≤ B/6 usually do not have problems with excessive settlement. Generally, a settlement analysis is necessary only if q_{toe} exceeds the preconsolidation pressure

4.7.2   Forces Acting Against the Retaining Wall

The forces on the wall can be divided as acting on the driving side and resting the resistant side. The forces on the driving side are the active forces generated by the retained material itself, the truck load, and the weight from the concrete pavement. On the other side, the resistant forces are the friction forces generated in the interface between the sulphur concrete wall and the gravel base, and the passive force in front of the wall toe (see Figure 4.20).

The compacted lean oil sand backfill and the granular base beneath the wall shown in Figure 4.20 are considered sufficiently compliant to allow the movement required to reduce the earth pressure to values significantly lower than the at-rest pressures. Consequently the active earth pressure for the design can be calculated by the Coulomb

117

theory, as indicated by Duncan et al. (1990). Moreover, Clough and Duncan (1992) indicated that the induced compaction stresses are released because of the deformation given after compaction reaching the limiting active condition. Therefore, the induced compaction stresses are not included in the analysis. The coefficients of active earth pressure are calculated by the equation 4.17 and shown in Table 4.12.
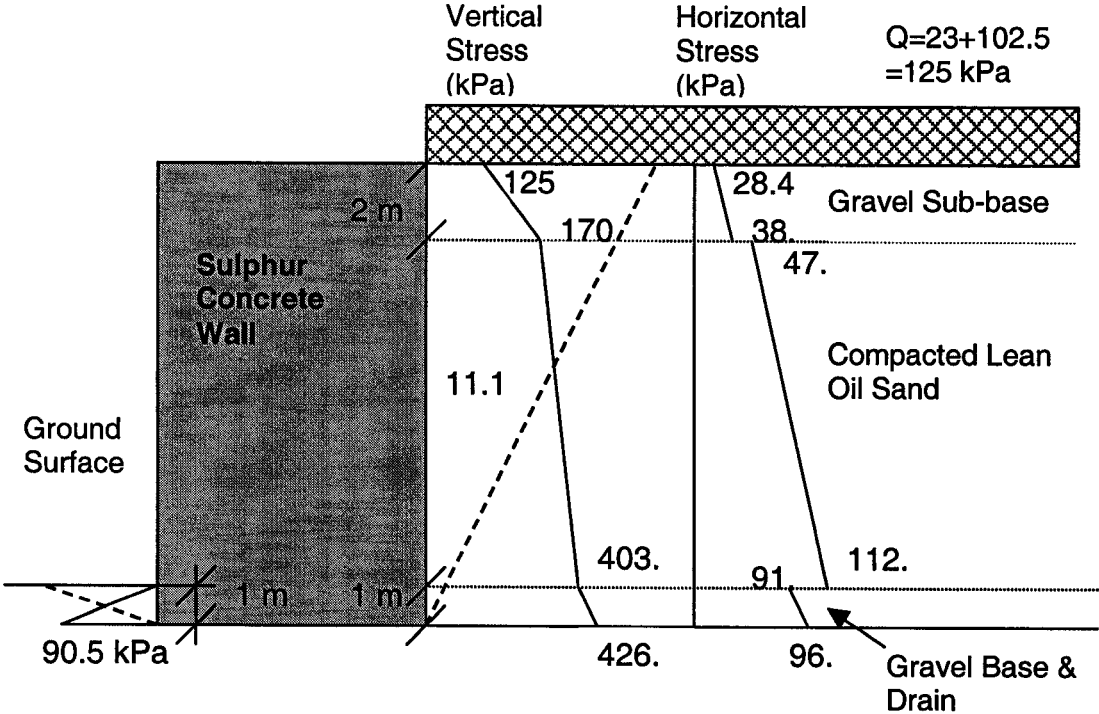
Figure 4.20 Horizontal stresses against the wall and the geometry (dotted line) to assess the sliding stability

Table 4.12 Coefficients of active earth pressure

Material	φ	θ	δ	α	K_a
Gravel Sub-base	38	0	19	0	0.2172
Compacted Oil Sand	32	0	16	0	0.2782
Gravel Base	38	0	19	0	0.2172

118

The coefficient of passive earth pressures estimated by the Coulomb theory are known to give high values on the unsafe side (Morgenstern and Eisentein, 1970). Although many other theories such as those of Shields and Tolunay (1973) and Caquot and Kerisel (1956) can be used to estimate this coefficient, the Rankine theory is chosen because the contribution of the passive force to resist sliding in this particular case is very small. The value of K_p estimated by using the equation 4.4 for the gravel base is 4.02. For design purposes, a factor of safety of 2 is applied to the coefficient of passive earth pressure.

The pore water pressure applies additional lateral force on the wall, at the same time the effective stress is reduced. In this particular case, a water table is not considered under working loads because drainage provisions which underlay the backfill are included. Consequently, the lateral stresses from pore water pressures are not included in the analysis. (See also section 4.5.3.)

The Mining Trucks and the concrete pavement are treated as a uniform linear surcharge. The concrete pavement is considered as a permanent surcharge of 23 kPa applied to top of the wall. The Mining Trucks waiting line introduces a uniform surcharge of 102.5 kPa. Both surcharges are multiplied by the coefficient of active earth pressure of each layer shown in Table 4.12, to calculate the horizontal stress against the wall.

Figure 4.20 shows the resultant horizontal stresses against the wall. In the same way, horizontal maximum passive stress of 90.5 kPa is calculated at the toe, as is shown on the left side of Figure 4.20. This stress distribution and the weight of the wall are used to calculate the horizontal and vertical forces per metre on the driving and resistant side of the wall.

4.7.3 Sliding Stability of the Sulphur Concrete Wall

This section refers to the stability of a slip surface that involves the active zone, passing throughout the interface between the wall and the gravel base, and coming out through the passive zone, as represented by the dotted line in Figure 4.20. In this case, this type of sliding is resisted by the interface friction between wall and the gravel base, and by the passive earth pressure of the gravel base in front of the wall. The factor of safety against sliding is calculated by Limit Equilibrium (see Section 4.6.1.1, and equation 4.18).

The factor of safety was calculated under two loading situations: 1) the first condition is presented in Figure 4.20 in which the load of 125 kPa represents the trucks waiting line and the pavement, and 2) The second condition includes an additional load of 205 kPa, which represents a truck on the wall, dumping the ore. During the first condition, the weight of the truck contributes to an increase in the friction resistance, resulting in a Factor of Safety of 2.2. When no truck is on top of the wall, the Factor of Safety decreases to 1.88, greater than the minimum required of 1.5. The detailed calculation of the sliding stability is included in Appendix A.

4.7.4 Overturning Stability of the Sulphur Concrete Wall

The factor of safety against overturning is determined by dividing the sum of moments tending to resist rotation of the wall about its toe, by the sum of the moments tending to produce the overturning, (see equation 4.19).

120

Traditionally, the centre of rotation is taken at the toe. However, during overturning, a local bearing capacity failure around the toe can happen, which results in moving the centre of rotation towards the backfill (Coduto, 1994). The most critical location, measured from the toe, is found to lie between 0.1 and 0.3 the base width, (see Section 4.6.1.2). The same two loading conditions as used in Section 4.7.3 are taken into account in the analysis.
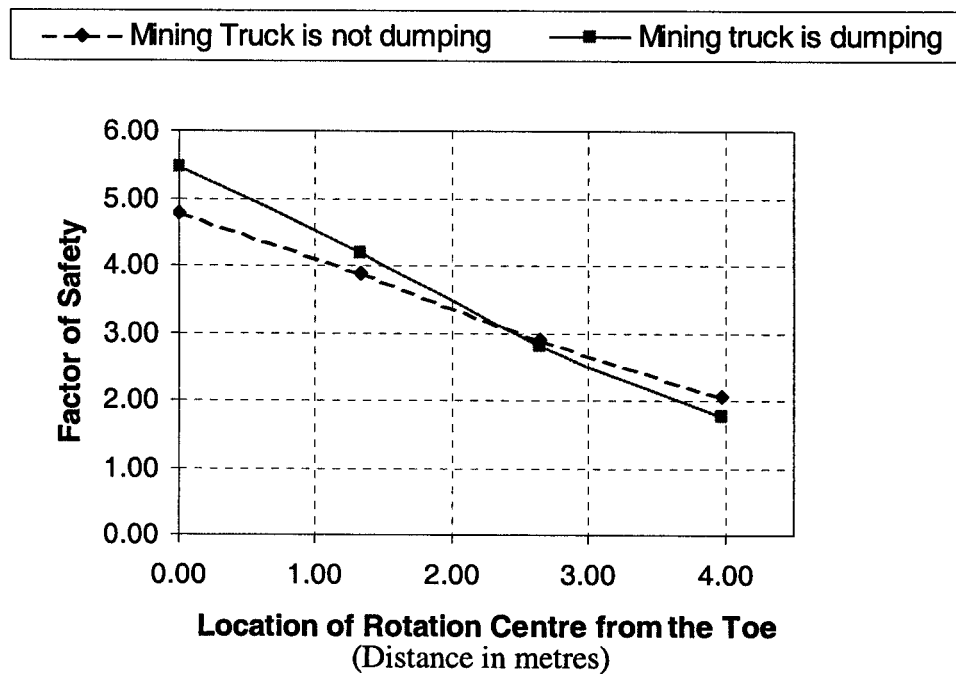
Figure 4.21 Factor of Safety against overturning

Figure 4.21 shows how the factor of safety against overturning decreases while the centre of rotation is moved away the toe. A factor of safety of 1.77 results by assuming that the rotation centre is located at 0.3 times the base width (about 4 metres from the wall face) and that the mining truck is located on top of the wall. These assumptions resulted in the lowest Factor of Safety, (Figure 4.21). When the truck is not on top of the

wall, the factor of safety is about 2.0. The complete overturning stability calculation is presented in Appendix B.

4.7.5 Contact Pressure Below the Wall (Bearing Capacity Failure) of the Sulphur Concrete Wall

The design of the sulphur-concrete wall requires an estimate of the allowable soil pressure on the foundation. However, because we are suggesting a solution equivalent to the existing reinforced-earth wall, the allowable soil pressure indicated in the contract drawings of 476 kPa is used (See McCavour Engineering LTD, Drawing S01A dated 02/16/00).

The wall has to support the working loads not exceeding the allowable contact pressure, and the lateral load produces a moment that is supported by the foundation. This rotation creates a non-uniform stress distribution beneath the wall, generating the maximum contact pressure in the outer edge and the minimum contact pressure in the inner edge of the wall, known as q_{max} and q_{min}. They are calculated by static equilibrium using equations 4.21 and 4.22, respectively.

The contact pressure is calculated using the two conditions, 1) when the mining truck is dumping from the top of the wall and 2) when no mining truck is on top. For both conditions, the surcharge caused by the waiting line of trucks is acting. The maximum bearing pressures, estimated under the first two conditions, are 548 kPa and 464 kPa, respectively. The pressure of 548 kPa exceeds the maximum allowable pressure by 13%. Without any mining truck, the maximum contact pressure is 390 kPa, almost 18% less than the allowable.

4.8 Summary

The existing reinforced earth retaining structure was evaluated using the Limit Equilibrium Method. The geometry was defined from the contract drawings (Figure 4.3) and the surcharge loads were defined from the weight (Table 4.2) and dimensions (Figure 4.4) of the CAT 797 mining truck. The reinforcement forces were estimated based on the contract drawings and introduced in Slope/W to calculate the global Factor of Safety and the location of the critical slip surface:

1. A Factor of Safety of 1.53 is the minimum found under the condition of a functioning drainage layer (No PWP) and maximum surcharge (Figure 4.14(a)). This result represents the global Factor of Safety under the most probable and reasonable working conditions.

2. A Factor of Safety of 3.64 was found for the slip plane passing through the maximum tension line (Figure 4.12). This result is consistent with design practice in which a high factor of safety is used to control the internal stability.

The sulphur-concrete retaining wall was evaluated using the same approach as above. The peak shear strength of the sulphur-concrete is based on cohesion only, and the friction is ignored. The cohesion is based in the unconfined compressive strength (equation 4.17b). The results of these stability analyses (Figure 4.16) show that as the cohesion of the sulphur-concrete increases the Factor of Safety increases nonlinearly. From the results the following is concluded:

1. To meet the Factor of Safety of 1.5 obtained for the RE retaining wall the cohesion of the sulphur concrete wall must be equal to 300 kPa.

2. Because the sulphur-concrete is a brittle material and the cohesion is lost after a small amount of plastic strain, a minimum Factor of Safety of 2 is recommended. Increasing the cohesion to 400 kPa is obtained a Factor of

123

Safety of 2.09. This is obtained with the drainage layer functioning (No PWP) and under maximum surcharge. From equation (4.17) a cohesion of 400 kPa could be reached using a sulphur-concrete with a unconfined compressive strength of 800 kPa.

3. The sulphur-concrete wall was evaluated using the yield compressive strength of 11,700 kPa, obtained after 100 freeze-thaw cycles, from the 15Su3FA sulphur-concrete mix. This compressive strength provides a cohesive strength of 5,850 kPa. This is more than exceeds the strength required for an acceptable factor of safety.

4. The stability analyses results of the sulphur concrete wall show that when the cohesion reaches approximately 500 kPa the slip surfaces touches the heel of the wall, rather than going throw the wall. This is the reason for the non-linearity relationship of Factor of safety versus cohesion in Figure 4.16. Therefore, the shear strength of the gravel base and the compacted lean oil sand backfill become more important in the global stability of the structure when the sulphur-concrete is used to construct the retaining wall.

The sliding, overturning and bearing capacity failures were evaluated for the sulphur-concrete retaining wall; however, these results could apply to the existing RE retaining wall, since both retaining walls under study have the same geometry and similar unit weight. The forces acting against the retaining wall were calculated in Section 4.7.2. The active earth pressures were calculated by the Coulomb theory, as indicated by Duncan et al. (1990), and the passive earth pressures were estimated by the Rankine theory because the contribution of the passive force to resist sliding in this particular case is very small.

1. The lowest Factor of Safety against sliding of 1.88 results from a situation when the mining truck was not positioned on top of the wall, because the

weight of the mining truck contributes to an increase in the friction resistance force at the retaining wall base.

2. The evaluation of the overturning stability indicated that the critical condition was obtained when the mining truck was situated on top of the wall giving a minimum Factor of Safety of approximately 1.77.

3. The contact pressure of the sulphur-concrete wall achieves a maximum value of 548 kPa when the mining truck is located on top of the wall, and this value is greater than the maximum allowable soil pressure of 476 kPa, as indicated in the contract drawings of the existing structure.

5 FINITE ELEMENT ANALYSIS

Using the same geometry for the wall as was evaluated in Chapter 4, and the material properties determined from Chapter 3, a stress-deformation analysis using the finite element method was carried out. The use of sulphur concrete to construct the retaining wall will result in a massive rigid block. The stability of this block must be checked for potential cracking that could lead to slabs falling from the face of the retaining wall. In the current reinforced earth wall this is not an issue as the face of the retaining wall is heavily reinforced. To assess the potential for cracking both compressive and tensile stresses need to be considered.

The finite element analyses described in this section were conducted to determine the maximum induced tensile stress and compressive stress that could potentially develop in the sulphur concrete wall. In normal retaining wall construction the backfill is constructed in layers which induce maximum deformations near the base of the wall. Such staged procedures often leads to overall reduced deformations, and hence lower wall stresses. However, for the analysis that option, which is available in Sigma/W was not used, for two reasons: (1) by applying gravity loading to the constructed wall the maximum deformations occurs at the top of the wall which leads to greater tilting potential and higher induced stresses and (2) it is not clear that the compacted lean oil sands would be used as backfill, i.e., the sulphur concrete wall may be placed directly on the natural soil. For these reasons the finite element analysis should be considered as scoping calculations to obtain a reasonable possible range of induced stresses.

The focus of the finite element analysis was to estimate the stresses in the sulphur concrete mass under several working (loading) conditions, including different applied loads, pore water pressures, and a simulation of possible problems that could affect the

wall, due to inappropriate preparation of the foundation layer. Furthermore, various assumptions of materials properties, such as the backfill and foundation, that may directly impact the stresses inside the sulphur concrete mass, were analysed and compared. The interface interaction between the sulphur concrete wall and the backfill, and between the wall and the foundation material, was examined and its effect on the stresses in the wall determined.

One aim, here, was to cover sensitivity analyses of several possible deviations from design, because of the uncertainties in the behaviour of the soil-structure interfaces, backfill, and foundation materials. Therefore, a discussion comparing the stress levels between different conditions is included.

5.1   Overview of the Finite Element Method

At present, there are many different calculation methods are available for analysing geotechnical structures. Potts and Zdravkovic (1999) summarized the fundamental considerations required for an exact theoretical solution. These conditions involve equilibrium, compatibility, material behaviour, and boundary conditions. The only method of analysis satisfying all these requirements is the Full Numerical Analysis (Potts and Zdravkovic, 1999).

Furthermore, Potts and Zdravkovic (1999) pointed out that the ability of these numerical methods to accurately reflect field conditions essentially depends on the ability of the constitutive model to represent real soil behaviour, and the correctness of the imposed boundary conditions. Therefore, the user has to define only the appropriate geometry, construction procedure, soil parameters, and boundary conditions. Thus, the user has to do the modelling.

Potts and Zdravkovic (1999) summarized the steps of the finite element method as follows:

- Element discretisation: This is the process of modelling the geometry of the problem under investigation through an assemblage of small regions, termed "finite elements." These elements have nodes defined on the elements' boundaries.

- Primary variable approximation: A primary variable must be selected (e.g., displacements, stresses etc.) and rules for how it should vary over a finite element established.

- Elements equations: An appropriate variational principle to derive element equations should be used:

$$[K_E]\{\Delta d_E\} = \{\Delta R_E\} \ , \qquad (5.1)$$

where $[K_E]$ is the element stiffness matrix, $\{\Delta d_E\}$, is the vector of incremental element nodal displacement, and $\{\Delta R_E\}$ is the vector of incremental element nodal forces.

- Global Equations: Element equations are combined to form global equations

$$[K_G]\{\Delta d_G\} = \{\Delta R_G\} \ , \qquad (5.2)$$

where $[K_G]$ is the global stiffness matrix, $\{\Delta d_G\}$, is the vector of all incremental nodal displacements, and $\{\Delta R_G\}$ is the vector of all incremental nodal forces.

- Boundary conditions: Boundary conditions are formulated and global equations are modified.

- Solve the global equations: The global equations 5.2 are in the form of a large number of simultaneous equations. These are solved to obtain the displacements

128

$\{\Delta d_G\}$ at all the nodes. From these nodal displacements, secondary quantities, such as stresses and strains, are evaluated.

5.2 Finite Element Software

The software selected for this study was Sigma/W, produced by Geo-Slope International (Geo-Slope, 2001). This is a general, finite element software product for stress and deformation analyses of geotechnical structures. The user can choose to use a variety of different stress-strain constitutive relationships, which range from simple linear-elastics to non-linear elasto-plastic models. Also, loads and pore water pressures can be applied, and construction stages can be simulated.

5.3 Geometric Idealisation

Because of the special geometric characteristics of many of the physical problems treated in soil mechanics, simplifications of considerable magnitude can be applied. Problems, such as the analysis of retaining walls, continuous footing, and the stability of slopes, generally have one dimension that is very large in comparison with the other two. Hence, if the force and/or applied displacement boundary conditions are perpendicular to, and independent of, this dimension, all cross sections will be the same. If the z dimension of the problem is large, and it can be assumed that the state existing in the x-y plane holds for all planes parallel to it, the displacement of any x-y cross section, relative to any parallel x-y cross section, is zero. The conditions consistent with these approximations are known as "the case of plane strain" (Potts et al., 1999).

5.4 Finite Element Mesh

5.4.1 Mesh Design

The geometry of the problems under investigation must be defined and quantified. Potts et al. (1999) pointed out that simplifications and approximations may be necessary during this process, and that the problem geometry is replaced by an equivalent finite element mesh which is composed of small regions called "finite elements." Naylor and Pande (1981) suggested that the selection of the size and shape of elements is a matter of experience and intuition; furthermore, elements should be smaller where the "action" is concentrated, such as those areas in which the stress and strains change rapidly.

The amount of computation memory and processing time required to solve the finite element equations is proportional to the number of nodes in the problem, the difference between node numbers in each element, and the integration order (Geo-Slope, 2001).

5.4.2 Elements

The starting point of the analysis is the division of the structure into elements. Naylor and Pande (1981) pointed out that the triangular and quadrilateral elements in a plane strain analysis are most commonly used.

Potts et al. (1999) noted that the accuracy of a finite element analysis depends on the elements' size and the nature of the displacement approximation. They also pointed out that compatibility conditions have to be satisfied to obtain an increase in accuracy by reducing the size of the elements. These conditions are summarized as follows: the displacement field should have continuity, the displacement approximations should be

130

able to represent rigid body movement; and the displacement approximations should be able to represent constant strain rates.

In addition, Potts et al. (1999) explained that the variation of the unknown displacements within an element is expressed as a simple function of the displacements at the nodes; therefore, the displacement field throughout the finite element mesh results from determining the displacement components at a finite numbers of nodes. Thus, for two-dimensional plane strains analysis, only two degrees of freedoms are at each node: the X and Y displacement.

Geo-Slope (2001) mentioned that the accuracy and performance of an element is affected to some extent by its shape. The best performance of quadrilateral elements is obtained when the interior angles are all 90 degrees and, for triangular elements, when one interior angle is 90 degrees and the other two are 45 degrees. Even though acceptable performance can be obtained with elements that deviate from 45 and 90 degrees, it deteriorates rapidly when any internal angle approaches zero or 180 degrees. Furthermore, Geo-Slope (2001) added that the aspect ratio of elements could also affect the performance. As the aspect ratio increases, the element performance deteriorates; consequently, a ratio of one gives the best performance.

Naylor and Pande (1981) defined isoparametric elements as the elements for which the equations describing the shape of their boundaries are of the same order as those describing the variation of the nodal unknown (e. g., displacement) across the element. Thus, for parabolic elements the equations are quadratic.

Sigma/W uses the set of general interpolating functions for finite elements presented in Bathe (1982). Sigma/W utilises isoparametric ordinary 4-noded quadrilateral elements and isoparametric 3-noded triangular elements. When an element has secondary nodes at the midpoints between the corner nodes, the element is known as a "higher order" element, since the equations describing the deformation within the element are of a higher order than when there are no secondary nodes. As well, the higher order elements are isoparametric. The interpolating functions, proposed by Bathe (1982), are linear when the secondary nodes are not used and quadratic when the secondary nodes are included.

5.4.3   Finite Element Mesh of the Sulphur Concrete Wall

As pointed out by Potts et al. (1999) element discretisation is the first step in a finite element analysis. The geometry of the sulphur-concrete retaining wall is given in Figure 4.14, and it is the same geometry evaluated using the Limit Equilibrium Method. The types of elements utilized to build the mesh were 6-noded triangular and 8-noded quadrilateral, parabolic isoparametric elements.

To model the interfaces between the wall and its surrounding material, the backfill and the foundation, 4-noded quadrilateral elements were used, with an aspect ratio of 10, as shown in Figure 5.1.

To arrive at the final mesh design, several trial steps were taken. First, higher order elements, 8-noded quadrilateral and 6-noded triangular, were used in the entire mesh. Next, the 4-noded quadrilateral elements used to model the interfaces of the wall, foundation and backfill were added. The modelling of the concrete pavement required the introduction of several features. First, interface elements were required between the concrete pavement and the gravel sub-base, as shown in the Figure 5.1, because of their contrasting stiffness. Furthermore, a gap was left between the concrete pavement on top of the wall and the concrete pavement on top of the sub-base. Actually, the contract drawings showed that on top of the wall there is concrete pavement, but on top of the sub-base roller compacted concrete (RCC) is specified. Thus, there is no continuity in the material. The concrete pavement and the RCC were modelled using the same material parameters for convenience.

At the wall's heel, just at the corner, an element with a very low Young's modulus was introduced. Figure 5.1 shows that the sulphur concrete wall is surrounded by interface elements; however, at the heel the wall was in contact with the drainage layer in the node at the corner. Therefore, an element with a very low modulus was introduced, to avoid an unrealistic stress concentration.

Figure 5.1 shows an enlarged view of the finite element mesh. Notice that most of the elements were quadrilateral, and only triangular elements were used in the drainage layer and in the transition between quadrilateral elements of differing sizes.
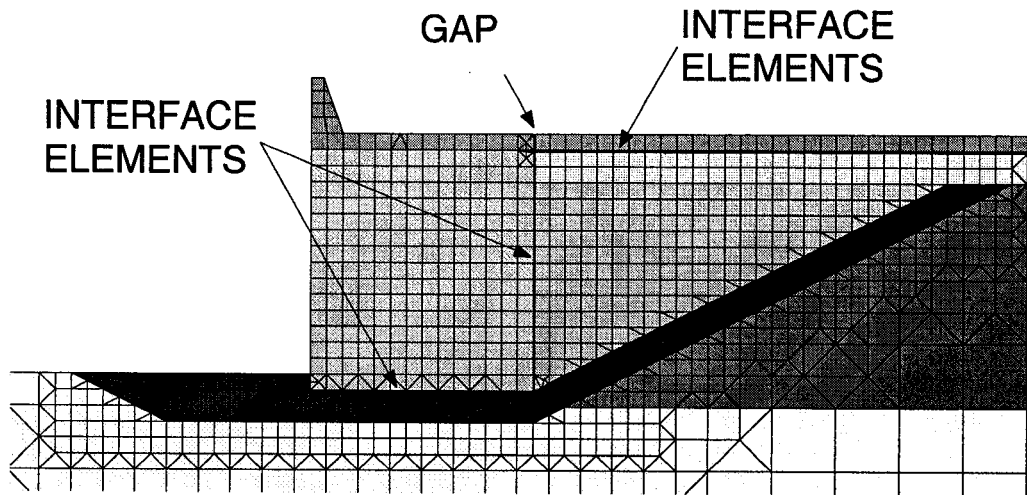
Figure 5.1 Finite element mesh and interface elements

Also, it was enforced to maintain the most accurate finite elements' shapes as possible, including squares and right triangles, as pointed out in Section 5.4.2. Figure 5.2 presents the entire finite element mesh used for analysis. The entire mesh included approximately 1800 nodes and 4700 elements, and the CPU time was approximately 10 minutes.

Figure 5.2 shows the boundary conditions introduced in the model. At the bottom, vertical and horizontal displacements were restricted, and on the vertical sides, only the horizontal displacement were restricted.
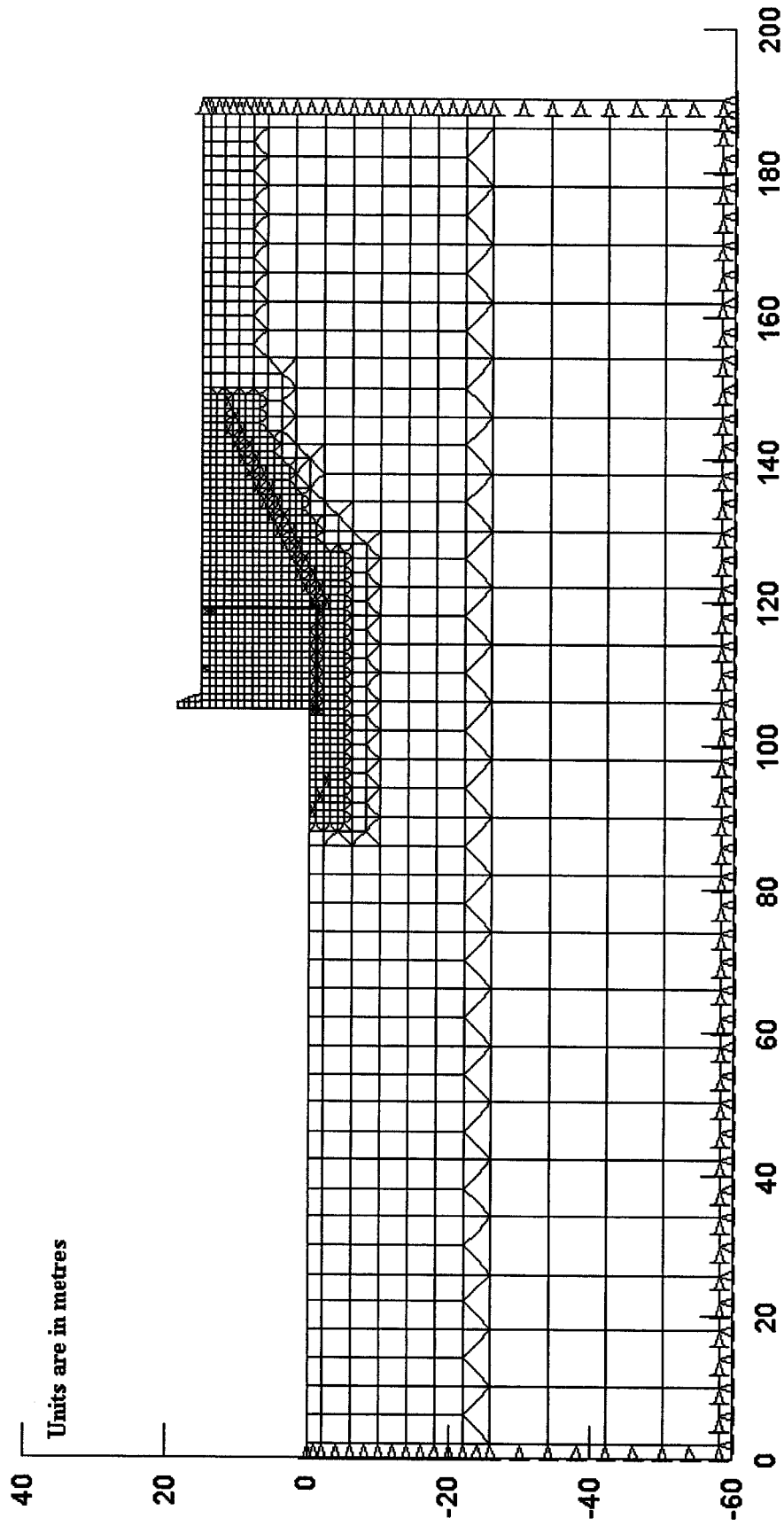
Figure 5.2 – Finite Element Mesh

Units are in metres

135

5.5 Modelling the Soil-Structure Interface

5.5.1 Finite Elements to Model Interfaces

Soil-structure interaction may occur in a situation of relative movement of the structure with respect to the soil. Potts et al. (1999) noted that continuum elements, with compatibility of displacements, in a finite element analysis of these situations prohibit relative movement at the soil-structure interface because the nodal compatibility constrains the soil and the structural face so that they move together. Thus, the interface, or joints elements, can be used to model the soil-structure boundary such as along the sides of a wall or pile or the underside of a footing. In addition, Potts et al. (1999) listed several methods that have been proposed to model discontinuous behaviour at the soil-structure interface.

In this thesis, interface elements of finite thickness were used. Goodman et al. (1968) used this special interface or joint elements to model jointed rocks. Clough and Duncan (1971) described a procedure realistically representing the soil-structure interface of the retaining wall. They used the elements defined by Goodman et al. (1968) to represent the interface in finite element analysis. Clough and Duncan (1971) used hyperbolic models, similar to those developed by Duncan and Chang (1970) to model the stress-strain behaviour of soils and to represent the non-linear stress dependent interface behaviour. They performed direct shear tests in which the soil was compacted in the upper part of the shear box and the lower part consisted of a specimen of concrete, simulating a concrete wall. Using the information from these tests, they derived four parameters K_I (dimensionless stiffness number), n (dimensionless stiffness exponent), R_f (failure ratio), and δ (angle of wall friction). The first three parameters were derived similarly to those

136

derived by Duncan and Chan (1970). In Section 5.6.2, this hyperbolic constitutive model is addressed.

Clough and Duncan (1971) performed incremental analysis changing the soil property values as appropriate for each stage of the analysis; therefore, tangent stiffness values estimated from the slope of a tangent to the shear stress-displacement curve were employed. The tangent stiffness (K_{st}) was computed from the following expression:

$$K_{st} = K_I \gamma_w \left(\frac{\sigma_n}{p_a}\right)^n \left(1 - \frac{R_f \tau}{\sigma_n \tan \delta}\right)^2 , \tag{5.3}$$

where σ_n is the normal stress, τ is the shear stress, γ_w is the unit weight of water, p_a is the atmospheric pressure (in the same unit of σ_n) and the others parameters are defined as previously. The interface elements developed by Goodman et al (1968) had properties consisting of a normal stiffness, K_n, and a shear stiffness, K_s, which are related to the normal and shear stresses acting on the element as follows:

$$K_n \Delta_n = \sigma_n \tag{5.4}$$

$$K_s \Delta_s = \sigma_s , \tag{5.5}$$

in which Δ_n is the average relative normal displacement across the element, and Δ_s is the average relative shear displacement along the element. To perform finite element analysis, Clough and Duncan (1971) assigned a large value to K_n $(10^9$ pcf), while equation 5.3 was used to estimate K_s. After an element failed in shear, with the interface still in compression, the value of K_s was reduced to a negligible value, but the value of K_n was kept large. If the elements develop tension, both K_s and K_n were assigned very small values.

137

Sigma/W allows the use of four-noded quadrilateral elements having a resistance to compression and a resistance to sliding, and their normal and shear stiffness are defined as follows:

$$K_{normal} = \frac{force}{unit\ defomation\ in\ thickness} \tag{5.6}$$

$$K_{shear} = \frac{force}{unit\ defomation\ in\ length} \tag{5.7}$$

Geo-Slope (2001) recommended setting a high value for K_{normal}, indicating that the slip surface element has a little or no compressibility, and K_{shear} usually is set to a low value to allow for slippage along the surface. A shortcoming of this formulation is that the elements are linear elastic, and no yield is included in the model. However, when the elements are in tension, the stiffnesses are set to zero.

5.5.2 Soil-Structure Interface of the Sulphur Concrete Wall

Sigma/W (Geo-Slope, 2001) used similar elements as those defined by Goodman et al. (1968) to model jointed rocks. This may be concluded by comparing equations 5.6 and 5.7, with equations 5.4 and 5.5, respectively. The only difference is that in equations 5.4 and 5.5, the stiffness is in units of stress/deformation, and in the Sigma/W's equations 5.5 and 5.7, the stiffness is in units of force/deformation. Thus, the slip surface elements included in Sigma/W were used to model the contact interface between the wall and the backfill, and between the wall and the foundation.

138

The modelling technique presented by Clough and Duncan (1971) was implemented with some limitations. The interface elements included in Sigma/W do not take into account shear strength, since they are linear elastic, and the shear stiffness was calculated separately, and introduced as a material property, to each interface element. Even though the elasto-plastic model allowed the introduction of shear strength to the interface elements, it was discarded because this model did not provide different stiffness in orthogonal directions (for example, in the x-y axes). The interface elements required a high stiffness perpendicular to the elements, to directly transmit the horizontal stresses to the wall, and low stiffness parallel to the elements to permit slippage of the backfill along the wall face. Thus, it was preferential to specify different orthogonal stiffness rather than to allow the elements to yield.

The normal stiffness (K_n) and the shear stiffness (K_s) of the interface elements in the wall's backside (facing the backfill) were calculated as follows:

- The normal and shear stresses along the back face were calculated by a finite element analysis in which all the material's constitutive models were linear elastic. In this analysis K_s and K_n were assumed to have the values of 1,000 and 1×10^8 kN/m, respectively.

- Equation 5.3 was used to evaluate K_s and with a high value of K_n (1×10^8 kN/m) as recommended by Clough and Duncan (1971). The friction angle of the compacted oil sand was 32°, thus the wall friction angle (δ) was 2/3 of ϕ given 21.3°. The values of the parameters K_I, n, and R_f in equation 5.3, were taken from Clough and Duncan (1971). When $\delta=2/3\phi$, they recommended the following values: $K_I=40,000$, n=1.0, and $R_f=0.9$.

- Having established the variation of the normal and shear stresses, and the parameters obtained in the previous paragraph, the parameter Ks was evaluated throughout the entire height of the wall, as shown in the Figure 5.3.

- Figure 5.3 shows the K_s values, at the nodes. To find the stiffness value at the element's midheight, K_s was averaged from the values, at both ends. This approximation was required, because in Sigma/W the stiffness is introduced as a material property of the elements.

- In Figure 5.4, equation 5.3 is divided into two terms. Term 1 is the initial shear stiffness, and Term 2 is a factor that modifies the initial stiffness, depending on the ratio of shear stress (τ) to normal stress (σ_n). Figure 5.4 shows that the value of K_{st} is directly dependent on the τ/σ_n ratio. If $\tau > \sigma_n$ then Term 2 may become much greater than 1, resulting in high K_{st} values. However, it is not reasonable that the value of K_{st} increase when decreasing the normal stress. Therefore, from an elevation of 7 to 14 metres, K_{st} was held constant at the value computed at the elevation of 7 metres. From an elevation of 2 to 7 metres the K_{st} values shown in Figure 5.4 were used. In contrast, from an elevation of 0 to 2 metres, the stiffness value from 2 metres was adopted.
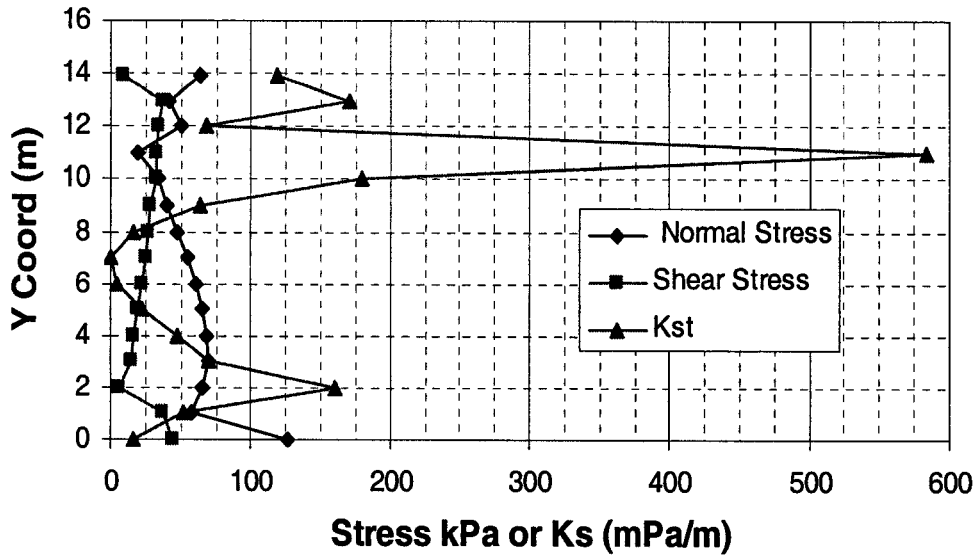
Figure 5.3 K_{st} vs shear and normal stresses along the back interface

$$K_{st} = \left[\gamma_w K_I \left(\frac{\sigma_n}{P_a} \right)^n \right] \left[\left(1 - \frac{R_f \tau}{\sigma_n \tan \delta} \right)^2 \right]$$

Term 1   Term 2
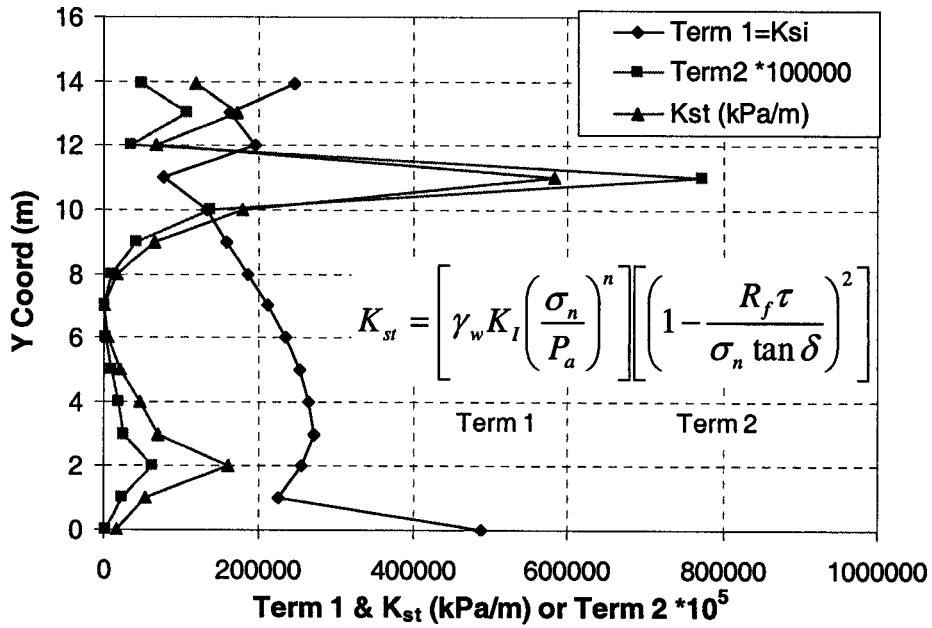
Figure 5.4 Effect of terms 1 and 2 on K_{st} values along the back interface

The shear stiffness (K_{st}) at the base of the wall was calculated in a similar manner. Figure 5.5 shows the variation of K_{st}, normal stress, and shear stress along the bottom interface. The normal and shear stress were obtained using the

same analysis in as along the back face. It was observed that the magnitude of K_{st} did not vary considerably, along the bottom interface. At both ends, as shown in Figure 5.5, the second term of equation 5.3 becomes very small, since the ratio of the shear stress to the normal stress is close to one. From these results, a K_{st} value of 1300 MPa/m was used for the bottom interface.
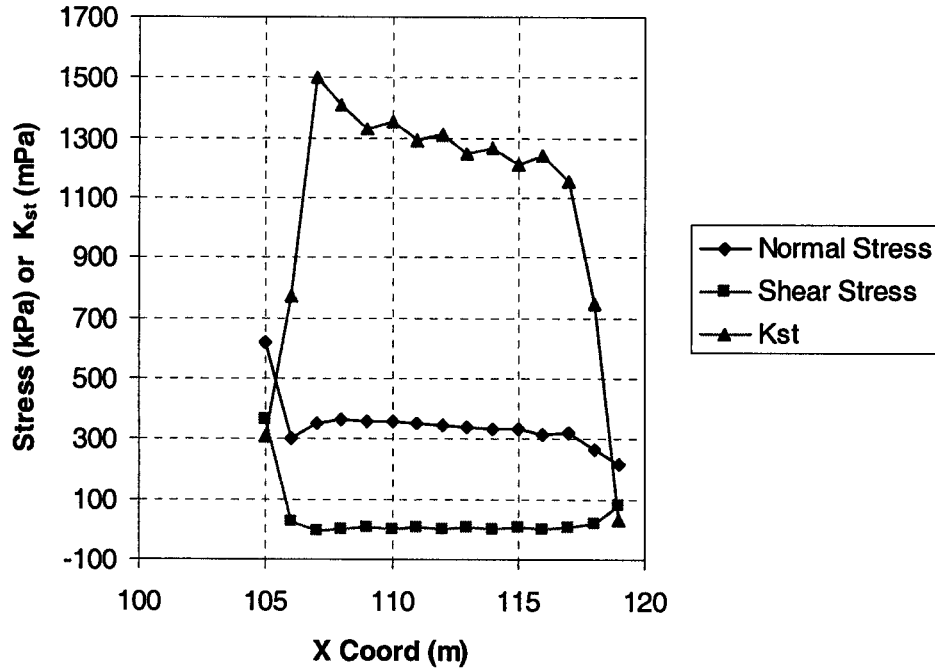
Figure 5.5 Variation of K_{st} along the bottom interface

Table 5.1 summarises the shear and normal stiffness along the three different interface that were evaluated. The variable refers to the K_{st} as explained in the previous paragraph, and estimated from the values presented in Figure 5.4. The notation under the key column shows the manner in which these interface models will be referred to, throughout, this thesis.

	K_s (kN/m)		K_n (kN/m)		
Interface Case	Back	Bottom	Back	Bottom	Key
1	1,000	1.3×10^6	1×10^8	1×10^8	ksback1000 ksbot1e6
2	Variable	1.3×10^6	1×10^8	1×10^8	ksbackvar ksbot1e6
3	Variable	1,000	1×10^8	1×10^8	ksbackvar ksbot1000

Table 5.1 K_s and K_n interface cases

5.6 Constitutive Models

5.6.1 Linear Elastic Model

The linear elastic model is the simplest soil model in which the stresses are directly proportional to the strains (Geo-Slope, 2001). The proportionality constants are the Young's Modulus (E), and Poisson's ratio (v). The stresses and strains are related as follows:

$$\begin{Bmatrix} \sigma_x \\ \sigma_y \\ \sigma_z \\ \tau_{xy} \end{Bmatrix} = \frac{E}{(1+v)(1-2v)} \begin{bmatrix} 1-v & v & v & 0 \\ v & 1-v & v & 0 \\ v & v & 1-v & 0 \\ 0 & 0 & 0 & \frac{1-2v}{2} \end{bmatrix} \begin{Bmatrix} \varepsilon_x \\ \varepsilon_y \\ \varepsilon_z \\ \gamma_{xy} \end{Bmatrix} \tag{5.8}$$

The value of the Poisson's ratio is limited to 0.49 because if v approaches to 0.5, the term $E/[(1+v)(1-2v)]$ tends to approach infinity as (1-2v) approaches zero. Physically, this behaviour means that the volumetric strain tends toward zero as Poisson's ratio approaches 0.5.

5.6.2 Hyperbolic Model

The hyperbolic model is the non-linear stress-strain constitutive model included in Sigma/W. The original model is attributed to Kondner (1963); however, it has been extensively developed by Duncan and his co-workers and is commonly known as the 'Duncan and Chan' model following Duncan and Chan (1970). These authors have shown that the stress-strain curves of many soils can be reasonably approximated by using the following:

$$(\sigma_1 - \sigma_3) = \frac{\varepsilon}{\dfrac{1}{E_i} + \dfrac{\varepsilon}{(\sigma_1 - \sigma_3)_{ult}}} \qquad (5.9)$$

The terms shown in the equation 5.9 can be better defined by inspecting Figure 5.5. The initial tangent modulus (E_i) is the initial slope of the stress-strain curve (Figure 5.6(a)), and $(\sigma_1\text{-}\sigma_3)_{ult}$ is the asymptotic value of stress difference, which is related closely to the strength of the soil. As usual, σ_1 and σ_3 are the maximum and the minimum principal stresses, respectively, and ε is the axial strain.

If the stress-strain curve is modified by changing the axes of Figure 5.6(a) to the axes shown in Figure 5.6(b), then equation 5.9 is transformed into equation 5.10.

$$\frac{\varepsilon}{(\sigma_1 - \sigma_3)} = \frac{1}{E_i} + \frac{\varepsilon}{(\sigma_1 - \sigma_3)_{ult}} \qquad (5.10)$$

Figure 5.6(b) demonstrates that the parameters used to define the hyperbolic stress-strain curve can be estimated from triaxial tests and has a physical meaning. Duncan et

144

al. (1980) described in a detailed manner the procedures for estimating the required parameter from drained and undrained triaxial tests.

Janbu (1963) suggested the following expression to estimate the initial tangent modulus:

$$E_i = K p_a \left(\frac{\sigma_3}{p_a} \right)^n ,$$

(5.11)
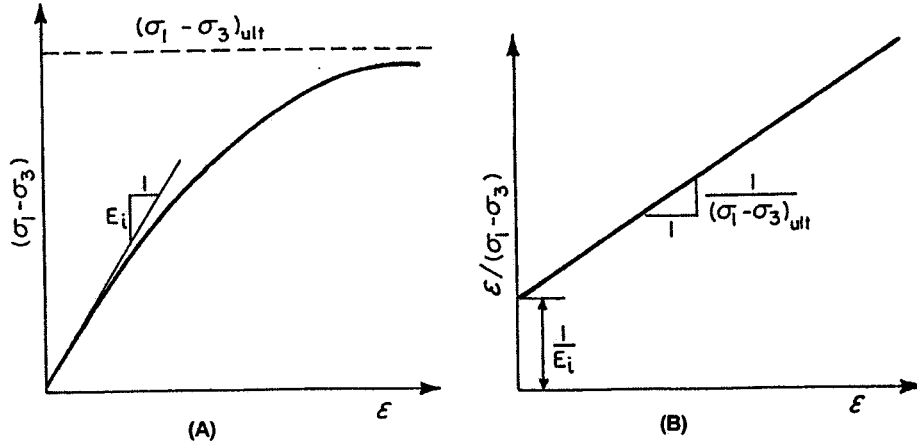
Figure 5.6 Hyperbolic Stress-Strain Curve, (a) original and (b) transformed.
Modified from Duncan et al. (1980).

where K is the modulus number and n is the modulus exponent (both parameters are dimensionless). The atmospheric pressure (p_a) is introduced into the equation to make the conversion from one system of units to another more convenient; therefore, the units of E_i, σ_3, and p_a are the same. Equation 5.11 estimates the initial modulus based on the variation of the confinement stress (σ_3). Wong and Broms (1994) pointed out that a high value of n (e.g. $n=0.8$) indicates that the initial modulus increases rapidly with increasing σ_3 and a corresponding decrease in the major principal strains at failure.

145

Figure 5.6(a) shows that the principal deviatoric stress (σ_1-σ_3) is the governing variable. Its value at failure can be computed as follows:

$$(\sigma_1 - \sigma_3)_f = \frac{2c\cos\phi + 2\sigma_3\sin\phi}{1 - \sin\phi} \qquad (5.12)$$

where the strength is a function of the cohesion (c), the friction angle (ϕ), and the confinement stress (σ_3) and is independent of the stress path and the boundary conditions. The ultimate deviatoric stress (σ_1-σ_3)$_{ult}$ is related to the deviatoric stress at failure with a simple expression:

$$(\sigma_1 - \sigma_3)_f = R_f (\sigma_1 - \sigma_3)_{ult} \quad , \qquad (5.13)$$

in which R_f is the failure ratio. Wong and Broms (1994) indicated that the failure ratio defines the shape of the stress-strain curve. If $R_f = 0$, the stress strain curve is a straight line up to failure; however, if $R_f = 1$, then the stress-strain curve is a perfect hyperbola. Nevertheless, since the deviatoric stress at failure is always less than the ultimate, this ratio is less than one. Duncan et al. (1980) noted typical values from 0.5 to 0.9 for most of the soils.

The instantaneous slope of the stress-strain curve is the tangent modulus (E_t) and is obtained by differentiating equation 5.9. Duncan and Chan (1970) derived the following expression:

$$E_t = \left[1 - \frac{R_f (1-\sin\phi)(\sigma_1 - \sigma_3)}{2c\cos\phi + 2\sigma_3\sin\phi} \right]^2 K p_a \left(\frac{\sigma_3}{p_a} \right)^n \qquad (5.14)$$

This equation can be used to calculate the appropriate values of tangent modulus for any stress condition if the values of the parameters K, n, c, ϕ and R_f are known.

When the soil is unloaded from a higher shear stress state, the Duncan and Chan model uses the unload-reloading modulus, E_{ur}. This modulus is computed similarly to the initial modulus (equation 5.11), but replaces K by K_{ur}, so that the expression changes as follows:

$$E_{ur} = K_{ur}\, p_a \left(\frac{\sigma_3}{p_a}\right)^n \qquad (5.15)$$

Won and Broms (1994) pointed out that it has been observed that the bulk modulus (B) varies with the confinement stress and that this modulus is relatively unaffected by the stress level; i.e., B is approximately constant for a given value of σ_3. Duncan et al. (1980) adopted the bulk modulus approach to characterize the volume change. The bulk modulus is calculated in the same manner as was shown in equations 5.11 and 5.15:

$$B = K_b\, p_a \left(\frac{\sigma_3}{p_a}\right)^m \quad , \qquad (5.16)$$

in which K_b is the bulk modulus number, and m is the bulk modulus exponent; furthermore, the effect of m is similar to the effect of n in equation 5.11. As well, both parameters are dimensionless. The rest of the parameters were defined previously. From the theory of elasticity, the tangent modulus (E_t) and the bulk modulus (B) can be related to the Poisson's ratio as shown in equation 5.17 a:

$$B = \frac{E_t}{3(1-2\nu)} \qquad \text{(5.17a)} \qquad \text{or} \qquad \nu = 0.5 - \frac{E_t}{6B} \qquad \text{(5.17b)}$$

Figure 5.6(a) reveals that when the stress level is low, E_t is high and that in equation 5.17b, ν can sometimes become negative. In contrast, when the soil is approaching failure, E_t low and ν can approach a value of 0.5. Therefore, in order to avoid numerical problems, some restrictions have to be used in Sigma/W, such as those proposed by Geo-Slope (2001).

5.6.3 Strain-Softening Model

Figure 5.7 shows the strain-softening model included in Sigma/W (Geo-Slope, 2001). This stress-strain curve is composed of 3 segments: an elastic portion up to the peak strength in which the slope is the Young's Modulus, a softening portion in which the strength reduces from peak to residual with a rate R, and a constant residual shear strength portion. This model is similar to that proposed by Chan (1986), who used a hyperbolic curve to describe the post-peak behaviour.

This strain-softening model is an elastic-softening plastic model, and its yield criterion is a function of the stress state and the equivalent plastic strain. Geo-Slope (2001) indicated that the yield function (F) for the strain softening model can be written in terms of the shear stress (q) and the shear strength (c_u) as follows:

$$F = q - \sqrt{3}c_u \qquad \text{(5.18)}$$

148
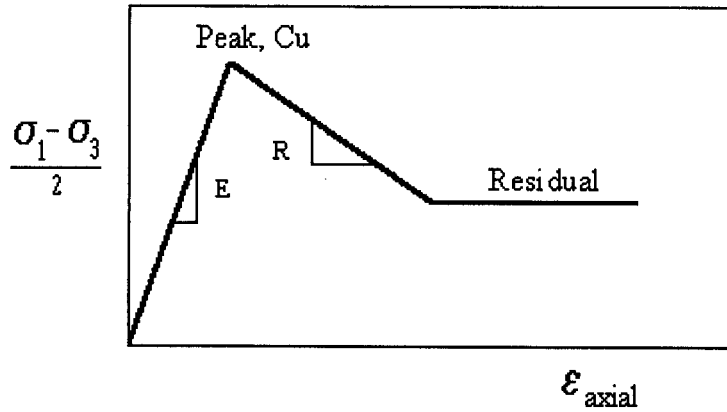
Figure 5.7 Strain-softening stress-strain curve

Geo-Slope 2001 pointed out that under plane strain conditions, it can be shown that at

failure, $\sigma_2 = (\sigma_1+\sigma_3)/2$, which gives a shear strength (c_u) at failure estimated as follows:

$$c_u = \frac{\sigma_1 - \sigma_3}{2} \tag{5.19}$$

Furthermore, the shear strength (c_u) depends on the total equivalent plastic strain (ε_p),

as given by the following equation:

$$c_u = \begin{cases} C_u & when\ \varepsilon_p = 0 \\ C_u - R\varepsilon_p & when\ 0 < \varepsilon_p \le \varepsilon_{pr} \\ C_r & when\ \varepsilon_p < \varepsilon_{pr} \end{cases} , \tag{5.20}$$

where C_u is the peak strength, C_r is the residual cohesive shear strength, ε_p is the total

plastic strain, ε_{pr} is the plastic strain where the softening line intersects the residual line,

and R is the rate of softening or the slope of the softening portion. Geo-Slope (2001)

remarked that ε_p is the softening parameter for this model and is a measure of the total

149

(accumulated) deviatoric plastic strain. An expression to evaluate this parameter and also the plastic matrix are given in Geo-Slope (2001).

5.6.4   Cam Clay Model

The Cam Clay model is a critical state model as well as an elastic and hardening plastic model (Geo-Slope, 2001). Geo-Slope (2001) stated that the formulation of the Cam Clay model in Sigma/W is based on Atkinson and Bransby (1978), and Britto and Gunn (1987).

Figure 5.8 shows a typical stress-strain curve for a metal. Atkinson and Bransby (1978) divided the curve into three portions: elastic, plastic, and unload-reload. The behaviour from point A to B is elastic and from point B to C is plastic. If a specimen is loaded up to a stress level below point B and then unloaded, the strain will return to the initial point A. Strains of this kind are known as "elastic strains" or "recoverable." If a specimen is loaded up to point C and unloaded, it will return to point D. The strains given from point A to D are known as "plastic strains" or "irrecoverable." If the same specimen is loaded again, its stress path will be throughout the DC line, elastic strains, and after the stress level at C, the specimen will be subject to plastic strains again. Points B and C are known as "yield stress". Atkinson and Bransby (1978) defined the effect of raising the yield stress from B to C (as shown in Figure 5.8, after the specimen experienced plastic strains) as "strain hardening".

Before starting a brief discussion of Critical State, the invariants q and p' for a triaxial test are defined as follows:

$$q = \sigma'_1 - \sigma'_3 \qquad (5.21)$$

150

$$p' = \frac{(\sigma'_1 + 2\sigma'_3)}{3} \quad , \tag{5.22}$$

where σ_1 and σ_3 are the maximum and minimum principal stresses, respectively. Furthermore, Atkinson and Bransby (1978) defined the specific volume (v) as the volume of the soil sample containing a unit volume of soil grains, and as equal to 1 plus the void ratio (e).
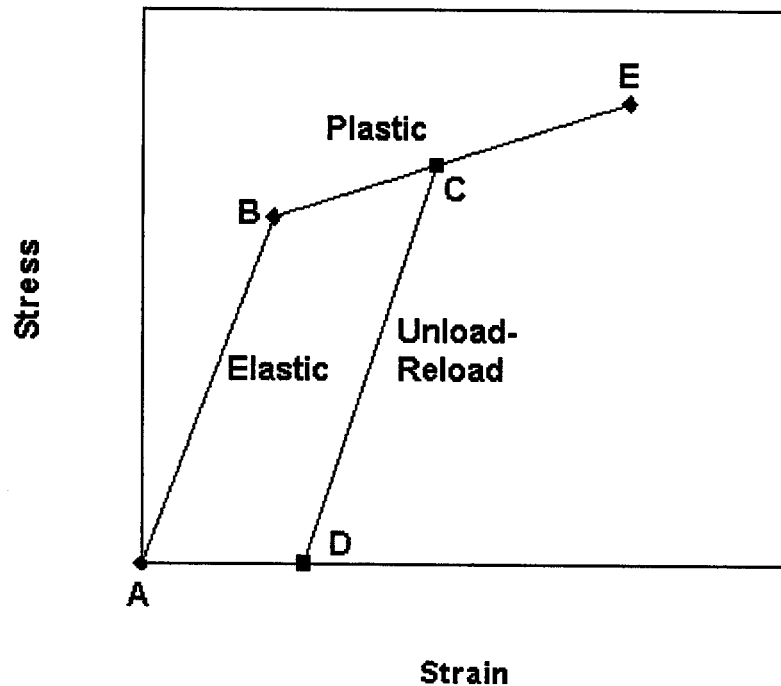
Figure 5.8 Elastic - plastic behaviour of metals

If Figure 5.8 is rotated clockwise, a figure similar to the one shown in Figure 5.9 is found. This figure reveals that the plastic line becomes the normal consolidation line, and the elastic line becomes the swelling line. Therefore, in soils also the characteristic of an elastic-hardening plastic stress-strain curve is also given, as Geo-Slope (2001) pointed out. Furthermore, Atkinson and Bransby (1978) remarked that recoverable and

151

irrecoverable strains are experienced in soils. Thus, points A and D presented the same stress level; however, at point D, a lower specific volume than at point A is shown. Consequently, irrecoverable plastic strains were observed to go from point A to D. If the stress path is ABCD, the plastic strains are given between points B and C, along the normal consolidation line. Along the swelling lines AB and CD, the strains are elastic and recoverable. An alternative path for going from point A to D required that the specimen be subjected to irrecoverable shear strains (at constant p'), travelling from the point A to a point into the yield surface, and moving through the yield surface up to a point where after unloading the shear stress (q), the sample deforms elastically as it moves to D. A detailed explanation is found in Atkinson and Bransby (1978).

Atkinson and Bransby (1978) stated that the Cam Clay theory was originally developed for normally consolidated and lightly overconsolidated soils and can really be applied successfully to these materials. The parameters required to define the Cam Clay model can be defined by using Figures 5.10 (a) and (b). Figure 5.10(a) presents the normal consolidation line (NCL), the overconsolidation or swelling line (OCL), and the critical state line (CSL). The first two lines were defined in the previous discussion.

Atkinson and Bransby (1978) pointed out that the crucial property of the CSL is that failure of initially isotropically compressed samples will occur once the stress states of the samples reach the line, irrespective of the test path followed by the samples on their way to the critical state line. They also added that failure will be manifested as a state at which large shear distortion occurs with no change in stress or in specific volume.
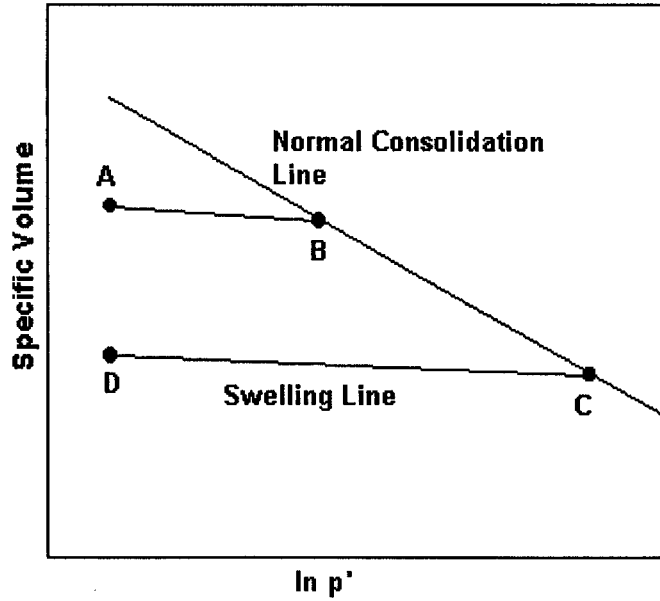
Figure 5.9 Elastic-plastic behaviour of soils

Using Figure 5.10(a), the parameters of the Cam Clay model can be defined. This figure is presented in a specific volume (v)-natural logarithm of p' space. The slope of the normal consolidation line (NCL) is named λ. The critical state line (CSL) is considered parallel to NCL; thus, the slope of CSL is also λ. The slope of the overconsolidation line (OCL), in Figure 5.10(a), is known as κ. In Figure 5.10(b), the critical state line is shown in q-p' space, and the slope in know as M. In a triaxial test, M can be calculated from the friction angle (ϕ') as follows:

$$M = \frac{6 \sin \phi'}{3 - \sin \phi'}$$
(5.23)

In Figure 5.10(a), the parameter N can be found by projecting the normal consolidation line onto the specific volume (v) axis intercepting when p' is equal to 1. Once N is known, the parameter Γ can be computed by the following equation:

$$\Gamma = N - \lambda + \kappa$$
(5.24)

153

The parameter Γ is defined as the intersection point of the critical state line with the specific volume axis when p' is equal to 1.0. Atkinson and Bansby (1978) give the derivation of equation 5.24.

In addition, Atkinson and Bransby (1978) also presented the associated yield curve of the Cam Clay model by using the following expression:

$$\frac{q}{Mp'} + \ln\left(\frac{p'}{p'_x}\right) = 1 \qquad (5.25)$$

where p'_x is the value of p' at the intersection of the yield curve with the projection of the critical state line at point X , as shown in Figure 5.10(b). The slope of the yield curve at X is zero, implying that the change of the volumetric strain per shear strain is zero at the critical state line. Geo-Slope (2001) used equation 5.25 to define the yield function in Sigma/W.

(a)   (b)
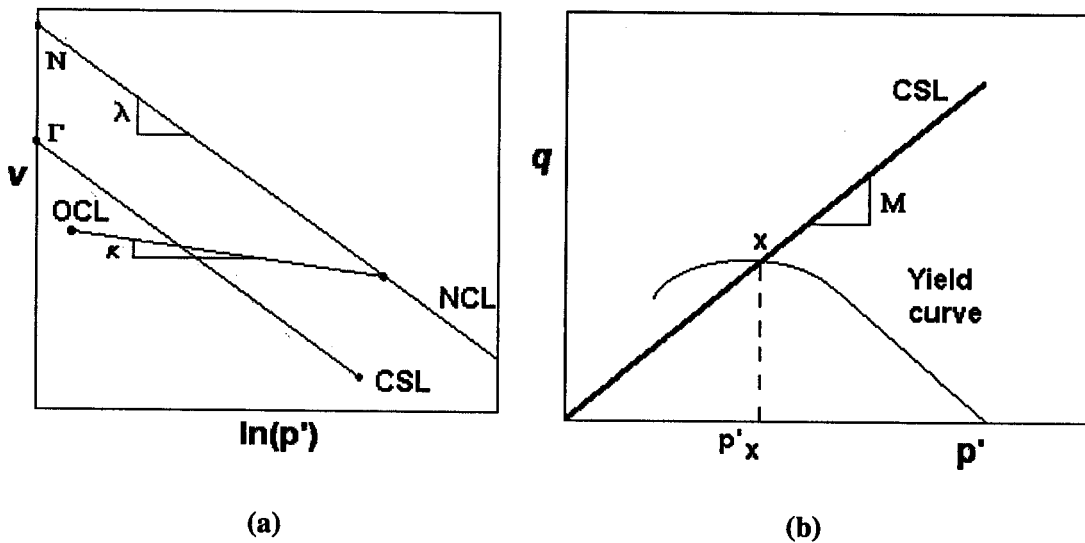
Figure 5.10 – Critical State Parameters

154

5.7 Material Properties and Selection of the Constitutive Models

Figure 4.15 gave the cross-section of the structure that is analysed using the recommended material parameters in Table 3.6 for the 15Su3FA mix. The main objective of this study is to evaluate the stresses in the sulphur-stabilized wall. The model used to represent the sulphur concrete was the strain-softening model proposed by Chan (1986), as discussed in Section 5.6.3. However, to estimate the stresses in the wall, it is necessary to also properly model the material surrounding the sulphur concrete wall and apply appropriate boundary condition. Therefore, to model the compacted oil sand backfill, and the gravel base drain layer the Hyperbolic model was implemented, as presented in Section 5.6.2. The gravel road sub-base was also simulated using this model. The behaviour of the compacted oil sand was investigated using the Cam Clay model presented in Section 5.6.4.

The linear elastic model was utilised to represent the behaviour of the concrete pavement, in-situ oil sand, and the unweathered limestone, as no yielding occurred in these materials.

5.7.1 Constitutive Model of the Sulphur Concrete

Sulphur concrete is a brittle material and hence a strain-softening model was used to represent the brittle behaviour. Table 3.6 presents the parameters derived from the laboratory tests, after 100 freeze-thaw cycles, and at the initial condition after construction for the 15Su3FA mix.

Figure 5.7 shows the parameters required to define the strain softening model, such as peak shear strength (C_u), residual shear strength (C_r), Young's Modulus (E) and the rate

155

of softening (R). Table 5.2 presents these parameters for the initial condition, and the condition after 100 freeze-thaw cycles for the 15Su3FA sulphur-concrete mix.

The parameters C_u, E, and v were defined from the results of the laboratory tests. C_u was defined from equation 5.19 at yield strength, as explained in Section 4.6.1. The softening rate was estimated at 1000 times the Young's modulus, to simulate the brittle nature of the material, and the residual shear strength was estimated as 10% of C_u.

Parameters	Initial Condition	After 100 cycles
Peak Shear Strength, C_u (kPa)	11,400	5,850
Residual Shear Strength, C_r (kPa)	1,140	585
Young's Modulus, E (MPa)	18,000	11,200
Softening Rate, R (MPa)	18,000,000	11,200,000
Poisson's ratio, v	0.1	0.1

Table 5.2 Strain softening model parameters for the 15Su3FA sulphur-concrete mix

5.7.2 Constitutive Model of the Gravel Base and Drain, and the Gravel Sub-base

The model selected for this material was the hyperbolic model, as presented by Duncan and Chang (1971) as presented in Section 5.6.2. Duncan et al. (1980) recommended the parameters presented in Table 5.3, to model the soil behaviour by using the hyperbolic model.

To model the road sub-base and the gravel base drain layer, the parameters shown in Table 5.3 (Row No. 2) were selected based on the average unit weight presented in Suncor (2000) (see Table 4.1 for 20-mm gravel), and on the fact that this material was compacted to 98% of the Standard Proctor, also as indicated in the Suncor (2000) report.

Thus, based on the Standard Proctor and the Unit Weight, the properties shown in Row 2 of Table 5.3 are the closest to representing the 20-mm gravel described in Suncor (2000).

Furthermore, the variation of the stresses in the sulphur concrete wall, due to varying the parameters from the maximum stiffness (line No. 1) to the minimum stiffness (line No. 4), was evaluated. This was the only case in which the parameters for the gravel base drain layer were changed.

No.	UCS	Relative Compaction (Std. Proctor, %)	γ (kN/m^3)	ϕ	K	N	R_f	K_b	m
1	GW,	105	23.5	42°	600	0.4	0.7	175	0.2
2	GP,	100	22.8	39°	450	0.4	0.7	125	0.2
3	SW,	95	22	36°	300	0.4	0.7	75	0.2
4	SP.	90	21.2	33°	200	0.4	0.7	50	0.2

Table 5.3 – Parameters for the hyperbolic model, taken from Duncan et al. (1980)

5.7.3 Constitutive Model of the Compacted Lean Oil Sand

Section 4.4 defines lean oil sand as excavated oil sand with bitumen content of 6% or less. This material was also modelled using the Duncan and Chang model. The tailing sand produced after the extraction of the bitumen was classified as SP (Section 3.2.2). The contract drawings of the existing structures specified a compaction of 98% of the Standard Proctor. In the Suncor (2000) Report, the samples of lean oil sand were also compacted up to 98% of the Standard Proctor. Lord and Cameron (1985) indicated a friction angle of 32°, due to the presence of the bitumen into the sand, and an average unit

157

weigh of about 20 kN/m³. Therefore, the parameters shown in Row 3 of Table 5.3 were selected as representative of the compaction, friction angle and the unit weight.
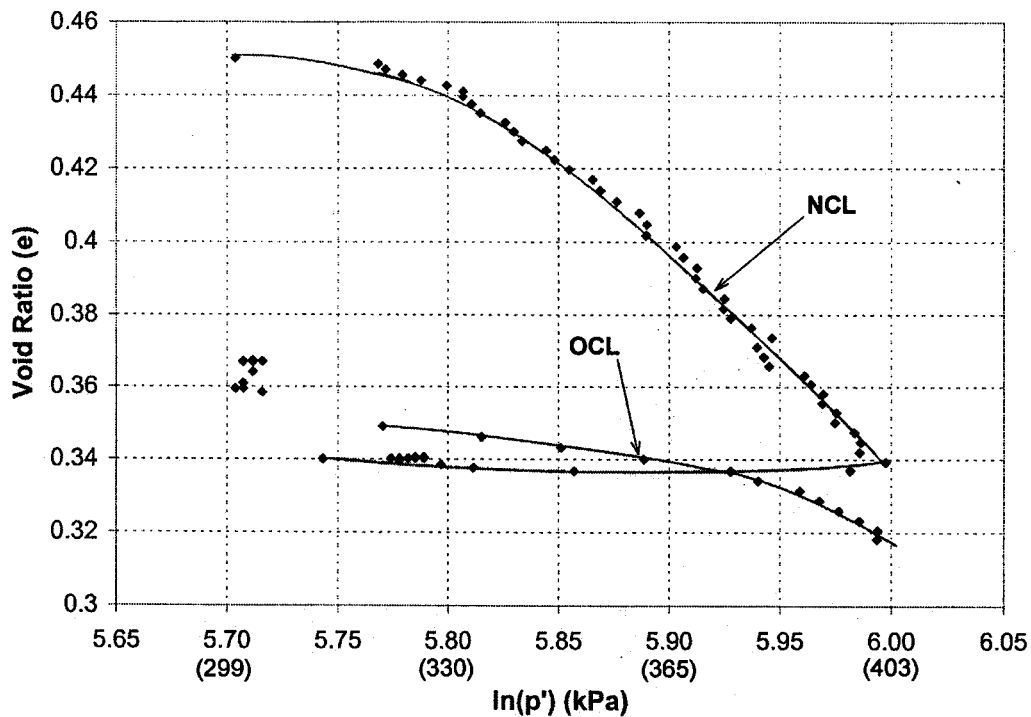
Figure 5.11 Compacted lean oil sand triaxial test

The effect of dilation of the backfill was considered by modelling its behaviour using the Cam Clay model. Section 5.6.4 addresses the theory related to this model. Two triaxial compression tests were used to determine the parameters required by this model. One performed up to failure, and the other was a loading-unloading cycling test. The first test was used to confirm the data from the second test, in which the slope of the normal consolidation line and the preconsolidation pressure of both tests match very well. These triaxial tests were performed at the University of Alberta, as part of the investigation reported in Suncor (2000). Unfortunately, the volumetric strains were not measured; thus, it was not possible to determine if the compacted lean oil sand dilated during shearing. However, the Cam Clay parameters were defined by plotting the test in a void ratio (e) versus natural logarithm of the mean stress (ln p'), as defined in Section

158

5.6.4. Note that the specific volume (v) is equal to the void ratio (e) plus one. Figure 5.11 shows the points recorded during the compression test; the Normal Consolidation Line (NCL), and the Over Consolidation Line (OCL) were drawn to fit the data points.

From the slopes of NCL and OCL, λ and κ were calculated, respectively. The value of N was estimated by projecting the NCL to the void ratio axis, and the value of Γ from equation 5.24. The slope of the critical state line in q-p' space was estimated using formula 5.23. The preconsolidation pressure (P'_c) was estimated using the graphical method proposed by Casagrande (1936). Table 5.4 shows the parameters determined for the Cam Clay model.

λ	κ	N	Γ	M	p'_c (kPa)
0.567	0.035	4.73	4.20	1.28	342

Table 5.4 – Parameters for the Cam Clay Model

5.7.4 Constitutive Model for the In-situ Oil Sand, the Unweathered Limestone and the Concrete Pavement.

The initial elastic finite element analysis showed no yielding in the in-situ oil sand, and the unweathered limestone; therefore, the linear elastic constitutive model was chosen to model their behaviour. For the concrete pavement, the linear-elastic model was adopted, from the beginning. Table 5.5 presents the Young's modulus and the Poisson's ratio used to model these materials. These values were used in all the finite element analyses presented in this thesis.

Samieh and Wong (1997) presented a series of stress-strain curves of the Athabasca Oil Sands. Based on the estimation of maximum and minimum principal stresses and strains from previous finite element analyses, the stress-strain curve measured by Samieh

159

and Wong (1997) using a confinement stress (σ_3) of 100 kPa, was selected. Since the problem lies in a very low stress and strain range, it was considered that the linear elastic model could well represent the behaviour of the oil sand, in this particular case. Thus, a Young's modulus of 150 MPa was calculated from the aforementioned curve, and a Poisson's of 0.3 was assumed.

Properties	In-Situ Oil Sand	Unweathered Limestone	Concrete Pavement
Young Modulus (E) (MPa)	150	45,000	30,000
Poisson's ratio (v)	0.3	0.2	0.2

Table 5.5 Linear-elastic constitutive model parameters

The parameters for the unweathered limestone were taken from Hoek and Bray (1981), and they indicated typical values for the Young's modulus and the Poisson's ratio of 45,000 MPa and 0.20, respectively.

The values selected for the Portland cement concrete pavement were taken from Fintel (1985) who pointed out that values of Poisson's ratio generally range from 0.11 to 0.28; furthermore, he indicated that for elastic strains, under normal working stresses, the Poisson's ratio is taken as 0.20.

5.8   Finite Element Analyses and Results

Many sensitivity analyses were performed to predict the behaviour of the sulphur-stabilized wall, under study. These are described in the following sections.

5.8.1   Base Model

A base model consists of the following:

- The finite element mesh as defined in Figures 5.1 and 5.2.

160

- Parameters to model the interfaces between the wall and the backfill, and the wall and the gravel base as defined in Table 5.1.

- An initial set of parameters for each constitutive model (Table 5.6).

Material	Constitutive Model		Unit Weight (kN/m^3)
	Type	Parameters	
Sulphur Concrete	Brittle	Cu=5,850 kPa; E=11,200 MPa; v=0.1 R=11,200,000 MPa; C$_r$=585 kPa	21
Gravel Base	Hyperbolic	E=200 MPa; v=0.3; ϕ=38° K=450; n=0.4; R$_f$=0.7; K$_b$=125; m=0.2	20
Road Sub-Base	Hyperbolic	E=200 MPa; v=0.3; ϕ=38° K=450; n=0.4; R$_f$=0.7; K$_b$=125; m=0.2	20
Comp. Oil Sand	Hyperbolic	E=30 MPa; v=0.3; ϕ=32° K=300; n=0.4; R$_f$=0.7; K$_b$=75; m=0.2	19
In-situ Oil Sand	Elastic	E=150 MPa; v=0.3	20
Unweathered Limestone	Elastic	E=45,000 MPa; v=0.2	23
Concrete Pavement	Elastic	E=30,000 MPa; v=0.2	23

Table 5.6 Base constitutive model for the finite element analyses

5.8.2 Evaluation of the Sulphur-Concrete Wall under the Full and the Partial Loading Conditions

The base model was subjected to the loading conditions, as defined in Section 4.5.1. The partial loading condition is as shown in Figure 4.6, and the full loading condition is as shown in Figure 4.7. The base model was maintained constant under the application of these loading conditions.

Figures 5.12 and 5.13 present the maximum (σ_1) and minimum (σ_3) stress contours, respectively, which resulted from the analysis using the interface model ksback1000

ksbot1e6. Note the maximum stress at the toe of the wall of 954 kPa. Figure 5.13 presents a zone of tension due the surcharge of 205 kPa located on the top left corner of the wall, and as defined by the zero contour. However, in this zone the tensile stresses are very small, less than 25 kPa. This zone of tension is present in all the conditions which include the surcharge of 205 kPa representing the mining trucks during the dumping operation.

Figure 5.14 shows the deformed mesh under the Full Loading Condition. The figure shows that the wall is deformed and tilted forward under the application of this load condition. Also, it shows the backfill settlement, and how the interface elements enable the sliding of the backfill against the wall. Figures 5.15 and 5.16 present the X and Y displacements contours in metres.

The results under Full Load Condition, using the interface model ksback1000 ksbot1e6, have been chosen, because this presents the higher stress concentrations and the larger deformations in the wall. The results for all cases, including partial and full loading conditions, are presented in the Appendix C.

Furthermore, Figure 5.17 shows the variation of the σ_1 stresses along the bottom of the wall. Note how the tilting forward of the structure is reflected in the stresses distribution. Figures 5.18 and 5.19 show that the distribution of principal stresses versus the y-coordinate (Elevation). Note that above the y-coordinate of 2 metres, the stresses are essentially independent of the interface model.

Figure 5.12 Maximum stress contours under Full loading – ksback1000 ksbot 1e6

Figure 5.13 Minimum stress contours under Full loading – ksback1000 ksbot1e6

205 kPa   102.5 kPa

10X

Figure 5.14 Full load mesh displacement (10X)-ksback1000 ksbot1e6

X Displacement (m)

205 kPa   102.5 kPa

-0.1

-0.08

-0.06

-0.04

-0.02

0

Figure 5.15 Full load X displacement – ksback1000 ksbot1e6

Y Displacement (m)

205 kPa   102.5 kPa

`Figure 5.16 – Full load Y displacement – ksback1000 ksbot1e6
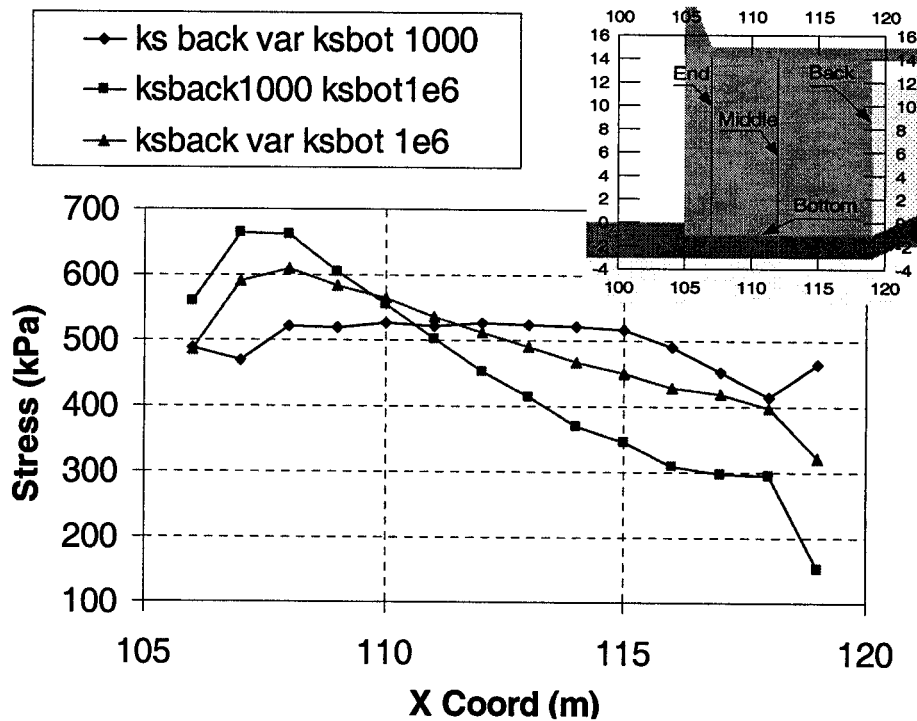
Figure 5.17 - σ_1 stresses at the bottom line

165
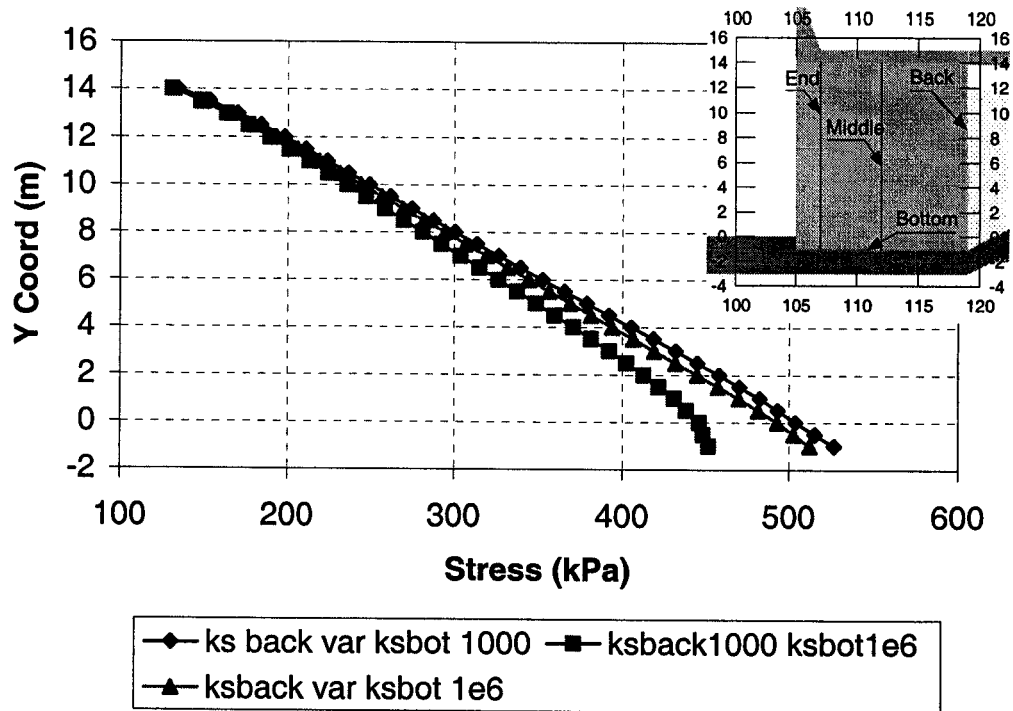
Figure 5.18 σ_1 stresses at the middle line
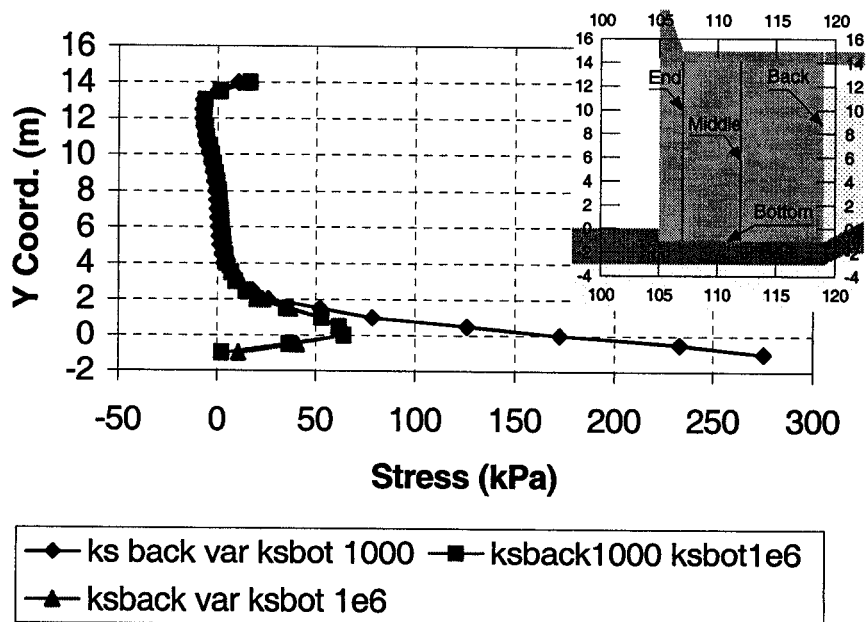
Figure 5.19 σ_3 stresses at the End line

166

5.8.3 Finite Element Analysis Including Pore Water Pressure

In order to evaluate the effect of the pore water pressure on stresses in the structure, a water table throughout the top of the gravel base drain layer was added, as shown in Figure 5.20. Sigma/W generates the initial pore water pressures from the water table using the hydrostatic pressure. Then, the change in pore-water pressure generated due to a change in total stress can be estimated by the equation proposed by Henkel (1960).
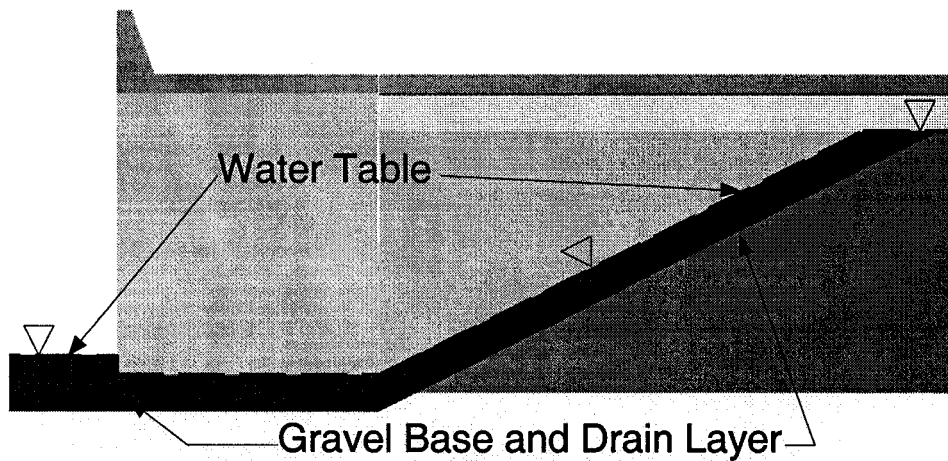
Figure 5.20 Water table for the finite element analysis

σ_1 Effective Contours

752

Figure 5.21 Full loading condition including pore water pressures - σ_1 effective

contours (in kPa)

Comments: No PWP Included
File Name: ksvar ksbot1e6_10.siz
Analysis Type: Load/Deformation

σ_1 Effective Contours

814
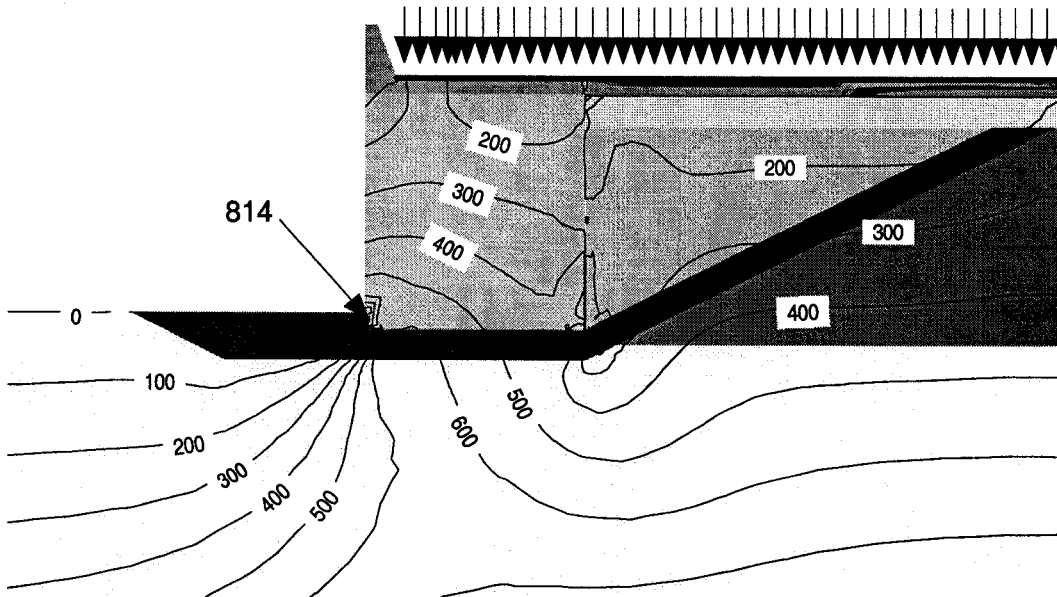
Figure 5.22 Full loading condition no including pore water pressure - σ_1 effective

contours (in kPa)

168

The base model presented in Section 5.8.1 was used for this evaluation, and the only change was the addition of the water table. However, only the results using the interface model ksback1000 ksbot1e6 are included, here. Figure 5.21 presents the maximum effective principal (σ_1) stresses. In this figure, the Full Loading Condition is applied on top of the structure, and the maximum value of σ_1 is presented at the toe of the structure. Figure 5.22 presents the same type of contours under the same loading condition, but it does not include pore water pressures. Although the water table is exactly below the retaining wall, as shown in Figure 5.20, a difference in the effective stress of about 7% can be observed at the toe of the retaining wall. However, the effective stress contours in both cases are very similar throughout the entire sulphur concrete wall.

5.8.4 Change in the Poisson's Ratio in the Sulphur Stabilized Wall.

Fintel (1985) shows that typical values of Poisson's ratio for Portland cement concrete varies from 0.11 to 0.28; therefore, the values of 0.1 and 0.3 were selected to investigate their influence on the stress distribution in the sulphur concrete. In this case, the value of the Poisson's ratio changes in the sulphur concrete. The interface model used was ksbackvar-ksbot1e6, the full loading conditions was applied, and no pore water pressures were included. The rest of the parameters defined in the Base model remain unchanged

Figures 5.23 and 5.24 show the variation in σ_3 and σ_1, respectively, near the face and bottom of the retaining wall, respectively. There is a minor variation in σ_3 when Poisson's ratio is increased from 0.1 to 0.3. Figure 5.23 presents the greater difference found between both analyses using the Poisson's ratio values of 0.1 and 0.3. Figure 5.25 also shows that maximum principal stresses along the centre of the wall are not sensitive to change in Poisson's ratio. In Appendix C, additional information, regardless of the

169

maximum and minimum principal stress, and the maximum shear stress are included, as well.
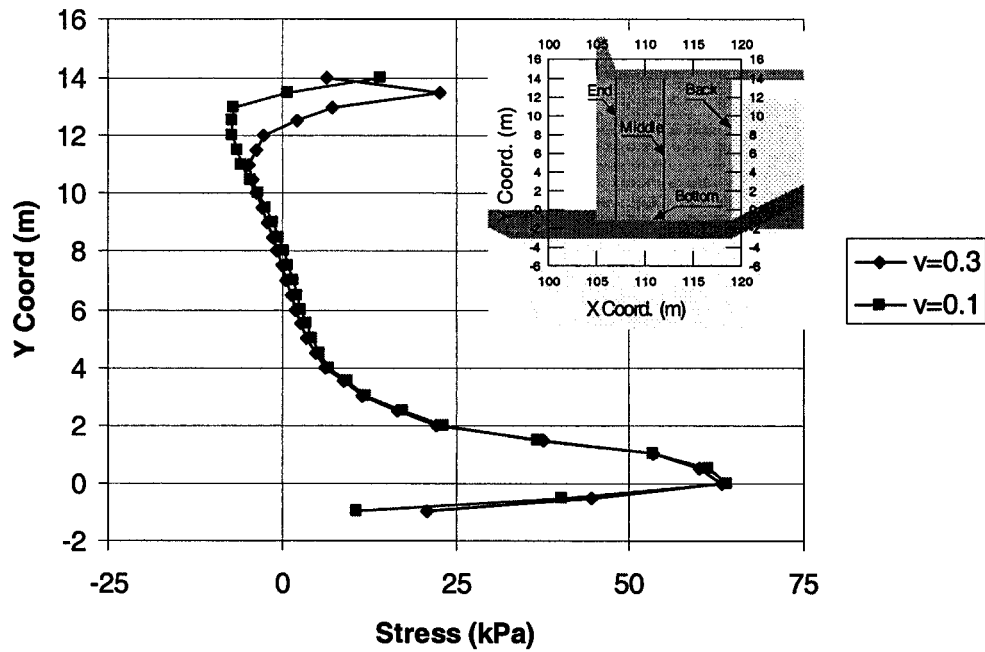
Figure 5.23 σ_3 stresses along the End line due the variation of Poisson's ratio

5.8.5   Irregular Surface between the Unweathered Limestone and the Gravel Base.

The preparation of the foundation surface is paramount for the proper performance of a structure with the characteristic of the wall under study. An irregular bedrock surface promotes concentration of stresses along the base of the retaining wall.
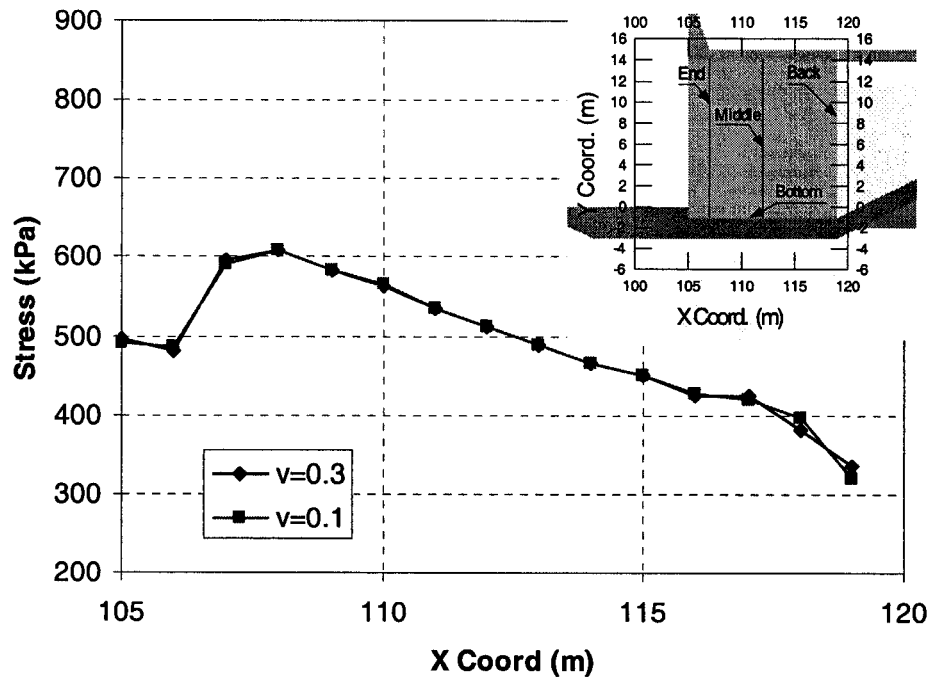
Figure 5.24 σ_1 along the Bottom line due the variation of the Poisson's ratio
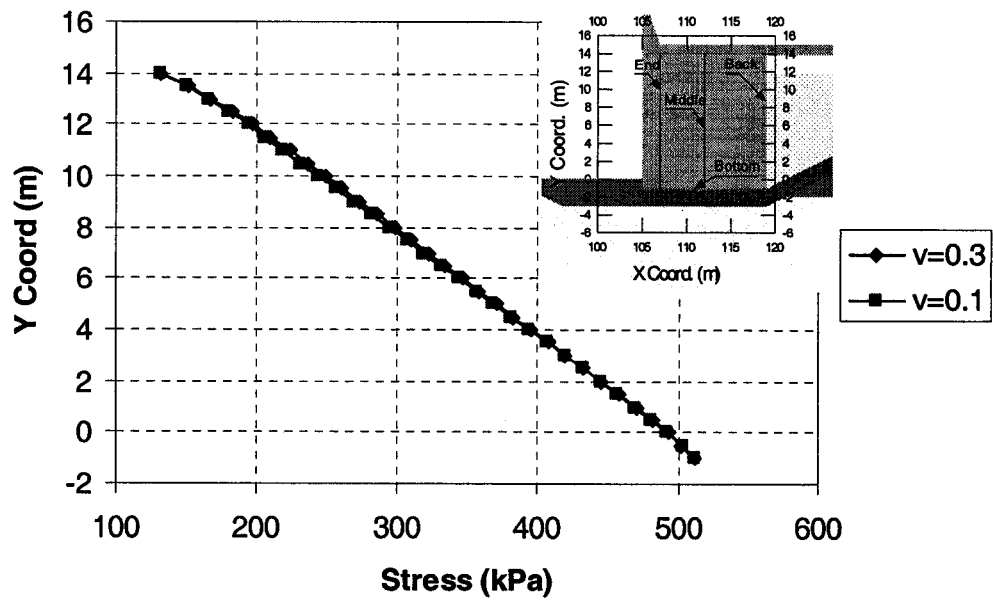
Figure 5.25 σ_1 along the Middle line due the variation of the Poisson's ratio

Moreover, is concentrations of stresses may generate tensile stresses in a similar manner to the stresses generated during the split tensile test. This section presents two cases in which the finite element mesh was modified to simulate the effects of the foundation surface not being prepared properly. In this case, the finite element mesh is modified, as presented in the Figures 5.26 and 5.27, the interface model used is the ksbackvar-ksbot1e6, the surcharge applied is the full loading condition, and the rest of the parameters of the base model remain unchanged. Also, the pore water pressures are not included.

Figure 5.26 shows a wedge-shaped rock protruding into the foundation layer. This "piece of rock" is modeled as a wedge to produce extreme stress concentrations in the wall. Figure 5.27 shows a case that could occur in normal practice, i.e. that the assumed height of the "piece of Rock" is half the thickness of the gravel base with its tip "rounded".

Figure 5.28 shows the effect of the wedge-shaped rock on the σ_3 stress distribution in the retaining wall. Note that in this case the rock is in contact with the bottom of the wall, generating a maximum tensile stress of 333 kPa during construction. Figure 5.29 shows the stress distribution of σ_3 caused by a rock wedge that has a rounded tip and covered by 1-m of gravel. This possible construction situation does not generate tensile stresses in the retaining wall.

Contact
Surface

Gravel Base
and Drain Layer

Unweathered
Limestone
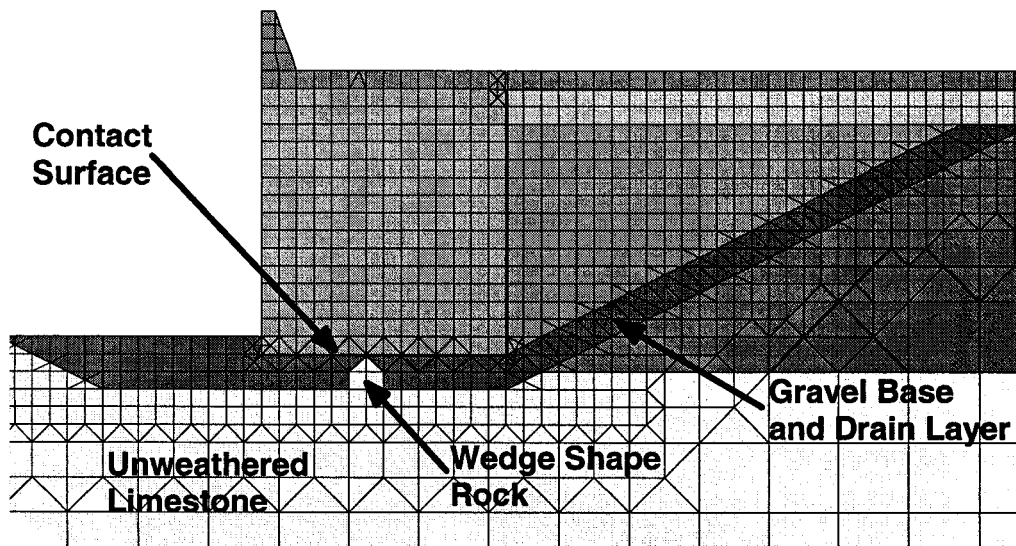
Wedge Shape
Rock

Figure 5.26 Finite element mesh showing a wedge shape rock

Contact
Surface

Gravel Base
and Drain Layer

Unweathered
Limestone
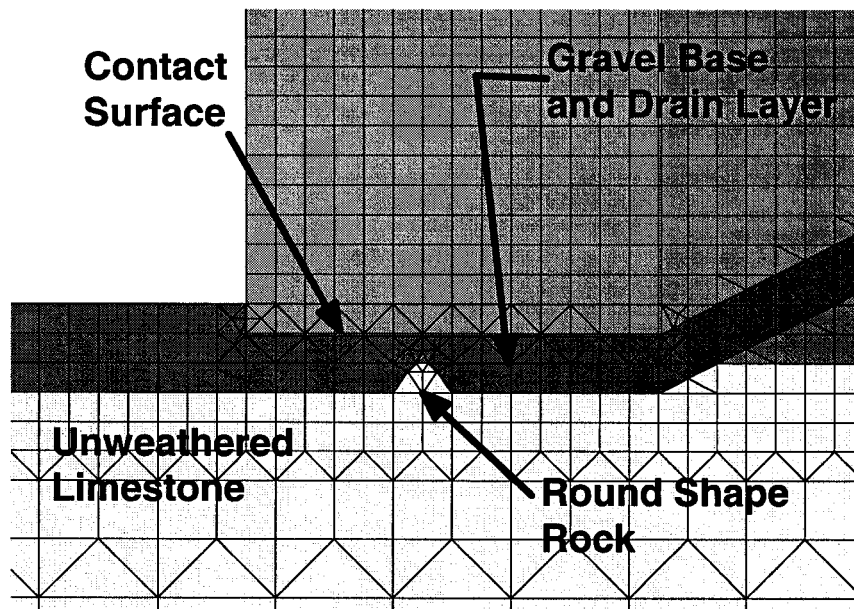
Round Shape
Rock

Figure 5.27 Finite element mesh showing a round shape rock

173
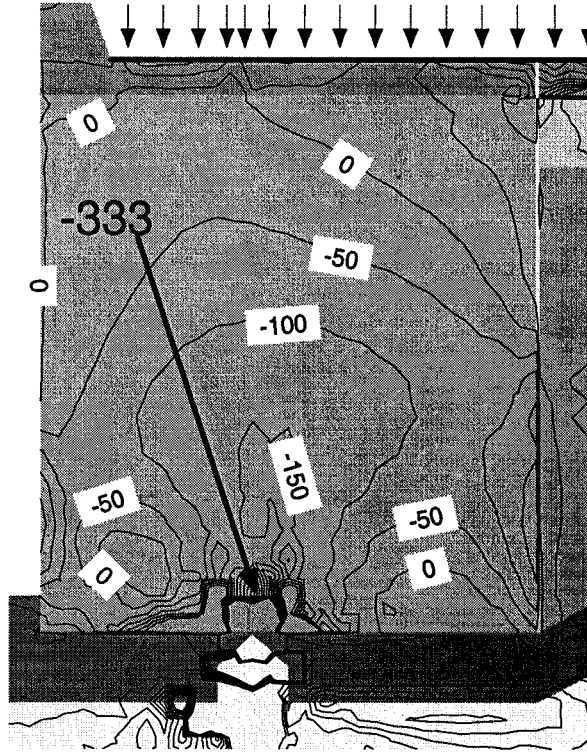
Figure 5.28 σ_3 contours cause by the wedge-shaped rock
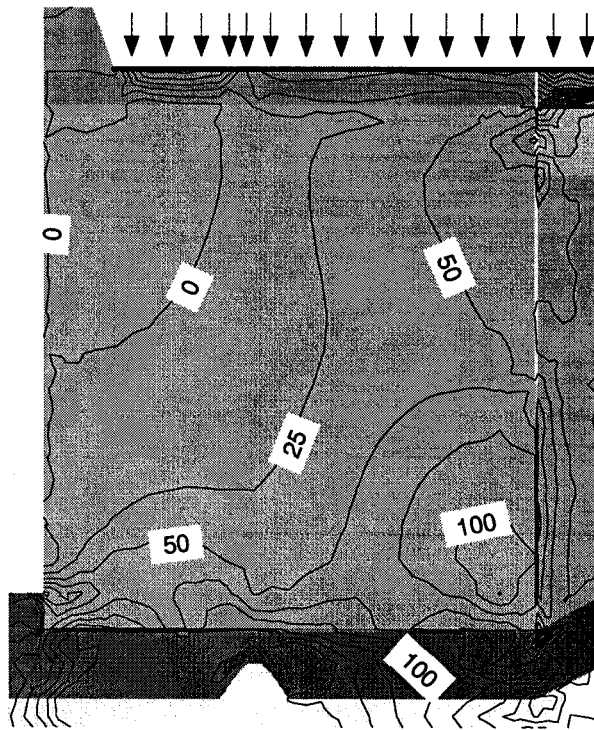
Figure 5.29 σ_3 contours caused by the round-shaped rock

5.8.6 Variation of the Stiffness in the Gravel Base Drain Layer

In this case only the material properties of the gravel base drain layer had been modified. The full loading condition is applied, and the pore water pressures are not included. Moreover, the interface model used is the ksbackvar-ksbotle6 (Table 5.1). The remainder of the parameters of the base model remain unchanged.

To investigate the influence of the stresses in the sulphur concrete wall if the stiffness of this layer varies, the modulus number into the hyperbolic model was varied from K=600 to K=200. The rest of the hyperbolic parameters were introduced in the finite element model, as shown in Table 5.3.

Figures 5.30 and 5.31 show the maximum (σ_1) and minimum (σ_3) principal contours for the case when K=600 and K_b=175, and Figures 5.32 and 5.33 present the σ_1 and σ_3 contours, when K=200 and K_b=50. When comparing the figures, it is noted that the concentration of σ_1 at the toe varies slightly. When K is decreased σ_1 stress concentration decreased 8%. The σ_3 contours do not show significant variation. Appendix C presents additional stress profiles showing the variation of the stresses in the sulphur concrete wall.

σ_1

Figure 5.30 σ_1 contours using K=600 and K_b=175

σ_3

Figure 5.31 σ_3 contours using K=600 and K_b=175

σ_1

Figure 5.32 - σ_1 contours using K=200 and K_b=50.

σ_3
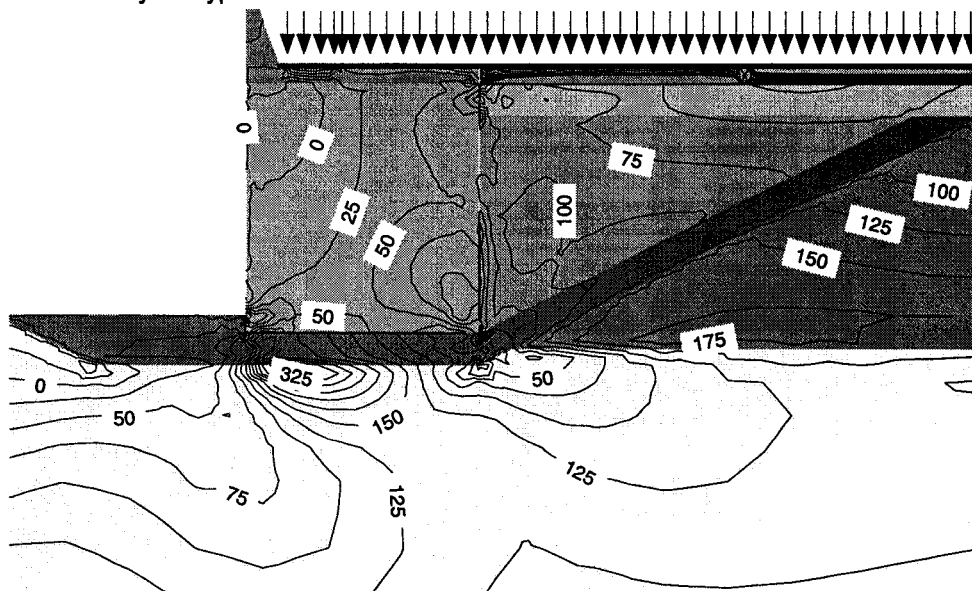
Figure 5.33 - σ_3 contours using K=200 and K_b=50

177

5.8.7 Cam Clay Model to Represent the Behaviour of the Compacted Oil Sand.

The compacted oil sand was modeled in a previous, section using the hyperbolic model presented by Duncan and Chang (1970). The properties selected were based on the friction angle, unit weight, and the required compaction, as indicated in section 5.7.3. However, the hyperbolic model is not able to simulate dilation during shearing. As a result, the Cam Clay model was selected to evaluate the effect of dilation of the compacted lean oil sand on the stresses in the retaining wall. The Cam Clay parameters were presented in Table 5.4. The interface model was represented using the ksbackvar-ksbot1e6 parameters (Table 5.1), and the applied surcharge was the full loading condition (Figure 4.6).

Figures 5.34 and 5.35 present the σ_1 and σ_3 contours, respectively. Note that the stress concentration at the toe area reaches a compressive stress of 858 kPa, which is not significantly different from the previous results presented (see Figures 5.12, 5.22, and 5.30).

Figures 5.36 and 5.37 show the X and Y displacement, respectively. The effect of a dilating backfill can be observed in the X displacement contours. Notice how these contours expand in Figure 5.36 compared to the displacement pattern in Figure 5.15.

σ_1

Figure 5.34 σ_1 contours using the cam clay model for the compacted oil sand

σ_3

Figure 5.35 σ_3 contours using the cam clay model for the compacted oil sand

179
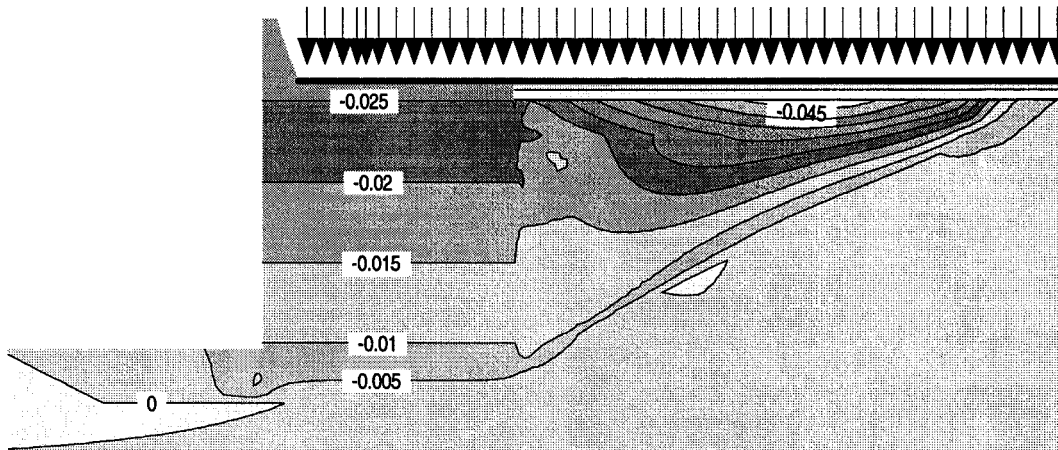
X Displacement (m)

Figure 5.36 X displacement contours using the cam clay model in the compacted oil sand backfill
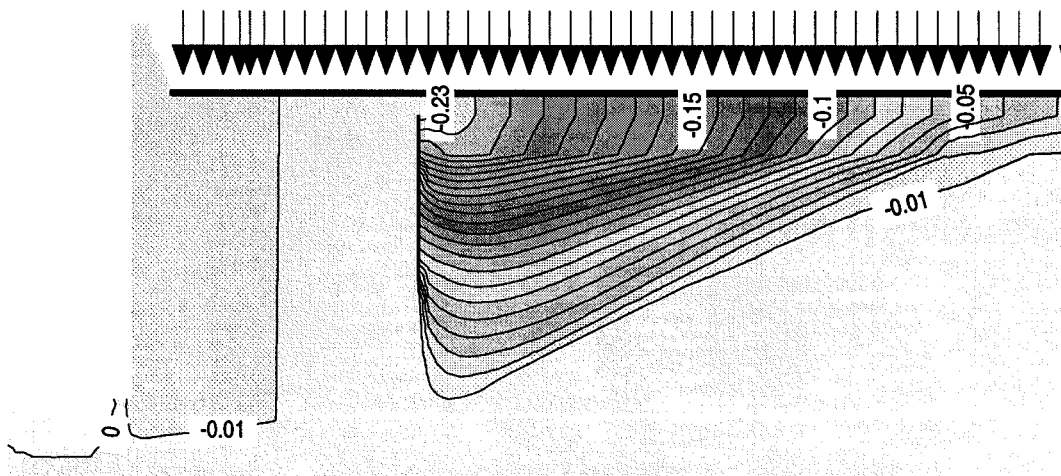
Y Displacement (m)

Figure 5.37 Y displacement contours using the cam clay model in the compacted oil sand backfill

5.8.8 Factor of Safety Against Compression and Tension Failure

This section evaluates the Factor of Safety against compression and tension failures using the results from the finite element analyses. The Factor of Safety in compression was calculated based on the yield stress as follow:

$$FofS_c = \frac{f_y}{\sigma_1} \qquad (5.26)$$

where f_y is the compressive strength at yield.

Furthermore, the Factor of Safety against tension was estimated in a similar manner, but based on the tensile strength as follows:

$$FofS_t = \frac{f_t}{\sigma_3} \qquad (5.27)$$

in which f_t is the tensile strength and σ_3 is the minimum principal stress in tension.

Figure 5.38 presents the most critical condition of tension stresses found during this study. This is the case when a wedge-shaped rock is found at the bottom of the structure touching its base. The location of the stress profile is also shown in Figure 5.38. The minimum Factor of Safety was 2, at elevation zero; thus, the maximum tension was not generated at the contact surface. It was found 1 metre into the sulphur concrete mass. This finding is very similar to the results of a split tensile test, in which the point where the load is applied is under compression, and the tensile stresses are generated away from the borders in the middle of the samples.

The highest compressive stresses were found in the case study using the interface model ksback1000 ksbot1e6 (see Section 5.8.2). Figure 5.39 gives the Factor of Safety for this case against compressive failure, along the bottom line. The lowest value was about 11, at the toe of the retaining wall. Furthermore, for the same case study, Figure 5.40 shows the Factor of Safety against tension failure along the End line.
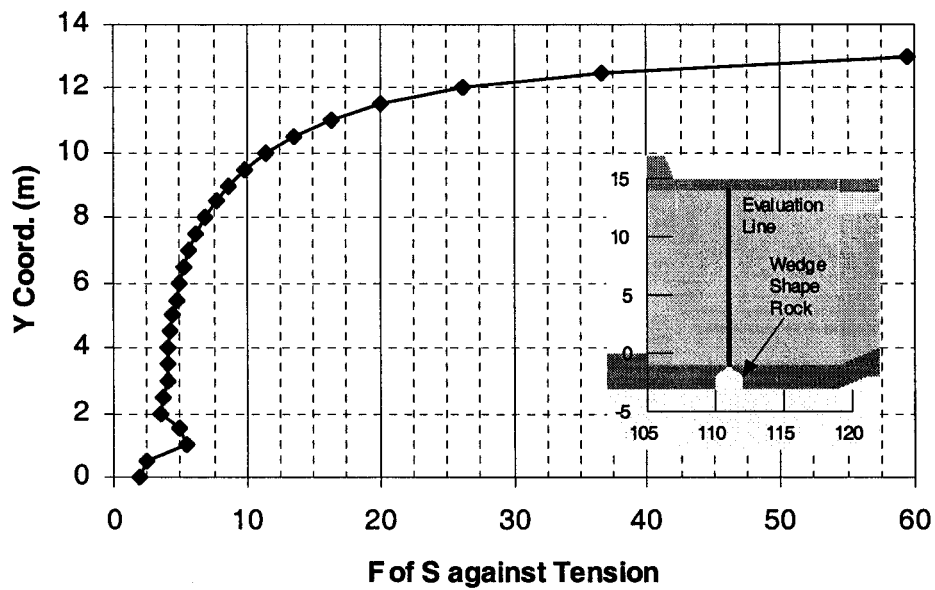
Figure 5.38 Factor of Safety against tension failure of the wedge shaped rock case

Along the End Line (ksback1000-ksbot1e6)
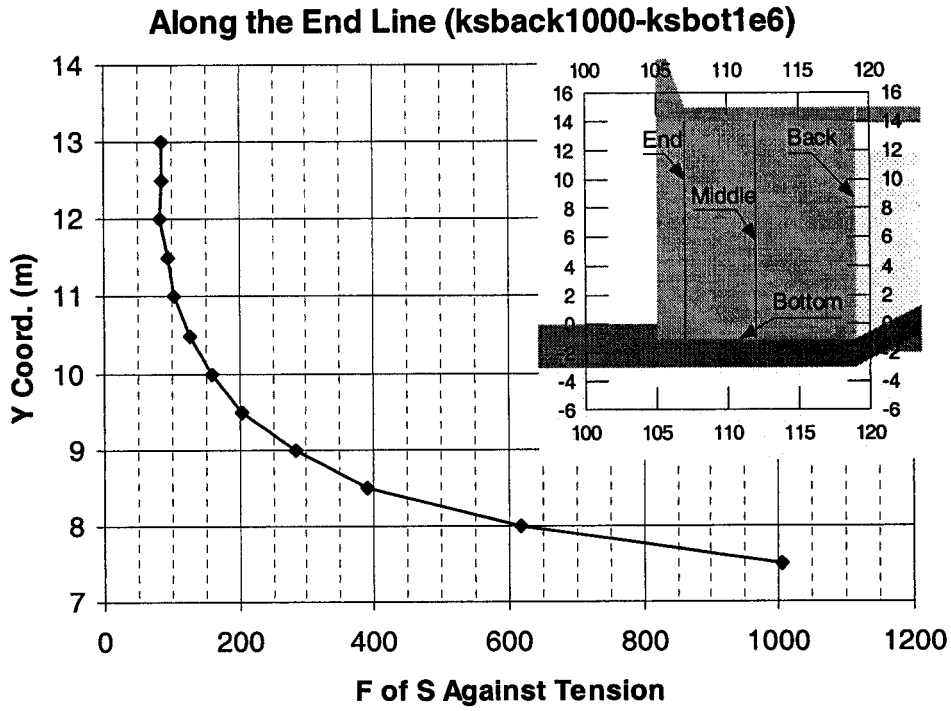
Figure 5.40 Factor of Safety against tension failure along the end line

Along the Bottom Line (ksback1000-ksbot1e6)
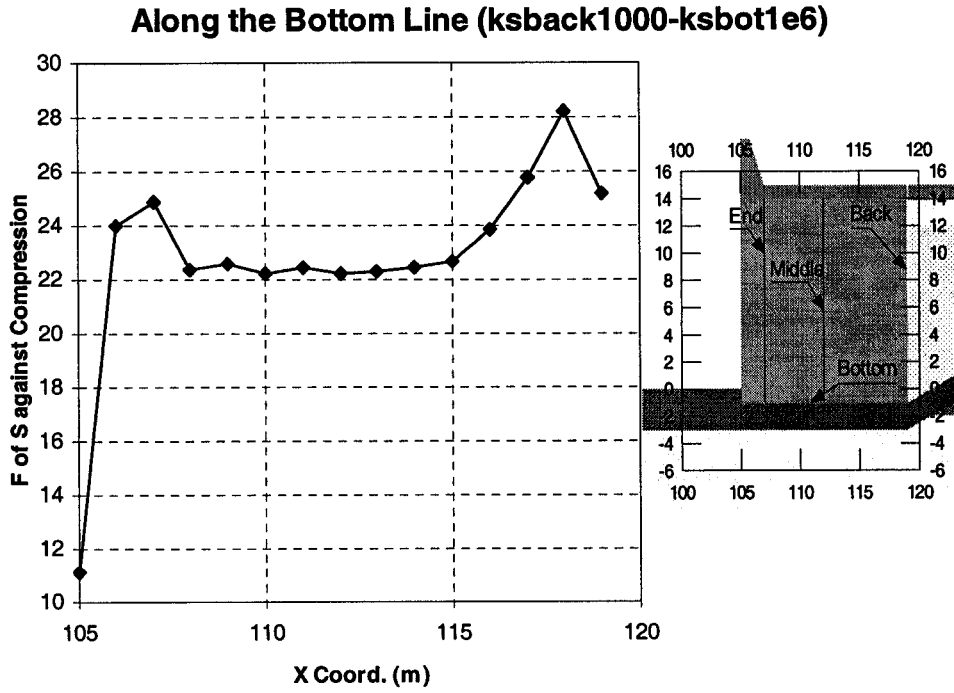
Figure 5.39 Factor of Safety against compressive failure along the bottom line

183

5.9 Summary

The purpose of this chapter was to evaluate loading conditions that could affect the stresses in the sulphur concrete wall. A summary of the cases presented herein includes:

1. The Base model, as presented in Section 5.8.1, was subjected under the Full Load and Partial Load conditions. This model also included an evaluation of three different interface models.

2. Effect of the pore water pressures.

3. Effect of the Poisson's ratio.

4. Effect of preparation of the foundation layer that will receive the structure was taken into account.

5. Effect of the stiffness of the gravel base drain layer.

6. Effect of dilation of the Compacted Lean Oil Sand was also considered.

Section 5.8.2 presents the worst-case scenario, in which the wall develops the highest compressive stresses into the sulphur concrete wall. This stress level is reached due to the combination of the interface model utilised, and the application of the Full Load surcharge. The interface model ksback1000 ksbot1e6 indicated that the shear stiffness in the wall back face is very low, simulating a smooth interface (low friction) between the backfill and the wall itself. This condition shows that the wall tilts forward, increasing the stresses at the toe. Figure 5.17 corroborates the previous finding, showing that the analysis with the lowest shear stiffness, in the back face (ksback1000 ksbot1e6), produces the higher concentration of stress in the area surrounding the toe. Figure 5.14 vividly shows the retaining wall movement due these assumptions, tilting and moving forward.

The inclusion of the pore water pressure clearly demonstrates, in Section 5.8.3, that its addition did not affect the retaining wall stresses. However, this takes into consideration

184

that the drain layer will work efficiently. In the same manner, Section 5.8.4 presents that the effect of the variation of the Poisson's ratio also did not show any adverse effect to the stress distribution, throughout the retaining wall.

The purpose of Section 5.8.5 is to demonstrate the importance of appropriate surface preparation, prior to constructing the retaining wall. Figure 5.28 shows how the structure can go into a state of tension in almost the entire structure, and Figure 5.29 suggests that proper preparation of the surface will significantly reduce the possibility of generating tensile stresses in the wall. Hence reducing the potential for tension-induced cracking.

The interaction of the backfill and the foundation layer with the retaining wall governs how the stresses change in the wall. This is observed in the case presented in Section 5.8.2, in which three different interface models are used. Furthermore, the constitutive models of the backfill and gravel base were changed keeping the same interface model constant. Figure 5.30 demonstrates that if the stiffness of the gravel base is increased, the concentration of stresses at the toe also increases. The stress increases, because the wall supports the same loads from the backfill and surcharge, but its foundation deforms less, generating an increase in stress. In contrast, Figure 5.32 shows that the stress decreases when the stiffness of the gravel base also decrease; therefore, the gravel base experiences greater deformations.

Moreover, the constitutive model of the compacted lean oil sand is changed to take into account possible dilation of the backfill, during shearing. The results in Figure 5.34 used the Cam Clay model and the results in Figure 5.22 used the Hyperbolic model (with K=450). The inclusion of the dilation in the compacted oil sand through the Cam Clay model increases σ_1 stress concentration by 5% in the toe area.

185

Equations 5.26 and 5.27 show Factor of Safety related to the computed compressive and tensile stresses, respectively. The lowest Factor of Safety against tensile failure occurred with the adverse rock foundation (Figure 5.38). However, the author does not consider this condition is realistic as good construction practice will eliminate this condition. The Factor of Safety shown in Figures 5.39 and 5.40 are very high values; nevertheless, the material properties of the 15Su3FA mix were determined after 100 freeze-thaw cycles. Beyond 100 cycles the strength of the sulphur-concrete decreased rapidly.

This discussion direct attention to one question: How long will it take to perform 100 cycles in a natural environment? The answer to this question clearly will defines the lifespan of the structure.

6 CONCLUSIONS AND RECOMMENDATIONS

6.1 Conclusions

The conversion of oil sands mining to truck and shovel operation presents opportunities and challenges. Because of the large mobile nature of the mining method, temporary engineered structures are required to facilitate the mining operation; e.g. haul roads, sizer-walls, containment dykes, etc. In this thesis the construction of sizer-walls using sulphur-concrete is evaluated. Traditionally, these sizer-walls are constructed using reinforced earth technology. The use of sulphur-concrete would 1) alleviate the growing volumes of sulphur in the Fort McMurray area and 2) create new opportunities for using sulphur-concrete in the mining operation e.g. construction of haul roads.

This thesis investigated the use of sulphur concrete in sizer-wall construction by:

1. Conducting a laboratory testing program to define the properties of sulphur-concrete,

2. Asses the stability of a sizer-wall constructed of sulphur-concrete using limit equilibrium; and ,

3. Assess the stresses and deformation in the sulphur-concrete sizer-wall using the finite element method.

The conclusions that arise from this work are:

1. As long as the temperature of the mix during the preparation of sulphur concrete is maintained below 149°C, the concentrations of Hydrogen Sulphide (H_2S), Sulphur Dioxide (SO_2) and Sulphur remained below the maximum allowable concentrations (MAC) suggested by the American Conference of Governmental Industrial Hygienists (ACGIH).

   In relation to the environment, a comprehensive study was presented in the literature review, in which it was concluded that exposure to weathering and in-service

187

conditions had a negligible effect on the sulphur concrete materials. Run-off, either by wind or rain, produced little or no effect in the immediate environment.

From the literature reviews, it may also be concluded that sulphur concrete can be used as a construction material in a safe manner, with no detrimental effect to human health or the environment.

2. The laboratory results showed that, with the materials available from the oil sands industry, such as sulphur, tailing sand, and fly ash, a competent construction material, such as the mixes listed in Table 3.6, can be produced. One great advantage is the rapid gain of strength; after only one day of cooling, it reaches approximately 85% of its strength. However, it is emphasised again that the impact of the freeze-thaw cycles on the strength of these materials is critical, and, depending on its application, a sulphur modifier may be required.

3. The fabrication of the sulphur-concrete samples using the methodology given in ACI 548 (1988) resulted in construction joints in the samples; however, their existence and influence on deteriorating the sample were noted only during the freeze-thaw cycles.

4. Sulphur-concrete strength deteriorates when subjected to freeze-thaw cycles. The laboratory test indicate that sulphur-concrete made from 15% unmodified sulphur, 3% fly ash and 82% tailing sand (by weight) loss 50% of its compressive strength and 38% of its Young's modulus after 100 freeze-thaw cycles. Beyond 100 cycles the strength of sulphur concrete degrades rapidly and samples had failed after 150 cycles.

The construction joint that formed during the fabrication of the samples appeared to play a significant role in the freeze-thaw induced strength loss. Construction procedures would have to be developed to minimise this during field construction using sulphur concrete.

5. Limit Equilibrium Analysis -

a) The existing, reinforced earth retaining wall was evaluated, based on the information contained in the contract drawings. The stability analysis gave a minimum Factor of Safety of approximately 1.5. This result was found for the condition of no pore water pressure, and represents the minimum external stability Factor of Safety under the most probable and reasonable working conditions.

b) The sulphur-concrete retaining wall was evaluated, using the same approach as above. The results showed that, to obtain a Factor of Safety of approximately 1.6, the sulphur concrete must have a minimum cohesive strength of 300 kPa. A cohesion of 400 kPa provided a Factor of Safety of 2.0. This cohesion suggests that the material must have a peak strength of 800 kPa, which is considerably less than that obtain from the uniaxial strength test (Mean = 13,200 kPa). The shear strengths of the gravel base and the compacted lean oil sand backfill become more important in the global stability of the structure when the sulphur-concrete is used to construct the retaining wall.

c) The sliding, and overturning were evaluated in the case of the sulphur-concrete wall. In relation to the sliding stability, the lowest Factor of Safety of approximately 1.88 results from a situation when a mining truck was not positioned on top of the wall. In contrast, the evaluation of the overturning stability indicated that the critical

189

condition was obtained when the mining truck was situated on top of the wall, giving a minimum Factor of Safety of approximately 1.77. This finding is obtained, when considering sliding, the weight of the truck on top of the wall increases the friction force, at the base of the wall.

d) The contact pressure of the sulphur-concrete wall, evaluated by simple static equilibrium, achieves a maximum value of 548 kPa when a mining truck is located on top of the wall. This value is greater than the maximum allowable soil pressure of 476 kPa, as indicated in the contract drawings of the existing structure. The results of the finite element analysis in Chapter 5 also present similar contact pressures. Figure 5.12 also demonstrates that, at the toe, stresses exceed the allowable contact pressure. Thus, a change in the geometry of the wall is required to decrease the contact pressure below the maximum allowable.

6.   Finite Element Analysis -

A sensitivity analysis was performed to evaluate the development of stresses and deformations in the sulphur concrete wall. Loading conditions, pore water pressures, variation in material parameters, and constitutive models were considered. From these scenarios considered, it can be concluded that up to 100 freeze-thaw cycles, the sulphur concrete wall performance was acceptable when evaluated against the properties for 100 freeze-thaw cycles.

a) Even though a tensile stress of 333 kPa, was obtained under the extreme condition of inadequate preparation of the foundation surface (see Figure 5.23), the maximum allowable tensile stress of 660 kPa would provide a Factor of Safety of 2.0 against tensile failure.

b) The upper corner of retaining wall face is observed to be constantly in tension, under the truck loads. This is a very low tension of less than 25 kPa; however, a fatigue process could be initiated, due to the repetitive loading and unloading of the mining trucks. A possible reinforcement may be required, but only in the area affected by the truck loads.

c) The interface models used between the sulphur concrete and the backfill, and the sulphur concrete and the base, become the most important variables in the determination of the stresses in the sulphur concrete wall. A low value of shear stiffness (ksback1000-ksbot1e6) in the back face results in the larger tilting and forward movement of the wall. This condition is similar to the assumption of a smooth interface, between the wall and the backfill. The more realistic interface model is when the variable shear stiffness (ksbackvar-ksbot1e6) is assumed along the back face. These scenario results in approximately 10% in the variation range of values of σ_1.

d) Utilising a dilatant constitutive model for the compacted lean oil sands did not significantly increase the stresses at the toe of the retaining wall although slightly greater horizontal movement were predicted in the compacted lean oil sands.

e) From the variation of the stiffness in the gravel base can be concluded: 1) If the stiffness of the gravel bases is increased the concentration of stresses at the toe also increases. Because the wall supports the same load from the backfill and surcharge, but its foundation deforms less, generating an increase in stress. 2) In contrast, the

191

stress at the toe decreases when the stiffness of the gravel base also decreases; therefore, the gravel base experiences greater deformations.

6.2   Recommendations

6.2.1   Preparation of Samples for the Resistance of Concrete to Rapid Freezing-Thawing Test

This test was performed in a different manner than that specified by the ASTM C 666 standards explained in Section 3.6.2. The appearance of the construction joints (see Figure 3.12) made it clear that the tamping of layers during the preparation of samples to be used in this test must be avoided. Probably the use of smaller molds, approximately 1.5 by 3-inches, will allow one to cast the sulphur concrete into the mold in one layer. In that way, the tamping will not produce an intermediate construction joint in the sample.

6.2.2   Placement of the Sulphur Concrete During Construction

The pop-up of the samples, during the freeze-thaw test, presents some concern about the placement in layers of the sulphur concrete during construction. A method of placement creating an interlocking between successive layers of sulphur concrete must be implemented. Possibly, the use of sheepsfoot compactors during placement of sulphur concrete to produce the interlocking could be required.

6.2.3   Parameters for Stress-Deformation Finite Element Analysis

Stress-deformation analysis requires knowledge of the constitutive models of the materials simulated in the finite element model. Therefore, triaxial tests are required to characterise the behaviour of the compacted lean oil sand, and to arrive at the appropriate

192

constitutive relationships for modelling. Also, this recommendation is extended to the gravel base material.

Furthermore, to model the interface between the sulphur concrete wall and the compacted lean oil sand, a shear test as performed by Clough and Duncan (1971), to determine the shear stiffness parameters is required.

6.2.4 Future Research for New Applications

Sulphur concrete reaches 85% of its strength after curing in air, for only 24 hours. The oil sands industry produces sulphur as a by-product material, and this fast setting characteristic could be exploited efficiently. Although the disadvantage of the unmodified sulphur cement in long term applications, due its lack of durability during freeze-thaw cycles, it can be used in many temporary applications such as concrete slabs or temporary roads. Furthermore, if the sulphur concrete is isolated, it could be used in long term applications. As an example, if sulphur concrete is places as a stiff base layer below a couple of metres of compacted fill, it will be isolated from the environment, and it could serve as a foundation layer for road embankments.

REFERENCES

Abdel-Jawad, Y. and Al-Qudah, M. 1993. The Combined Effect of Water and Temperature on the Strength of Sulfur Concrete. Cement and Concrete Research, Vol. 24, pp.165-175.

ACI 548 1988. Guide for Mixing and Placing Sulfur Concrete in Construction, reported by ACI Committee 548. ACI Materials Journal, July-August, pp. 314-325.

Atkinson, J.H. and Bransby, P.L. 1978. **The Mechanics of Soils: An Introduction to Critical State Soil Mechanics**. McGraw-Hill, London, p.375.

Bacon, R. F., Davis, H. S. 1921. Recent advances in the American sulphur industry. Chemical and Metallurgical Engineering, Vol. 24, No. 2, pp. 65-72.

Bathe, K. J. 1982. **Finite Element Procedures in Engineering Analysis**. Printice Hall.

Beaudoin, J. J. and Sereda, P. J. 1973. The Freeze Thaw Durability of Sulphur Concrete. Building research Notes, Division of Building Research, National Research Council, Ottawa, 53 p.

Berkowitz, J. and Marquart, J. R. 1963. J. Chem. Phys., 39, 275.

Bishop, A. W. 1958. Test requirements for measuring the coefficient of earth pressure at rest. Proceedings Brussels Conference on Earth Pressure Problems, Vol. 1, pp.15-27.

Boulon, M., Plytas, C. and Foray, P. 1986 Comportement d' interface et prévision du frottement latéral le long des pieux et tirants d'ancrage, Revue Francaise de Géotechnique, Vol. 2, Paris, pp. 129-135.

Brich Hansen, J. 1953. Earth Pressure Calculation. Danish Technical Press, Copenhagen.

Britto, A.M. and Gunn, M.J. 1987. **Critical State Soil Mechanics via Finite Elements**. Halsted Press, New York, p.488.

Brockbank, W. J., Kalynchuk, G., and Sherger, B. 1992. Use of Oil Sand for Construction of a Reinforced Earth Dump Wall. Proc. 45th Canadian Geotechnical Conference, Toronto, Canada, No.36,pp.1-10.

Broms, B and Ingleson I. 1971. Earth pressures against abutment of rigid frame bridge. Geotechnique, 1971, Vol. 21, No. 1, pp. 15-28.

Broms, B and Ingleson I. 1972. Lateral Earth Pressure on a Bridge Abutment. Proceedings of the 5th European Conference of Soil Mechanics and Foundation Engineering, Madrid, Vol. 1, pp.117-123.

Broms, B. 1971. Lateral earth pressures due to compaction of cohesionless soils. Proceeding of the 4th Budapest Conference on Soil Mechanics and Foundation Engineering, pp. 373-384.

Brooker, E. W. and Ireland, H. O. 1965. Earth pressures at rest related to stress history. Canadian Geotechnical Journal, Vol. 2, pp. 1-15

Bros, B. 1972. The influence of model retaining wall displacement on active and passive earth pressure in sand. Proc. 5th European Conference on Soil Mechanics and Foundation Engineering. Madrid, Vol. 1, pp. 241-249.

Casagrande, A. 1936. The Determination of the Pre-Consolidation Load and Its Practical Significance. Proceeings International Conference of Soil Mechanics and Foundation Engineering, Vol. III, pp.60-64.

Carder, D. R, Murray, R. T., and Krawczyk, J. V. 1980. Earth pressures against an experimental retaining wall backfilled with silty clay. Transport and Road Research Laboratory Report, No. LR 946.

Carder, D. R. Pocock, R. G. and Murray, R. T. 1977. Experimental retaining wall facility-lateral stress measurements with sand backfill, Transport and Road Research Laboratory Report, No. LR 766.

Chan, D. H.-K. 1986. Finite Element Analysis of Strain Softening Material. Ph. D. Thesis, Civil Engineering Department, University of Alberta, Edmonton, Alberta, Canada.

Clough, G. W. and Duncan, J. M. 1992. Earth Pressures. **Foundation Engineering Handbook**, Second Edition. Edited by Fang, H. Y. Van Nostrand Reinhold Company, New York , pp.223 - 235

Clough, G.W. and Duncan, J.M. 1971. Finite Element Analyses of Retaining Wall Behavior. Journal of the Soil Mechanics and Foundation Divison, ASCE, SM 12, December, pp.1657-1673.

Coduto, D. P. 1994. **Foundation Design: principles and practices**. Printice-Hall, Inc., 796 p.

Cohen, M. D. 1987. Damage Mechanism of Cyclic Freezing-Thawing in Sulfur Concrete. Cement and Concrete Research, Vol. 17, pp.357-360.

Coulomb, C. A., 1776. Essai sur une application des regles de Maximums et Minimis á quelques Problems de Statique, relatifs á l'Architecture, Memoires de Mathematique et de Physique, Présentés, á l'Academie Royale des Science, Paris, Vol. 3, 38.

Coyle, H. M., Bartoskewitz, R.E 1976. Earth pressures on precast panel retaining wall, Journal of the Geotechnical Engineering Division, ASCE, Vol. 102, No. GT5, pp.441-456.

Coyle, H. M., Bartoskewitz, R.E., Milberger, L. J., and Butler, H. D: 1974. Field measurements of lateral pressures on a cantilever retaining wall. Transportation Research Record, No. 517, pp. 16-29.

Crick, S. M. and Whitmore, D. W. 1998. Using Sulfur Concrete on a Commercial Scale. Concrete International, American Concrete Institute, Detroit, Michigan, February, pp. 83-86.

Crow, L. J., and Bates, R. C. 1970. Strength of Sulfur-Basalt Concretes. Report No. RI 7349, U.S. Bureau of Mines, Washington, D.C., 34 p.

Currel, B. R. 1976. New Sulphur-Based Coating. Polymers and Paint Journal, Spring, pp. 6-8.

Currel, B. R., William, A. J., Mooney, A. J., Nash, B. J. 1975. New Uses of Sulfur. Advances in Chemistry, Series 140, ACS, Washington, p. 1-17,

Czarnecki, B. and Gillot, J. E. 1989, Stress-Strain Behaviour of Sulfur Concrete made with Different Aggregates and Admixtures. Quarterly Journal of Engineering Geology, London, Vol. 22, pp.196-206.

Czarnecki, B. and Gillot, J. E. 1989. Effect of Different Admixture on the Strength of Sulphur Concrete. Cement, Concrete and Aggregates, CCAGDP, Vol. 11, No. 2, pp. 109-118.

Czarnecki, B and Gillot, J. E. 1990. The Effect of Mix Design on Properties of Sulfur Concrete. Cement, Concrete and Aggregates, CCAGDP, Vol. 12, No. 2, Winter, pp. 79-86.

Czarnecki, B. and Gillot, J. E. 1990. Effect of Different Admixtures on the Durability of Sulfur Concrete made with Different Aggregates. Engineering Geology, Amsterdam, Vol. 28, pp. 105-118.

Dale, J. M. and Ludwig, A. C. 1966. Feasibility Study for Using Sulfur-Aggregate Mixtures as a Structural Material. Technical report NO. AFWL-TR-66-57, Southwest Research Institute, San Antonio, Sept.,40 p.

Dale, J. M. and Ludwig, A. C. 1968. Advanced Studies of the Sulfur-Aggregate Mixture as a Structural Material. Technical report NO. AFWL-TR-68-21, Southwest Research Institute, San Antonio, Oct.,68 p.

Deme, I. 1974. Processing of Sand-Asphalt-Sulphur Mixes. Presented at the Annual Meeting of the Association of Asphalt Paving Technologists, Williamsburg, Virginia, February .

Deuel, L. E., Saylak, D 1981. Environmental and Safety Aspects of the Use of Sulfur in Highway Pavements: Part II – Weathering and In-Service Considerations. Proceedings of: SULPHUR-81 an International Conference on Sulphur, Calgary, May, pp. 681-709.

Diehl, L 1976. Dicyclopentadiene modified sulphur and its uses as a binder, quoting sulphur concrete as an example. Proceedings of New Uses for Sulphur and Pyrites; May 17-19, Madrid; The Sulphur Institute, Washington, D.C., pp.202-214.

Driscoll, D. D. 1979. Retaining Wall Design Guide, Foundation Services, Inc., Portland, OR. Prepared for the USDA Forest Service.

Duecker, W. W. 1934. Admixtures improve properties of sulphur cements. Chemical and Metallurgical Engineering, Vol. 41, No. 11, pp. 583-586.

Duecker, W. W., Estep, J. W., Mayberry, M. G., Schwab 1948. Studies of properties of sulphur jointing compounds. Journal of Am Waterworks Association, Vol. 7, pp. 715-728.

Duncan, J. M., Byrne, P., Wong, K.S., Mabry, P. 1980. Strength, stress-strain and bulk modulus parameters for finite element analyses of stresses and movements in soil masses. Report No. UBC/GT/80-01. Department of Civil Engineering, University of California, Berkeley, California. p.70.

Duncan, J.M, Clough, G. W., and Ebeling R. M. 1990. Behavior and Design of Gravity Earth Retaining Structures. Design and Performance of Earth Retaining Structures, Edited by P.C. Lambe and L. A. Hansen. Geotechnical Special Publication No. 25, ASCE, 1990, pp.251-277.

Duncan, J.M. and Chan, C.Y. 1970. Non-linear analysis of stress and strain in soils. Journal of the Soil Mechanics and Foundation Division, ASCE, September, SM 5, pp.1629-1653.

Dusseault, M. B. and Morgernstern, N. R. 1978 Shear strength of the Athabasca Oil Sands. Canadian Geotechnical Journal, Vol. 15, pp. 216-238

Fintel, M. 1985. **Handbook of Concrete Engineering**, 2nd Edition. Van Nostrand Reinhold Company, New York, 1985.

Forsyth, A 1978. Alternative Earth Reinforcements, ASCE Symp. Earth Reinforcement, Pittsburgh,pp. 358-370

Frasch, H. J., 1912. Ind. Eng. Chem. 4, 134. "Perkin Medal Award Address of Acceptance".

Funke, R. H., Jr. and McBee, W. C. 1982. An Industrial Application of Sulfur Concrete. ASC Symposium Series No. 183, American Chemical Society, Washington, D.C., pp. 195-208.

Gamble, B. R. and Shrive, N. G. 1978. Creep in Sulphur. Proceedings of the International Conference on Sulphur in Construction, CANMET, Energy, Mines, and Resource Canada, Sept. 12-15d, Ottawa, pp. 503-518.

Geo-Slope 2001. User's Guide Sigma/W – for finite element stress/deformation analysis – Version 5. Geo-Slope International Ltd., Calgary, Canada.

Gillot, J. E., Jordaan, I. J., Loov, R. J., and Shrive, N. G. 1983. Effect of different aggregates on the durability of sulphur concretes. Durability of Building Materials, Vol. 1, pp. 255-273.

Gillott, J. E.; Jordaan, I. J.; Loov, R. E.; and Shrive, N. G. 1980. Sulfur Concretes, Mortars and the Like. U.S. Patent No.4,188,230, Feb. 12.

Gillott, J. E.; Jordaan, I. J.; Loov, R. E.; and Shrive, N. G. 1982. Studies of sulphur concrete made with different aggregates. Proceedings of Sulphur-82, International Sulphur Conference, London, England, pp. 45-49.

Goodman, R. E., Taylor, R.L., and Brekke, T.L. 1968. A Model for the Mechanics of Jointed Rock. Journal of the Soil Mechanics and Foundation Division, ASCE, SM 3, May, pp.637-659.

Graham, J. 1968. Plane plastic failure in cohesionless soils. Geotechnique, Vol. 18, pp. 301-316.

Hajiabdolmajid, V., Martin, C. D., and Kaiser, P. K. 2000. Modelling brittle failure of rock. Proc. 4th North American Rock Mechanics Symposium. NARMS 2000, Girard, Liebman, Breeds and Doe Editors. Balkema, Rotterdam, pp.991-998.

Henkel, D. J. 1960. The shear strength of saturated remoulded clay. Proceedings od the ASCE Research Conference on Shear Strength of Cohesive Soil, Boulder, Colorado, USA, pp.533-544.

Hoek, E. and Bray, J.W. 1981. **Rock Slope Engineering**, 3rd Edition. The Institution of Mining and Metallurgy, London, p.308

Hyne, J. B. 1981. Understanding Sulphur – The Key of the Advancement of Its Technology. Proceeding of SULPHUR-81 an international conference on sulphur, Sulphur Development Institute of Canada, Calgary, Alberta, Canada, May25-28, pp. 25-37.

Ingold, T. S, 1983. Laboratory Pull-Out Testing of Grid Reinforcements in Sand. Geotechnical Testing Journal, ASTM, Vol. 6, September.

Izatt, J. 0. 1977. Sulphur-Extended Asphalt Paving Project Highway US 93-95, Boulder City, Nevada - A Construction Report. Prepared for the Sulphur Institute, January.

Jacky, J. 1957. The Coefficients of Earth Pressure at Rest, Journal of the Society of Hungarian Architects and Engineers, Vol. 7, pp. 355-358.

Johnston, C. D. 1978. Preparation, proportioning and properties of sulphur concrete. Proceedings of the International Conference on Sulphur in Construction, CANMET, Energy, Mines, and Resource Canada, Sept. 12-15, Ottawa, pp. 413-432.

Kennepohl, G. J. A., Logan, A., and Bean, D. C. 1975. Conventional Paving Mixes with Sulphur-Asphalt Binder. Presented to the Annual Meeting of the Association of Asphalt Paving Technologists, Phoenix, Arizona, February.

Koerner, R. M. 1994. **Designing with Geosynthetics**, 3rd Edition. 1994, Prentice Hall, New Jersey, 783 p.

Konder, R.L. 1963. Hyperbolic stress-strain response: cohesive soils. Journal of the Soil Mechanics and Foundation Division, ASCE, Vol.89, SM 1, February, pp.115-141.

Laishly, E. J. and Tyler, M. C. 1978. Biological Oxidation of Sulphur Construction Materials. Proceedings of the International Conference on Sulphur in Construction, CANMET, Energy, Mines, and Resource Canada, Sept. 12-15, Ottawa, pp. 171-180.

Lavoasier, A. 1794. "Elements of Chemistry", R. Kerr, Transl., Creech & Son, Edinburgh.

Lee, D. Y., Klaiber, F. W., and Khosraviani 1978. Fatigue behaviour of improved sulphur concrete. Proceedings of the International Conference on Sulphur in Construction, CANMET, energy, Mines and Resources Canada, Sept. 12-15, Ottawa, pp.489-502.

Lee, I. K. and Herrington, J. R 1974. **Soil Mechanics New Horizons**, edited by I. K. Lee, Newnws-Butterworths.

Litvan, G. G. 1976. Frost Action in Cement in the Presence of Deicers. Cement and Concrete Research, Vol. 6, No. 3, pp. 351-356.

Loov, R. E. 1974. Sulfur Concrete – State of the Art in 1974. Research Report No. CE75-2, Department of Civil Engineering, University of Calgary, 10 p.

Loov, R. E., Vroom, A. H., and Ward, M. A. 1974. Sulfur Concrete a New Construction Material. Prestressed Concrete Institute Journal, Vol. 19, No. 1, January-February, p. 86-95.

Lord E. R. F. and Cameron R. 1985. Compaction Characteristic of Athabasca Tar Sand. Proceedings of the 38th Canadian Geotechnical Conference, Edmonton, Alberta, pp. 359-368

Malhotra, V. M. 1974. Effect of specimen size on compressive strength of sulphur concrete. Division Report IR 74-25, Energy, Mines and Resource Canada.

Malhotra, V. M. 1979. Sulphur Concrete and Sulphur Infiltrated Concrete: Properties, Applications and Limitations. CANMET Report 79-28. Energy, Mines, and Resources Canada, Ottawa, 26 p.

Malhotra, V. M.; Soles, J. A.; Wheat, T. A.; and Berry, E. E. 1978, Editors, Proceedings, International Conference on Sulfur in Construction, Ottawa, Sept., V. 2, 555 pp.

Mayne, P W. and Kulhawy, F. H. 1982. K_0 –OCR relationships in soil. Journal of the Geotechnical Engineering Division, ASCE, 108, No. GT6, pp. 851-872.

McBee, W. C., and Sullivan, T. A. 1979. Development of Specialized Sulfur Concretes. BuMines Report No. RI 8346, U.S. Bureau of Mines, Washington, D.C., 21 p.

McBee, W. C., and Sullivan, T. A. 1982, (assigned to U.S. Department of Commerce). Modified Sulfur Cement. U.S. Patent No. 4,311,826, Jan 19.

McBee, W. C., and Sullivan, T. A. 1982, (assigned to U.S. Department of Commerce). Concrete Formulations Comprising Polymeric Reaction Products of

Sulfur/Cyclopentadiene, Oligmer/Dicyclopentadiene. U.S. Patent No. 4,348,313, Sept. 7.

McBee, W. C.; Sullivan, T. A.; and Jong, B. W. 1981. Modified Sulfur Cements for use in Concretes, Flexible Paving, Coatings, and Grouts. BuMines Report No. RI 8545, U.S. Bureau of Mines, Washington, D.C., 24 p.

McBee, W. C.; Sullivan, T. A.; and Jong, B. W. 1981. Modified Sulfur Concrete Technology. Proceedings, SULPHUR-81 International Conference on Sulphur, Calgary, May, pp. 367-388.

McBee, W. C.; Sullivan, T. A.; and Jong, B. W. 1983. Industrial Evaluation of Sulfur Concrete in Corrosive Environments. BuMines Report No. RI 8786, U.S. Bureau of Mines, Washington, D.C., 15 pp.

McBee, W. C.; Sullivan, T. A.; and Jong, B. W. 1983. Corrosion-Resistant Sulfur Concretes. BuMines Report No. 8758, U.S. Bureau of Mines, Washington, D.C., 28 p.

McBee, W. C.; Sullivan, T. A.; and Fike, H. F. 1986. Corrosion-Resistant Sulfur Concretes. Corrosion and Chemical, Resistant Masonry Materials Handbook, Noyes Publications, Park Ridge, pp. 392-417.

Meyer, B 1977. **Sulphur, Energy and Enviroment**, Elsevier Scientific Publishing, Amsterdam, The Netherlands, 448 p.

Mitchell, J. K. and Christopher, B. R. 1990. North American Practice in Reinforced Soil System. Design and Performance of Earth Retaining Structures, Geothecnical Special Publication No. 25, ASCE, Edited by Lambe, P. and Hansen, L., pp. 322-346.

Mohr, O., 1900. Welche Umstande Bedingen die Elastizitatsgrenze und den Bruch eines Materials?, Zeitschrift des Vereines Deutsher Ingenieure, Vol. 44, 1524-1530, 1572-1577.

Morgenstern, N.R. 1992. The Evaluation of Slope Stability - A 25 Year Perspective. ASCE Specialty Conference on Stability of Slopes and Embankments. 1:1-26.

Morgenstern, N. R. and Eisenstein, Z., 1970. Methods of Estimating Loads and Deformations. Proceedings of the Specialty Conference Lateral Stresses in the Ground and Design of Earth-Retaining Structures, ASCE, p. 51-102.

Morris, D. V. and Crockford, W. W. 1990. Cement Stabilized Soil Retaining Wall. Design and Performance of Earth Retaining Structures, Edited by P.C. Lambe and L. A. Hansen. Geotechnical Special Publication No. 25, ASCE, pp. 347-378.

NAVFAC DM-7.2, Foundation and Earth Structures, Design Manual 7.2, Department of the Navy, Naval Facility Engineering Command, Alexandria, May 1982, p. 270.

Naylor, D. J. and Pande, G. N. 1981. **Finite Elements in Geotechnical Engineering**. Pineridge Press, Swansea, UK, p. 245.

Nimer, F. L., and Campbell, R. W. 1983. Sulfur Cement-Aggregate-Organosilane Composition and Methods for Preparing. U.S. Patent No. 4,376,830, Mar. 15.

O'Rourke, T. D and Jones, C. J. F. P. 1990. Overview of Earth Retention Systems: 1970-1990. Geotechnical Special Publication No. 25, Design and Performance of Earth Retaining Structures, P. C. Lambe and L. A. Hansen Editors, ASCE, pp. 22-51.

Okamura, H. A. 1998. Early Sulfur Concrete Installations. Concrete International, American Concrete Institute, January, pp.72-75.

Packshaw, E. 1946. Earth Pressure and Earth Resistance. Journal of Institution of Civil Engineers, 1946, Vol. 25, pp.233-256.

Potts, D. M. 1993. The analysis of earth retaining structures. Retaining Structures, Edited by C. R. I. Clayton, Institution of Civil Engineers. Tomas Telford Services Ltd, London, pp. 167-186.

Potts, D. M. and Zdravkovic, L 1999. **Finite Element Analysis in Geotechnical Engineering – Theory**. Thomas Teldford, London, p.440.

Powers, T. C. 1975. Freezing Effects in Concrete. American Concrete Institute, Special Publication No. SP-47, pp.1-11.

Rankine, W. J. M. 1857. On the stability of loose earth. Phil. Trans. Roy. Soc., London, 147, Part 1, pp. 9-27.

Rehnman, S. E: and Broms, B. B. 1972 Lareral pressures on basement wall. Results from full scale tests. Proceedings of 5th European Conference on Soil Mechanics and Foundation Engineering, Madrid, Vol. 1, pp. 189-197.

Rennie, W. J. 1978. Sulphur Asphalts: The Pronk S/A Emulsion Binder System, 2nd Edition. New Uses for Sulphur Technological Series No. 3 SUDIC: Calgary, Alberta.

Rowe, P. W. 1954. A Stress-Strain Theory for Cohesionless Soil with Applications to Earth Pressures at Rest and Moving Walls. Geotechnique, Vol. 4, No. 2, pp. 70-88.

Rybezeynski, W., Ortega, A., Ali, W. 1974. Sulphur concrete and very low cost housing. Canadian Sulphur Symposium, Calgary, 1-9.

Saylak , D. et al. 1980. Environmental and Safety Aspects of the Use of Sulfur in Highway Pavements. Final Report No. FHWA-RD-80/191, Texas A&M University, August.

Saylak, D., Deuel, L. E., Zahray, R. 1981. Environmental and Safety Aspects of the Use of Sulfur in Highway Pavements: Part I – Mix Preparation and Construction. Proceedings of: SULPHUR-81 an International Conference on Sulphur, Calgary, May. pp. 651-679.

Schlosser, F. (1971).Terre Armé: reserches et réalisations, Bulletin de liaison des LCPC, No. 62).

Schlosser, F. 1990. Mechanically Stabilized Earth Retaining Structure in Europe. Design and Performance of Earth Retaining Structures, Edited by P.C. Lambe and L. A. Hansen. Geotechnical Special Publication No. 25, ASCE, pp. 347-378.

Schlosser, F. and De Buhan, P. 1990. State of the Art Report, Theory and design related to the performance of reinforced soil structures. Performance of reinforced soil stuctures. British Geotechnical Society, Edited by McGown, Yeo and Andrawes, pp. 1-13.

Schlosser, F. and Elias, V 1978. Friction in Reinforced Earth, ASCE Symp. Earth Reinf., Pittsburgh, pp. 735-763.

Schneider, R. A., and Simic, M. 1981. Plasticized Sulfur Composition. U.S. Patent No. 4,308,072, Dec. 29.

Sheppard, Jr., W. L. 1975. Sulphur mortars - a historical survey. Journal of the Sulphur Institute, Fall-Winter issue, Washington, D.C.

Shrive, N. G., Gillott, J. E., Jordaan, I. J and Loov, R. E. 1977. Basic properties of some sulphur-bound composite materials. Material Science and Engineering, Vol. 30, No. 1, pp. 71-79.

Shrive, N. G., Gillott, J. E., Jordaan, I. J and Loov, R. E. 1981. Freeze/Thaw Durability of Sulphur Concretes. Proceedings of: SULPHUR-81 an International Conference on Sulphur, Calgary, May, pp. 185-194.

Shrive, N. G., Gillott, J. E., Jordaan, I. J and Loov, R. E. 1977. A Study of Durability in Temperature Cycles and Water Resistance of Sulphur Concretes and Mortars. Journal of Testing and Evaluation, Vol. 5, No. 6, pp 484-493.

Stuedel, R. and Mausle, H. J. 1980. Chemie in unserer Zeit, 3, 14.

Suncor 2000. Haul Road Design Report. Suncor Energy, Mine Engineering, pp. 1-24.

Sullivan, T. A. 1986. Corrosion-Resistant Sulfur Concretes-Design Manual. The Sulphur Institute, Washington, D.C., 44 p.

Sullivan, I. A., and McBee, W. C. 1976. Development and Testing of Superior Sulfur Concretes, BuMines Report No. RI 8160, U.S. Bureau of Mines, Washington, D.C., 30 pp.

Sullivan, T. A.; MeBee, W. C.; and Blue, D. D. 1975. Sulfur in Coatings and Structural Materials. Advances in Chemistry Series No. 140, American Chemical Society, Washington, D.C., p. 55-74.

Terzaghi, K. and Peck, R. B. 1967. **Soil Mechanics in Engineering Practice,** 2nd Edition. John Wiley & Sons, Inc., New York, p. 729.

Terzaghi, K., Peck, R. B. and Mersri, G. 1996. **Soil Mechanics in Engineering Practice,** 3rd Edition. John Wiley & Sons, Inc., New York, p. 549.

U.S. Army Corps of Engineers 1994.Retaining and Flood Walls. Technical Engineering and Design Guides, No. 4, ASCE, New York, p. 313.

U.S. Department of the Navy 1962. Design Manual – Soil Mechanics, Foundation and Earth Structures. Bureau of Yards and Docks, Washington.

Vroom, A. H. 1977. Sulfur Cements, Process for Making Same and Sulfur Concretes Made Therefrom. U.S. Patent No. 4,058,500, Nov. 15.

Vroom, A. H. 1981. Sulfur Cements, Process for Making Same and Sulfur Concretes Made Therefrom. U.S. Patent No. 4,293,463, Oct. 6.

Vroom, A. H. 1998. Sulfur Concrete Goes Global. Concrete International, American Concrete Institute, Detroit, Michigan, January, pp. 68-71.

Wong, K.S. and Broms, B.B. 1994. Analysis of Retaining Walls Using the Hyperbolic Model. Soil-Structure Interaction: Numerical Analysis and Modeling. Edited by J.W. Bull. E&FN Spon, London. pp.605-645.

Woo, G. L. 1983. Phosphoric Acid Treated Sulfur Cement-Aggregate Compositions. U.S. Patent No. 4,376,831, Mar. 15.

Wu, T. H. 1975. Retaining Walls. **Foundation Engineering Handbook,** Edited by Winterkon, H. F. and Fang, H. Y. Van Nostrand Reinhold Company, New York, pp. 402-417

APPENDIX A LABORATORY RESULTS

This appendix presents the laboratory results from the compression test, split tensile test and the test of resistance to rapid freezing and thawing cycles performed on the six mixes studied in this thesis. The included results are the following:

Initial Condition
- Stress-strain curves.
- Peak compressive strength and yield compressive strength.
- Young's modulus.
- Tensile strength and maximum tensile strain.

After the test for resistance of concrete to rapid freezing and thawing.
- Peak compressive strength and yield compressive strength.
- Initial Young's modulus and corrected Young's modulus.
- Correction factors for specimens with l/d ratio less than 2.

10% Sulphur + 90% Tailing Sand
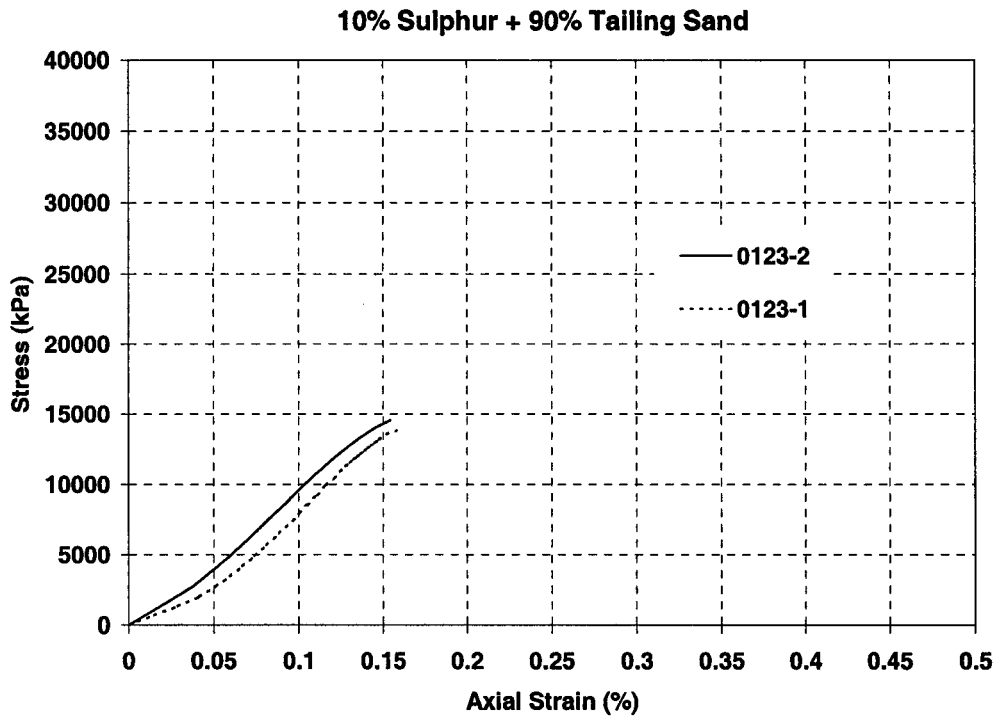
Figure A-1 10Su90Sa stress-strain curve

10% Sulphur + 2% Fly Ash + 88% Sand
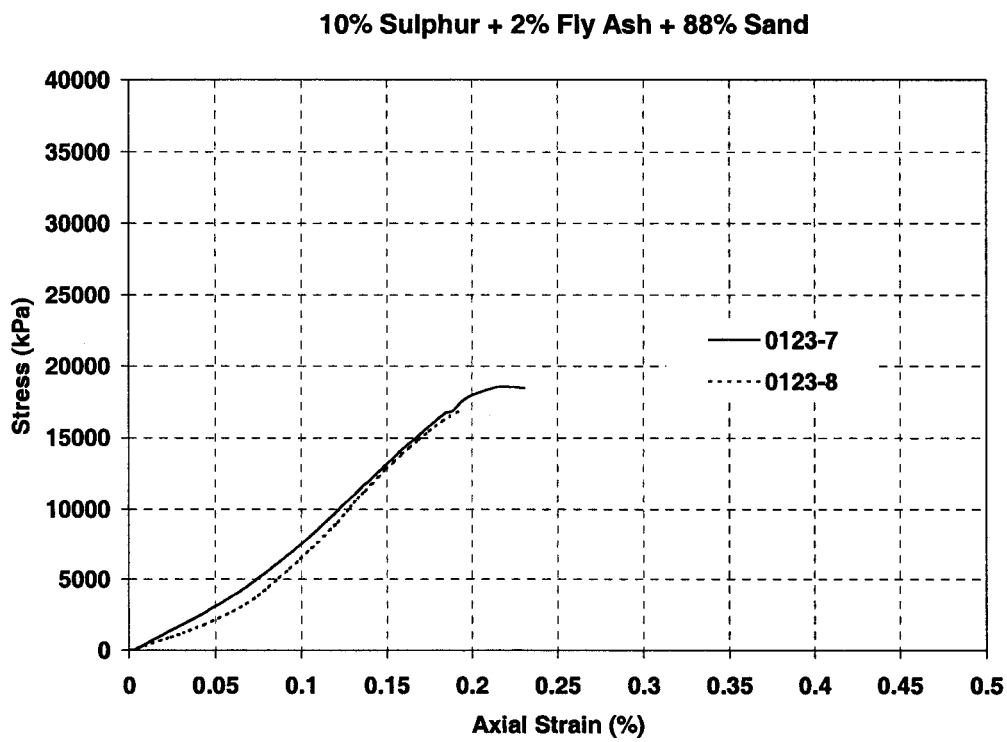
Figure A-2 10Su2FA stress-strain curve

15% Sulphur + 85% Sand
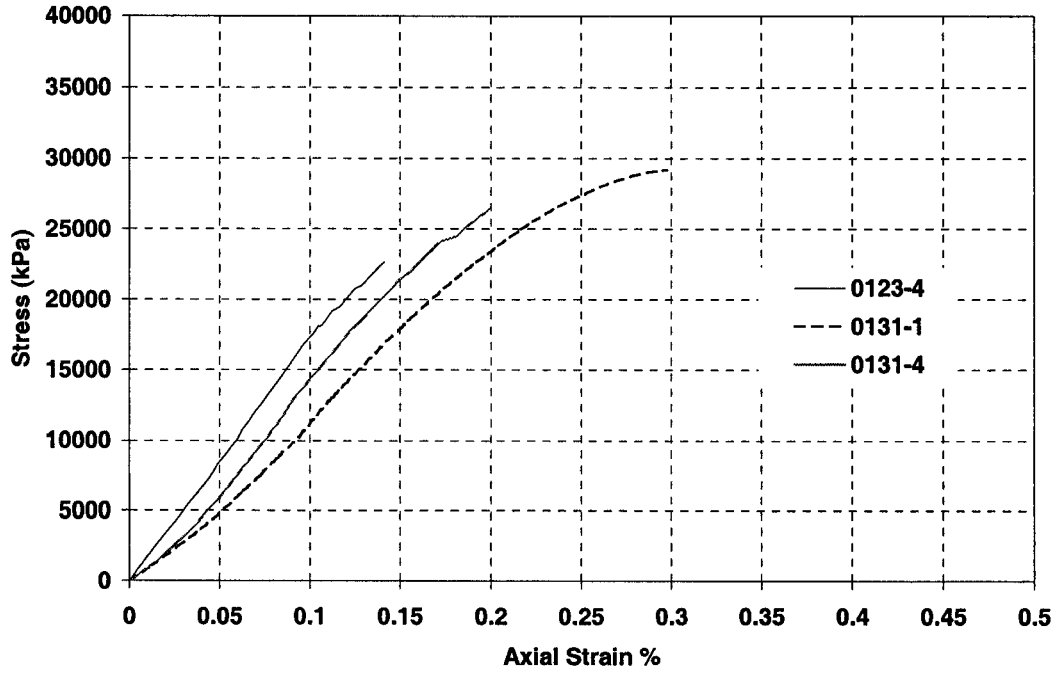
Figure A-3 15Su85Sa stress-strain curve

15% Sulphur + 3% Fly Ash + 82% Tailing Sand
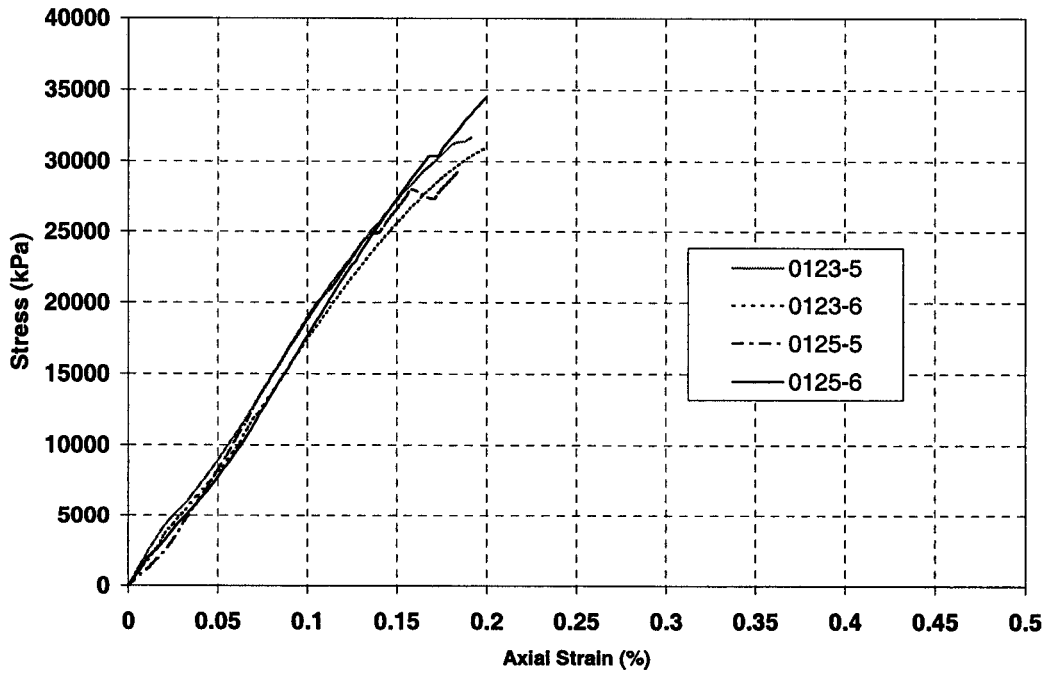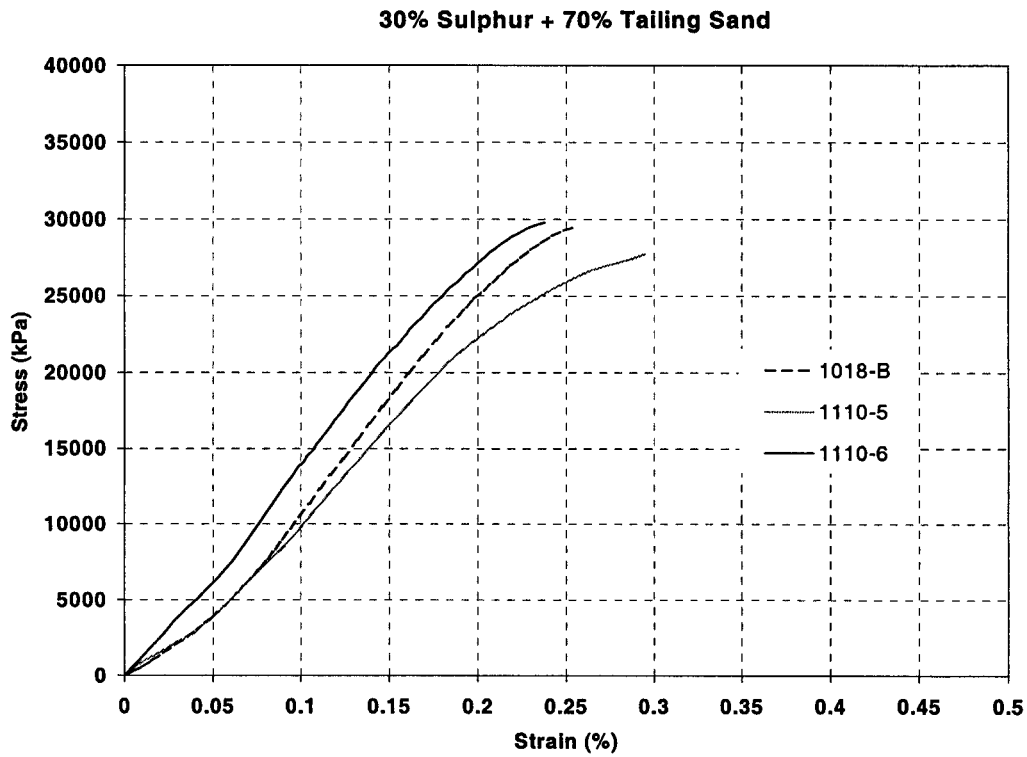

Figure A-4 15Su3FA stress-strain curve

30% Sulphur + 70% Tailing Sand

Figure A-5 30Su70Sa stress-strain curve

25% Su + 5% Fly Ash + 70% Tailing Sand
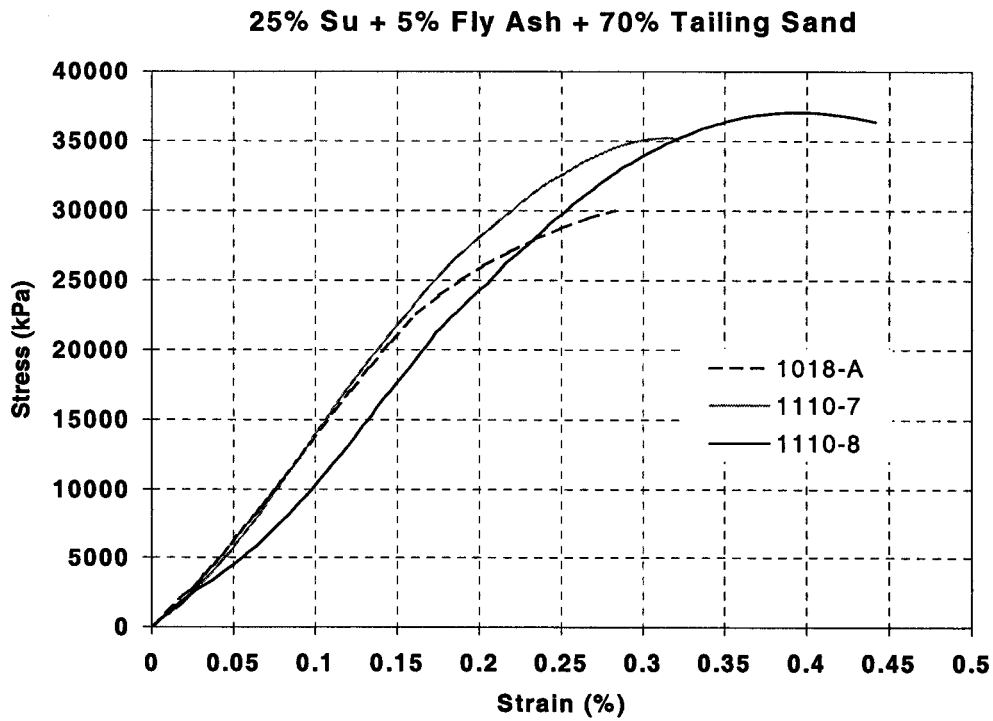
Figure A-6 30Su5FA stress-strain curve

Material:
10% Sulphur + 90% Tailing Sand

Sample	Peak Strength kPa	Yield Strength kPa	Statistiscs	Peak Strength	Yield Strength
			Mean	11718	10890
0123-1	13852	10452	Standard Error	1026	928
0123-2	11085	10970	Median	11411	10970
0920-3	7682	7368	Standard Deviation	2513	2274
1004-1	11085	10970	Sample Variance	6313996	5170043
1005-1	11737	11056	Range	7186	7157
1101-2	14868	14525	Minimum	7682	7368
			Maximum	14868	14525
			Sum	70309	65342
			Count	6	6

Material:
15% Sulphur + 85% Tailing Sand

Sample	Peak Strength kPa	Yield Strength kPa	Statistiscs	Peak Strength	Yield Strength
			Mean	21671	17057
0123-4	22677	16747	Standard Error	2535	1163
0131-1	29200	19394	Median	22935	17221
0131-4	26432	17695	Standard Deviation	6210	2848
1006-4	14659	14297	Sample Variance	38567606	8108700
1006-1	13861	13433	Range	15339	7342
1005-3	23194	20775	Minimum	13861	13433
			Maximum	29200	20775
			Sum	130023	102341
			Count	6	6

Material:
30% Sulphur + 70% Tailing Sand

Sample	Peak Strength kPa	Yield Strength kPa	Statistiscs	Peak Strength	Yield Strength
			Mean	32860	18834
1018-B	29534	19949	Standard Error	2239	566
1110-5	27745	18107	Median	29665	18446
1110-6	29795	18446	Standard Deviation	6334	980
1010-1	45159		Sample Variance	40118204	960803
1008-3	28104		Range	17414	1842
1009-3	35287		Minimum	27745	18107
1009-1	38786		Maximum	45159	19949
1018-B	28467		Sum	262878	56503
			Count	8	3

Table A-1 Peak and yield strengths of sulphur and tailing sand mixes

209

Material:

10% Sulphur +2% Fly Ash + 88% Tailing Sand

Sample	Peak Strength kPa	Yield Strength kPa	Statistiscs	Peak Strength	Yield Strength
			Mean	13159	11613
0123-7	18445	14000	Standard Error	1849	1073
0123-8	16820	12781	Median	10505	11539
0918-1	10505	10298	Standard Deviation	4135	2146
0918-2	10329		Sample Variance	17102156	4603800
1006-5	9694	9373	Range	8751	4627
			Minimum	9694	9373
			Maximum	18445	14000
			Sum	65794	46451
			Count	5	4

Material:

15% Sulphur +3% Fly Ash + 84% Tailing Sand

Sample	Peak Strength kPa	Yield Strength kPa	Statistiscs	Peak Strength	Yield Strength
			Mean	27030	22809
0123-5	31678	19455	Standard Error	1926	1271
0123-6	30975	22286	Median	27758	23307
0125-5	29253	24328	Standard Deviation	5447	2542
0125-6	34517	25166	Sample Variance	29669765	6461542
0918-5	19332		Range	15185	5711
0918-7	21316		Minimum	19332	19455
1110-3	22904		Maximum	34517	25166
1110-4	26264		Sum	216238	91235
			Count	8	4

Material:

25% Sulphur +5% Fly Ash + 70% Tailing Sand

Sample	Peak Strength kPa	Yield Strength kPa	Statistiscs	Peak Strength	Yield Strength
			Mean	32251	22568
1018-A	30018	22581	Standard Error	2298	734
1110-7	37048	21290	Median	35217	22581
1110-8	35217	23833	Standard Deviation	6081	1272
1010-4	30052.65		Sample Variance	36981398	1616868
1011-1	35890.84		Range	16894	2543
0920-1	20317.48		Minimum	20317	21290
0920-2	37211.31		Maximum	37211	23833
			Sum	225754	67704
			Count	7	3

Table A-2 Peak and yield strengths of sulphur, tailing sand and fly ash mixes

210

Statistisc	10Su90Sa (mPa)	10Su2FA (mPa)	15Su85Sa (mPa)	15Su3FA (mPa)	30Su70Sa (mPa)	25Su5FA (mPa)
Mean	11623	12218	16578	18065	17379	18266
Standard Error	340	460	1044	704	1572	1282
Median	11686	12031	15431	18405	16378	16918
Standard Deviation	898	1126	2762	2113	4446	3393
Sample Variance	807073	1267005	7626066	4466768	19768968	11509562
Range	2479	3080	7611	5681	12497	7937
Minimum	10505	10920	12885	14825	10934	14583
Maximum	12983	14000	20496	20506	23431	22520
Sum	81362	73309	116043	162584	139034	127860
Count	7	6	7	9	8	7

Table A-3 Young's modulus statistics

10Su90Sa	
Sample	E (MPa)
1005-2	12983
1005-2	12066
1004-2	10505
0123-1	12321
0125-3	10825
0125-4	10977

10Su2FA	
Sample	E (MPa)
0918-4	11930
1006-6	12132
0123-7	11332
0123-8	12994
1120-6	10920

15Su85Sa	
Sample	E (MPa)
1006-2	14825
1006-3	15100
0123-4	17762
0131-1	12885
0131-4	15431
1122-2	20496
1122-2	19544

15Su3FA	
Sample	E (MPa)
1006-2	14825
0918-6	16853
0918-8	16479
0123-5	20490
0123-6	18405
0125-5	19766
0125-6	20506
1120-1	15895
1120-2	19366

30Su 70Sa	
Sample	E (MPa)
1010-2	23431
1009-2	10934
1009-4	23128
1018-B	15368
1110-5	13575
1110-6	15838
1122-5	19841
1122-6	16918

25Su 5FA	
Sample	E (MPa)
0919-3	22511
0919-4	22520
1018-A	14583
1110-7	14660
1110-8	16828
1122-5	19841
1122-6	16918

Figure A-4 Initial Young's modulus

211

Material: **10Su90Sa**

Sample	Max. Tensile Strain (%)	Tensile Strength (kPa)
1013-6b	0.19	1099
1013-5	0.04	668
AVG	0.12	883

Material: **10Su2FA**

Sample	Max. Tensile Strain (%)	Tensile Strength (kPa)
1110-1	0.14	793
1110-2	0.09	871
AVG	0.11	832

Material: **15Su85Sa**

Sample	Max. Tensile Strain (%)	Tensile Strength (kPa)
1013-3	0.02	1254
1013-4	0.11	1157
AVG	0.07	1205

Material: **15Su3FA**

Sample	Max. Tensile Strain (%)	Tensile Strength (kPa)
1013-9	0.05	1318
1013-10	0.08	1059
AVG	0.06	1189

Material: **30Su70Sa**

Sample	Max. Tensile Strain (%)	Tensile Strength (kPa)
1013-1	0.75	2087
1013-2	0.58	1767
AVG	0.67	1927

Material: **25Su5FA**

Sample	Max. Tensile Strain (%)	Tensile Strength (kPa)
1013-7	0.19	2427
1013-8	0.37	3184
AVG	0.28	2805

Table A-5 Maximum tensile strain and tensile strength

Material: **10% Sulphur + 90% Tailing Sand**

Sample	Cycles	Young Mod. MPa	Peak Strength kPa	Yield Strength kPa
41_10Su90Sa-1	41	2334	8337	6389
68_10Su90Sa-1	68	1143	5091	4147
68_10Su90Sa-2	68	784	6019	5307
82_10Su90Sa-1	82	831	3938	2897
82_10Su90Sa-2	82	383	3471	2042

Material: **15% Sulphur + 85% Tailing Sand**

Sample	Cycles	Young Mod. MPa	Peak Strength kPa	Yield Strength kPa
1015-6[a]	50	16479	11833	9856

(a) E corrected
1015-5 was damaged during coring to obtain 2:1 samples
1016-3 and 1016-4 failed the test after 100 cycles
1020-3 and 1020-4 failed the test after 150 cycles

Material: **30% Sulphur + 70% Tailing Sand**

Sample	Cycles	Young Mod. MPa	Peak Strength kPa	Yield Strength kPa
1015-1	50	5620	15539	14534
1015-2	50	4603	14559	12767
1016-1	100	3349	10685	8670
1020-2[a]	150	1619	8633	7684

(a) Another sample failed the test after 150 cycles.
1016-2 failed the test after 100 cycles.

Table A-6 Peak and yield compressive strength after freeze-thaw cycle for mixes composed of sulphur and tailing sand

213

Material: 10% Sulphur +2% Fly Ash + 88% Tailing Sand

Sample	Cycles	Young Mod. MPa	Peak Strength kPa	Yield Strength kPa
39_10Su2FA-1	39	3875	10080	7576
41_10Su2FA-1	41	4062	17272	13996
41_10Su2FA-2	41	3245	10419	7455
68_10SuFA2-1[a]	68	5676	6253	5150
82_10Su2FA-2	82	515	4364	3197
86_10Su2FA-1	86	456	4983	4302

(a) E corrected.

Material: 15% Sulphur + 3% Fly Ash + 82% Tailing Sand

Sample	Cycles	Young Mod. MPa	Peak Strength kPa	Yield Strength kPa
41_15Su3FA-1	41	4603	17581	14215
41_15Su3FA-2	41	7383	15871	12999
50_15Su3FA-1[a]	50	9265	16976	16024
1101-6[a]	50	16415	18846	15791
100_15Su3FA-1[a]	100	8835	13245	11734
1016-10[a]	100	13659	17005	12359
162_1017-7[b][c]	162	6231	20188	15436

(a) E corrected.
(b) 2 samples of 150 and 1 sample of 162 cycles failed the test.
(c) One inch at the bottom was sand with no sulphur bonds.

Material: 25% Sulphur + 5% Fly Ash + 70% Tailing Sand

Sample	Cycles	Young Mod. MPa	Peak Strength kPa	Yield Strength kPa
1015-8	50	12313	34484	23023
1015-7	50	15759	39654	29201
100_25Su5FA-1	100	7401	31925	23322
100_25Su5FA-2	100	5879	28857	22927
100-25Su5FA-3	100	9566	37436	26191

1020-7 and 1020-8 failed the test after 150 cycles.

Table A-7 Peak and yield compressive strength after freeze-thaw cycle for mixes composed of sulphur and tailing sand

Material:	10Su2FA						
Description	No. of Cycles	E AVG mPa	EMIN	EMAX	No. of Samples	% of Eo	E related to the Baldwin
Eo Baldwin		12218	10920	14000	7		12218
Eo Instron		1227	1193	1282	3		
E Baldwin	39	3874	n/a	n/a	1	32	3874
E Baldwin	41	3653	3244	4062	2	30	3653
E Instron	68	570			1	46	5676
E Baldwin	82	515			1	4	515
E Baldwin	86	455			1	4	455

Material:	15Su 3FA 82Sa						
Description	No. of Cycles	E AVG mPa	EMIN	EMAX	No. of Samples	% of Eo	E related to the Baldwin
Eo Baldwin		16578	12885	20496	7		16578
Eo Instron		1732	1406	2028	4		
E Instron	50	1340	967	1714	2	77	12826
E Instron	100	1175	923	1427	2	68	11247
E Baldwin	162	6231	N/A	N/A	1	38	6231

Material:	25Su5FA70Sa						
Description	No. of Cycles	E AVG mPa	EMIN	EMAX	No. of Samples	% of Eo	E related to the Baldwin
Eo Baldwin		18266	14583	22520			18266
E Baldwin	50	14035.5	12312	15759	2	77	14036
E Baldwin	100	7615	5879	9566	3	42	7615

Table A-8 Correction of the Young's modulus measured in the Instron compression machine and Young's modulus values related to the Baldwin compression machine for samples tested after the freeze-thaw cycles – Sulphur and tailing sand mixes

Material:		10Su90Sa		Sample_10SuFA2-1			
Description	No. of Cycles	E AVG mPa	EMIN	EMAX	No. of Samples	% of Eo	E related to the Baldwin
Eo Baldwin		11623	10505	12983			11623
E Baldwin	41	2333			1	20	2333
E Baldwin	68	963	784	1142	2	8	963
E Baldwin	82	606.5	383	830	2	5	607

Material:		15Su 85Sa					
Description	No. of Cycles	E AVG mPa	EMIN	EMAX	No. of Samples	% of Eo	E related to the Baldwin
Eo Baldwin		16578	12885	20496	7		16578
Eo Instron		1501	1462	1548	3		
E Instron	50	1492				99	16479

Material:		30Su70Sa					
Description	No. of Cycles	E AVG mPa	EMIN	EMAX	No. of Samples	% of Eo	E related to the Baldwin
Eo Baldwin		17379	10934	23431	8		17379
E Baldwin	50	5111	4603	5619	2	29	5111
E Baldwin	100	3348	n/a	n/a	1	19	3348

Table A-9 Correction of the Young's modulus measured in the Instron compression machine and Young's modulus values related to the Baldwin compression machine for samples tested after the freeze-thaw cycles – Sulphur, fly ash, and tailing sand mixes.

No.	Sample	H (mm)	D (mm)	Area m2	H/D Ratio	f'c,NS (kPa)	Fl/d Zmc=0.5	f'c,S (kPa)
1	68_10S2FA-1	79.09	74.60	0.00437	1.060	6924	0.891	6171
2	33_10S2FA-1	81.54	76.53	0.00460	1.065	3818	0.884	3376
3	33_10S2FA-2	73.77	76.20	0.00456	0.968	5844	0.865	5057
4	100_15S85Sa-1	80.28	76.19	0.00456	1.054			
5	100_15S3FA-1	88.28	76.40	0.00458	1.156	15019	0.929	13959
6	50_15S3FA-1	86.81	76.15	0.00455	1.140	17994	0.933	16796
7	39_10Su2FA-1	78.59	76.20	0.00456	1.031	11092	0.896	9940
8	41_10Su90Sa-1	78.02	76.21	0.00456	1.024	9242	0.889	8218
9	50_15Su90Sa-1	84.99	76.21	0.00456	1.115			
10	41_15Su3FA-2	72.99	76.24	0.00456	0.957	17350	0.900	15616
11	41_15Su3FA-1	83.00	76.30	0.00457	1.088	18739	0.927	17370
12	41_10Su2FA-1	72.71	76.19	0.00456	0.954	18796	0.904	16995
13	41_10Su2FA-2	78.97	76.14	0.00455	1.037	11439	0.898	10276
14	100_25Su5FA-1	75.29	76.44	0.00459	0.985	35870	0.963	34526
15	100_25Su5FA-2	72.07	76.17	0.00456	0.946	32792	0.949	31130
16	100_25Su5FA-3	71.91	76.03	0.00454	0.946	42718	0.982	41966
17	86_10Su2FA-1	68.86	76.29	0.00457	0.903	5774	0.847	4893
18	86_10Su2FA-2	71.07	76.13	0.00455	0.933	5262	0.854	4495
19	82_10Su90Sa-1	69.87	76.21	0.00456	0.917	4564	0.847	3866
20	82_10Su90Sa-2	61.42	76.09	0.00455	0.807	4172	0.813	3391
21	33_10Su90Sa-1	69.32	75.53	0.00448	0.918			
22	82_10Su2FA-2	59.25	75.96	0.00453	0.780	5262	0.809	4258
23	68_10Su90Sa-1	65.10	75.84	0.00452	0.858	5967	0.836	4986
24	68_10Su90Sa-2	65.31	76.02	0.00454	0.859	7019	0.840	5896
25	162-1017-7	112.00	76.48	0.00459	1.464	20595	0.976	20109

$$f'_{c,S} = \left[1 + \left(-0.144 + 0.027 Z_{mc} + 0.00044 f'_{c,NS} \right) \left(2 - \frac{l}{d} \right)^2 \right] f'_{c,NS}$$

Table A-10 Correction factors (Fl/d) for specimen l/d ratio less than 2

APPENDIX B EXTERNAL STABILITY

This appendix presents the external stability calculations such as sliding, overturning, and contact pressure below the wall (bearing capacity). The pore water pressures were not included because is assumed that the water table highest elevation is the top of the drainage layer.

Figures B1, B2, B3, and B4 show the calculation including the truck loads. The waiting line truck is always applied. Also, two calculations are given one adding a truck load when is dumping the ore on top of the wall and another when there is not a truck on top of the wall dumping the ore. The first case corresponds to Full loading condition showed in Figure 4.4; however, the surcharge of 102.5 kPa is not applied on top of the wall. Because the most critical situation is when the mining truck is dumping the ore and there is no more trucks on the wall at the same moment.

Figures B5, B6, B7, and B8 presents the sliding, overturning and contact pressures calculations for the case when there is not mining trucks on top of the wall and neither trucks in the waiting line; thus the surcharge of 102.5 kPa and 205 kPa are not applied.

FORCES APPLIED TO THE WALL
DRIVING SIDE

	U/W Kpa	φ	C(kPa)
Subrade	22.5	37	0
Oil Sand	21	32	0
Base	22.5	37	0

NOTES:

(1) The the truck dumping the material (205 kPa) is located the Wall, this surcharge does not contribute to the horizontal pressure applied to the wall.

(2) The surcharge (q) is estimated from the concrete pavement and the live load surcharge from the mining trucks on waiting line.
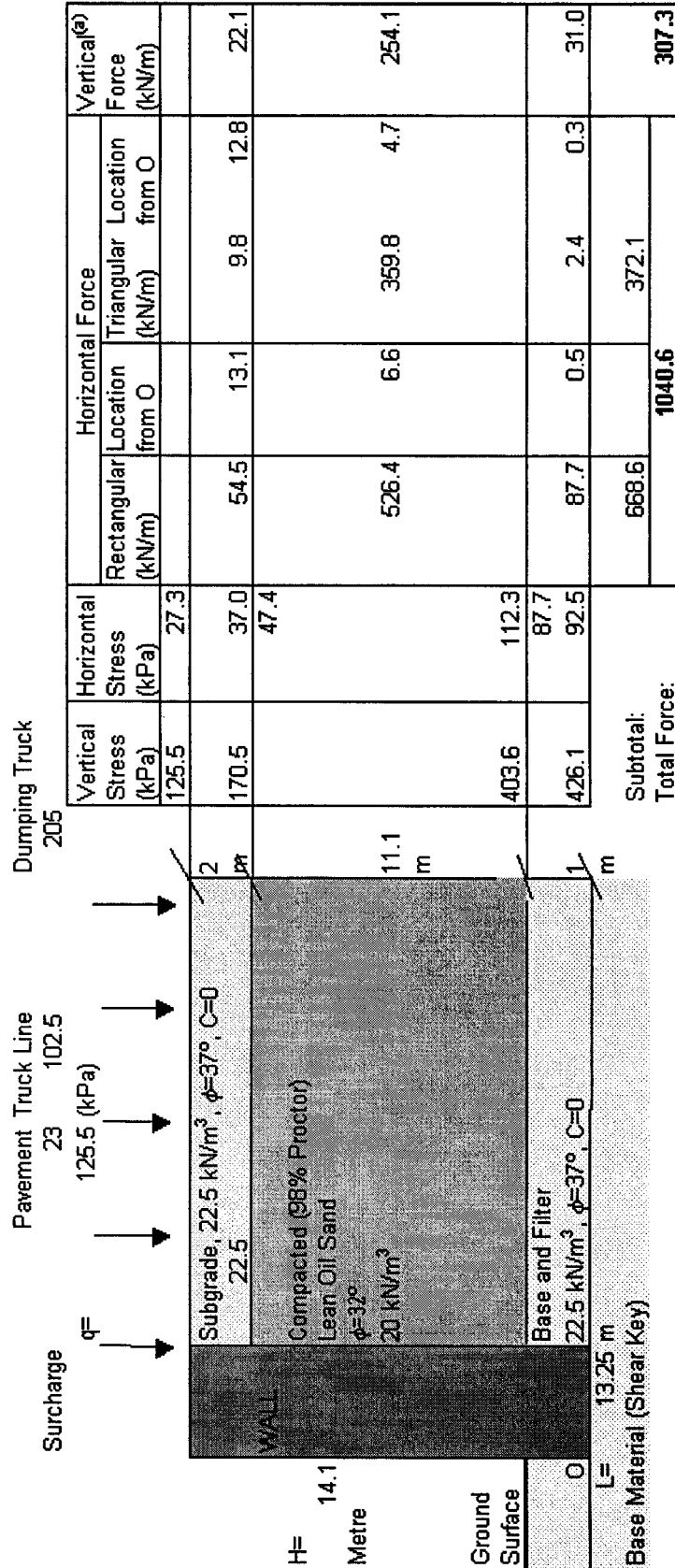
Dumping Truck 205

Pavement Truck Line 23   102.5

Surcharge 125.5 (kPa)

	Vertical Stress (kPa)	Horizontal Stress (kPa)	Horizontal Force				Vertical[a] Force (kN/m)
			Rectangular (kN/m)	Location from O	Triangular (kN/m)	Location from O	
	125.5	27.3					
	170.5	37.0	54.5	13.1	9.8	12.8	22.1
		47.4					
	403.6	112.3	526.4	6.6	359.8	4.7	254.1
	426.1	87.7					
		92.5	87.7	0.5	2.4	0.3	31.0
Subtotal:			668.6		372.1		
Total Force:			1040.6				307.3

(a) Vertical Force: Horizontal force x (tan δ)

q=

Surcharge

H= 14.1 Metre

Subgrade, 22.5 kN/m³, φ=37°, C=0

Compacted (98% Proctor) Lean Oil Sand φ=32° 20 kN/m³

11.1 m

WALL

Ground Surface

Base and Filter 22.5 kN/m³, φ=37°, C=0

O

L= 13.25 m

Base Material (Shear Key)

2

1

Figure B-1 External Stability Including Truck Loads Forces Applied to the Wall - Driving Side

RESISTANT SIDE

Passive Force
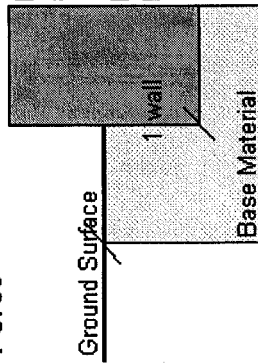
It is asumed that the friction is not mobilized in fron of the wall, and the Rankine theory was used to estimate the horizontal passive force.

Kp= 4.02279121   SF= 2

		Loc.(m)
Passive		From O
Force	22.6 kN	0.33

Friction Force at the Wall Base

Assuming a friction coeficient between the wall and the gravel base of tan δ

δ= 24   (From NAVFAC DM 7.2 p.7.2-63)

Unit Weight of wall=   20 kN/m³

Vertical Forces=   W1=   3736.5 (Weight of wall (kN))
                   W2=   307.3   (Total vertical force on the face to the backfill (kN))

Total   W3=   304.8   (Weight of the concrete pavement (kN))
Vertical   W4=   738.0   (Truck Weight(kN))

Force	Friction Force
kN/m	kN/m
4348.5 x (tan δ) =	1936.1 (a)	(a) (W1+W2+W3)
5086.5 x (tan δ) =	2264.7 (b)	(b) (W1+W2+W3+W4)

SLIDING FACTOR OF SAFETY

Driving	Resisting	F of S	
1040.6	1958.7	1.88	(a)
1040.6	2287.3	2.20	(b)

Figure B-2 External Stability Including the Truck Loads. Forces Applied to the Wall - Resisting Side and Sliding Factor of Safety

220

CONTACT PRESSURE BELOW THE WALL (Bearing Capacity)

Resistant Moments		Driving Moments
From		From
Fp=	7.5	
Fav=	4071.6	Fah 6022.8
W=	26773.3	M_D= 6022.8 kN/m*m
Mtruck	4068.2	
M_R=	34920.6 kN/m*m	

V1= W1+W2+W3+W4

V1= 5086.53691 kN/m

V2= W1+W2+W3

V2= 4348.54

e=B/2-(M_R-M_D)/V

e= 0.94 m

0.92

q=V/A +- Vec/I   I=BH^3/12   c=L/2   A=BL

q=(V/BL)(1+- 6e/L)   B= 1 m

L= 13.25 m

qmax = **548.0** Kpa   **464.2**

qmin= 219.8 Kpa   192.2

q adm = *476* Kpa
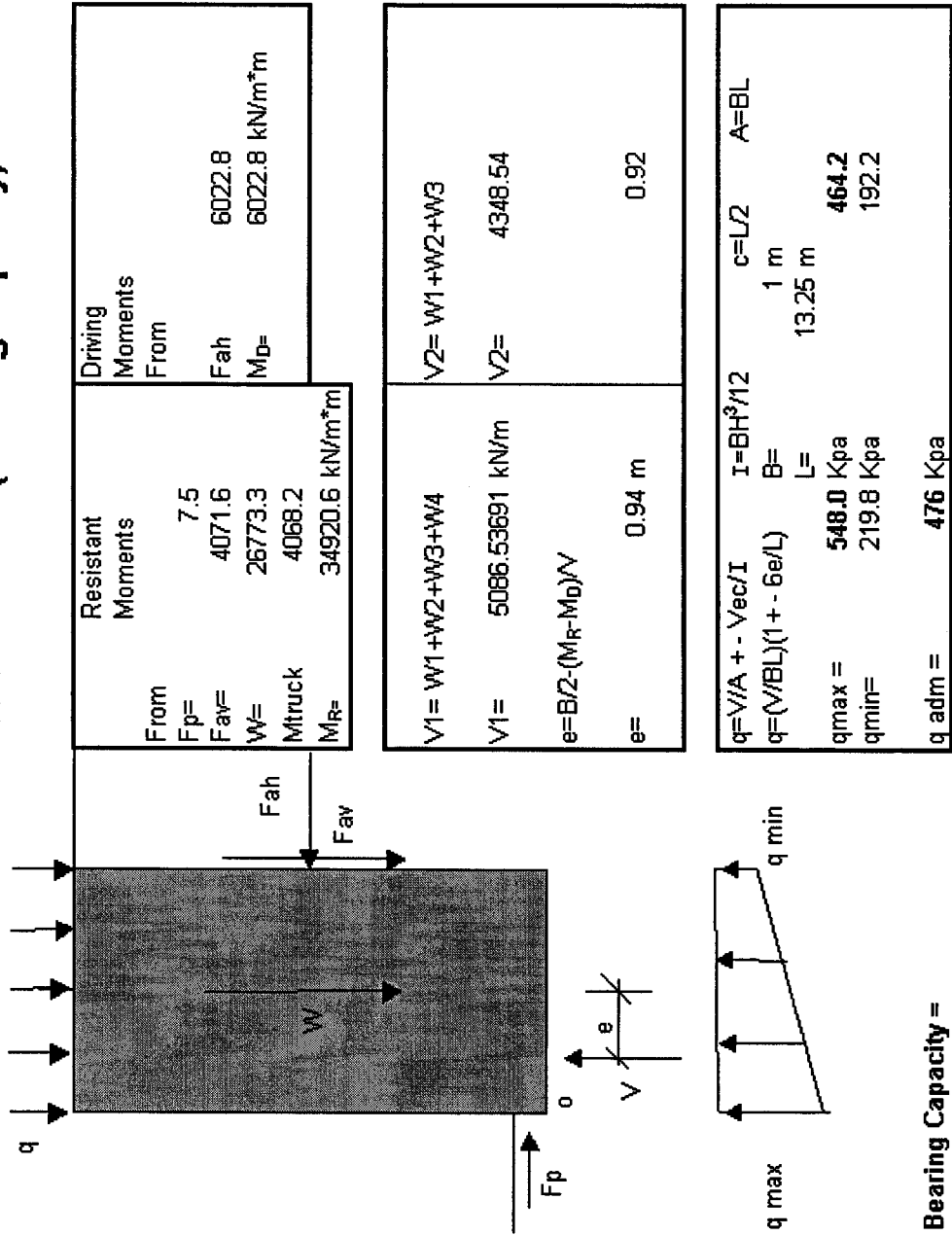
Bearing Capacity =

(See McCavour Engineering LTD, Drawing S01A dated 02/16/00)

Figure B-3 External Stability Including the Truck Loads Contact Pressure Below the Wall

FACTOR OF SAFETY AGAINST OVERTURNING

Note: The Pasive Pressure is not included

d= 0.1 to 0.3 L
Require a trial and error analysis to find the critical location of "O".
(Due local bearing capacity failure during overturning)
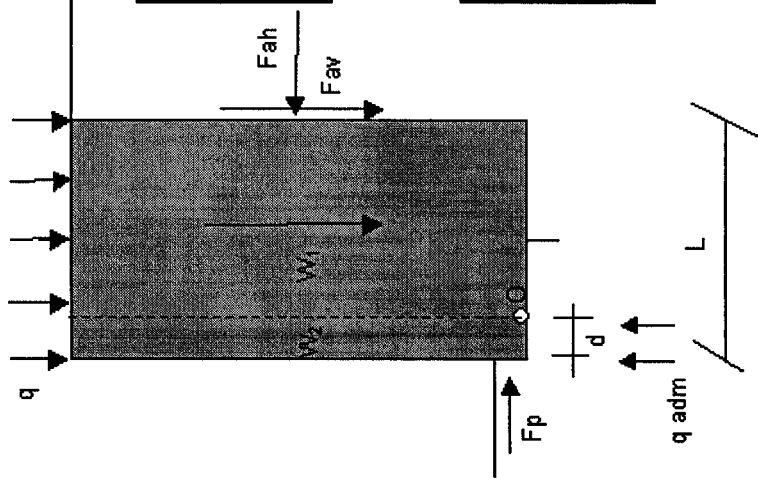
d	Mr			Mfah	Md	F of S
	Mw1	Mfav	Mqadm		Mw2	
0.00	24754.3	4071.6	0.0	6022.8	0.0	4.79
1.33	20051.0	3664.4	630.7	6022.8	247.5	3.88
2.65	15842.8	3257.2	1261.4	6022.8	990.2	2.90
3.98	12129.6	2850.1	1892.1	6022.8	2227.9	2.04

0.1*L=
0.2*L=
0.3*L=

Including the truck load when the trucks are dumping the ore:

d	Mr			Mfah	Md	F of S
	Mw1	Mfav	Mqadm		Mw2	
0.00	28822.5	4071.6	0.0	6022.8	0.0	5.46
1.33	22587.9	3664.4	630.7	6022.8	427.5	4.17
2.65	17208.3	3257.2	1261.4	6022.8	1710.0	2.81
3.98	12683.7	2850.1	1892.1	6022.8	3847.5	1.77

0.1*L=
0.2*L=
0.3*L=

M_{w1}= Moment due load W_1 M_{fav}= Moment due the force Fav
M_{w2}= Moment due load W_2 M_{qadm}= Moment at the toe by the bearing capacity q a

Note:
* The calculation of Mfah and Mfav include the effect of surcharge from the mining trucks waiting line.
* On top of the wall the surcharge from the mining truck waiting line is not considered, because this load will tend to stabilize. This is a conservative assumption.

Figure B-4   External Stability Including the Truck Loads Overturning Factor of Safety

FORCES APPLIED TO THE WALL
DRIVING SIDE

NOTES:

	U/W Kpa	φ	C(kPa)
Subrade	22.5	37	0
Oil Sand	21	32	0
Base	22.5	37	0

(1) The the truck dumping the material (205 kPa) is located the Wall, this surcharge does not contribute to the horizontal pressure applied to the wall.

(2) The surcharge (q) is estimated from the concrete pavement and the live load surcharge from the mining trucks on waiting line.

Surcharge

Pavement Truck Line
23 (kPa)

q= 23 (kPa)

Dumping Truck

Subgrade, 22.5 kN/m³, φ=37°, C=0
22.5

Compacted (98% Proctor)
Lean Oil Sand
φ=32°
20 kN/m³

11.1
m

Base and Filter
22.5 kN/m³, φ=37°, C=0

2

1
m

WALL

H= 14.1 Metre

Ground Surface

O   L= 13.25 m

Base Material (Shear Key)

Vertical Stress (kPa)	Horizontal Stress (kPa)	Horizontal Force				Vertical[a] Force (kN/m)
		Rectangular (kN/m)	Location from O	Triangular (kN/m)	Location from O	
23.0	5.0					
68.0	14.8	10.0	13.1	9.8	12.8	6.8
	18.9					
		209.9	6.6	359.8	4.7	163.4
301.1	83.8					
	65.4					
323.6	70.3	65.4	0.5	2.4	0.3	23.4
Subtotal:		285.3		372.1		193.5
Total Force:		657.4				

(a) Vertical Force: Horizontal force x (tan δ)
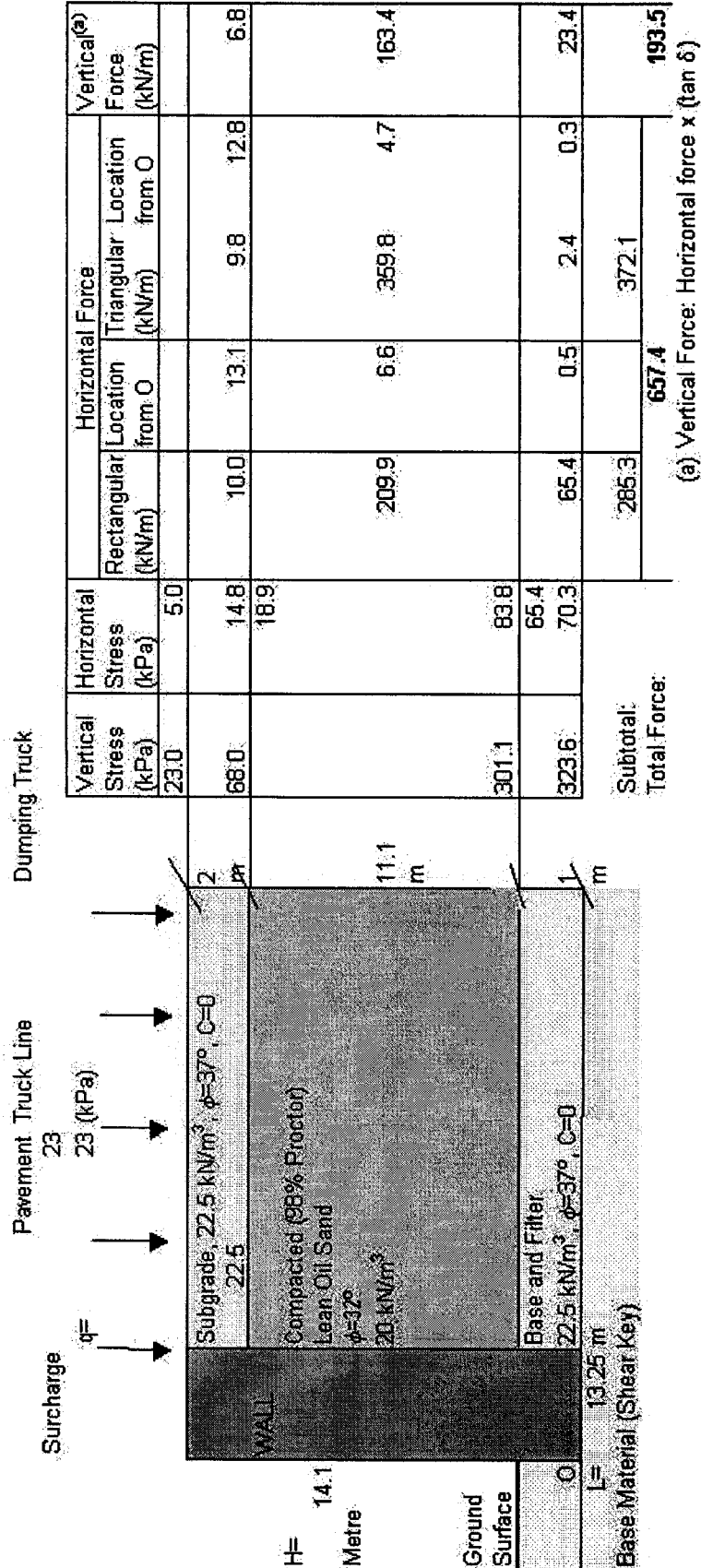
Figure B-5 External Stability No Including Truck Loads Forces Applied to the Wall - Driving Side

223

RESISTANT SIDE

Passive Force

It is asumed that the friction is not mobilized in fron of the wall, and the Rankine theory was used to estimate the horizontal passive force.

K_p= 4.02279121   SF= 2

Ground Surface

wall

Base Material

Passive	Loc.(m)
Force	From O
22.6 kN	0.33

Friction Force at the Wall Base

Assuming a friction coeficient between the wall and the gravel base of tan δ

δ= 24   (From NAVFAC DM 7.2 p.7.2-63)

Unit Weight of wall= 20 kN/m³

Vertical Forces=

W1=	3736.5	(Weight of wall (kN))
W2=	193.5	(Total vertical force on the face to the backfill (kN))
Total	W3=	304.8	(Weight of the concrete pavement (kN))
Vertical	W4=	0.0	(Truck Weight(kN))

Force	Friction Force
kN/m	kN/m
4234.8 x (tan δ) =	1885.5 (a)	(a) (W1+W2+W3)
4234.8 x (tan δ) =	1885.5 (b)	(b) (W1+W2+W3+W4)

SLIDING FACTOR OF SAFETY

Driving	Resisting	F of S	
657.4	1908.1	2.90	(a)
657.4	1908.1	2.90	(b)

Figure B-6   External Stability No Including the Truck Loads. Forces Applied to the Wall - Resisting Side and Sliding Factor of Safety

224

CONTACT PRESSURE BELOW THE WALL

Resistant Moments		Driving Moments	
From		From	
Fp=	7.5	Fah	
Fav=	2564.5	M_D=	3355.6
W=	26773.3		3355.6 kN/m*m
Mtruck	0.0		
M_R=	29345.3 kN/m*m		

V1= W1+W2+W3+W4		V2= W1+W2+W3	
V1=	4234.8 kN/m	V2=	4234.80
e=B/2-(M_R-M_D)/V			0.49
e=	0.49 m		

$q = V/A + - Vec/I$ $I = BH^3/12$ $c = L/2$ $A = BL$
$q = (V/BL)(1 + - 6e/L)$ B= 1 m
                           L= 13.25 m
qmax = **390.2** Kpa   **390.2**
qmin= 249.0 Kpa   249.0

q adm = *476* Kpa

Bearing Capacity =
(See McCavour Engineering LTD, Drawing S01A dated 02/16/00)

**Figure B-7 External Stability No Including the Truck Loads
Contact Pressure Below the Wall**

225

FACTOR OF SAFETY AGAINST OVERTURNING

Note: The Pasive Pressure is not included

d= 0.1 to 0.3 L
Require a trial and error analysis to find the critical location of "O".
(Due local bearing capacity failure during overturning)

d		Mr		Mqadm	Md		F of S
		Mw1	Mfav		Mfah	Mw2	
0.1*L=	0.00	24754.3	2564.5	0.0	3355.6	0.0	8.14
0.2*L=	1.33	20051.0	2308.1	630.7	3355.6	247.5	6.38
0.2*L=	2.65	15842.8	2051.6	1261.4	3355.6	990.2	4.41
0.3*L=	3.98	12129.6	1795.2	1892.1	3355.6	2227.9	2.83

Including the truck load when the trucks are dumping the ore:

d		Mr		Mqadm	Md		F of S
		Mw1	Mfav		Mfah	Mw2	
0.1*L=	0.00	24754.3	2564.5	0.0	3355.6	0.0	8.14
0.2*L=	1.33	20051.0	2308.1	630.7	3355.6	247.5	6.38
0.2*L=	2.65	15842.8	2051.6	1261.4	3355.6	990.2	4.41
0.3*L=	3.98	12129.6	1795.2	1892.1	3355.6	2227.9	2.83

Mw1= Moment due load W_1 Mfav= Moment due the force Fav

Mw2= Moment due load W_2 Mqadm= Moment at the toe by the bearing capacity q a

Note:
* The calculation of Mfah and Mfav include the effect of surcharge from the mining trucks waiting line.
* On top of the wall the surcharge from the mining truck waiting line is not considered, because this load will tend to stabilize. This is a conservative assumption.

Figure B-8 External Stability No Including the Truck Loads Overturning Factor of Safety

APPENDIX C FINITE ELEMENT ANALYSES RESULTS

This appendix includes the results of several finite element analyses performed in this thesis work. These are listed as follows:

- Finite element analyses were performed considering the Full Loading Condition and the three interface models presented in Table 5.1. The σ_1, σ_3, and τ_{max} contours are presented from Figure C-1 to C-9. From Figure C-10 to C-12 are presented the σ_1, σ_3, and τ_{max} contours of a finite element analysis performed under full load condition, using the interface model ksback1000 ksbot1e6, and the Cam clay model was used for the backfill.

- From Figure C-13 to C-24 show the stress profiles along four evaluation lines to examine the stresses in the retaining wall under the condition explained above.

- Finite element analyses were performed considering the Partial Loading Condition and the interface models as presented in Table 5.1. The σ_1, σ_3, and τ_{max} contours are presented from Figure C-25 to C-33.

- Figure C-34 and C-35 show the stress profiles along a vertical line located on the "rock" for the irregular surface cases showed in Figures 5.21 and 5.22, wedge shape rock and round shape rock, respectively.

- Finite Element Analyses were performed varying the stiffness of the base gravel drain layer as presented in Section 5.6.6. The σ_1, σ_3, and τ_{max} contours are presented from Figure C-36 to C-41. Moreover, the stress profiles along four evaluation lines are presented from Figure C-42 to C-51.

File Name: ksvar ksbot1e6_10.siz

σ_1

814
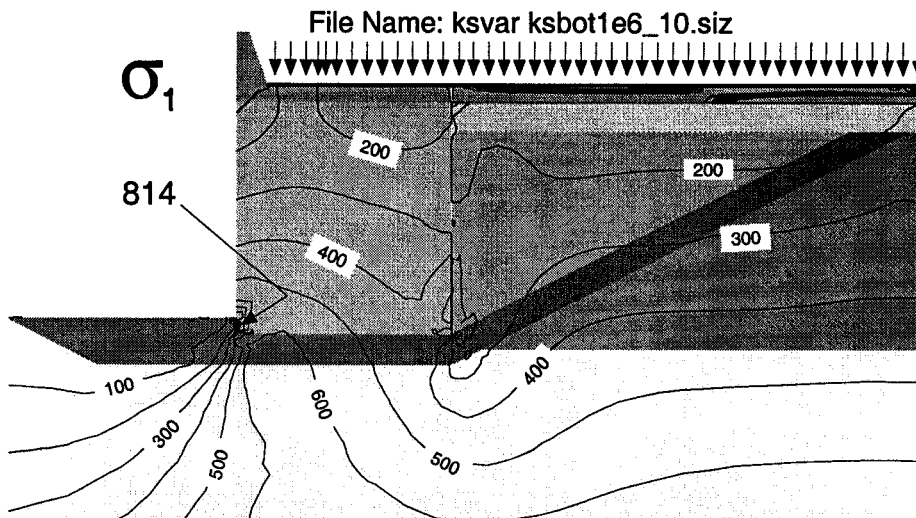
Figure C-1 Full Load Condition-ksbackvar ksbot1e6-σ_1 Contours.

File Name: ksvar ksbot1e6_10.siz

σ_3

154
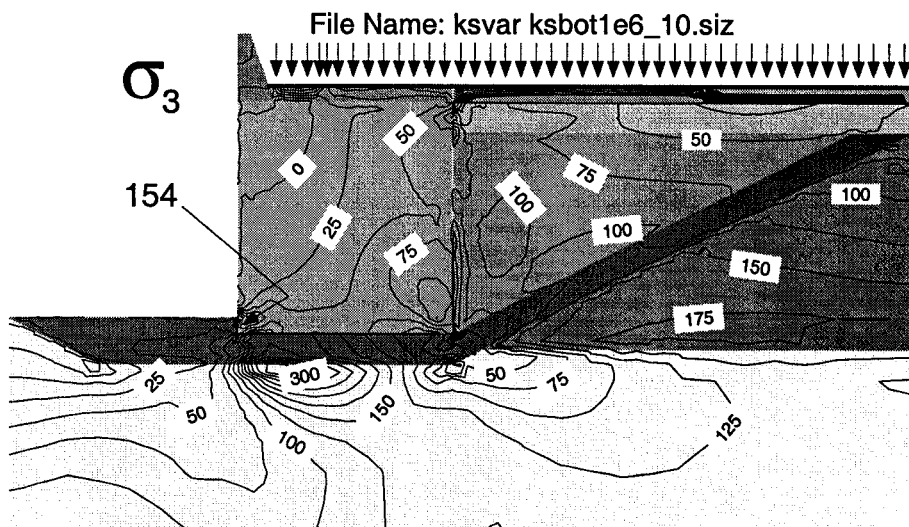
Figure C-2 Full Load Condition-ksbackvar ksbot1e6-σ_3 Contours.

File Name: ksvar ksbot1e6_10.siz

τ_{max}

365
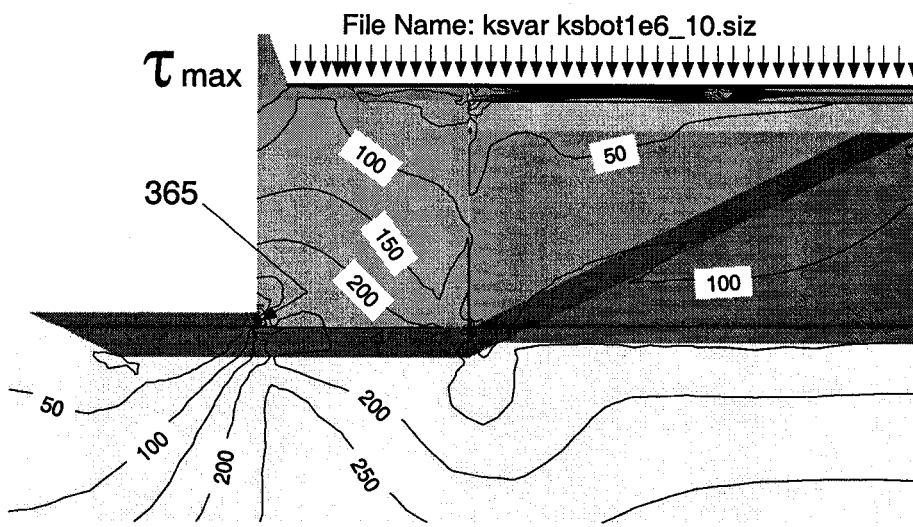
Figure C-3 Full Load Condition-ksbackvar ksbot1e6-τ_{max} Contours.

228

σ_1

1051
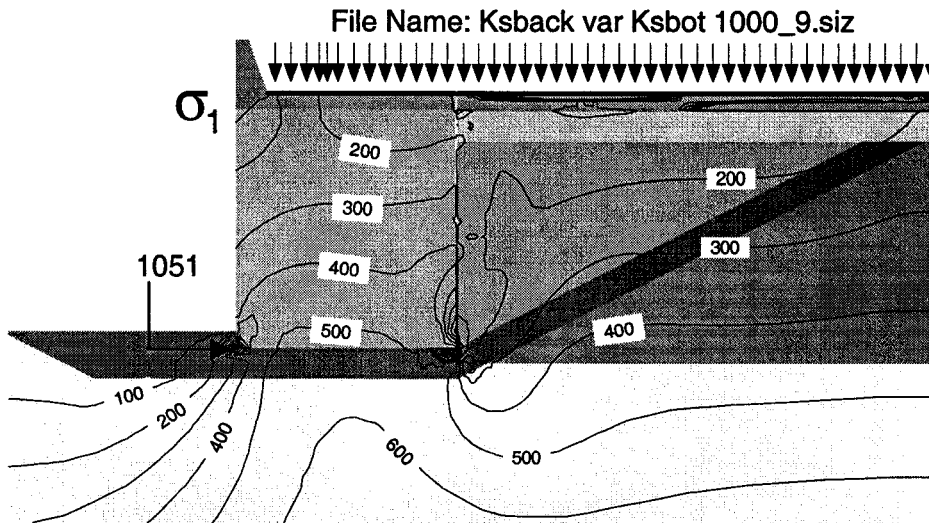
Figure C-4 Full Load Condition-ksbackvar ksbot1000-σ_1 Contours. .

σ_3

152
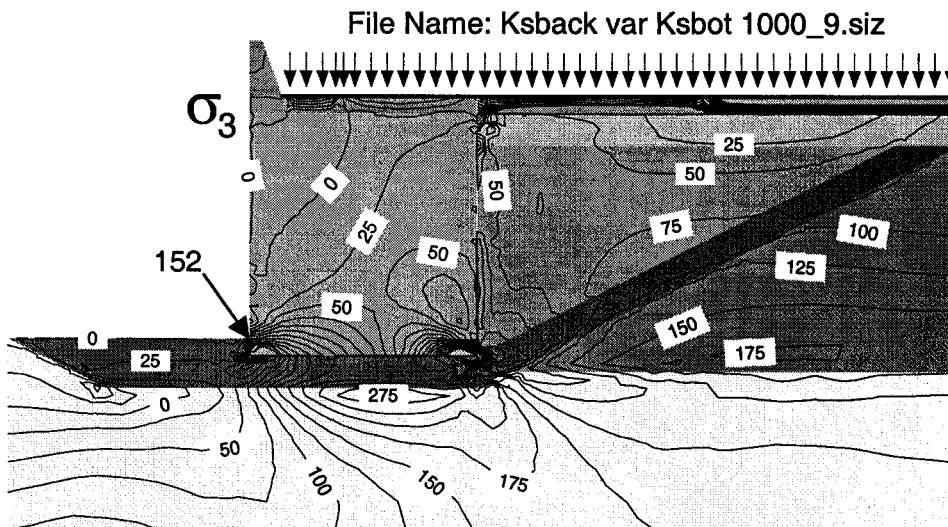
Figure C-5 Full Load Condition-ksbackvar ksbot1000-σ_3 Contours.

τ_{max}
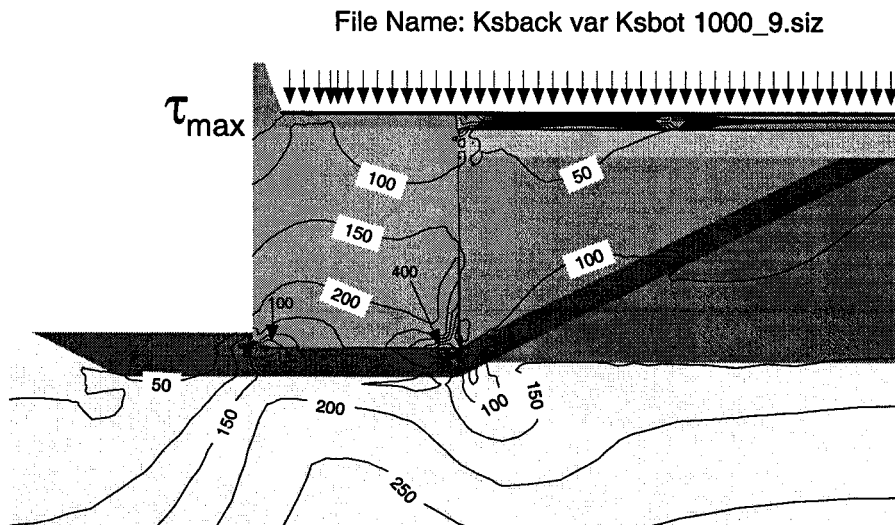
Figure C-6 Full Load Condition-ksbackvar ksbot1000 - τmax Contours.
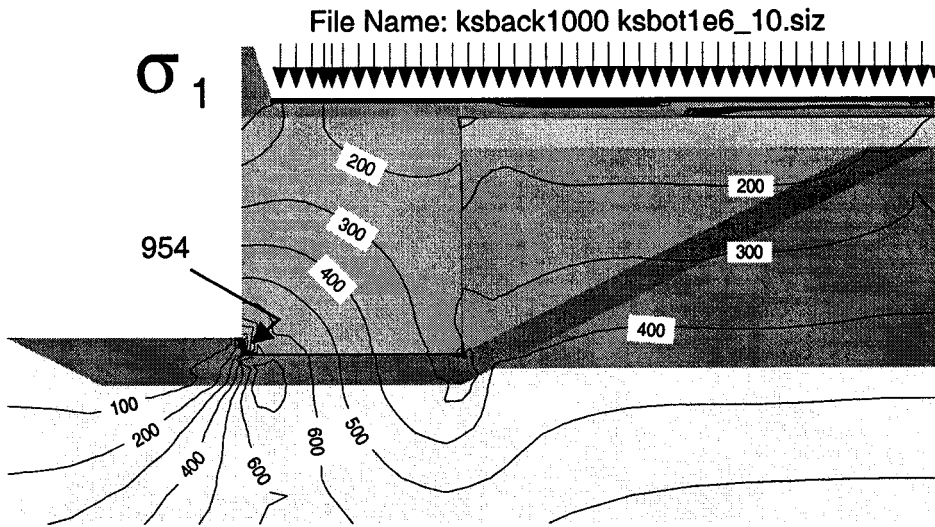
Figure C-7 Full Load Condition-ksback1000 ksbot1e6 - σ_1 Contours.
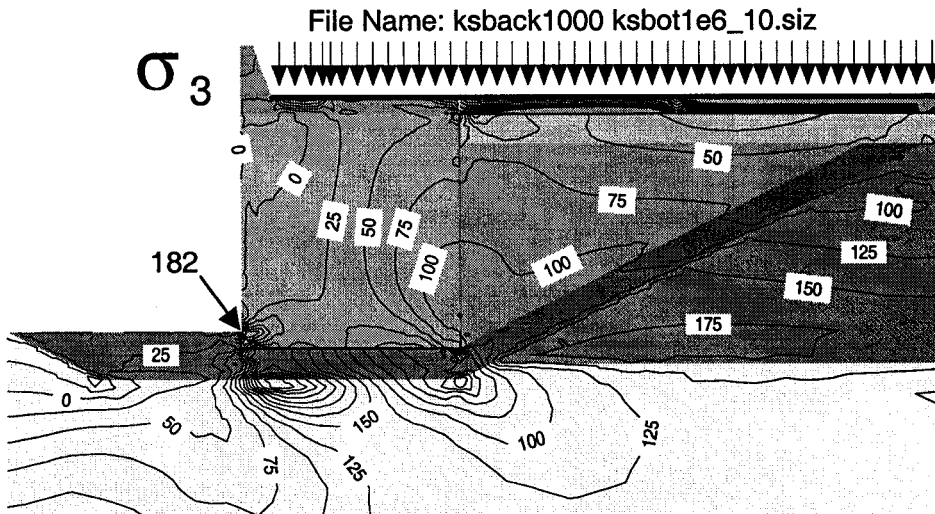
Figure C-8 Full Load Condition-ksback1000 ksbot1e6 - σ_3 Contours.
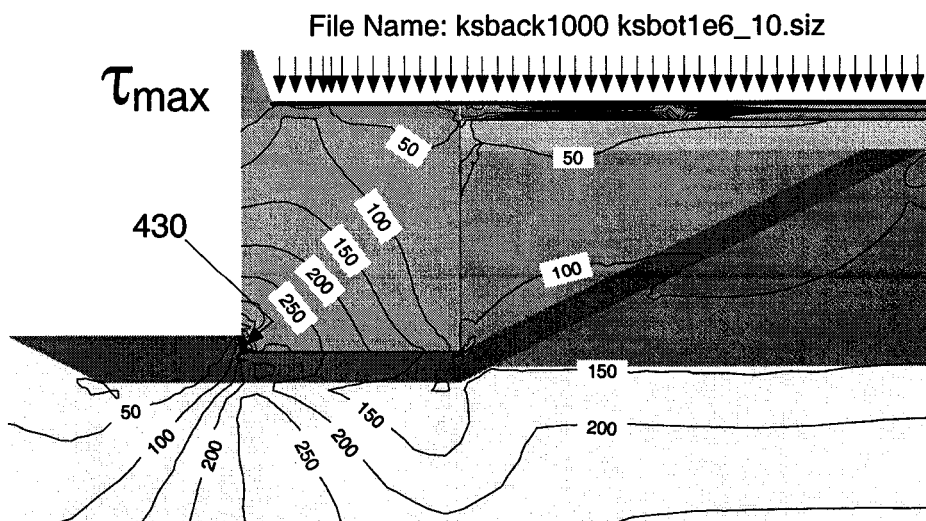
Figure C-9 Full Load Condition-ksback1000 ksbot1e6 - τ_{max} Contours.

230
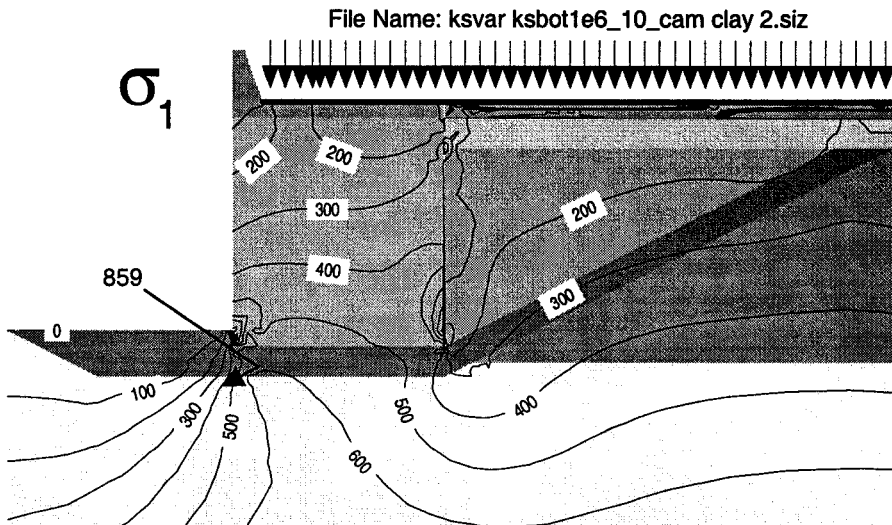
Figure C-10 Full Load - ksback1000 ksbot1e6 & Cam Clay at Backfill- σ_1 Contours.
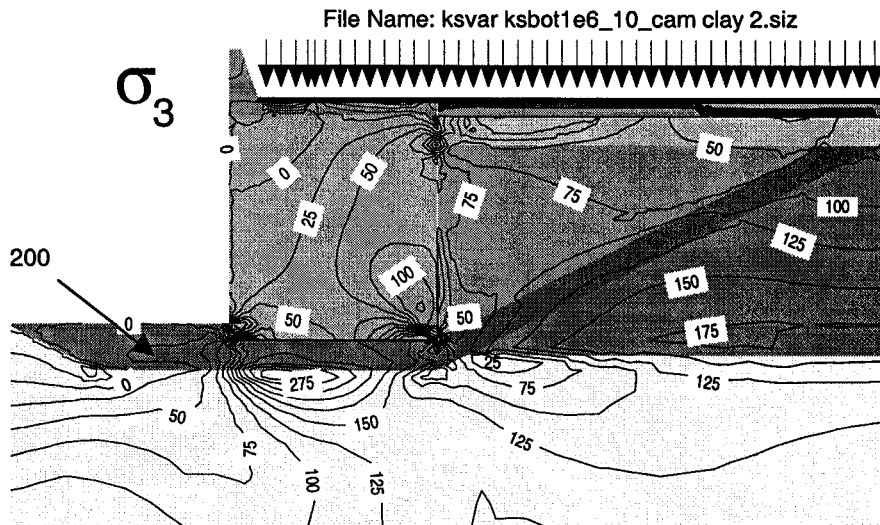
Figure C-11 Full Load - ksback1000 ksbot1e6 & Cam Clay at Backfill- σ_3 Contours.
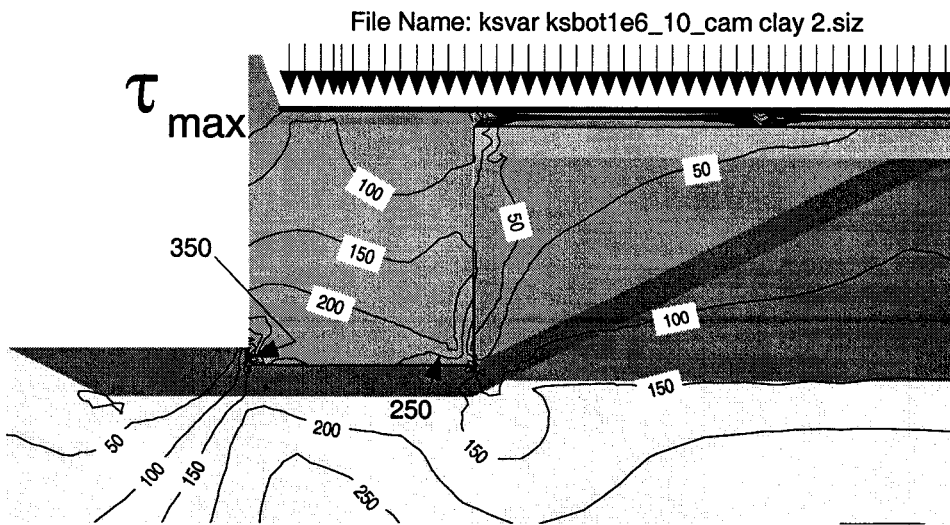
Figure C-12 Full Load - ksback1000 ksbot1e6 & Cam Clay at Backfill- τ_{max} Cont.
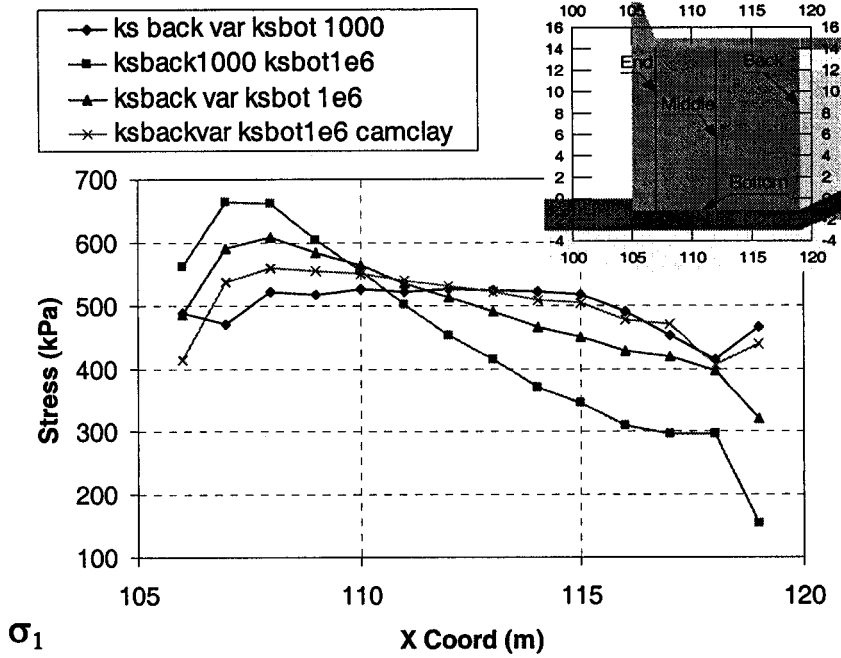
Figure C-13 Full Load Condition – Bottom Line - σ_1 Stress.
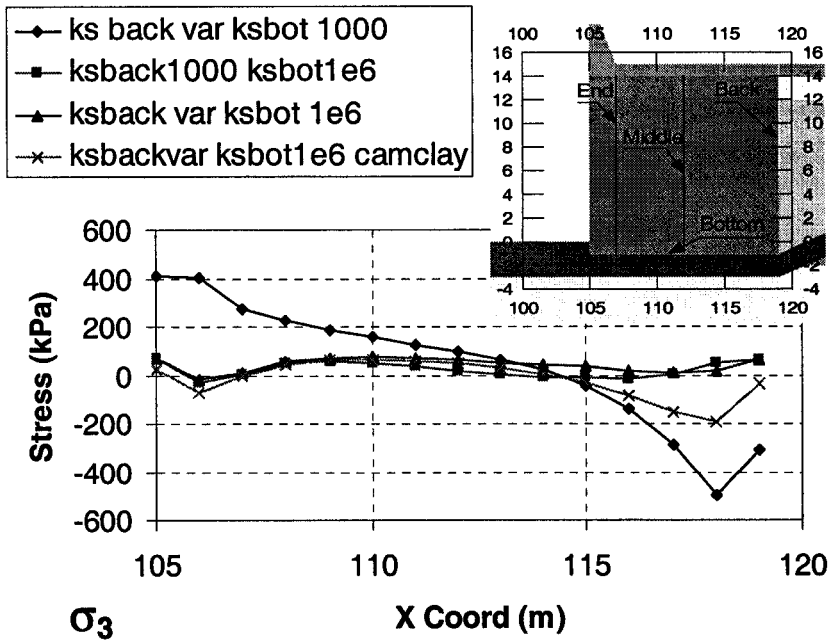
Figure C-14 Full Load Condition – Bottom Line - σ_3 Stress.

232
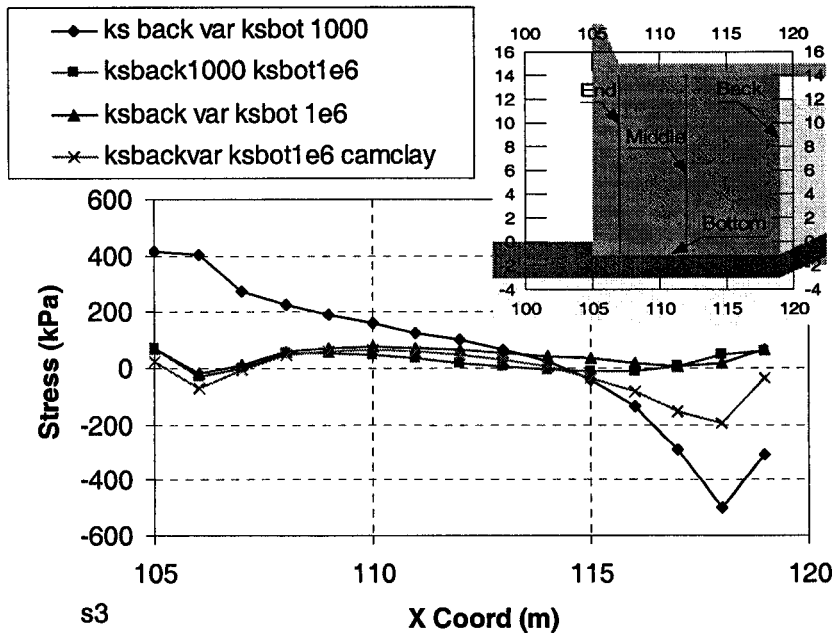
Figure C-15 Full Load Condition – Bottom Line - τ_{max} Stress.
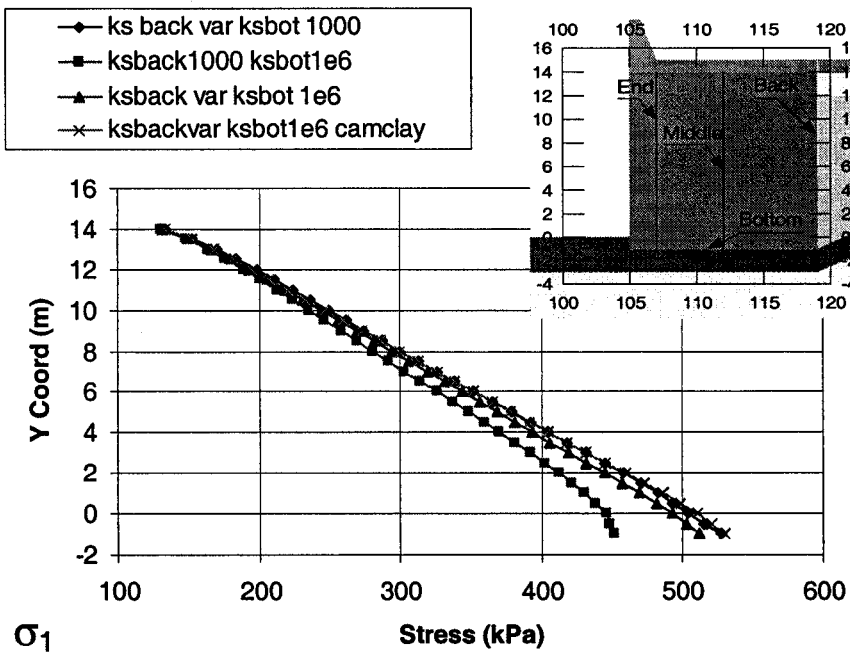
Figure C-16 Full Load Condition – Middle Line - σ_1 Stress.

233
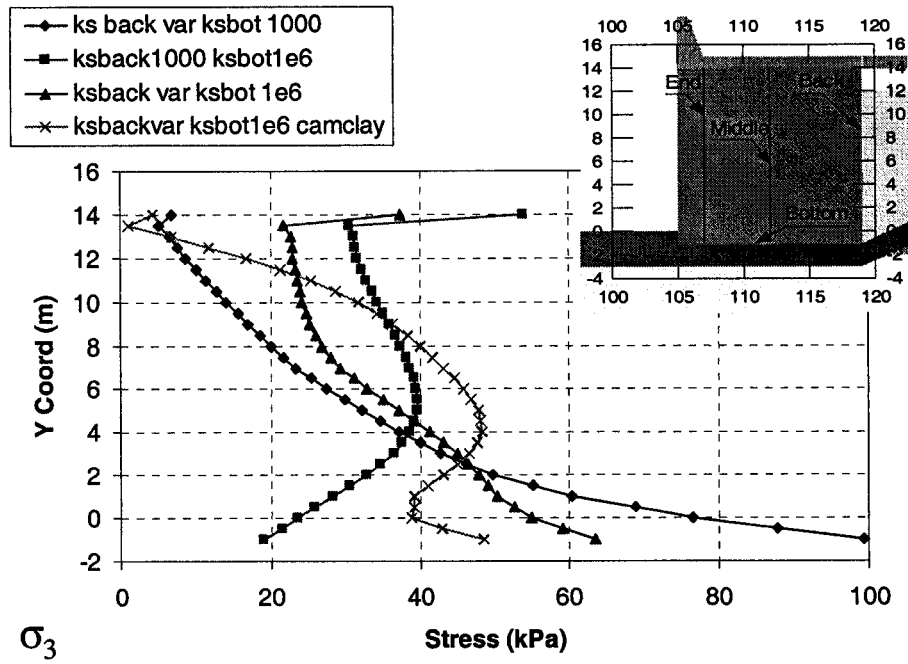
Figure C-17 Full Load Condition – Middle Line - σ_3 Stress.
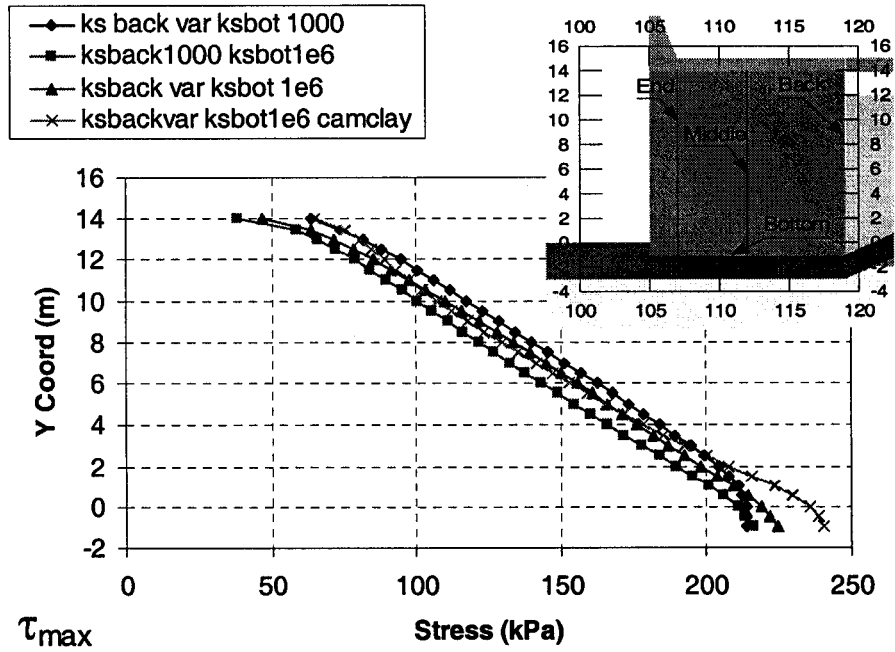
Figure C-18 Full Load Condition – Middle Line - τ_{max} Stress.

234
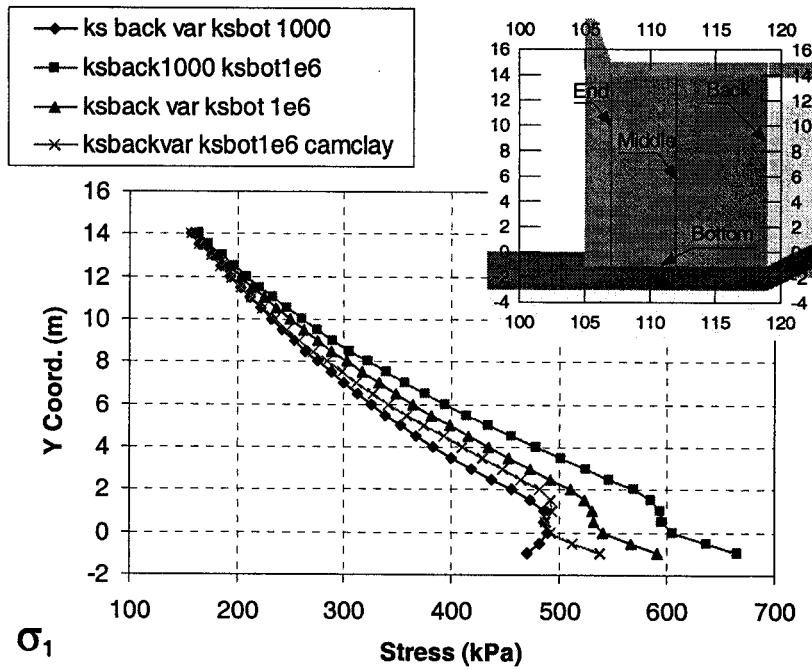
Figure C-19 Full Load Condition – End Line - σ_1 Stress.
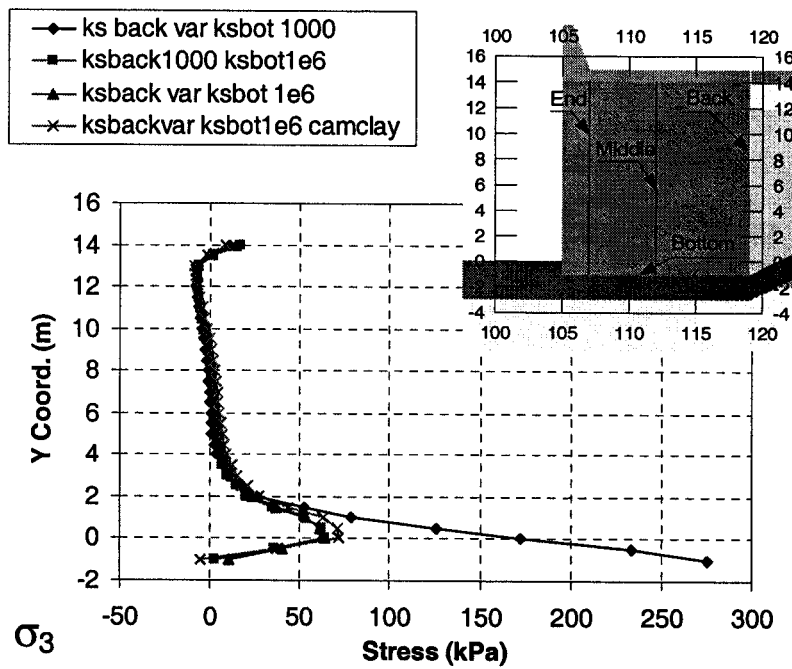
Figure C-20 Full Load Condition – End Line - σ_3 Stress.

235
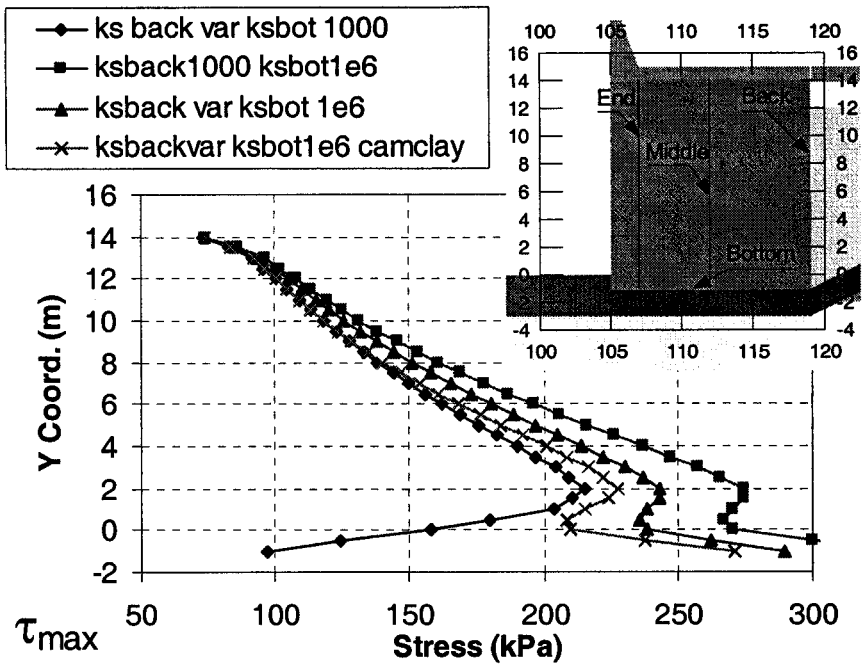
Figure C-21 Full Load Condition – End Line - τ_{max} Stress.
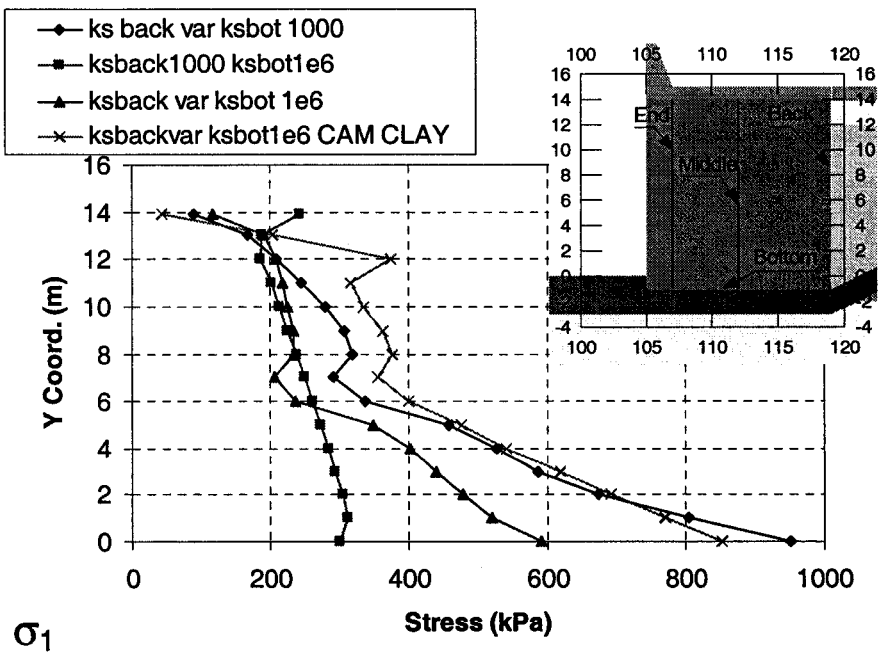
Figure C-22 Full Load Condition – Bottom Line - σ_1 Stress.

236
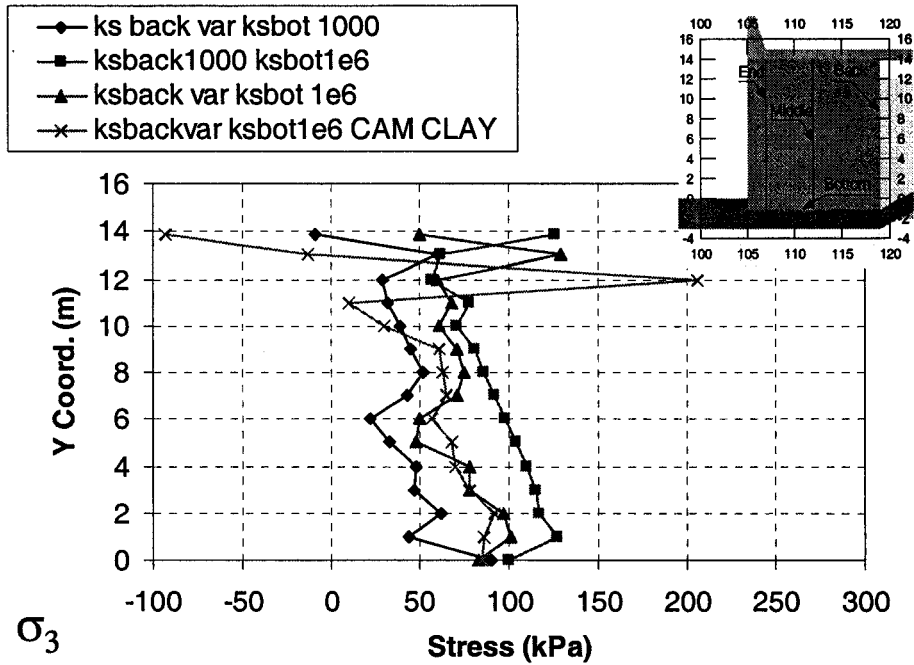
Figure C-23 Full Load Condition – Bottom Line - σ_3 Stress.
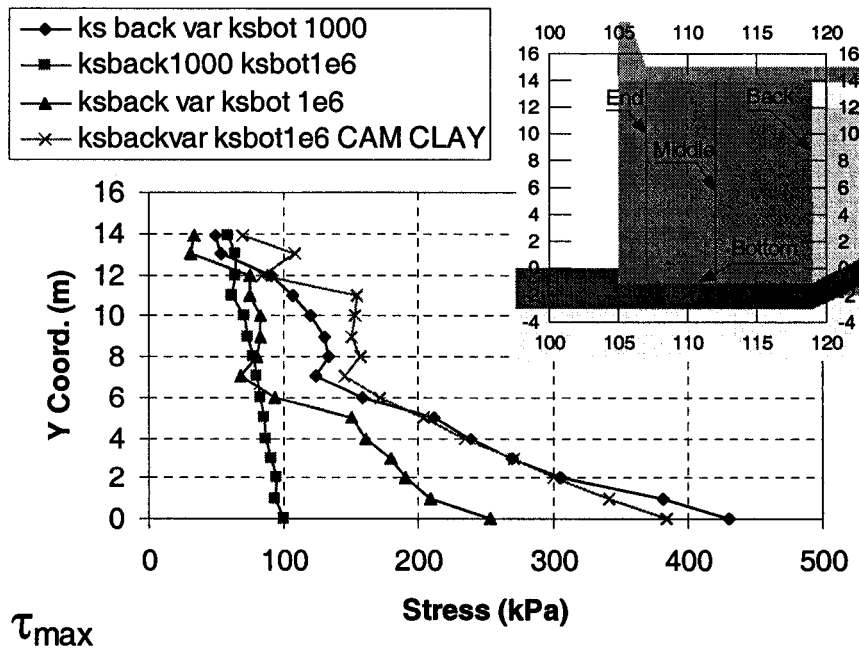
Figure C-24 Full Load Condition – Bottom Line - τ_{max} Stress.

237
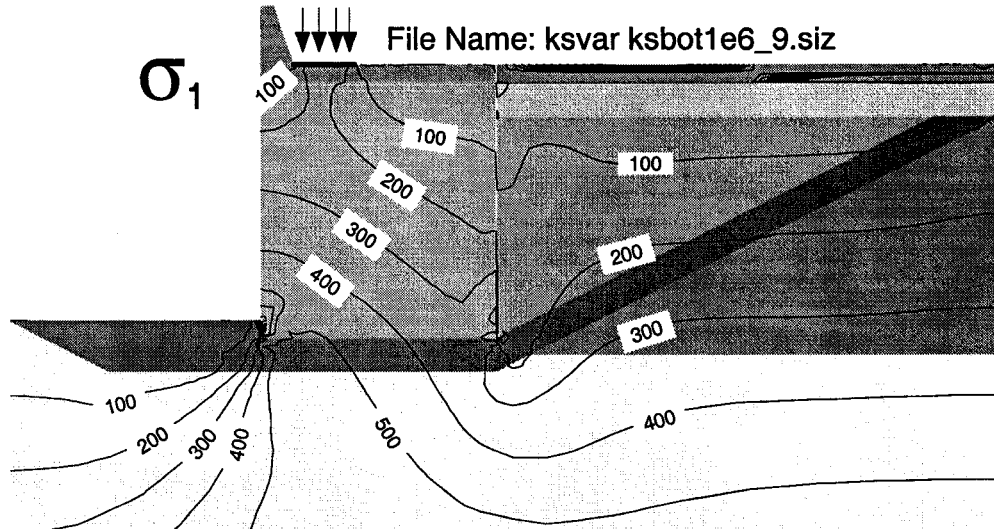
Figure C-25 Partial Load Condition – ksbackvar ksbot1e6 - σ_1 Contours.
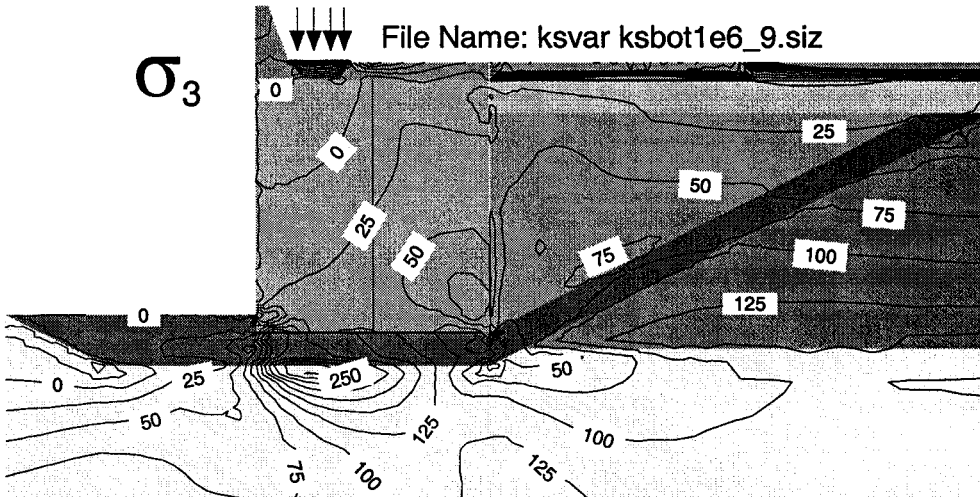
Figure C-26 Partial Load Condition – ksbackvar ksbot1e6 - σ_3 Contours.
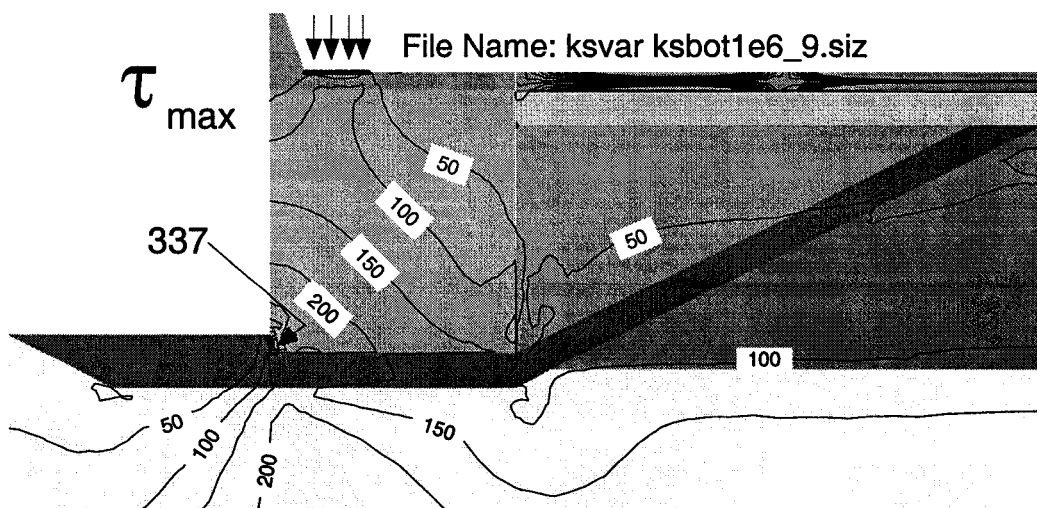
Figure C-27 Partial Load Condition – ksbackvar ksbot1e6 - τ_{max} Contours.

σ_1

709
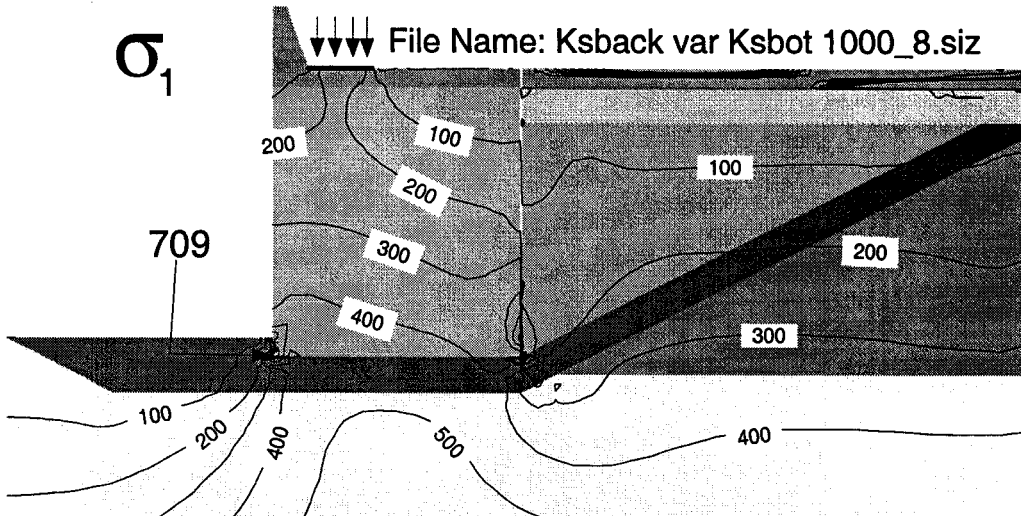
Figure C-28 Partial Load Condition – ksbackvar ksbot1000 - σ_1 Contours.

σ_3

316
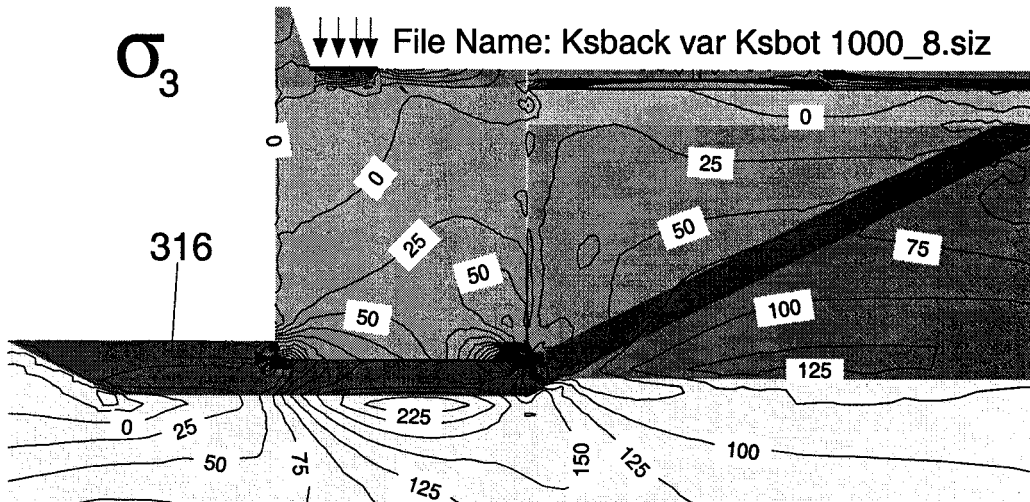
Figure C-29 Partial Load Condition – ksbackvar ksbot1000 - σ_3 Contours.

τ_{max}

196
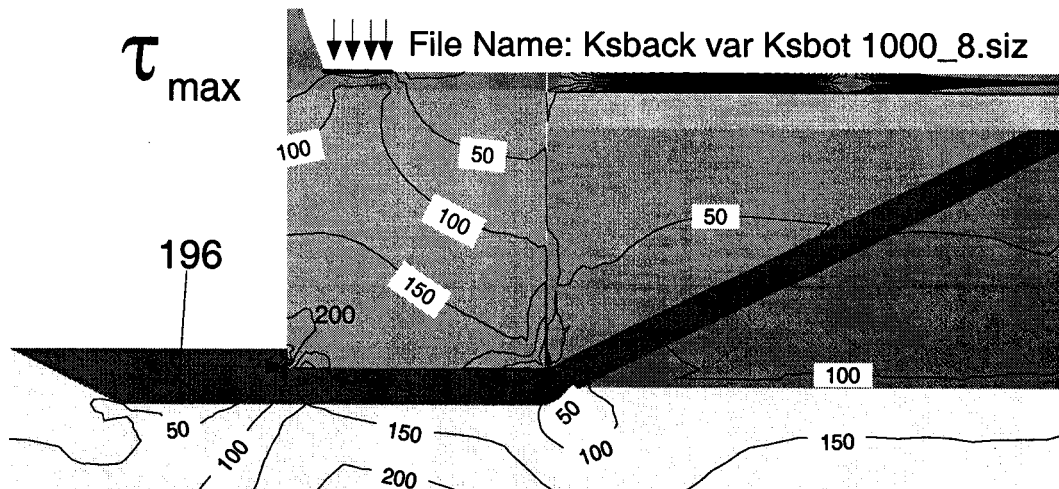
Figure C-30 Partial Load Condition – ksbackvar ksbot1000 - τ_{max} Contours.
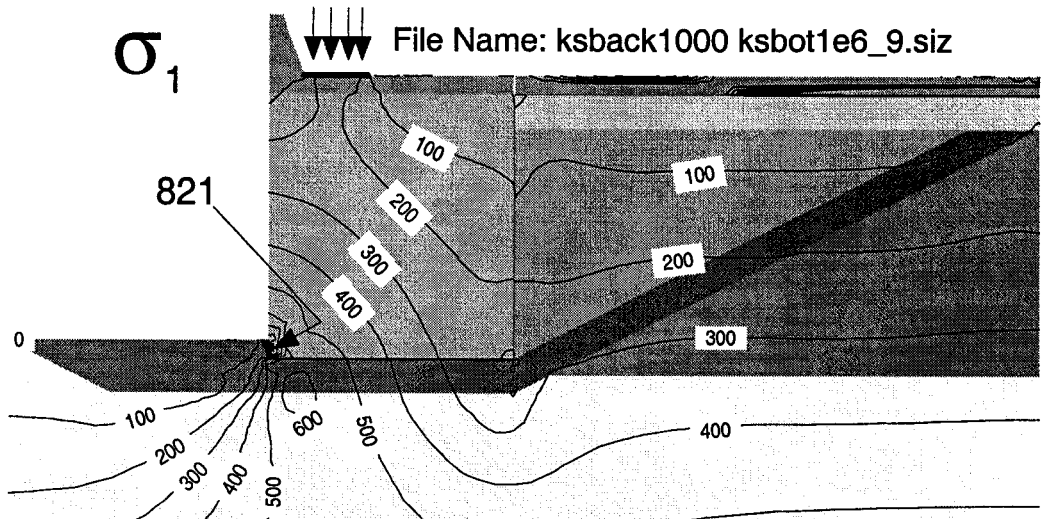
Figure C-31 Partial Load Condition – ksback1000 ksbot1e6 - σ_1 Contours.
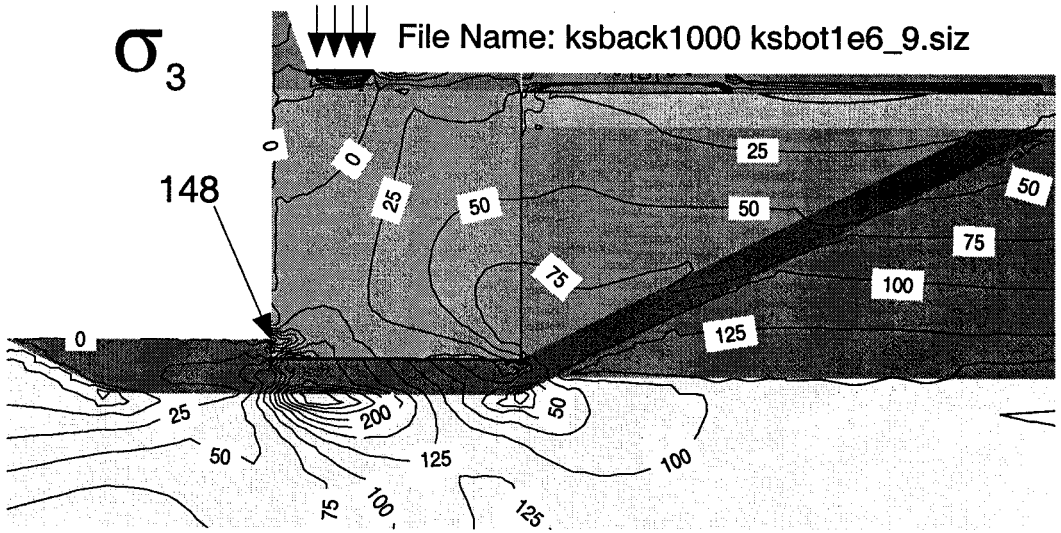
Figure C-32 Partial Load Condition – ksback1000 ksbot1e6 - σ_3 Contours.
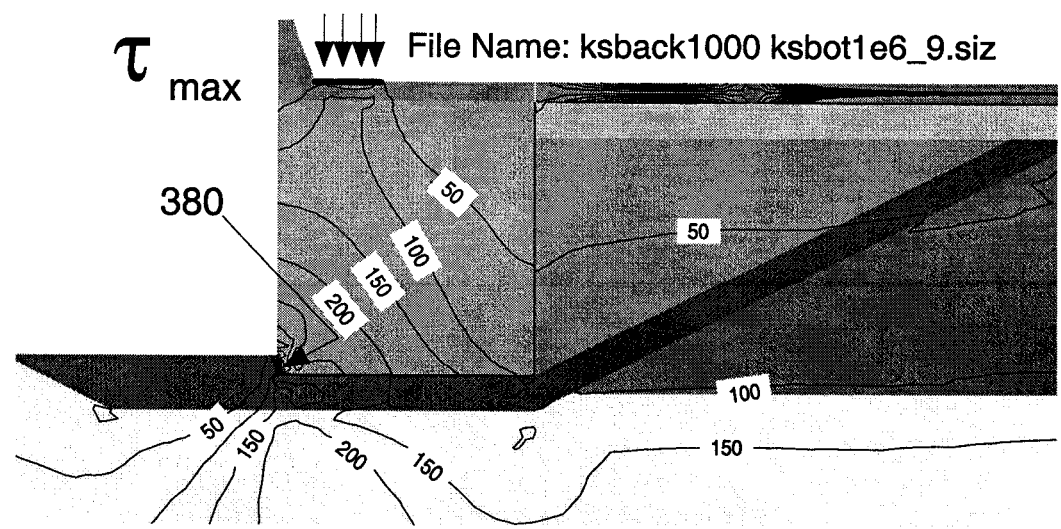
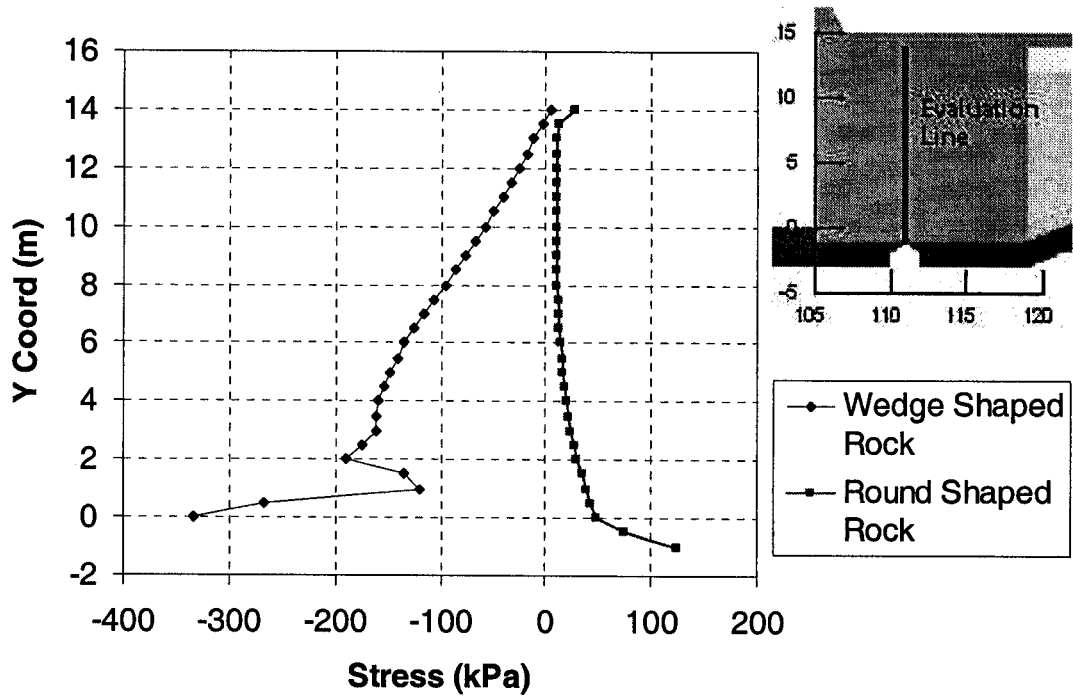**Figure C-33 Partial Load Condition – ksback1000 ksbot1e6 - τ_{max} Contours.**

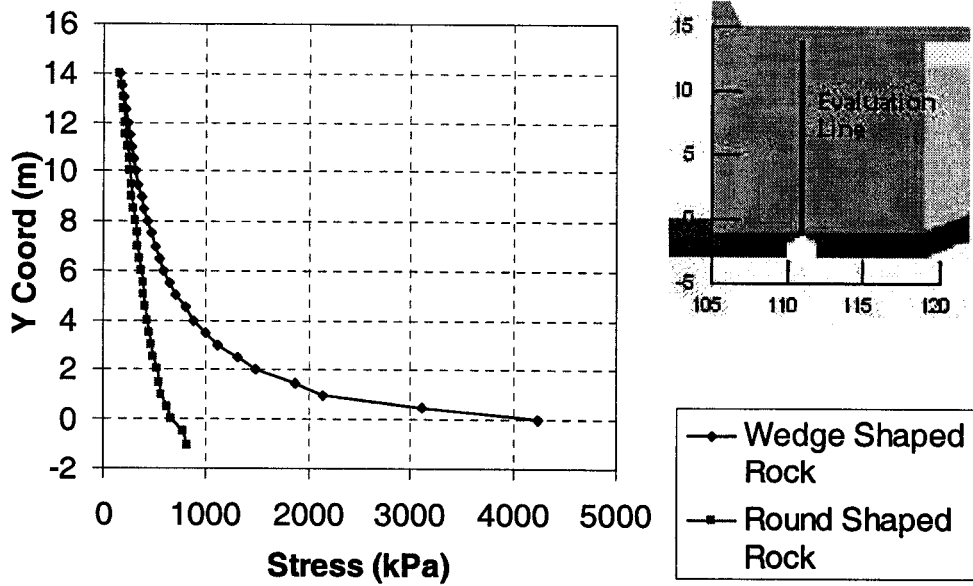**Figure C-34 Irregular Surface-Evaluation Line - σ_3 Stress.**
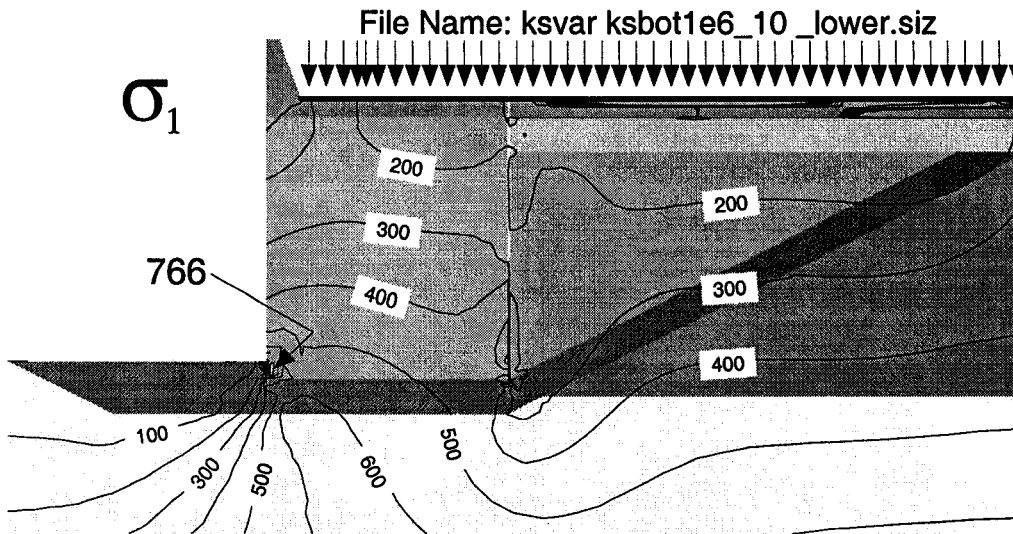

Figure C-35 Irregular Surface – Evaluation Line - σ_1 Stress.

σ_1

766

Figure C-36 Full Load – ksbackvar ksbot1e6- K=200 & K$_b$=50 - σ_1 Contours.

σ_3

159
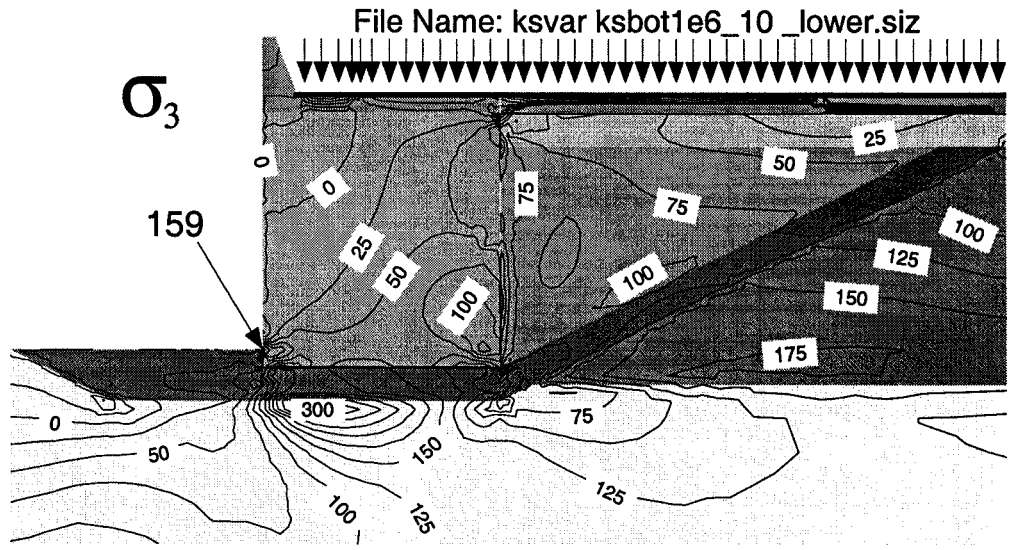
Figure C-37 Full Load – ksbackvar ksbot1e6- K=200 & K$_b$=50 - σ_3 Contours.

τ_{max}

766
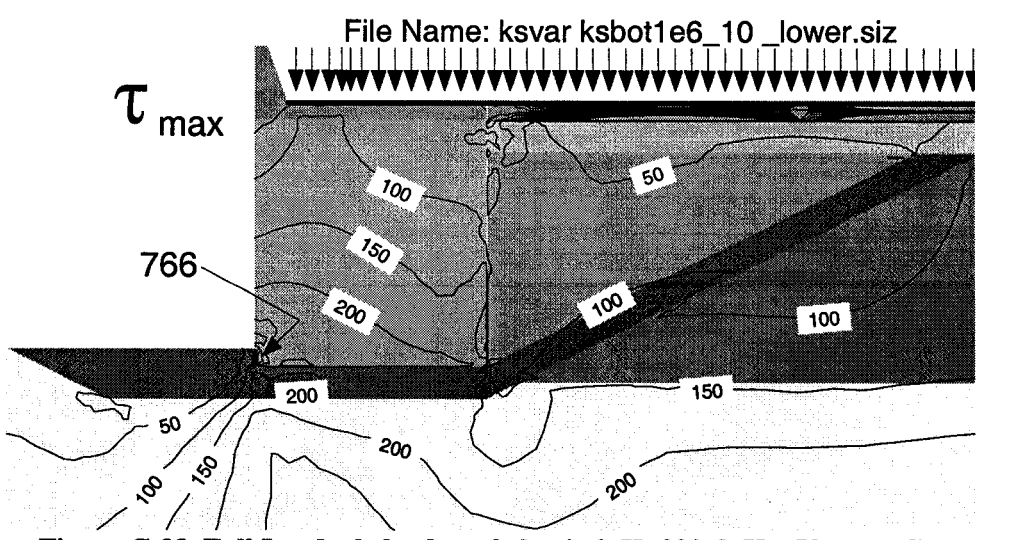
Figure C-38 Full Load – ksbackvar ksbot1e6- K=200 & K$_b$=50 - τ_{max} Contours.

File Name: ksvar ksbot1e6_10 _upper.siz

σ_1

836
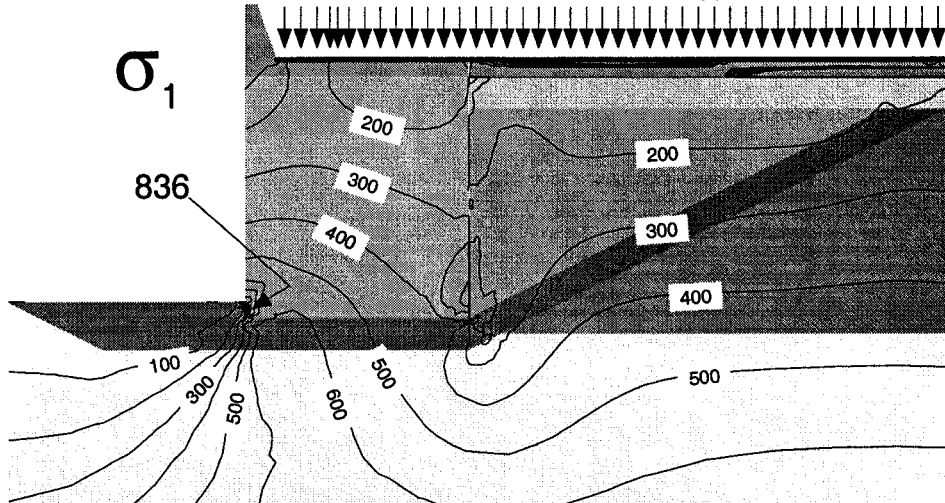
Figure C-39 Full Load – ksbackvar ksbot1e6- K=600 & K$_b$=170 - σ_1 Contours.

File Name: ksvar ksbot1e6_10 _upper.siz

σ_3

151
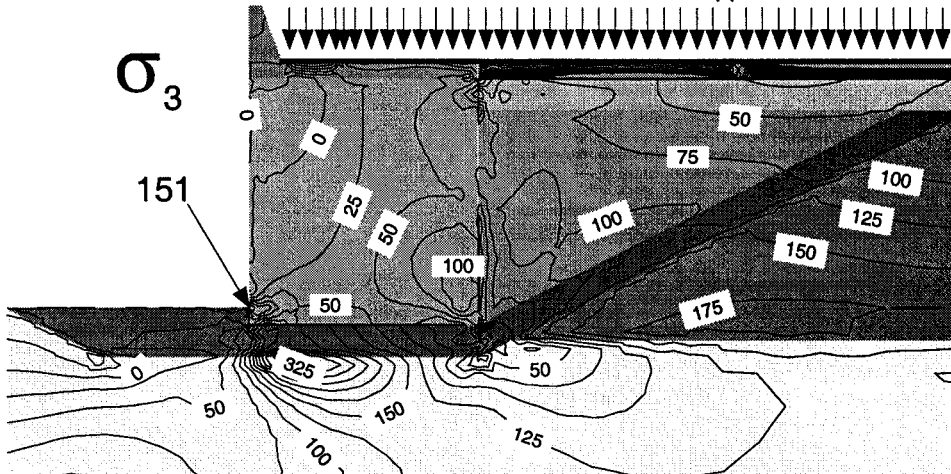
Figure C-40 Full Load – ksbackvar ksbot1e6- K=600 & K$_b$=170 - σ_3 Contours.

File Name: ksvar ksbot1e6_10 _upper.siz
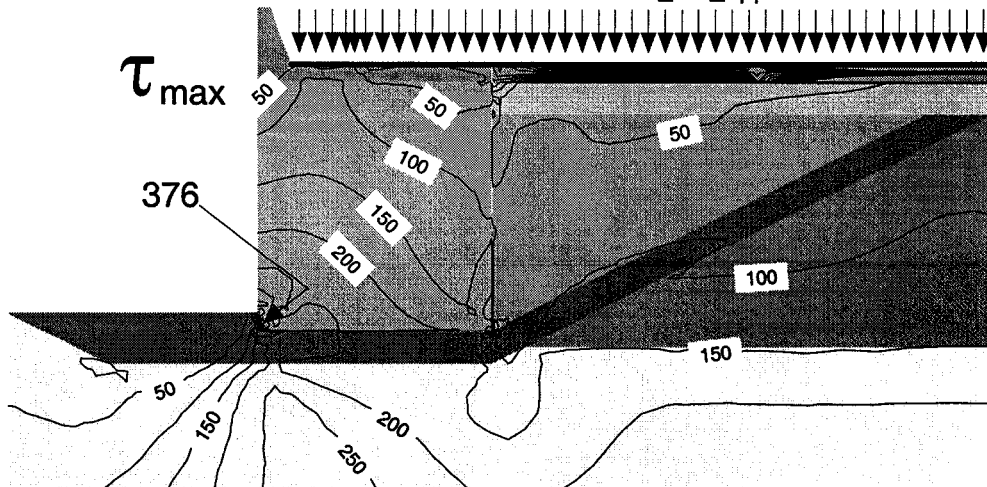
τ_{max}

376

Figure C-41 Full Load – ksbackvar ksbot1e6- K=600 & K$_b$=170 - τ_{max} Contours.

Figure C-42 Full Load – Bottom Line - ksbackvar ksbot1e6- K=600 & K_b=170 - σ_1 Stress.
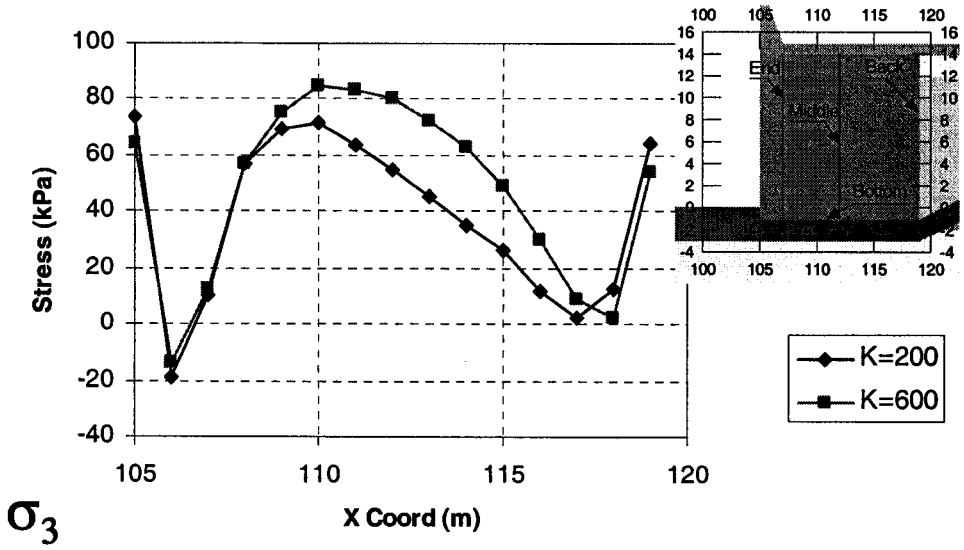
Figure C-42 Full Load – Bottom Line - ksbackvar ksbot1e6- K=600 & K_b=170 - σ_3 Stress.

Figure C-43 Full Load – Bottom Line - ksbackvar ksbot1e6- K=600 & K_b=170 - τ_{max} Stress.
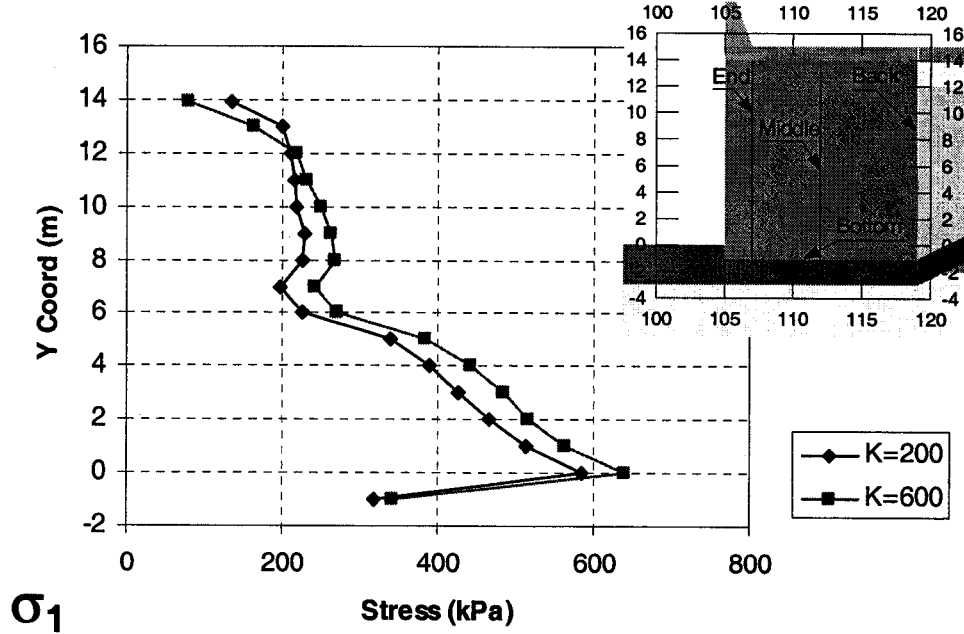
Figure C-44 Full Load – Back Line - ksbackvar ksbot1e6- K=600 & K_b=170 - σ_1 Stress.

Figure C-45Full Load – Back Line - ksbackvar ksbot1e6- K=600 & K_b=170 - σ3 Sress.
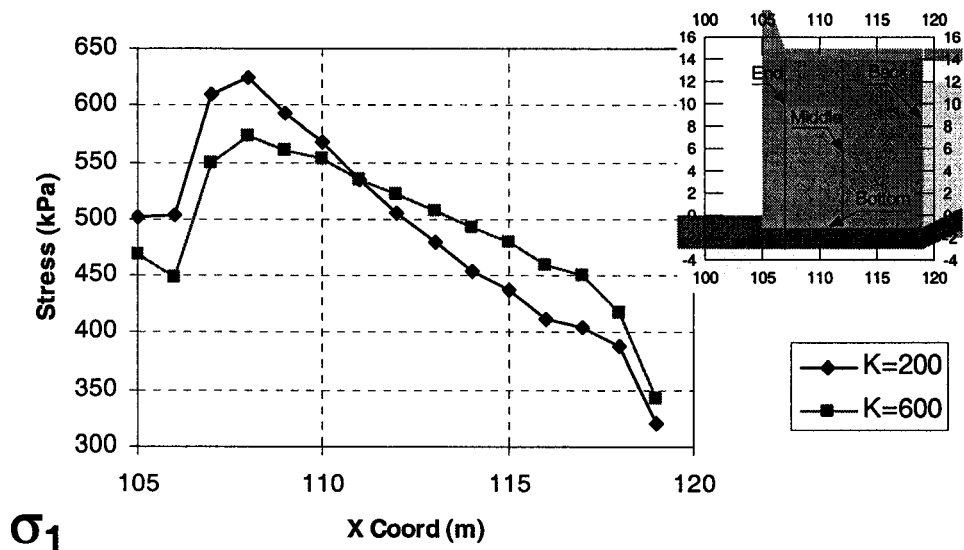

Figure C-45Full Load – Back Line - ksbackvar ksbot1e6- K=600 & K_b=170 - τ_max Stress.

Figure C-46 Full Load – Middle Line - ksbackvar ksbot1e6- K=600 & K_b=170 - σ_1 Stress.

Figure C-47 Full Load – Middle Line - ksbackvar ksbot1e6- K=600 & K_b=170 - σ_3 Stress.

Figure C-48 Full Load – Middle Line - ksbackvar ksbot1e6- K=600 & K_b=170 - τ_{max} Stress.
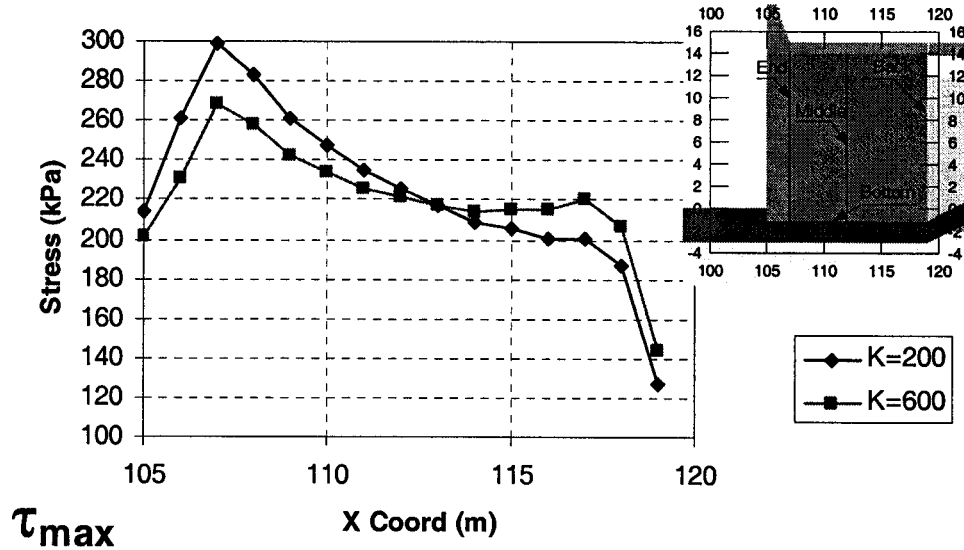

Figure C-49 Full Load – End Line - ksbackvar ksbot1e6- K=600 & K_b=170 - σ_1 Stress.
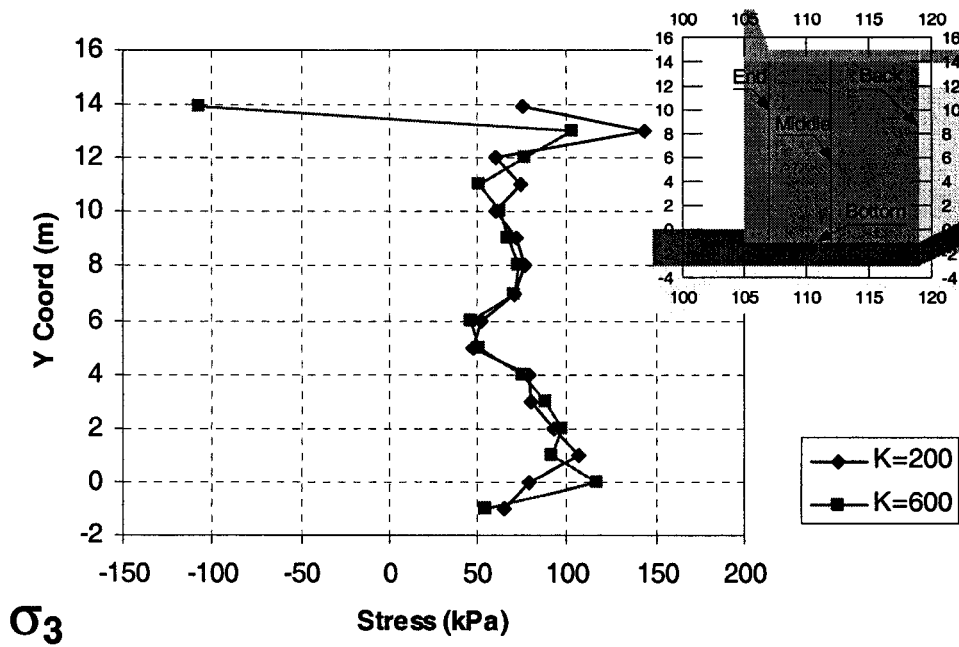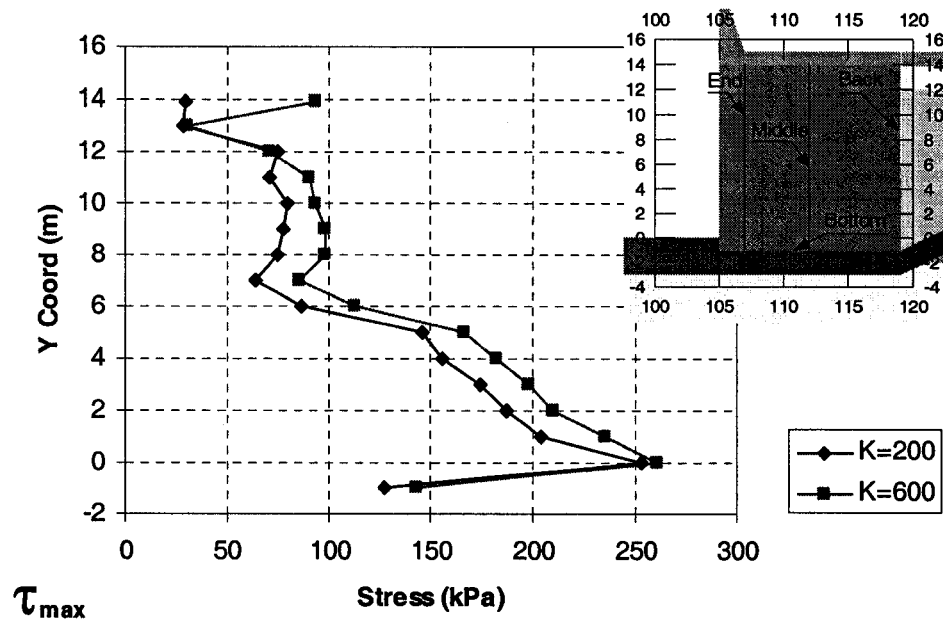
Figure C-50 Full Load – End Line - ksbackvar ksbot1e6- K=600 & K_b=170 - σ_3 Stress.

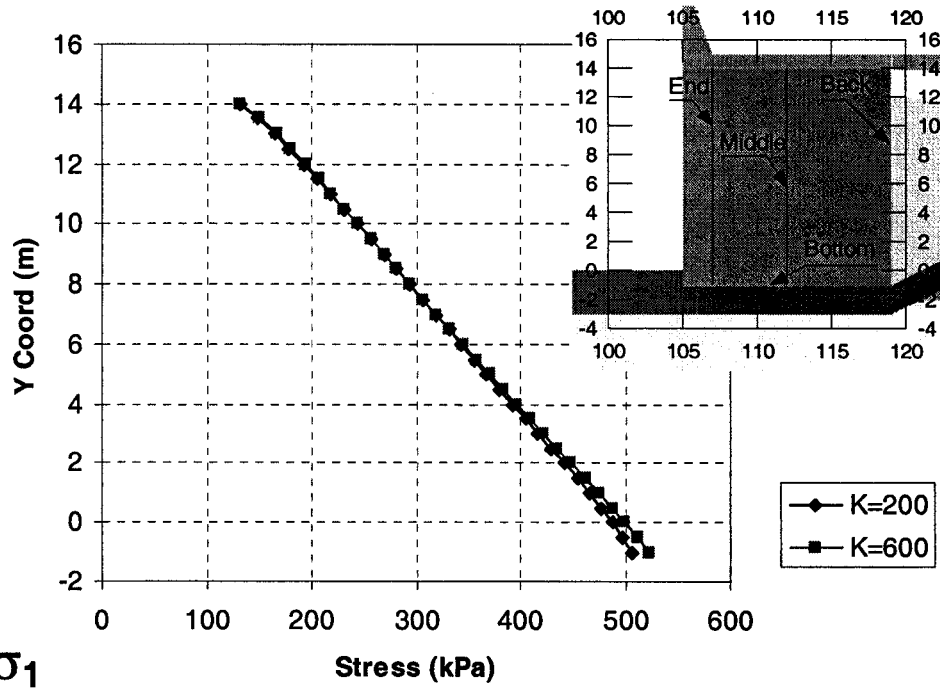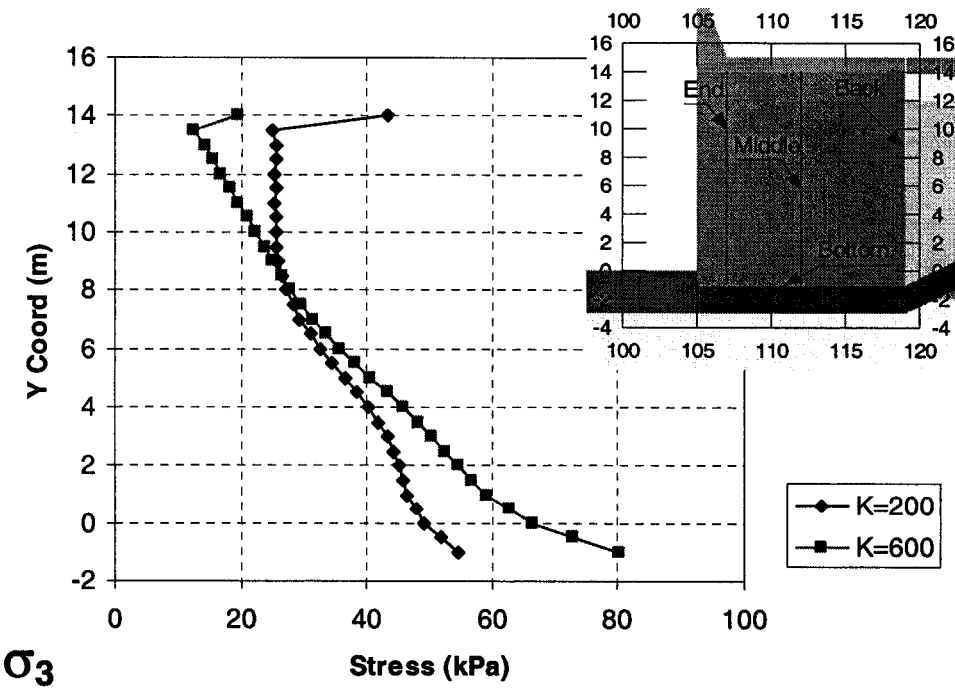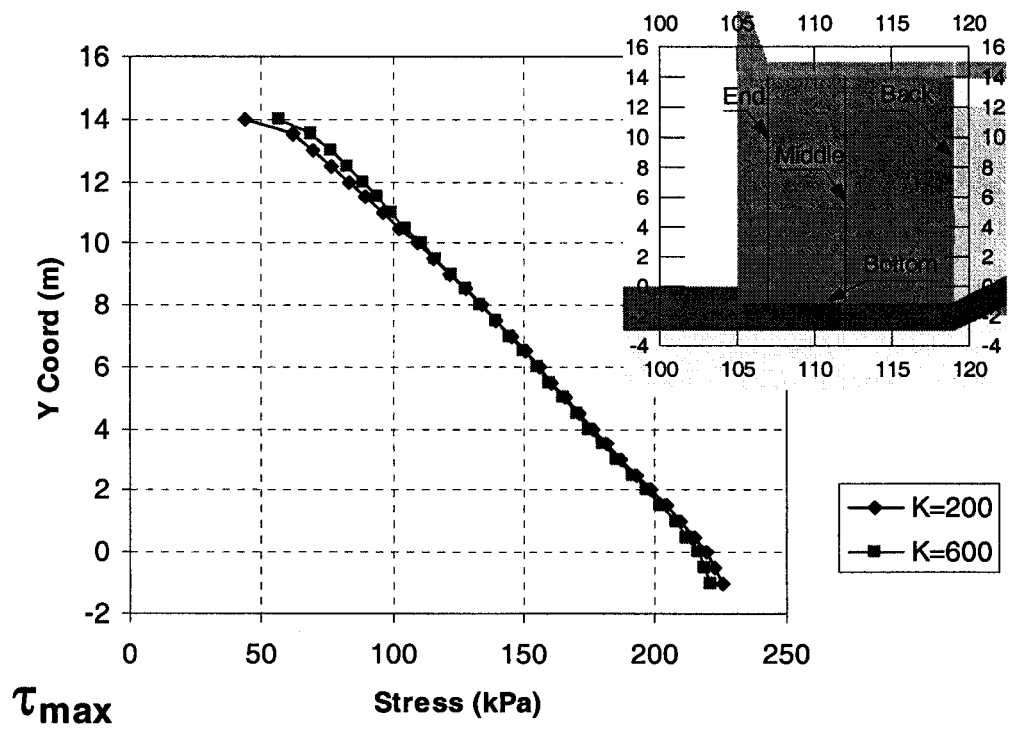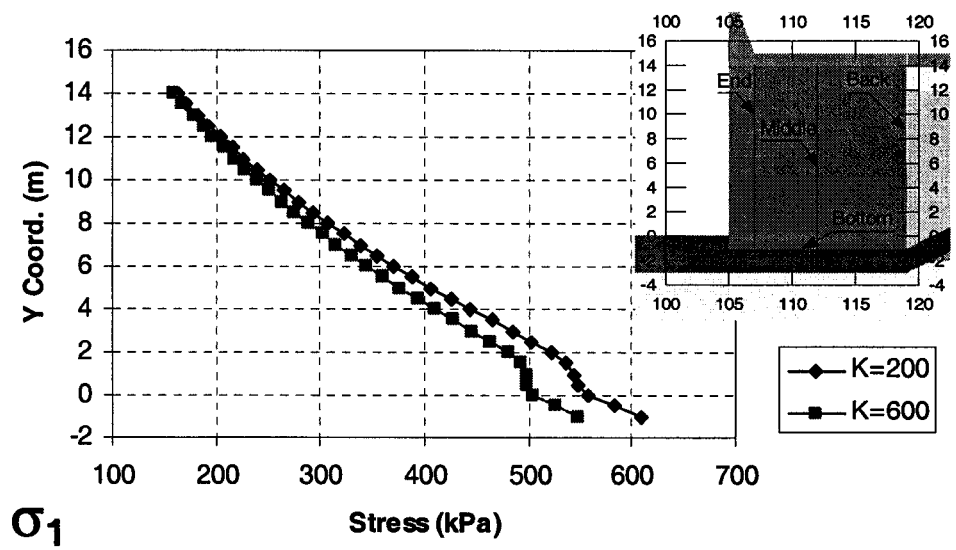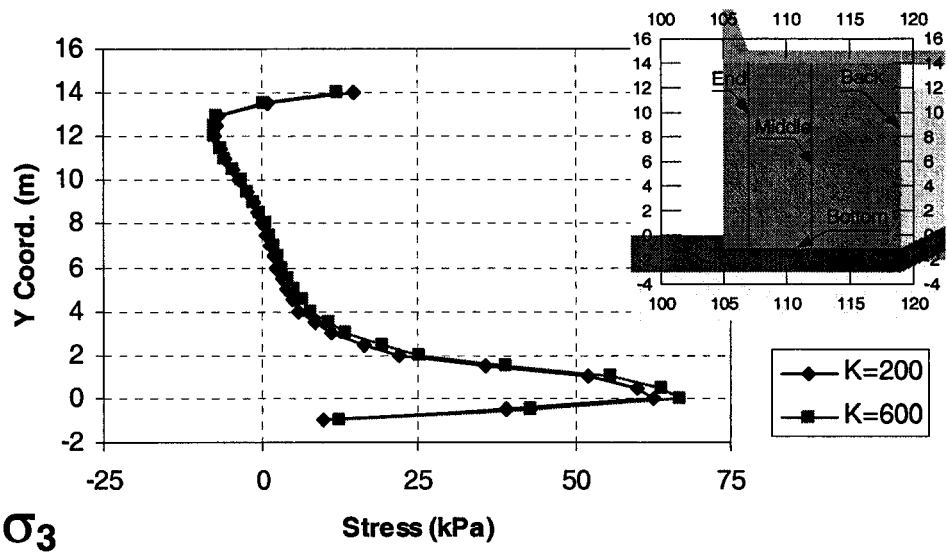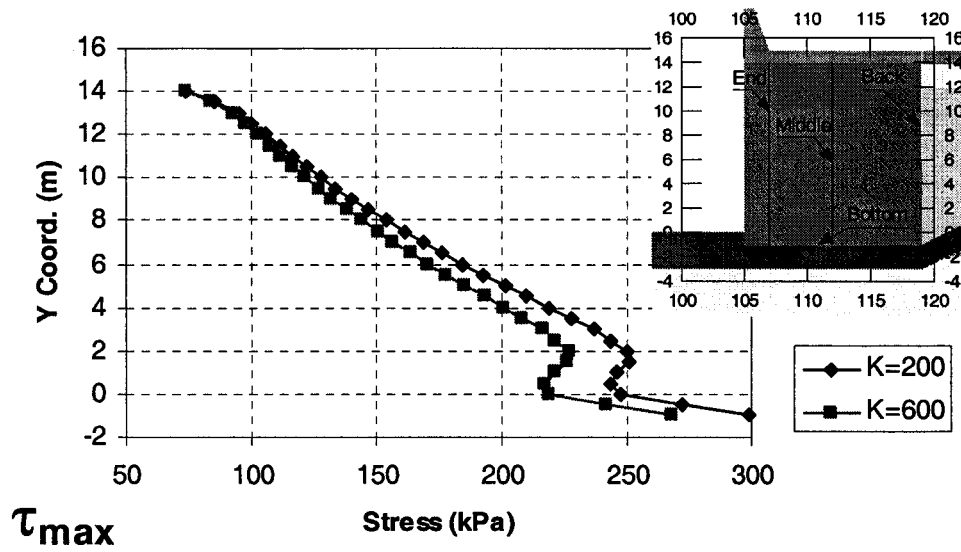**Figure C-51 Full Load – End Line - ksbackvar ksbot1e6- K=600 & K_b=170 - τ_{max} Stress.**

APPENDIX D LABORATORY STANDARD PROCEDURES

D.1   Standard Procedures for Measuring Compressive Strength, Young's Modulus and Stress-Strain Curve

As was mentioned previously, this method is described in the ASTM C 39 and covers the determination of compressive strength of cylindrical concrete specimens such as molded cylinders or drilled cores. The ASTM C 39 summarised the test method as follows: " This test method consists of applying a compressive axial load to molded cylinders or cores at a rate which is within a prescribed range until failure occurs. The compressive strength of the specimen is calculated by dividing the maximum load attained during the test by the cross-sectional area of the specimen"(p.18).

The standard indicates that care must be exercised in the interpretations of the significance of compressive strength determinated by this test method since strength is not a fundamental or intrinsic property of concrete made from the given materials. The ASTM C 39 also points out that the values obtained depend on the size and shape of the specimens, the batching, the mixing procedures, and the methods of sampling, molding, and fabrication. This consideration may also apply to sulphur concrete. In Sections 2.1.6.1 and 2.1.6.6, it is remarked that the compressive strength of the sulphur concrete specimens do not vary significantly with age. The moisture condition during curing is obviously not applicable because the sulphur concrete cylinders are cured in air at room temperature (20°C) in contrast with Portland cement concrete that is cured in a moisture room maintained at 100% relative humidity.

The ASTM C 39 indicates that neither end of compressive test specimens when tested should depart from the perpendicularity to the axis by more than 0.5°. The ends of specimens not planed within 0.050 mm should be sawed or ground to meet that tolerance, or capped in accordance with

either practice C 617 or C 1231. Furthermore, the diameter should be the average of two diameters measured at right angles to each other at about the midheight of the specimen.

The testing machine must have sufficient capacity and be capable of providing the rates of loading prescribed in this section. The machine also has to apply the load continuously and smoothly. The standard also indicated that the verification of the calibration must be made within 18 months, and preferably after an interval of 12 months. In testing machines of the screw type, the moving head must travel at a rate of approximately 1 mm/min. In hydraulically operated machines, the load must be applied at a rate of movement corresponding to a loading rate in the specimen within the range of 15 to 350 kPa/s. Moreover, this ASTM standard also specified that the rate of movement shall be maintained at least during the latter half of the anticipated loading phase of the testing cycle. However, a higher rate of loading is permitted during the anticipated first half of the loading phase. Finally, the standard required the application of the load until the failure of the specimen and the recording of the maximum load carried.

The calculation of the compressive strength is computed by dividing the maximum load carried (by the specimen) by the average cross-sectional area and expressing the results to the nearest 0.1 mPa. The determination of the stress-strain curve is covered in the ASTM C 469, and this procedure is explained in Section 3.4.2.1.

The procedure for calculating the Young's modulus was adopted from Brown (1981). The axial strain is calculated from the following equation:

$$\varepsilon_a = \frac{\Delta l}{l_o} \, , \qquad\qquad (D.1)$$

where l_0 is the original axial length and Δl is the change in measured axial length. The stress-strain curve is obtained by plotting the axial strain versus the axial stress from zero up to the failure stress of the specimen.

In addition, the calculation of the Young's modulus (E), or modulus of elasticity, followed Brown (1981), and is defined as the ratio of the axial stress change to the axial strain produced by the stress change. Engineering practice uses three methods to calculate the modulus. In this present thesis, the average Young's modulus is adopted (E_{av}) and is determined from the average slopes of the more or less straight-line portion of the axial stress-axial strain curve. In the following, the "static modulus of elasticity" will be called "Young's modulus." Both terms are widely used in practice and refer to the same material property.

D.2 Standard Procedures Measuring the Young' Modulus and Poisson's Ratio

The measurement of the Young's modulus, and the Poisson's ratio of concrete specimens in compression is covered in the ASTM C 469 standard method.

To measure the axial strains, the ASTM C 469 specified that an unbounded sensing device can be used for measuring to the nearest 5 millionths the average deformation of two diametrically opposite gauge lines, each parallel to the axis, and each centred to the midheight of the specimen. This standard also specified that the effective length of each gauge line must not be less than three times the maximum size of the aggregate in the concrete, nor more than two-thirds the height of the specimen. If the Poisson ratio is to be measured, as it was in our case, the ASTM C 469 specified that an unbounded extensomerter should be used and must be capable of measuring to the nearest 0.635 μm the change in diameter at the midheight of the specimen, or at two bonded strain gauges mounted circumferentially at diametrically opposite points at the midheight

of the specimen, and also capable of measuring the circumferential strain to the nearest 5 millionths.

The ASTM C 469 required that companion specimens have to be tested to obtain the compressive strength prior to the test, in order to determine its maximum load. The specimen must be loaded at least twice, but no data is recorded during the first loading. The first loading is primarily for the seating of the equipment. After the equipment seating, the ASTM C 469 recommends performing at least two loadings. The load must be applied continuously and smoothly up to 40% of the previously measured compression strength.

This standard suggested that if the stress-strain curve is desired, then a continuous reading should be taken by using suitable instruments. Furthermore, the strength and the modulus of elasticity may be obtained from the same loading providing an appropriate measure to protect the equipment.

This standard method required that the diameter be measured by calliper to the nearest 0.25 mm by averaging the two diameters measured at right angles to each other near the centre of the specimen.

The procedures to calculate the Young's modulus and the Poisson's ratio were taken from Brown (1981). Section 3.4.1.1 includes the recommendations for calculating the Young Modulus. The suggested procedures for estimating the Poisson's ratio are covered in this section.

Brown (1981) suggested that the diametric strain might be determined by measuring the changes in the specimen's diameter or by measuring the changes in the circumference, as the ASTM C 469 also recommends. The formulations to estimate these strains were taken from

Brown (1981). If the change in diameter is measured the diametric strain is calculated from the following equation:

$$\varepsilon_d = \frac{\Delta d}{d_o} \quad , \qquad\qquad (D.2)$$

where d_o is the original undeformed diameter of the specimen, and Δd is the change in diameter (defined to be negative for an increase in diameter). In measuring the circumferential strain ε_c, the circumference is $C=\pi d$; thus, the change in circumference is $\Delta C=\pi \Delta d$. Consequently, the circumferential strain is related to the diametric strain by

$$\varepsilon_c = \frac{\Delta C}{C_o} = \frac{\Delta d}{d_o} ; \text{ therefore, } \varepsilon_c = \varepsilon_d , \qquad\qquad (D.3)$$

where C_o and d_o are the specimen's original circumference and diameter, respectively. The Poisson's ratio is calculated from the following equation:

$$\upsilon = -\frac{\Delta \sigma_a / \Delta \varepsilon_a}{\Delta \sigma_a / \Delta \varepsilon_d} \quad , \qquad\qquad (D.4)$$

where $\Delta \sigma_a$ is the axial stress, $\Delta \varepsilon_a$ is the axial strain, and $\Delta \varepsilon_d$ is the diametric strain. Note that the Poisson's ratio in equation 3.4 has a positive value, since the slope of the diametric curve is negative.

D.3 Splitting Tensile Test Standard Procedure

The ASTM C 496 summarised the test method as follows: "This test method consists of applying a diametral compressive force along the length of a cylindrical concrete specimen.... This loading induces tensile stresses on the plane containing the applied load and relatively high compressive stresses in the area immediately around the applied load. Tensile failure occurs rather than compressive failure because the areas of load application are in a state of triaxial compression..."(p. 268).

The splitting tensile test rather than the direct tensile test was selected for investigating the tensile strength of the sulphur concrete cylinders because the former test procedure is simpler. The testing machine utilized was the same compression machine used in the compression test program; therefore, it is not described again in this section. The ASTM standard required the use of supplementary bearing plates in case when the length of the cylinders is larger than the diameter of the upper or lower bearing blocks; however, this factor did not apply because the dimension of the cylinders was only 3 by 6-inches.

The ASTM C 496 specified the use of two bearing strips of nominally 3.2-mm thick plywood, free of imperfections, approximately 25-mm wide, and with a length equal to or slightly longer than the cylinders' length. The strips must be placed between the cylinder and both the upper and lower bearing blocks of the testing machine. Furthermore, the standard specified that the strips should not be reused for subsequent tests.

The proper execution of this test requires marking the specimens by drawing diametral lines on each end of the specimens by using a suitable device to ensure that they were in the same axial plane. As well, the diameter of the samples must be obtained to the nearest 0.25 mm by averaging three diameters, lying on the marked planes, at both ends and at the middle of the specimen. The length is determined by averaging at least two measurements through the plane containing the lines marked on two ends. The marked lines guide the proper positioning of the cylinders in the test apparatus. A plywood strip is placed along the centre of the lower bearing block. Then, the cylinder is placed on top of the strip by aligning the marked lines vertically and centred over the plywood strip. The second strip is placed on top of the cylinder by aligning the marked line on the strip centre. The positioning must ensure that the vertical marked plane is on the upper bearing block centre. Finally, the load is applied continuously and smoothly at a

constant rate within the range of 689 to 1380 kPa/min until failure of the specimen. The splitting tensile strength (T) is calculated as follows:

$$T = \frac{2P}{\pi l d},$$

(D.5)

where P is the maximum applied load, l is the specimen length, and d is the specimen's diameter. The units are given in kPa if kN, and metres are the units.

D.4 Standard Procedure of the Test Method for Resistance of Concrete to Rapid Freezing and Thawing

The ASTM C 666 specified that the freezing and thawing apparatus must consist of a suitable chamber or chambers in which the specimens may be subjected to the specified freezing and thawing cycle. Furthermore, the apparatus must be capable of producing continuously and automatically reproducible cycles within the specified temperature requirements. If the equipment does not operate automatically, provisions shall be made for either a day of its continuous manual operation on a 24-hour basis or for the storage of all specimens in a frozen condition when the equipment is not in operation.

Procedure A requires that the specimens shall be completely surrounded by no less than 1mm and no more than 3 mm of water at all times during the freeze-thaw cycles. Also, the bottom of a specimen must not be in direct contact with the bottom of the container, in order to avoid substantially different conditions from the remainder areas of the sample. The standard also recommended the use of a flat spiral of 3-mm wire placed at the bottom of the container to support the specimens. The temperature-measuring equipment consists of thermometers, resistance thermometers, or thermocouples capable of measuring to within 1.1°C the temperature at various points within the specimen chamber and at the centres of the control specimens.

The nominal freezing and thawing cycle of this test method should consist of alternatively lowering the temperature from 4.4 to –17.8°C and raising it from –17.8 to 4.4°C in not less than 2 hours and no more than 5 hours. Procedure A also required that not less than 25% of the time should be used for thawing. At the end of the cooling period, the temperature at the centre of the specimens should be –17.8 ± 1.7°C, and at the end of the heating period, the temperature should be 4.4 ± 1.7°C. During the entire experiment, the maximum and minimum temperature should be between 6.1 and –19.4°C, respectively.

During the freezing and thawing test, the specimens are removed for testing the fundamental transverse frequency at intervals not exceeding 36 cycles. The specimens are returned to the freeze-thaw apparatus, either to random positions or to a predetermined rotation scheme to ensure that all the specimens are subjected to the conditions at all parts of the freezing apparatus. The test continues until 300 cycles of freeze-thaw are reached or their relative dynamic modulus of elasticity deteriorates to 60% of the initial modulus.